Amine End-Functional Poly(*N*-vinylpyrrolidone) as a Macroinitiator for L-lysine *N*-carboxyanhydride Polymerization - Towards the Preparation of pH-Responsive Micelles for Drug Delivery

By

Alexander Ilchev

Thesis presented in partial fulfillment of the requirements for the degree,

Doctor of Philosophy in Polymer Science

Supervisor: Prof. Bert Klumperman

Department of Chemistry and Polymer Science

Stellenbosch University

Declaration

I, the undersigned, hereby declare that the work contained in this thesis is my own original work and that I have not previously in its entirety or in part submitted it at any university for a degree.

……..

Alexander Assenov Ilchev 04 December 2014

/ƨLJè₥ƗƎKǘ ϭ нлмр {ǘŜfƒŜyʊƟƨǎǑK ¦ y₥ØŜ₥ǎʎǘè

! ƒƒ ₥ƗƎKǘǎ ₥ŜǎŜ₥ØŜŘ

Abstract

Cancer is a notorious affliction that knows no age, gender, ethnic, racial, or species bounds and is responsible for over 14% of annual worldwide human deaths. There is no universal cure and the treatments that exist have poor probabilities of success. Chemotherapy is often considered the staple for cancer treatment as it can enter areas of the body that are unsafe for surgery and can treat tumors that are too small to be detected, even with modern imaging techniques. However, chemotherapy can induce many harmful and fatal side-effects. It can also lose its therapeutic effect if the cancer mutates to become multi-drug resistant. These shortcomings can be linked to the poor selectivity and pharmacokinetics of conventional chemotherapy drugs. Modern research focusses on improving these aspects of existing chemotherapy regimens through the incorporation of drug delivery principles. This dissertation focusses on the development of a novel, polymeric, pH-responsive drug delivery system for chemotherapy that incorporates the chemotherapeutic drug as well as a cell-penetrating peptide in a prodrug formulation. The system was designed to inhibit the release of its components into healthy tissues while selectively accumulating, through the enhanced permeability and retention effect, and releasing its payload, through reversible hydrolysis of imine bonds, within tumor tissues. Poly(L-lysine) was chosen as the cell-penetrating peptide since it is able to form imine bonds through its ε-amine functional groups on its residues. It was prepared by the primary amine-initiated ring-opening polymerization of N^{ε}-(benzyloxycarbonyl)-L-lysine *N*-carboxyanhydride at 0 °C and pressures lower than 1 mbar as these conditions allow for a controlled, living polymerization to occur. The benzyloxycarbonyl end-group was removed by acidolysis with HBr in a mixture of dichloromethane and 1,4-dioxane at 0 °C. The initiator used for the ring-opening polymerization was poly(*N*-vinylpyrrolidone) with a primary amine end-group, prepared by RAFT-mediated polymerization with *O*-ethyl-*S*-(phthalimidylmethyl)xanthate. This RAFT agent was shown to display slow pre-equilibrium kinetics which was linked to the lower relative stability of the phthalimidylmethyl radical compared to the poly(N-vinylpyrrolidone) propagating radical. The pre-equilibrium and main equilibrium kinetics of the RAFT polymerization were optimized by performing the polymerization in semi-batch mode. During the semi-batch polymerization, the monomer to RAFT agent ratio could be controlled by adjusting the monomer feed. This ratio was shown to be inversely proportional to the probability of radical transfer from the propagating radical to the phthalimidylmethyl radical. The phthalimide end-group could be converted to a primary amine both by reacting with hydrazine in methanol as well as reduction with sodium borohydride in water followed by hydrolysis in 1 M HCl at 60 °C. Doxorubicin and

benzaldehyde could be conjugated, via imine bonds, to the poly(N-vinylpyrrolidone-*block*-L-lysine) copolymer spontaneously in methanol. Both types of conjugates would self-assemble into micelles when dispersed in water. However, the Doxorubicin conjugates were unstable, precipitating out of solution within 24 hours. The benzaldehyde conjugates were stable in water for over 24 hours. This suggested that a formulation of Doxorubicin and benzaldehyde conjugated to the block copolymer may be sufficiently stable under the physiological conditions of blood plasma.

Opsomming

Kanker is 'n berugte toestand wat geen ouderdom, geslag, etniese, ras- of spesiegrense ken nie en is verantwoordelik vir meer as 14% van die jaarlikse wêreldwye menslike sterftes. Daar is geen universele kuur vir hierdie siekte nie en die behandelings wat bestaan het swak waarskynlikhede van sukses. Chemoterapie is handig want dit behandel tumore waar operasies nie as veilig beskou word nie of as dit te klein is om te spoor, selfs met moderne beeldingstegnieke. Chemoterapie kan egter skadelike en dodelike newe-effekte tot gevolg hê. Dit kan ook die terapeutiese effek verloor as die kanker muteer en multi-middelweerstandig word. Hierdie tekortkominge kan gekoppel word aan die swak selektiwiteit en farmakokinetika van konvensionele chemoterapiemiddels. Moderne navorsing probeer om hierdie probleme op te los deur die inlywing van geneesmiddel-leweringsbeginsels. Hierdie proefskrif fokus op die ontwikkeling van 'n nuwe, polimeriese, pH-reaktiewe geneesmiddel-leweringstelsel vir chemoterapie wat die chemoterapeutiese middel sowel as 'n sel-indringende peptied in 'n progeneesmiddel formulering inkorporeer. Die stelsel is ontwerp om die ophoping of vrystelling van die medikasie en die peptied in gesonde weefsel te inhibeer. Terselftertyd word die medikasie deur middel van gevorderde deurlatings en terughoudings in die tumor vrygestel deur omgekeerde hidrolise van die imienbindings. Poli (L-lisien) is gekies as die sel-indringerpeptied omdat dit imienbindings kan vorm deur middel van die ε-amien funksionele groep en ook omdat dit bioafbreekbaar is. Die reaksie is daargestel deur die primêre amien-geïnisieerde ring-openingpolimerisasie van *Nε*-(bensieloksikarboniel)-L-lisien *N*-karboksianhidried. Die temperatuur is by 0 °C en die druk onder 1 mBar gehou aangesien hierdie omstandighede gekontroleerde lewende polimerisasie toelaat. Die bensieloksikarboniel eindgroep is verwyder deur middel van HBr in 'n mengsel van dichlorometaan en 1,4-dioksaan by 0 °C. Die inisieerder wat gebruik word vir die ring-openingpolimerisasie is poli(*N*-vinielpirrolidoon) met 'n primêre amien eindgroep. Dit is berei deur RAFT-bemiddelde polimerisasie van *N*-vinielpirrolidoon met *O*-etiel-*S*-(ftalimidielmetiel)xantaat. Hierdie RAFT-agent het stadige voorewewig kinetika getoon as gevolg van die laer relatiewe stabiliteit van die ftalimidielmetielradikaal in vergelyking met die poli(*N*-vinielpirrolidoon) voortsettingsradikaal. Die voorewewig en hoofewewig kinetika van die RAFT-polimerisasie is geoptimaliseer deur die polimerisasie in ‘n semi-bondel manier uit te voer.

Die monomeer / RAFT-agent verhouding kon deur die tempo van monomeertoevoeging beheer word. Hierdie verhouding is omgekeerd eweredig aan die waarskynlikheid van radikale oordrag van

die voortsettingsradikaal aan die ftalimidielmetielradikaal. Die ftalimied eindgroep kon na 'n primêre amien omgeskakel word deur die reaksie met hidrasien in metanol sowel as deur die vermindering van natriumboorhidried in water, gevolg deur hidrolise met 1 M HCl by 60 °C. Doksorubisien en bensaldehied het spontaan imienbindings met poli-(*N*-vinielpirrolidoon-*blok*-L-lisien) kopolimeer in metanol gevorm. Altwee tipes konjugate sou self-omskakel in miselle wanneer hulle in water versprei word maar die doksorubisien konjugate was relatief onstabiel en het binne 24 uur neergeslaan in water. Die bensaldehied kojugaat was egter stabiel in water vir langer as 24 uur. Dit dui daarop dat ’n oplossing van doksorubisien en bensaldehied gekonjugeer aan die blokkopolimeer genoegsaam stabiel onder die fisiologiese toestande van bloedplasma sal wees.

Acknowledgements

I would like to take this opportunity to express my dearest appreciation for the people who were instrumental towards the preparation of my dissertation. I must begin with the copious gratitude I possess towards my supervisor, Professor Bert Klumperman. He was the first person I spoke with at the Polymer Science department in Stellenbosch and was the man that made it all possible. His devotion and collaboration with all the students under his care is quite amazing, especially considering all the long distance trips he has to make annually. Secondly, I wish to mention that without the further aid and guidance of Dr. Rueben Pfukwa, my first few months of literature review and project planning could have very well been years. I also have to thank him for his aid during the period in which he was in charge of running and maintaining the SEC system I needed for the analysis of my polymers. I wish to thank Dr. Nadine Pretorius for performing that role as his successor. I also would like to regard my utmost admiration to Dr. Jacu Brand and Dr. Elsa Malherbe for the extra time they took to indulge my gratuitous queries on the theory and practice of nuclear magnetic resonance while I was using their department's instruments. I have to thank Dr. M. Jaffer for his aid in preparing and analyzing all my cryo-TEM samples. A heartfelt indebtedness is felt for Dr. Maggie Brand due to her devotion towards my understanding and application of our dynamic light scattering instrument. I would like to thank our lab captain Dr. Paul Reader for establishing the protocols in our lab as well as the digital cataloguing system which all made our experimental work far more convenient. Also, as a colleague with a similar research topic, there were many inspiring discussions we had on similar problems with our research that I shall not easily forget. A solemn recognition to Piere-André Siebert and Nedine Van Deventer for helping me translate my abstract to an Afrikaans version. I wish to also thank all my other colleagues for the exciting work environment they created. Our technical staff Kelvin Maart, Jim Motshweni and Deon Koen are really a marvel and deserve every bit of respect they receive from our group. They always ensured that the facilities ran smoothly and the orders were on time and not mishandled. Our administrative staff Anelli Louw and Erinda Cooper also performed their roles in a manner attracting gracious appraisal. I wish to thank the NRF for generously funding so much of our research in our department. Most notably, I have to thank my father Dr. Assen Ilchev for raising me as well as aiding in my understanding and appreciation for the mathematical problems I faced in my thesis. I also wish to thank my mother Stoya Ilcheva in a similar manner as, with her knowledge in linguistics, she ensured that the eloquence in my writing was of a standard beyond my reach alone. For the rest of my family, I am grateful to you for believing in me and ensuring that I was never alone.

Contents

Declaration ii

Abstract iii

Opsomming v

Acknowledgements vii

Contents viii

List of Figures xvii

List of Tables xxi

List of Schemes xxii

List of Abbreviations xxiii

List of Symbols xxix

1.) Prologue 1

1.1) Introduction 1

1.2) Objectives 1

1.3) Layout of Thesis 3

1.3.1) Chapter 1: Prologue 3

1.3.2) Chapter 2: Literature Review 3

1.3.3) Chapter 3: RAFT-Mediated Polymerization of *N*-vinylpyrrolidone with *O*-ethyl-*S*-(phthalimidylmethyl)xanthate Performed in Batch-Mode 3

1.3.4) Chapter 4: Designing a Semi-Batch RAFT-Mediated Polymerization of *N*-vinylpyrrolidone with *O*-ethyl-*S*-(phthalimidylmethyl)xanthate 3

1.3.5) Chapter 5: Deprotection of the Primary Amine α-End-Group on PVP 4

1.3.6) Chapter 6: Hydrolysis of the Xanthate and Alkene End-Groups on PVP 4

1.3.7) Chapter 7: Preparation of Poly(*N*-vinylpyrrolidone)-*block*-poly(L-lysine) Copolymers by *N*-Carboxyanhydride Ring-Opening Polymerization 4

1.3.8) Chapter 8: Deprotecting the N^{ε}-Amine of the Lysine Residues on PVP-*block*-poly(N^{ε}-(CBZ)-L-lys) 4

1.3.9) Chapter 9: Conjugation of Doxorubicin to PVP-*block*-poly(L-lysine) 5

1.3.10) Chapter 10: Epilogue 5

1.3.11) Appendices 5

1.4) References 5

2.) Literature Review 8

2.1) Cancer and Chemotherapy 8

2.1.1) Overview of Cancer 8

2.1.2) Concepts of Chemotherapy 9

2.1.3) Doxorubicin (Adriamycin) as a Chemotherapeutic Drug 12

2.2) Drug Delivery 13

2.2.1) Principles of Drug Delivery 13

2.2.2) Nanotechnology in Drug Delivery 14

2.2.3) Stimuli-Responsive Polymers in Drug Delivery 15

2.2.4) Prodrugs 16

2.2.5) Polymeric Prodrugs 17

2.2.6) Targeted Drug Delivery 18

2.2.7) Cell-penetrating Peptides and Drug Delivery 21

2.3) Radical Polymerization 22

2.3.1) Overview of Radical Polymerization 22

2.3.2) PVP as a Biomaterial 24

2.3.3) Controlled Radical Polymerization and RAFT Polymerization 25

2.4) *N*-Carboxyanhydrides and their Ring-Opening Polymerization 28

2.4.1) Overview of Ring-Opening Polymerization 28

2.4.2) Overview of *N*-Carboxyanhydrides 29

2.4.3) NCAs as Monomers for Ring-Opening Polymerization 30

2.5) Brief Deduction of the Researched Literature 33

2.6) References 35

3.) RAFT-Mediated Polymerization of *N*-vinylpyrrolidone with *O*-ethyl-*S*-(phthalimidylmethyl)xanthate Performed in Batch-Mode 48

3.1) Introduction 48

3.2) Materials and Experimental Methods 49

3.2.1) Synthesis of XA2 49

3.2.2) RAFT-Mediated Polymerization of NVP with XA2 - R = 196 49

3.2.3) RAFT-Mediated Polymerization of NVP with XA2 – R = 117 50

3.2.4) ^{1}H-NMR *In-situ* Polymerization of NVP with XA2 – R = 5 50

3.2.5) SEC Analysis 51

3.2.6) NMR Analysis 51

3.3) Results and Discussion 52

3.3.1) Analysis of Polymers Prepared in Sections 3.2.2 and 3.2.3 52

3.3.2) Pre-Equilibrium Kinetics Study by *In-Situ* ^{1}H-NMR 59

3.4) Conclusions 63

3.5) References 64

4.) Designing a Semi-Batch RAFT-Mediated Polymerization of *N*-vinylpyrrolidone with *O*-ethyl-*S*-(phthalimidylmethyl)xanthate 66

4.1) Introduction 66

4.2) Simulating the Convergent Discrete Semi-Batch Process 70

4.3) Simulating the Steady Discrete Semi-Batch Process 74

4.4) Simulating the Continuous Semi-Batch Process 76

4.5) Materials and Experimental Methods 79

4.5.1) Determining the Observed Rate Constant for the Polymerization of NVP with XA2 79

4.5.2) Polymerization of NVP with XA2 by the Convergent Discrete Semi-Batch Process 79

4.5.3) Polymerization of NVP with XA2 by the Steady Discrete Semi-Batch Process 80

4.6) Results and Discussion 81

4.6.1) Calculating the Observed Rate Constant for the Polymerization of XA2 with NVP 81

4.6.2) Polymerization of NVP with XA2 by the Convergent Discrete Semi-Batch Process 82

4.6.3) Polymerization of NVP with XA2 by the Steady Discrete Semi-Batch Process 84

4.7) Conclusions 88

4.8) References 89

5.) Deprotection of the Primary Amine α-End-Group on PVP 90

5.1) Introduction 90

5.2) Materials and Experimental Methods 91

5.2.1) Thermolysis of the Xanthate End-Group 91

5.2.2) Deprotection of the Primary Amine End-Group 92

5.2.3) Dialysis of the Deprotected PVP 92

5.2.4) Derivatization with 3,5-Bis(trifluoromethyl)Benzaldehyde 92

5.2.5) Derivatization with Pentafluorobenzaldehyde 93

5.3) Results and Discussion 93

5.3.1) Thermolysis of the Xanthate End-Group 93

5.3.2) Deprotection of the Primary Amine α-End-Group and Isolation of the Product by Dialysis 95

5.3.3) Derivatization with 3,5-Bis(trifluoromethyl)Benzaldehyde 98

5.3.4) Derivatization with Pentafluorobenzaldehyde 102

5.4) Conclusions 103

5.5) References 103

6.) Hydrolysis of the Xanthate and Alkene End-Groups on PVP 105

6.1) Introduction 105

6.2) Materials and Experimental Methods 108

6.2.1) *In-Situ* ^{1}H-NMR Kinetic analysis of Xanthate End-Group Hydrolysis 109

6.2.2) *In-Situ* ^{1}H-NMR Kinetic analysis of Alkene End-Group Hydrolysis 110

6.2.3) Reduction of the Aldehyde End-Group with Simultaneous Phthalimide Deprotection 110

6.3) Results and Discussion 111

6.3.1) Hydrolysis of the Xanthate End-Group 111

6.3.2) Hydrolysis of the Alkene End-Group 116

6.3.3) Reduction of the Aldehyde End-Group with Simultaneous Phthalimide Deprotection 120

6.4) Conclusions 123

6.5) References 124

7.) Preparation of Poly(*N*-vinylpyrrolidone)-poly(L-lysine) Block Copolymers by *N*-Carboxyanhydride Ring-Opening Polymerization 125

7.1) Introduction 125

7.2) Materials and Experimental Methods 127

7.2.1) Synthesis of N^{ε}-(Benzyloxycarbonyl) L-Lysine 128

7.2.2) Synthesis of N^{ε}-(CBZ) Lys-NCA 129

7.2.3) Polymerization of N^{ε}-(CBZ) Lys-NCA Using 1-Octylamine 129

7.2.4) Polymerization of N^{ε}-(CBZ) Lys-NCA Using Amine-functionalized PVP 130

7.2.5) Preparation of Colloidal Dispersion of PVP-*block*-poly(N^{ε}-(CBZ)-L-lys) in H_2O 131

7.3) Results and Discussion 132

7.3.1) Synthesis of poly(N^{ε}-(CBZ)-L-lysine) 132

7.3.2) Synthesis of PVP-block-poly(N^{ε}-(CBZ)-L-lysine) 133

7.4) Conclusions 137

7.5) References 138

8.) Deprotecting the N^{ε}-Amine of the Lysine Residues on PVP-*block*-poly(N^{ε}-(CBZ)-L-lys) 140

8.1) Introduction 140

8.2) Materials and Experimental Methods 140

8.2.1) Deprotection of the CBZ Group by Acidolysis with HBr in TFAA 141

8.2.2.) Deprotection of the CBZ Group by Acidolysis with HBr in a 1,4-Dioxane and DCM Mixture 141

8.2.3) Deprotection of the CBZ Group by Catalytic Hydrogenation 141

8.3) Results and Discussion 142

8.3.1) Deprotection of PVP-*block*-poly(N^{ε}-(CBZ)-L-lys) by Acidolysis with HBr 142

8.3.2) Deprotection of PVP-*block*-poly(N^{ε}-(CBZ)-L-lys) by Catalytic Hydrogenation 144

8.4) Conclusions 145

8.5) References 146

9.) Conjugation of Doxorubicin to PVP-*block*-poly(L-lysine) 147

9.1) Introduction 147

9.2) Materials and Experimental Methods 148

9.2.1) Synthesis of PVP-*block*-poly(L-lysine)-Doxorubicin Dispersion in H_2O 148

9.2.2) Synthesis of PVP-*block*-poly(L-lysine)-Benzaldehyde Dispersion in H_2O 148

9.2.3) Synthesis of Doxorubicin Dispersion in H_2O 149

9.3) Results and Discussion 149

9.3.1) Synthesis of PVP-*block*-poly(L-lysine)-Doxorubicin as well as free Doxorubicin Dispersions 149

9.3.2) Synthesis of PVP-*block*-poly(L-lysine)-Benzaldehyde Dispersion 151

9.4) Conclusions 153

9.5) References 154

10.) Epilogue 156

10.1) Thesis Synopsis 156

10.2) Implications of the Research 157

10.3) Future Research and Developments 158

Appendices 160

A1) Conversion of SEC Traces to Molecular Weight Distributions 160

A2) Least Squares Approximation of Kinetic Data 162

A2.1) Kinetic Data from Section 3.2.4 162

A2.2) Kinetic Data from Sections 3.2.2 and 3.2.3 162

A2.3) Comparison of P(T) for XA2 with that for

O-ethyl-*S*-(cyanoisopropyl)xanthate 162

A3) Calculating [M] for a Continuous Semi-Batch Process (CSB) 163

A4) Calculation of [M] for a Discrete Semi-Batch Process (DSB) 168

A5) Calculating Observed Rate Constants 169

A6) Calculating the Feed Times for the CDSB 170

A7) Calculating the Reaction Time as well as χ for R-group

and Xanthate-Functionalized Chains for the CDSB 173

A8) Calculating the Reaction Time as well as χ for R-group

and Xanthate-Functionalized Chains for the SDSB 174

A9) Calculating the Reaction Time as well as χ for R-group

and Xanthate-Functionalized Chains for the s-CSB 175

A10) Determining the Amount of Diethyl Ether in a Polymer Sample with a Known $M_{n,NMR}$ 176

A11) Normalizing the NMR Spectrum of the PFBA-Derivatized PVP using the Peak for the Vinyl Protons 178

A12) Normalizing the ^{1}H-NMR Spectrum of PVP-block-poly(N^{ϵ}-(CBZ)-L-lysine) 179

A13) References 181

List of Figures

Figure 2.1: A) Molecular Structure of Doxorubicin. B) Major Degradation Product at pH > 6.5.

Figure 2.2: Fundamental Structure of a RAFT Agent.

Figure 2.3: General Structure of α-Amino Acid *N*-Carboxyanhydrides.

Figure 3.1: ^{1}H-NMR Spectra for the Reaction Mixture of the Trial with R = 196. A) Initial Conditions. B) 50% Monomer Conversion.

Figure 3.2: ^{1}H-NMR Spectrum for the Isolated Polymer from the Trial with R = 196 at 50% Monomer Conversion.

Figure 3.3: Normalized Molar Mass Distributions for RAFT-mediated Polymerizations with A) R = 196, B) R = 117 at Different Monomer Conversions.

Figure 3.4: Plot of [XA2] and [NVP] During *In-situ* ^{1}H-NMR Polymerization with R = 5.

Figure 3.5: $\mathrm{P(T)}$ for the ^{1}H-NMR *In-situ* Polymerization with R = 5.

Figure 3.6: [XA2]/[NVP] as a Function of Time for the ^{1}H-NMR *In-situ* Polymerization.

Figure 3.7: $\mathrm{P(T)}$ for the Polymerizations with Different Initial Monomer to RAFT Agent Ratios (R). A) R = 117 and B) R = 196. C) Comparison of $\mathrm{P(T)}$ for the Polymerizations with R = 5, 117 and 196.

Figure 4.1: Calculated Mole Fractions of A) Phthalimide-Functionalized Chain Ends and B) Dormant Polymer Chains for the RAFT-Mediated Polymerization of NVP with XA2 by the CDSB.

Figure 4.2: Reaction Time Required to Reach a Specific M_n During the CDSB.

Figure 4.3: Calculated Mole Fractions of A) Phthalimide-Functionalized Chain Ends and B) Dormant Polymer Chains for the RAFT-Mediated Polymerization of NVP with XA2 by the SDSB.

Figure 4.4: Reaction Time Required to Reach a Specific M_n During the SDSB.

Figure 4.5: Calculated Mole Fractions of A) Phthalimide-Functionalized Chain Ends and B) Dormant Polymer Chains for the RAFT-Mediated Polymerization of NVP with XA2 by the d-CSB.

Figure 4.6: Reaction Time Required to Reach a Specific M_n During the d-CSB.

Figure 4.7: Calculated Mole Fractions of A) Phthalimide-Functionalized Chain Ends and B) Dormant Polymer Chains for the RAFT-Mediated Polymerization of NVP with XA2 by the s-CSB.

Figure 4.8: Reaction Time Required to Reach a Specific M_n During the s-CSB.

Figure 4.9: Monomer Conversion Profile for CDSB.

Figure 4.10: A) Molar Mass Distributions for the CDSB. B) Comparison of Molar Mass Distributions for the Final Product of the CDSB to those for the Batch-Mode Polymerizations Performed in Section 3.2.2 and 3.2.3.

Figure 4.11: Monomer Conversion Profile for SDSB.

Figure 4.12: 600 MHz ^{1}H-NMR Spectrum of Reaction Mixture in $CDCl_3$ for (-) 3rd Interval of SDSB and (-) 4th Interval of SDSB.

Figure 4.13: A) Molar Mass Distributions for SDSB. B) Comparison of Molar Mass Distributions for the Product of the SDSB. with those for the Polymerizations Performed in Batch-Mode with R = 117 and R = 196 that had a Similar $M_{n,SEC}$.

Figure 5.1: ^{1}H-NMR Spectra for (-) Xanthate-Functionalized PVP Starting Material and (-) Thermolyzed Product.

Figure 5.2: Comparison of the Normalized Molecular Weight Distributions for the Xanthate-Functionalized PVP and the Thermolyzed Product.

Figure 5.3: ^{1}H-NMR Spectra for (-) Thermolyzed Polymer. (-) Deprotected Polymer.

Figure 5.4: A) Normalized Molecular Weight Distribution for the (-) Polymer Isolated from Sample 1 in Section 5.2.3 Superimposed with those for the (-) Thermolyzed Polymer. B) SEC Trace for the Thermolyzed Polymer.

Figure 5.5: Normalized Molecular Weight Distributions of the Deprotected Polymer Samples (-) Isolated from A) Sample 2 and B) Sample 3, prepared in Section 5.2.3. (-) Thermolyzed Polymer.

Figure 5.6: Normalized ^{19}F-NMR Spectrum of TFBA Stock Solution Prepared in Section 5.2.4.

Figure 5.7: Normalized ^{1}H-NMR Spectrum of TFBA Stock Solution Prepared in Section 5.2.4.

Figure 5.8: ^{1}H-NMR Spectrum of TFBA-Derivatized PVP Prepared in Section 5.2.4.

Figure 5.9: ^{1}H-NMR Spectrum of Thermolyzed Polymer used as the Starting Material for the Preparation of Sample 2 in Section 5.2.3.

Figure 5.10: ^{19}F-NMR Spectrum of TFBA-Derivatized PVP Prepared in Section 5.2.4.

Figure 5.11: ^{1}H-NMR Spectrum for the PFBA-derivatized PVP.

Figure 6.1: Initial Conditions for the *in-situ* NMR Experiment Performed on Vial 1 in Section 6.2.1.

Figure 6.2: Concentration Profile for the Xanthate End-Group during Hydrolysis in D_2O at 40 °C and in 1M DCl at 60 °C.

Figure 6.3: Conditions at the end of the *in-situ* NMR Experiment Performed on Vial 1 in Section 6.2.1.

Figure 6.4: ^{1}H-NMR spectrum of the PVP Isolated after Hydrolysis of the Xanthate End-Group in 1 M DCl at 60 °C.

Figure 6.5: Normalized Molecular Weight Distributions for the Hydrolysis of the Xanthate End-Group in D_2O and 1 M DCl.

Figure 6.6: SEC Trace for the Xanthate-Functionalized PVP Hydrolyzed at 40 °C in D_2O.

Figure 6.7: ^{1}H-NMR of Alkene-Functionalized PVP used for the Hydrolysis Experiments Described in Section 6.2.2.

Figure 6.8: Concentration Profiles for the Alkene End-Group during Hydrolysis in D_2O as well as in 1 M DCl.

Figure 6.9: ^{1}H-NMR Spectrum of Alkene-Functionalized PVP after Hydrolysis in 1 M DCl at 65 °C.

Figure 6.10: Normalized Molecular Weight Distributions for the Thermolysis of the Xanthate End-Group and its Hydrolysis in 1 M DCl at 65 °C.

Figure 6.11: ^{1}H-NMR Spectrum of PVP Isolated for Crude Reaction Mixture by Dialysis and Hydrolysis.

Figure 6.12: ^{1}H-NMR Spectrum of PVP after Reduction with $NaBH_4$.

Figure 6.13: ^{1}H-NMR Spectrum of the Reduced PVP after hydrolysis and PFBA-Derivatization.

Figure 6.14: Normalized Molecular Weight Distributions Obtained by SEC for the Xanthate-Functionalized PVP and the Product of Deprotection by Hydrolysis and Reduction.

Figure 7.1: 1H-NMR of poly(N^{ε}-(CBZ)-L-lysine).

Figure 7.2: ^{1}H-NMR Spectrum of PVP-*block*-poly(N^{ε}-(CBZ)-L-lys) with Presaturation of the Water Peak.

Figure 7.3: Normalized Molecular Weight Distributions for the PVP-Amine Macroinitiator and the PVP-*block*-poly(N^{ε}-(CBZ)-L-lys) Product.

Figure 7.4: A) Representative Cryo-TEM Image of PVP-*block*-poly(N^{ε}-(CBZ)-L-lys) Collodial Dispersion. B) Histogram of Measured Micelle Diameters.

Figure 7.5: DLS Analysis of PVP-*block*-poly(N^{ε}-(CBZ)-L-lys) in DMF and in H_2O.

Figure 8.1: ^{1}H-NMR Spectrum of PVP-*block*-poly(L-lysine) Deprotected with HBr in TFAA.

Figure 8.2: ^{1}H-NMR Spectrum of PVP-*block*-poly(L-lysine) Deprotected with HBr in a Mixture of 1,4-Dioxane and DCM.

Figure 8.3: DLS Results for PVP-*block*-poly(L-lysine), Deprotected by Acidolysis in the 1,4-Dioxane and DCM Solvent Mixture, as well as that of the PVP Macroinitiator Used to Prepare it.

Figure 8.4: ^{1}H-NMR Spectrum for PVP-*block*-poly(L-lysine) Deprotected by Catalytic Hydrogenation and that of its Starting Material.

Figure 9.1: Hydrodynamic Diameter Distributions for the PVP-*block*-poly(L-lysine)-Doxorubicin Dispersion.

Figure 9.2: Hydrodynamic Diameter Distribution for the Free Doxorubicin Dispersion.

Figure 9.3: A) Cryo-TEM Image of PVP-*block*-poly(L-lysine)-Doxorubicin Dispersion. B) Histogram of Measured Particle Diameters.

Figure 9.4: Hydrodynamic Diameter Distributions for the PVP-*block*-poly(L-lysine)-benzaldehyde Dispersion as well as that for PVP-*block*-poly(L-lysine).

Figure 9.5: A) Cryo-TEM Image of PVP-*block*-poly(L-lysine)-benzaldehyde Dispersion. B) Histogram of Measured Particle Diameters.

Figure A5.1: Plots of $ln\left(\frac{[M]}{[M]_0}\right)$ versus $\sqrt{\frac{I_0}{k_d V}}\left(e^{\left(-\frac{k_d(t-t_0)}{2}\right)}-1\right)$ for the Polymerizations Performed in Sections A) 3.2.4, B) 4.5.1, C) 3.2.3 and D) 3.2.2.

List of Tables

Table 3.1: Results for RAFT-mediated Polymerizations of NVP with XA2 as described in Section 3.2.2 and 3.2.3. (a) – Measured using the isolated polymer samples.

Table 4.1: Monomer and AIBN Feed Profile for CDSB.

Table 4.2: Monomer and AIBN Feed Times for SDSB.

Table 4.3: Observed Rate Constant (φ) during RAFT-mediated Polymerization of NVP with XA2 at Different Initial Monomer to RAFT agent Ratios. (a) Obtained by Linear Least Squares approximation of All the Data.

Table 4.4: Results for CDSB Polymerization. (a) – Measured for the isolated polymer sample.

Table 4.5: Results for SDSB Polymerization. (a) – Measured using a 600 MHz Spectrometer.

Table 5.1: Hydrazine Stock Solution Dilution with Methanol for the 3 Trials.

Table A5.1: Parameters for the Calculation of φ for the Polymerization of NVP with XA2 at Various Monomer to RAFT Agent Ratios.

Table A10.1: Results of Iterative Procedure for Normalizing the ^{1}H-NMR Spectrum obtained for the sample prepared in Section 5.2.4 with respect to number of PVP chains for the sample prepared in Section 5.2.1.

Table A11.1: Results for the Iterative Procedure, Described in Appendix A11.

Table A12.1: Results of Iterative Procedure for Normalizing the ^{1}H-NMR Spectrum for PVP-block-poly(N^{ε}-(CBZ)-L-lysine).

List of Schemes

Scheme 2.1: General Mechanism for a RAFT Polymerization.

Scheme 2.2: Mechanisms of Initiating NCA Polymerization.

Scheme 2.3: NCA Polymerization Using Zerovalent Transition Metal Initiators.

Scheme 2.4: Preparation of Functionalized Transition Metal Initiators.

Scheme 2.5: Initiation Using TMS-amine Initiators.

Scheme 3.1: Thermolysis of a RAFT agent from a Polymer Chain.

Scheme 5.1: Imine Formation of TFBA with Primary Amines.

Scheme 6.1: Addition of HBr to Alkene End-Groups of PVP and Subsequent Hydrolysis of the Bromide.

Scheme 6.2: Formation of Aldehyde End-Groups via Elimination of Pyrrolidone.

Scheme 6.3: Two-Step Removal of Phthalimide Protecting Group with Simultaneous Reduction of Aldehyde End-Groups.

Scheme 6.4: Mechanism of Xanthate Hydrolysis by Nucleophilic Attack.

Scheme 6.5: Mechanism of Xanthate Hydrolysis by Elimination of Xanthic Acid.

Scheme 6.6: Mechanism of Xanthate Hydrolysis by Substitution of Xanthic Acid with Water.

Scheme 7.1: Preparation of N^{ε}-(Benzyloxycarbonyl)-L-Lysine.

Scheme 7.2: Synthesis of N^{ε}-(CBZ)-Lys-NCA by the Fuchs-Farthing Method.

Scheme 7.3: Synthesis of N^{ε}-(CBZ)-Lys-NCA by the Modified Leuch's Method.

Scheme 9.1: General Mechanism of Schiff Base Formation.

Scheme 9.2: Oligomerization of Doxorubicin on Lysine Residues of PVP-*block*-poly(L-lysine).

Scheme 10.1: Preparation of PVP-*block*-poly(L-lysine) with an Acyl Hydrazone Bond Between the two Blocks.

List of Abbreviations

ACS – American chemical society

ADME – Absorption, distribution, metabolism and elimination

AIBN – Azobisisobutyronitrile

(aq) – Aqueous phase

ATP – Adenosine triphosphate

ATRP – Atom transfer radical polymerization

:B – Any base

BHT – Butylated hydroxytoluene

Br - Broad

BzCl – Benzyl chloride

CBZ – Benzyloxycarbonyl

$CDCl_3$ – Deuterated chloroform

CDSB – Convergent discrete semi-batch process

CH – Catalytic hydrogenation

$CHCl_3$ – Chloroform

CMC – Critical Micelle Concentration

CPP – Cell-penetrating peptide

Cryo – Cryogenic

cryo-TEM – Transmission electron microscopy in vitreous ice

CSIRO – Commonwealth Scientific and Industrial Research Organization

$CuCO_3$ – Copper carbonate

$Cu(OH)_2$ – Copper(II) hydroxide

DCl – Deuterium chloride

DCM – Dichloromethane

d-CSB – Dead-end continuous semi-batch process

DDS – Drug Delivery System

DLS – Dynamic light scattering

DMAC – *N,N*-dimethylacetamide

DMF – *N,N*-dimethylformamide

DMSO-d6 – Deuterated dimethyl sulfoxide

DNA – Deoxyribonucleic acid

D_2O – Deuterated water

DOSY – Diffusion-ordered spectroscopy

DRI – Differential refractive index

E1 – Intramolecular elimination

E2 – Intermolecular elimination

EDTA – Ethylenediaminetetraacetic acid

EGFR – Epidermal growth factor receptor

EPR – Enhanced permeability and retention

ESI – Electrospray ionization

EtOAc – Ethyl acetate

FcRn – Neonatal Fc receptor

FFF – Field-flow fractionation

GC – Gas chromatography

GFLG – Glycine-phenylalanine-leucine-glycine oligopeptide

HBr – Hydrobromic acid

HBr Method 1 – Deprotection of PVP-*block*-poly(N^{ε}-(CBZ)-L-lys) by acidolysis with HBr in TFAA

HBr Method 2 – Deprotection of PVP-*block*-poly(N^{ε}-(CBZ)-L-lys) by acidolysis with HBr in a DCM and 1,4-dioxane solvent mixture

HCl – Hydrochloric acid

H_2 – Molecular hydrogen

H_2O – Water

HPLC – High performance liquid chromatography

HPMA – 2-(hydroxypropyl)methacrylamide

I – Initiator

IgM – Immunoglobulin M

IUPAC – International union of pure and applied chemistry

LHS – Left-hand side

Lys-NCA – Lysine *N*-carboxyanhydride

m – Multiplet

M – Monomer

MALDI-TOF – Matrix-assisted laser desorption ionization with time-of-flight detection

MS – Mass spectrometry

MW – Molecular weight

***N*$^{\alpha}$** – Alpha amino nitrogen of amino acid

***N*$^{\varepsilon}$** – Epsilon amino nitrogen of L-lysine

***N*$^{\varepsilon}$-(CBZ)-Lys-NCA** – N^{ε}-(benzyloxycarbonyl)-L-Lysine *N*-carboxyanhydride

$NaBH_4$ – Sodium borohydride

NaCl – Sodium chloride

Na_2CO_3 – Sodium carbonate

$NaHCO_3$ – Sodium bicarbonate

NCA – *N*-Carboxyanhydride

NMP – Nitroxide-mediated polymerization

NMR – Nuclear magnetic resonance

NRP – Normal radical polymerization

NVP – *N*-vinylpyrrolidone

[O] – Oxidation

PCl_5 – Phosphorus pentachloride

Pd/C – Palladium on carbon

PEG – Polyethylene glycol

PFBA – pentafluorobenzaldehyde

PG – Protecting group

PMMA – Poly(methyl methacrylate)

poly(N^{ε}-(CBZ)-L-lys) – Poly(N^{ε}-(benzyloxycarbonyl)-L-lysine)

PSS – Polymer standards service

PVP – Poly(*N*-vinylpyrrolidone)

q – Quartet

RAFT – Reversible Addition-Fragmentation Chain Transfer

RES – Reticuloendothelial system

RGD – Arginine-glycine-aspartic acid oligopeptide

R-group – Leaving group of RAFT agent

RNA – Ribonucleic acid

ROP – Ring-opening polymerization

s – Singlet (NMR data)

s-CSB – Steady continuous semi-batch process

SDSB – Steady discrete semi-batch process

SEC – Size-exclusion chromatography

t – Triplet

Tat – Trans-activating transcriptional activator

TEM – Transmission electron microscopy

TFAA – Trifluoroacetic acid

TFBA – 3,5-bis(trifluoromethyl)benzaldehyde

TFT – α, α, α-Trifluorotoluene

THF – Tetrahydrofuran

TMS – Trimethylsilyl

TMS-amine – *N*-(Trimethylsilyl)amine

UK – United Kingdom

UNCA – Urethane-protected *N*-carboxyanhydride

UV – Ultraviolet light

VEGFR – Vascular endothelial growth factor receptor

VT – Variable temperature

$\boldsymbol{X}$ – Any RAFT agent

XA2 - *O*-ethyl-*S*-(phthalimidylmethyl)xanthate

X1 – *O*-ethyl-*S*-(cyanoisopropyl)xanthate

Z-group – Stabilizing group of RAFT agent

List of Symbols

a – Second Mark-Houwink parameter

a_c – First linear calibration constant for DMAC SEC

b – Dilution factor for monomer additions during discrete semi-batch processes

b_c – Second linear calibration constant for DMAC SEC

Å – Angstrom

cm – Centimeter

C – Constant concentration of monomer in the reaction mixture

$C_m(t)$ – Concentration of monomer in the feed at time t

C_{int} – Integration constant

cP – Centipoise

C_{tr} – Apparent transfer constant

dm – decimeter

$Đ$ – Dispersity

$Đ_{SEC}$ – Dispersity measured by SEC

δ – Chemical Shift

°C – Degrees celcius

DP – Degree of polymerization

e – Natural exponent

ε – Error (in numerical computations)

$F(\delta)$ – Normalized and baseline-corrected NMR spectrum as a function of chemical shift

f – Efficiency factor of the initiator

g – Gram

$\boldsymbol{I_0}$ – Initial number of moles of initiator in the reaction mixture

$\boldsymbol{I^{\bullet}}$ – Initiator-derived radicals

$\boldsymbol{K}$ – First Mark-Houwink parameter

$\boldsymbol{k_d}$ – Rate constant for initiator decomposition

kDa – Kilodalton

$\boldsymbol{k_p}$ – Propagation rate constant

$\boldsymbol{k_p^i}$ – Rate constant for propagation of chains with length i

$\boldsymbol{k_t}$ – Termination rate constant

$\boldsymbol{k_t^*}$ – IUPAC average termination rate constant

L – Litre

$\boldsymbol{ln}$ – Natural logarithm

$\boldsymbol{log}$ – Logarithm with a base of 10

M – Molar concentration

$\boldsymbol{M_{add}}$ – No. of moles of monomer added at the end of each interval

$\boldsymbol{M_0}$ – Initial number of moles of monomer in the reaction mixture

$\boldsymbol{M_f}$ – Total amount of monomer fed into reactor from t_0 until t

$\boldsymbol{M_r}$ – Monomer which has been converted to polymer

Mbar – Millibar

mg - Milligram

MHz – Megahertz

mL – Milliliter

mm – Millimeter

MWCO – Nominal molecular weight cut-off

µm – Micrometer

M_n – Number-average molecular weight

$M_{n,NMR}$ – Number-average molecular weight measured by NMR

$M_{n,SEC}$ – Number-average molecular weight measured by SEC

$M_{n,theory}$ – Theoretical number-average molecular weight

M_w – Weight-average molecular weight

MW_i – Molecular weight corresponding to ith elution volume in the SEC data

mol – Moles

N_I – Number of initiator-derived polymer chains

n_i – Baseline-corrected DRI signal at ith data point

N_i – Number of polymer chains with corresponding MW_i

nm – Nanometer

$Norm_i$ – Normalized and baseline-corrected DRI signal

$[\eta]$ – Intrinsic viscosity

$\mathbb{N}$ – Field of natural numbers

$P^\bullet$ – Propagating radicals

pH – Negative logarithm, with a base of 10, of the hydronium ion concentration

pKa – Negative logarithm, with a base of 10, of the acid dissociation constant

ppm – Parts per million

PT – Number of polymer chains that formed via termination by combination

$\mathbf{P(T)}$ – The probability that a propagating radical would transfer its radical to the phthalimidylmethyl leaving group of XA2 instead of continuing to propagate at a specific moment

PX – Poly-RAFT agent

R – Ratio of monomer to RAFT agent

R$^{\bullet}$ – RAFT agent leaving group radical

$\boldsymbol{R_i}$ – Rate of initiation

$\boldsymbol{R_t}$ – Rate of termination of propagating radicals

rpm – Revolutions per minute

s – Seconds

$\boldsymbol{t}$ – Time

T1 – Longitudinal relaxation time (Spin-lattice relaxation time)

$\boldsymbol{V}$ – Volume of the reaction mixture

$\boldsymbol{v}$ – Total volume added to the reaction mixture from t_0 to t

∀ – For all

$\boldsymbol{W_i}$ – Weight of the ith data point used for the analysis of the SEC data

w/v – Weight to volume

w/w – Weight to weight

$\boldsymbol{x_i}$ – The amount of monomer added at the beginning of interval i during the SDSB

$\boldsymbol{\chi_{\alpha_R}}$ – Mole fraction of R-group-initiated polymer chains

$\boldsymbol{\chi_{CHO}}$ – Initial fraction of aldehyde end-groups relative to xanthate-functionalized PVP before any aldol addition or condensation had occurred

$\boldsymbol{\chi_{\omega_X}}$ – Mole fraction of dormant polymer chains

% – Percent

$\boldsymbol{\varphi}$ – Observed rate constant

CHAPTER 1

Prologue

1.1) Introduction

One of the cornerstones of civilization is the development of medicine to improve the average duration and quality of life. This is an endlessly changing and improving field of science as new diseases are emerging all the time.[1] Also, there are still many known ailments that are either very difficult to cure or even untreatable with our current understanding. Cancer is one such disease that has notoriously plagued mankind physically and intellectually. It has been considered in the past as an incurable affliction[2] due to the fact that it is, simply put, the patient's own body turning against them. Formally, cancer is an unregulated growth of a group of genetically mutated cells within the patient. These cells usually cannot be recognized by the patient's immune system and continue to grow until they overwhelm the body, causing death. This makes it very difficult to selectively treat the cancerous cells without affecting the patient. Another reason cancer is so difficult to treat is that symptoms often only emerge once the cancer has been well established.

Unfortunately, cancer is not a rare affliction and was responsible for up to 14.6% of recent annual worldwide deaths.[3-6] In developed countries, such as America, it is the second highest cause of death. Hence, there is a great demand for improvement in cancer treatment.

1.2) Objectives

The main objective of this research was to prepare a novel drug delivery system (DDS) that incorporates conventional chemotherapeutic compounds as well as a cell-penetrating peptide[7-11] (CPP) and transports them through the body, accumulating selectively within tumor tissues.[12-14] Doxorubicin was the model drug used in this study. A nano-sized block copolymer micelle with a size range of 10 – 150 nm is the basic architecture for the DDS. The hydrophobic core will be composed of poly(L-lysine) as this polypeptide has shown cell-penetrating properties[7,8] and can bond to molecules containing aldehyde or ketone functional groups via reversible imine bonds. Doxorubicin is one such compound and will be used as the chemotherapeutic compound in this case. Imines were chosen as they are usually unstable under aqueous or acidic conditions,[15] releasing the drugs and the cell penetrating peptide simultaneously, although they should be stable within the hydrophobic micelle core. The hydrophilic corona of the DDS was chosen to be composed of poly(*N*-

vinylpyrrolidone) (PVP) as this polymer offers excellent biocompatibility[16-18] and has been researched extensively by our group.[19-22] The PVP block will be prepared by a reversible addition-fragmentation chain transfer (RAFT) mediated radical polymerization.[23] The RAFT agent used was chosen to allow for a primary amine to be incorporated into one of the polymer chain ends. In order to prepare the desired block copolymer, the amine-functionalized PVP will be used as a macroinitiator for the ring-opening polymerization of N^{ε}-(benzyloxycarbonyl)-L-lysine *N*-carbonxyanhydride.[24-28] Subsequent deprotection of the lysine residues and incorporation of Doxorubicin should provide the desired DDS.

The main aims of this research are:

1) Determine if sufficiently stable micelles can be prepared by this route. The micelles need to have a very low critical micelle concentration (CMC) as they will be greatly diluted during blood circulation.[29-31] They should also be stable under the physiological conditions of blood plasma for at least 24 hours. This translates to a necessity for a very slow hydrolysis rate of the imine linkages within the micelle core. If the polymer-drug conjugates are not sufficiently stable on their own then the addition of a cross-linker, modifier or a ternary stabilizing block will be investigated.
2) Fine-tune the micelles to decompose readily under the physiological conditions of endosomes and lysosomes (pH ≈ 4 - 6).[32,33] Tumor tissues also tend to be slightly acidic (pH ≈ 6.5)[34-36] and it would prove beneficial if the micelles could be optimized to be sufficiently stable in blood plasma but begin to decompose in tumor tissues. The drug could then be transported into the surrounding cells by the cell-penetrating peptide, provided a small fraction is still conjugated to it via the reversible imine bonds.
3) Determine if the stability of Doxorubicin in neutral and slightly alkaline solutions is augmented when it is incorporated in the DDS. Doxorubicin is known to decompose increasingly rapidly in aqueous solutions with an increase in pH above 6.5.[37] By incorporating the drug in a hydrophobic core of a micelle, this instability may be circumvented.
4) Determine if there is a synergism occurring for the uptake of Doxorubicin and poly(L-lysine). Polycationic peptides are known to traverse through cell membranes by non-classical mechanisms.[9,10,38] Poly(L-lysine) is one such peptide and since the imine linkages are reversible, some doxorubicin may still be conjugated to the peptide as it penetrates a tumor cell. This may improve the uptake of the drug within tumor tissues as well as the drug efficacy against multi-drug resistant cancer cells.

1.3) Layout of Thesis

1.3.1) Chapter 1: Prologue

This chapter provides a description of the research proposal as well as the goals that the research is aiming to achieve. It also contains a breakdown of the thesis structure.

1.3.2) Chapter 2: Literature Review

This chapter contains the research topics that were reviewed and seen as beneficial or indicative towards the research focused on in this thesis. Each topic is discussed in a separate section although some sections inevitably deal with more than one of these topics. These are discussed in both sections with the emphasis being focused on the topic of the current section. The literature review avoids excessively covering the theory of the various analytical techniques applied as well as any fundamental mathematical or chemical background beyond what is unavoidable as the many existing textbooks already cover these topics sufficiently. The topics covered in this review are on cancer, drug delivery, polymerization as well as controlled and living polymerization.

1.3.3) Chapter 3: RAFT-Mediated Polymerization of *N*-vinylpyrrolidone with *O*-ethyl-*S*-(phthalimidylmethyl)xanthate Performed in Batch-Mode

This chapter covers the RAFT-mediated polymerization of NVP, why a protecting group is necessary to prepare an amine end-functional polymer by RAFT-mediated polymerization and describes some of the shortcomings of the RAFT agent used to incorporate this functional group. The most notable limitation of this RAFT agent was the slow pre-equilibrium kinetics that resulted in hybrid behavior occurring during the polymerization.

1.3.4) Chapter 4: Designing a Semi-Batch RAFT-Mediated Polymerization of *N*-vinylpyrrolidone with *O*-ethyl-*S*-(phthalimidylmethyl)xanthate

This chapter focusses on the slow pre-equilibrium kinetics of the RAFT agent used in this research and describes a method for overcoming this limitation as well as optimizing the control of the molecular weight and end-group functionality during the polymerization.

1.3.5) Chapter 5: Deprotection of the Primary Amine α-End-Group on PVP

This chapter focuses on the removal of the phthalimide protecting group from the PVP chain end by reacting it with hydrazine in methanol. It also discusses the incompatibility of the xanthate end-group with strong nucleophiles and why this end-group needs to be removed or transformed before the deprotection can be carried out. It also covers a problem encountered when the simplest transformation is used that involves converting the xanthate to an alkene by thermolysis.

1.3.6) Chapter 6: Hydrolysis of the Xanthate and Alkene End-Groups on PVP

This chapter describes a kinetic analysis of the xanthate and alkene hydrolysis rates in D_2O and 1 M DCl. It also investigates a novel method for removing the phthalimide end-group while simultaneously hydrolyzing and then reducing the xanthate end-group to an aldehyde and primary alcohol, respectively.

1.3.7) Chapter 7: Preparation of Poly(*N*-vinylpyrrolidone)-*block*-poly(L-lysine) Copolymers by *N*-Carboxyanhydride Ring-Opening Polymerization

The preparation and ring-opening polymerization of N^{ϵ}-(benzyloxycarbonyl)-L-lysine *N*-Carboxyanhydride, using amine end-functional PVP as a macroinitiator is discussed in this chapter. The product was analyzed by cryo-TEM and DLS among the usual procedures to gauge the morphology that the block copolymer-conjugate would self-assemble into when dispersed in water.

1.3.8) Chapter 8: Deprotecting the N^{ϵ}-Amine of the Lysine Residues on PVP-*block*-poly(N^{ϵ}-(CBZ)-L-lys)

This chapter covers the deprotection protocols investigated for the removal of the benzyloxycarbonyl (CBZ) protecting group. It also describes some of the pitfalls involved with the various techniques investigated.

1.3.9) Chapter 9: Conjugation of Doxorubicin to PVP-*block*-poly(L-lysine)

This chapter is a preliminary study of the preparation of PVP-*block*-poly(L-lysine)-Doxorubicin conjugates as well as their self-assembly and stability in water. It also investigates benzaldehyde as a possible modifier and proposes terephthalaldehyde as a possible cross-linker.

1.3.10) Chapter 10: Epilogue

A synopsis of the research is given, followed by some implications drawn from the research. This chapter concludes with the perceived future research that should be performed on this topic.

1.3.11) Appendices

This section contains all the derivations and calculations used during the research.

1.4) References

1. Link, K. *Understanding New, Resurgent, and Resistant Diseases: How Man and Globalization Create and Spread Illness;* Praeger Publishers: USA, 2007.

2. Olson, J. S. *The History of Cancer: An Annotated Bibliography;* Greenwood Press: USA, 1989.

3. Ferlay, J.; Shin, H. R.; Bray, F.; Forman, D.; Mathers, C.; Parkin, D. M. Estimates of worldwide burden of cancer in 2008: GLOBOCAN 2008. *Int. J. Cancer* **2010***, 127*, 2893-2917.

4. National Cancer Institute Cancer. *http://www.cancer.gov/*2012).

5. Stewart, B. W.; Wild, C. *World Cancer Report 2014;* World Health Organization: 2014.

6. World Health Organisation Cancer - Health Topics. *http://www.who.int/topics/cancer/en/*2012).

7. Han, K.; Jeon, M. J.; Kim, S. H.; Ki, D.; Bahn, J. H.; Lee, K. S.; Park, J.; Choi, S. Y. Efficient intracellular delivery of an exogenous protein GFP with genetically fused basic oligopeptides. *Mol. Cells* **2001***, 12*, 267-271.

8. Ryser, H. J.; Hancock, R. Histones and Basic Polyamino Acids Stimulate the Uptake of Albumin by Tumor Cells in Culture. *Science* **1965***, 150*, 501-503.

9. Bechara, C.; Sagan, S. Cell-penetrating peptides: 20 years later, where do we stand? *FEBS Lett.* **2013***, 587*, 1693-1702.

10. Copolovici, D. M.; Langel, K.; Eriste, E.; Langel, Ã. Cell-Penetrating Peptides: Design, Synthesis, and Applications. *ACS Nano* **2014***, 8*, 1972-1994.

11. Frankel, A. D.; Pabo, C. O. Cellular uptake of the tat protein from human immunodeficiency virus. *Cell* **1988**, *55*, 1189-1193.

12. De Villiers, M. M.; Aramwit, P.; Kwon, G. S. *Nanotechnology in Drug Delivery;* Springer: New York, 2009.

13. Greish, K. Enhanced permeability and retention (EPR) effect for anticancer nanomedicine drug targeting. *Methods Mol. Biol.* **2010**, *624*, 25-37.

14. Khandare, J.; Minko, T. Polymer-drug conjugates: Progress in polymeric prodrugs. *Prog. Polym. Sci.* **2006**, *31*, 359-397.

15. Clayden, J.; Greeves, N.; Warren, S. *Organic Chemistry;* Oxford University Press: New York, 2012.

16. Wessel, W.; Schoog, M.; Winkler, E. Polyvinylpyrrolidone (PVP), its diagnostic, therapeutic and technical application and consequences thereof. *Arzneimittel-Forschung* **1971**, *21*, 1468-1482.

17. Pramanick, S.; Singodia, D.; Vikas, C. Excipient Selection in Parenteral Formulation Development. *Pharma Times* **2013**, *45*, 65-77.

18. Kaneda, Y.; Tsutsumi, Y.; Yoshioka, Y.; Kamada, H.; Yamamoto, Y.; Kodaira, H.; Tsunoda, S.; Okamoto, T.; Mukai, Y.; Shibata, H.; Nakagawa, S.; Mayumi, T. The use of PVP as a polymeric carrier to improve the plasma half-life of drugs. *Biomaterials* **2004**, *25*, 3259-3266.

19. Bailly, N.; Thomas, M.; Klumperman, B. Poly(N-vinylpyrrolidone)-block-poly(vinyl acetate) as a drug delivery vehicle for hydrophobic drugs. *Biomacromolecules* **2012**, *13*, 4109-4117.

20. Jacobs, J.; Pound-Lana, G.; Klumperman, B. Poly(N-vinylpyrrolidone-b-(gamma]-benzyl-l-glutamate)) - synthesis and self-assembly into pH-sensitive micelles. *Polym. Chem.* **2012**, *3*, 2551-2560.

21. Pfukwa, R.; Pound, G.; Klumperman, B. In *In Facile end group modification of RAFT made polymers, by radical exchange with hydrogen peroxide;* 236th National Meeting of the American-Chemical-Society, 5th Controlled/living Radical Polymerization Symposium; 2008.

22. Pound, G.; McKenzie, J. M.; Lange, R. F. M.; Klumperman, B. Polymer-protein conjugates from small omega]-aldehyde endfunctional poly(N-vinylpyrrolidone) synthesised via xanthate-mediated living radical polymerisation. *Chem. Commun.* **2008**, 3193-3195.

23. Postma, A.; Davis, T. P.; Li, G.; Moad, G.; O'Shea, M. S. RAFT Polymerization with Phthalimidylmethyl Trithiocarbonates or Xanthates. On the Origin of Bimodal Molecular Weight Distributions in Living Radical Polymerization. *Macromolecules* **2006**, *39*, 5307-5318.

24. Cheng, J.; Deming, T. J. In *Synthesis of Polypeptides by Ring-Opening Polymerization of α-Amino Acid N-Carboxyanhydrides;* Deming, T., Ed.; Peptide-Based Materials; Springer Berlin Heidelberg: 2012; Vol. 310, pp 1-26.

25. Deming, T. J. Facile synthesis of block copolypeptides of defined architecture. *Nature* **1997**, *390*, 386-389.

26. Habraken, G. J. M.; Wilsens, K. H. R. M.; Koning, C. E.; Heise, A. Optimization of N-carboxyanhydride (NCA) polymerization by variation of reaction temperature and pressure. *Polym. Chem.* **2011***, 2*, 1322-1330.

27. Hernández, J. R.; Klok, H. Synthesis and ring-opening (co)polymerization of L-lysine N-carboxyanhydrides containing labile side-chain protective groups. *J. Polym. Sci. A Polym. Chem.* **2003***, 41*, 1167-1187.

28. Kricheldorf, H. R. Polypeptides and 100 Years of Chemistry of α-Amino Acid N-Carboxyanhydrides. *Angew. Chem. Int. Ed.* **2006***, 45*, 5752-5784.

29. Xu, P.; Tang, H.; Li, S.; Ren, J.; Van Kirk, E.; Murdoch, W. J.; Radosz, M.; Shen, Y. Enhanced stability of core-surface cross-linked micelles fabricated from amphiphilic brush copolymers. *Biomacromolecules* **2004***, 5*, 1736-1744.

30. Wu, Y.; Chen, W.; Meng, F.; Wang, Z.; Cheng, R.; Deng, C.; Liu, H.; Zhong, Z. Core-crosslinked pH-sensitive degradable micelles: A promising approach to resolve the extracellular stability versus intracellular drug release dilemma. *J. Control. Release* **2012***, 164*, 338-345.

31. Shuai, X.; Merdan, T.; Schaper, A. K.; Xi, F.; Kissel, T. Core-cross-linked polymeric micelles as paclitaxel carriers. *Bioconjug. Chem.* **2004***, 15*, 441-448.

32. Geisow, M. J.; Evans, W. H. pH in the endosome. Measurements during pinocytosis and receptor-mediated endocytosis. *Exp. Cell Res.* **1984***, 150*, 36-46.

33. Sorkin, A.; von Zastrow, M. Signal transduction and endocytosis: close encounters of many kinds. *Nat. Rev. Mol. Cell Biol.* **2002***, 3*, 600-614.

34. Milane, L.; Ganesh, S.; Shah, S.; Duan, Z.; Amiji, M. Multi-modal strategies for overcoming tumor drug resistance: Hypoxia, the Warburg effect, stem cells, and multifunctional nanotechnology. *J. Control. Release* **2011***, 155*, 237-247.

35. Persidis, A. Cancer multidrug resistance. *Nat. Biotech.* **1999***, 17*, 94-95.

36. Kratz, F.; Senter, P.; Steinhagen, H. *Drug Delivery in Oncology: From Basic Research to Cancer Therapy;* Wiley-VCH Verlag & Co. KGaA: Weinheim, Germany, 2012.

37. Beijnen, J. H.; van der Houwen, O. A. G. J.; Underberg, W. J. M. Aspects of the degradation kinetics of doxorubicin in aqueous solution. *Int. J. Pharm.* **1986***, 32*, 123-131.

38. Nakase, I.; Konishi, Y.; Ueda, M.; Saji, H.; Futaki, S. Accumulation of arginine-rich cell-penetrating peptides in tumors and the potential for anticancer drug delivery in vivo. *J. Control. Release* **2012***, 159*, 181-188.

CHAPTER 2

Literature Review

2.1) Cancer and Chemotherapy

2.1.1) Overview of Cancer

Cancer is the group of diseases that arise from unregulated cell growth. More specifically, when a cell becomes cancerous it begins to divide and grow uncontrollably. This forms new cancer cells, which eventually make up a cancerous tissue known as a tumor or malignant neoplasm. It is a disease that, if not treated rapidly, often has fatal consequences. To make matters worse, it can only be detected when a tumor mass reaches approximately 1 cm^3 in volume. Cancer also often only produces notable symptoms late in its progression. This affliction is notoriously common (14% of worldwide deaths),[1,2] has no age, ethnic, gender or racial bounds and can be as diverse as the individuals afflicted with it.

The most crucial feature of a tumor is that it is malignant. This means that tumor cells can become detached from the tumor and enter the circulatory system where they can traverse throughout the body until they become lodged in another region, forming a new tumor. Benign tumors are not malignant hence are not considered cancerous but can still have negative effects to the body's health[3] and can become cancerous through tumor progression.[4]

Many types of cancer exist - basically, any type of cell can become cancerous. The most common types of cancer encountered are different for men (lung and prostate cancer) and women (breast and cervical cancer.) The most common cancer-related fatalities are from lung, stomach, liver, colon and breast cancer.[1]

The causes of cancer are only partially understood and consist of complex as well as diverse mechanisms. The direct biochemical cause is a mutation of the proto-oncogenes of a cell that are responsible for stimulating cell division as well as the tumor suppressor genes. These genes regulate cell growth and division.[5] There are five leading behavioral and dietary risks for developing cancer. These are high body mass index, low fruit and vegetable intake, lack of physical activity as well as tobacco and alcohol use. Of these, smoking has the highest risk factor.[5,6] Exposure to carcinogens (compounds which have been linked to inducing cancer formation) as well as a genetic predisposition can also increase an individual's risk of forming cancer.

There are various methods of cancer treatment. They can be grouped into three main classes:

- Physical resection of the afflicted tissue by surgery, transplantation, hyperthermia and cryotherapy.
- Physically-stimulated necrosis of the afflicted tissue by radiation, ultrasound and laser therapy.
- Chemically-stimulated necrosis of the cancerous cells by chemotherapy.

The basis of this research is focused on chemotherapy and hence it will be the only treatment discussed in detail. More information on the other modes of treatment is available from Ko *et al*.[5] as well as the World Health Organisation[6] and National Cancer Institute[7] websites.

2.1.2) Concepts of Chemotherapy

The main purpose of chemotherapy is to prevent cancerous cells from multiplying, invading, metastasizing and killing the patient. Since cancerous cells tend to multiply rapidly and uncontrollably, treating the patient with various cytotoxic or cytostatic agents usually results in a therapeutic effect. There are seven main classes of chemotherapeutic agents available these days.[8,9]

These are:

1. Alkylating agents
2. Antimetabolites
3. Anthracyclines
4. Plant alkaloids
5. Molecularly targeted agents, hormones and hormone antagonists
6. Biologic response modifiers
7. Miscellaneous agents

Alkylating agents such as the nitrogen mustards, nitrosoureas and alkyl sulfonates react by adding an alkyl group to DNA residues. This inhibits DNA transcription and replication.[8,9] Platinum-based chemotherapeutic drugs also damage DNA by forming stable coordination compounds with the residues.[8,9] Antimetabolites like folic acid, pyrimidine and purine analogues mimic natural metabolites involved in DNA synthesis and either inhibit critical enzymes involved in nucleic acid synthesis or become incorporated into the nucleic acid sequence, which disrupts the genetic code and alters the gene's function.[8,9] Anthracyclines cause topoisomerase II-dependent DNA cleavage

and intercalate with the DNA double helix. This also results in an inhibition of DNA transcription and replication.[8,9] Many different plant alkaloids act as topoisomerase inhibitors though some also act as microtubule inhibitors or modulators.[8,9] Targeting antitumor agents include enzymes, steroids and hormones, tyrosine kinase inhibitors and monoclonal antibodies. These affect certain metabolic pathways by interacting with specific cell receptors. The most common result is regulated or ceased cell proliferation.[8,9] There are also other chemotherapeutic compounds with unclear modes of action that are grouped as miscellaneous compounds.

Since rapid cell division is also an inherent process for many types of normal cells, chemotherapy is plagued by serious side-effects. They can range from relatively minor problems such as nausea, loss of hair and appetite, gastrointestinal distress, skin reactions and fatigue to more dangerous and even fatal adverse effects including depression of the immune system, vital organ failure and formation of secondary neoplasms.[8,9] The side-effects usually arise from the toxicity of chemotherapy towards many vital cells, especially fast growing ones. This results in a characteristically narrow therapeutic window for chemotherapy that limits the achievable therapeutic effect and causes devastating collateral damage.[8,9]

As the understanding of our body's physiology on a molecular level expands, new methods of fighting cancer with chemotherapy have begun to emerge. These methods focus on stimulating or administering certain biological response modifiers, such as monoclonal antibodies and interferons[8] for immunotherapy, or changing the physiology of the tumor so that it is no longer self-sustainable, as is the case with antiangiogenic therapy. Gene therapy is being investigated as a method of reversing the mutation in the oncogenes or tumor suppressor genes.[8,9]

However, even with this vast arsenal of chemotherapeutic agents, we still appear to be losing the war on cancer. Since the beginning of clinical chemotherapy, the average five-year survival rate for cancer patients has only increased by 5.7% in America.[9] On the other hand, there has been an improvement in the number of successful treatments thanks to better diagnostic procedures resulting in more regular early detection and better tumor profiling.[9] To understand this dilemma, both the virtues and pitfalls of chemotherapy need to be taken into account.

To account for the benefits of chemotherapy, it is considered the first and last line of defense against malignant neoplasms. This is a result of the drugs being able to enter areas of the body that are unsafe for surgery as well as chemotherapy being able to treat metastatic cancer cells that are too small to be detected, even by state of the art diagnostic procedures. Chemotherapy is often administered as neoadjuvant therapy prior to surgery in order to shrink the tumor to a safe size for

resection.[10-14] This is especially important when the tumor is located in a vital organ such as the liver, kidneys or brain. It is also applied post-surgery to capture any remaining cancer cells that may have metastasized or have been dislodged during the operation.[15,16]

Looking at the problems associated with chemotherapy, the most notable flaw is the less than adequate selectivity of the cytotoxic effects for aberrant cells. This results in a myriad of serious and potentially fatal side-effects. This, compounded with the low solubility issues for most chemotherapy compounds, usually limits the regimen to sub-optimal doses.[8] As a tumor develops, heterogeneity forms among its cell populations. Most chemotherapy agents however only affect cells at a specific stage in their growth cycle. Many cells in larger tumors remain in the quiescent phase of the cell cycle because the poorly-developed vasculature in the tumor results in inadequate nutrient distribution throughout its tissues which permeates into formation of hypoxic, acidic and necrotic regions within the tumor.[9] These cells are less responsive to cytotoxic and cytostatic compounds. The hypoxic as well as acidic environment (including other factors such as the chemotherapy regimen itself) where these cells are located also stimulates the expression of the multidrug resistance phenotype. Cancer cells which develop resistance to chemotherapy before initial treatments are said to have intrinsic drug resistance whereas cells that emerge with drug resistance after initial treatments are said to have acquired drug resistance. Intrinsic and acquired multidrug resistance is the highest obstacle for chemotherapy to overcome.[17-23]

Multidrug resistance is a phenotype often displayed by some or all the cells in a neoplasm. This allows them to be much more resistant to chemotherapy than ordinary cells.[4,24] A number of biochemical mechanisms are responsible for multidrug resistance. Changes in the cellular target of the respective drug by mutation will lower the binding efficiency of the drug and hence lower its therapeutic index. Alterations in enzymatic activation and detoxification mechanisms can increase the metabolism and clearance of a drug. Defective apoptotic pathways can prevent antigens or drugs from stimulating apoptosis. For example the mutation of the Fas gene as well as upregulation of Fas ligand secretion by tumors compromises immune responses.[25,26] Membrane changes and expression of drug efflux pumps within them drastically increases drug clearance from the cell. Efflux pumps are the most notorious traits of the multidrug resistance phenotype. The most studied efflux pumps are P-glycoprotein,[17,19,20,24] multiple resistance protein,[18,21] and breast cancer resistance protein.[22,23] These trans-membrane proteins belong to the ATP-binding cassette transporter family and actively expel chemotherapy drugs from the cytoplasm. Much effort is being focused on combinatorial chemotherapy, where compounds that inhibit the production or function of these efflux pumps are co-administered with the conventional cytotoxic compounds.[17]

Another serious issue caused by the heterogeneity of a solid tumor is the poor accessibility of chemotherapy drugs to the hypoxic, acidic and necrotic regions within the tumor tissue.[9] This is mainly due to the poorly developed vasculature of a tumor, which does not efficiently traverse its entire volume. The high osmotic pressure of the tissue (caused by an underdeveloped or non-existent lymphatic system) as well as changes to the drug itself (such as protonation, hydrolysis or oxidation) caused by the harsh environment results in an insignificant amount of the drugs penetrating deep enough into the tumor to affect all the cancerous cells.

From these observations, it is clear that traditional chemotherapy has many fundamental problems that would most likely not be solved by development of new chemotherapeutic compounds alone. Many of these issues are caused by the poor pharmacokinetics for the traditional drugs.

2.1.3) Doxorubicin (Adriamycin) as a Chemotherapeutic Drug

Doxorubicin is an anthracycline antibiotic prepared by semisynthesis from Daunomycin, which is extracted from the bacterium *Streptomyces Peucetius*. The molecular structure Doxorubicin is illustrated in Figure 2.1.

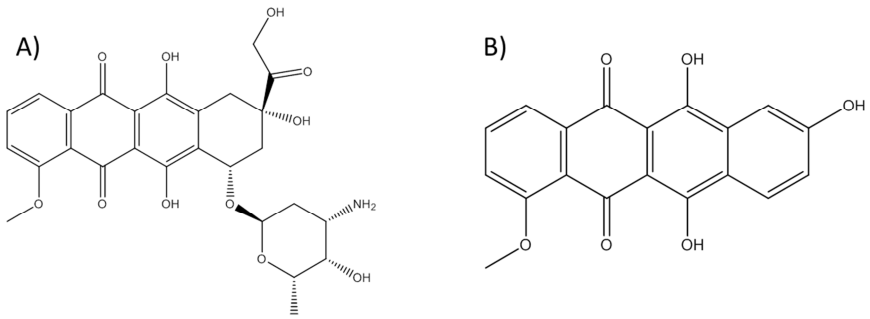

Figure 2.1: A) Molecular Structure of Doxorubicin. B) Major Degradation Product at pH > 6.5.

This compound has been used to treat many types of cancer including hematological malignancies, carcinomas and sarcomas.[8] It unfortunately causes many side-effects including myelosuppression, diarrhea, nausea, vomiting, oral mucositis, oesophagitis, loss of hair, anaphylaxis, liver dysfunction and cardiomyopathy.[8,27] According to Beijnen *et al*.[28], it is usually formulated in acidic solutions as it decomposes increasingly fast as the pH is increased above 6.5. They also studied the temperature dependence of the degradation and revealed that Doxorubicin has a half-life over four and a half days at 37 °C and pH = 7.4. The major degradation product formed is depicted in Figure 2.1.B. Incorporation of the drug in an appropriate drug delivery system has aided in decreasing the observed side-effects and has allowed it to be administered in solutions at physiological pH = 7.4.[29-31]

2.2) Drug Delivery

2.2.1) Principles of Drug Delivery

Drug design is a laborious (not to mention expensive) process involving target or disease identification, hit identification, hit optimization, lead selection and further optimization, candidate identification, and finally clinical trials of the candidate.[32] In the past, new drugs were discovered by combinatorial chemistry. This involved screening tens of thousands of random compounds, though systematically different, to find a few hits (compounds that have a desired physiological effect on the target/disease.) After identification and optimization of their structure-activity relationships, even fewer candidates entered into clinical trials. During the clinical trials, many candidates that showed promising results *in vitro* could have completely different results *in vivo*. In the late 1980s, Prentis *et al*. determined that, based on data from seven UK-based pharmaceutical companies, 39% of candidate compounds in clinical trials were rejected due to poor pharmacokinetic properties in humans.[32,33] On top of this, many of the other reasons for rejections were considered to be interrelated to the pharmacokinetics. Since the cost of clinical trials is far greater than that of the early developmental stages, new factors are now taken into account to determine the potential of a candidate. This new paradigm of drug discovery is known as rational design.[34] With rational design, new drugs are not only synthesized based on knowledge of a biological target. The pharmacokinetics, pharmacodynamics, toxicology and the compound's metabolism are also taken into account as these play crucial roles in the final approval of a compound during clinical trials.

Drug delivery deals mostly with the pharmacokinetics of a drug. This is the way a drug travels through the body and where it accumulates.[32] In other words, it deals with the Absorption, Distribution, Metabolism and Elimination (ADME) of a drug. The focus is to optimize the transport of a pharmaceutical compound in the body as needed to safely achieve its desired therapeutic effect. There are two main types of drug delivery – site-specific targeting and controlled drug release. Site-specific targeting aims to concentrate the drug in a specific region of the body while controlled drug release aims to control the concentration of the available drug in the body for a specific amount of time.

There are several techniques that are very popular for optimizing drug delivery:

- Formulations
- Administration method
- Prodrugs
- Receptor-mediated targeting

Often, several or all of these techniques are employed simultaneously when optimizing the pharmacokinetics of certain drugs. Recently, nanotechnology has imposed a great influence on the design of novel promising formulations for drug delivery.[35]

2.2.2) Nanotechnology in Drug Delivery

Nanotechnology is not bound to one strict, formal definition but the general idea remains the same. Simply stated, the concept of nanotechnology is the exploitation of materials with structural features at the intermediate range between the molecular and the macroscopic scale *i.e.* that at least one of the dimensions are in the nanometer length scale.[36,37] Nanomaterials differ from bulk systems by their surface-related properties as well as their quantum properties.[38]

The surface properties of nanomaterials are different because of the fact that their surface-to-volume ratios are generally larger than for larger objects of similar dimensions. For instance, the surface area to volume ratio for a cube is:

$$\frac{S}{V} = \frac{6 \times L^2}{L^3} = \frac{6}{L}$$

Where

S = Surface area of the cube

V = Volume of the cube

L = length of each of the sides of the cube

This simple equation indicates that as the length of the sides of the cube decrease, the surface to volume ratio will increase. On the other hand, any shape can be approximated by a linear combination of different-sized cubes. The total surface area and volume of the shape can then also be formulated as such a linear combination. Corrections made to take into account the fraction of the area of each cube that is exposed can be made by multiplying S for each cube by an appropriate coefficient. This also affects the dependence of each cube's surface to volume ratio. Thus the surface to volume ratio depends inversely on the cube dimensions as well as the sum of the coefficients.

The atoms or molecules at the surface of a material can display different properties than those within the bulk due to a reduced coordination number.[35] This usually has an effect on the physical behavior of those atoms/molecules as well as their chemical properties.

Atoms/molecules at the surface of a nanoparticle tend to display liquid-like characteristics that can affect its glass transition temperature, melting point and other phase transitions as well as its solubility. The nucleation and growth of particles is also governed by the thermodynamics at their surface, most notably their surface (or interfacial) energy. Many chemical properties of a nanomaterial display a transition from that of the bulk material towards quantum mechanical behavior due to the electrons in a nanosystem being confined to dimensions within the order of molecules. This causes the material's electronic structure to be more discrete, which can affect its electrical conductivity, magnetic and optical properties.

The various physiological barriers within the body portray an additional property of nanomaterials: the selective permeation of nanomaterials of a certain size and/or composition through them.[35] Further discussion of this phenomenon can be found in Section 2.2.6.

The ability to fine-tune a material's physicochemical properties through nanotechnology as well as the evolution of unique phenomena for nanomaterials and nanoarchitectures is an intensely researched field in modern medicine. Such innovations include selective distribution through certain biochemical barriers,[39] unique light absorption and scattering characteristics[40] as well as superparamagnetism.[41] These innovations have been implemented in drug delivery,[9,32,35,42] gene therapy,[43] tissue and bone engineering[44,45] as well as in imaging techniques such as computed tomography[46] and magnetic resonance imaging.[41]

2.2.3) Stimuli-Responsive Polymers in Drug Delivery

Synthetic polymers that can mimic the behavior of certain biopolymers towards various environmental stimuli are beyond fascination and offer a broad potential spectrum of applications in the biomedical and industrial fields. Plenty of research has been focused on developing such stimuli-responsive polymers and applications of these materials is seen in tissue engineering,[47] hydrophobic interaction chromatography,[48] size exclusion chromatography,[49] affinity chromatography,[50] ion exchange chromatography,[51] smart membranes,[52-55] lithography,[56] molecular imprinting[57] and drug delivery.[47,58-61]

Stimuli-responsive polymers are defined as polymers that undergo relatively large and abrupt, physical or chemical changes in response to small external changes in the environmental conditions.[62] Stimuli-responsive polymers can be arranged into two major groups according to the stimulus that causes their reaction. Both physical and chemical stimuli-responsive materials exist. Physical stimuli include temperature, light, electric and/or magnetic fields as well as mechanical

stress. Chemical stimuli include pH, ionic factors as well as chemical agents. The various structures that are of particular interest to construct from stimuli-responsive polymers are cross-linked and reversible hydrogels, micelles, modified surfaces and membranes as well as conjugated polymer solutions.[62] Stimuli-responsive hydrogels have been applied in sustained drug release.[63,64] Amphiphilic copolymers with one or more stimuli-responsive polymer blocks have been used to prepare stimuli-responsive micelles[58-62,65,66] or polymersomes[60,67] for site-specific drug delivery. Nanoparticles and bioconjugates containing stimuli-responsive polymers have also been investigated for various drug delivery applications.[65,68]

Due to the ability to control and optimize the pharmacokinetics of drugs through the incorporation of stimuli-responsive polymers in the design of drug delivery systems, they are among the most intensively researched topics in current cancer research and development.[58,65,69-71] The fundamental idea behind stimuli-responsive drug delivery systems is to encapsulate the drug and prevent it from interacting with the physiological environment until the appropriate stimulus is applied. The sudden or sustained release of the drug is then initiated. This methodology is closely related to that surrounding prodrug design, *vide infra*.

Poly-L-histidine and chitosan are two pH-responsive cationic polymers that are useful as components for drug delivery systems since they undergo their transition from neutral to cationic when the pH drops below that of blood plasma.[66,72,73]

2.2.4) Prodrugs

Prodrugs are drugs that are biologically inactive while in the initial form that they are administered in. They are converted into their active state within the body only once they have reached a specific region such as an organ, tissue, cell or organelle. There are two main types of prodrugs:[74]

- Bioprecursor Prodrugs
- Carrier Prodrugs

A bioprecursor prodrug enters a metabolic pathway to release the active form of the drug, sometimes releasing a small metabolite along with it. A carrier prodrug is a molecule/aggregate that incorporates the drug through a labile linker. Various linkers have been developed that can be cleaved either by enzymatic reactions or specific physiological conditions.[32,35,74,75]

The main difference between the two types of prodrugs is that carrier prodrugs are generally larger than the free drug or bioprecursor prodrug and may not necessarily target a metabolic pathway for release of the drug.

The major benefits of employing a prodrug over a free drug include improvement in the absorption and transport of the drug through cell membranes and other physiological barriers, improving patient compliance, inducing site-specific release or sustained release and minimizing the drug's side effects.[32]

2.2.5) Polymeric Prodrugs

In 1975, Helmut Ringsdorf proposed a novel class of carrier prodrugs based on using synthetic polymers as the carrier molecule.[76,77] In the general model, the polymer is functionalized with three types of functional groups attached to the polymer backbone.

The first type is a solubilizing group, which allows for modification of the pharmacokinetics of the conjugate. These are usually functional groups on the repeating units of the polymer. In the case of a copolymer, there may be more than one type of solubilizing group. Block copolymers with different solubility properties can be designed to self-assemble into polymeric micelles or vesicles in aqueous solution. They usually exhibit much lower critical micelle concentrations and greater stability than small molecule surfactant micelles or vesicles.[32] They can also incorporate the ability to be cross-linked, which increases their stability even more.

The second is the conjugated drug. The drug is usually attached to the polymer chain by a cleavable linker. Modern polymeric prodrugs also consider physical interactions, such as hydrophobic or electrostatic interactions, and coordination chemistry for incorporating the drug.[32,43,78] The linkers are often categorized by their cleavage mechanism. For instance, enzymatically cleavable linkers are substrates, such as oligopeptides, for certain metabolic enzymes. The oligopeptide glycine-phenylalanine-leucine-glycine (GFLG) is the most common one employed.[32] Some esters, α-acyloxyalkyl esters, alkoxycarbonyloxyalkyl esters, carbonates and carbamates can also be substrates for certain esterase enzymes.[32] Other linkers are reduced by certain enzyme-coenzyme systems. The most common is the reduction of disulfides by the glutathione-glutathione reductase system.[79] Other linkers have been designed to decompose when exposed to a specific physical stimulus. Linkers sensitive to stimuli such as temperature,[67,69,70] light,[80] and pH[9,32,70,81] have been developed. Temperature and pH-responsive linkers are among the most researched. Thermoresponsive polymers have been used to prepare reversible amphiphilic block copolymers that can self-assemble

into micelles or vesicles in an aqueous environment. Drugs can be loaded into a micelle core or encapsulated within a vesicle. When local hyperthermia or hypothermia is induced in a patient receiving the treatment, the drug delivery system will disintegrate at that site resulting in site-specific drug administration.[70] pH-responsive linkers are stable at a certain pH range but are readily hydrolyzed when there is either a significant increase or decrease in the pH. Some examples of these type of linkers include imine, hydrazone, acyl hydrazone, ketal, acetal, cis-aconityl, and trityl bonds.[9] There has been significant research on developing an acid-labile linker that reversibly binds an amine to a substrate.[32,82] However, very few practical applications of this type have been achieved since the linkages tend to be too unstable towards hydrolysis.[32] Imines, oxazolidines and thiazolidines seem to be the only viable linkers of this type and of these, only imines require just an amine and an aldehyde/ketone for the drug-linker conjugation. Imine stability under physiological conditions is improved when the nitrogen-carbon double bond is conjugated to an aromatic, lipophilic carbonyl compound because the pKa of the protonated imine is lowered.[32,83] Various types of linkers have been developed that can bind to many different types of functional groups. The most common functional groups targeted for binding are amines, thiols, carboxylic acids, alcohols, aldehydes or ketones, alkenes and alkynes.

The final component of the Ringsdorf model is a targeting moiety, which helps to improve the selective localization of the prodrug to a specific region within the body. All kinds of compounds have been used for this purpose. Substrates for certain cell surface receptors such as fatty acids, glycans, peptides, antibodies, vitamins and various antigens have all been used as targeting ligands in drug delivery systems for chemotherapy.[8,9] The selectivity of these ligands depends on the selectivity of their binding to a specific receptor as well as the distribution of the receptor throughout the different cells of the body. Targeting can also be a passive process such as the enhanced permeability and retention effect (EPR) that results in localization of molecules and aggregates of a specific size from the bloodstream into the tissue of a solid tumor.[9] This occurs due to a poorly developed basement membrane and lymphatic system within tumor tissue resulting in particles with a diameter 10 – 150 nm passing through the leaky vasculature and accumulating due to the absence of a functional lymphatic system. They would not do so in healthy blood vessels.

2.2.6) Targeted Drug Delivery

The poor selectivity of conventional chemotherapy drugs for tumor tissues is the cause for most of the serious side effects of chemotherapy and is also a limiting factor in the therapeutic effect of the

regimen due to the constraints of sub-optimal dosage being necessary for safety. This makes improving a drug's selectivity for tumor tissues an intensively investigated topic in cancer research. Over one hundred years ago, Dr. Paul Ehrlich, the father of chemotherapy, conceptualized a therapy for infectious diseases whereby the treatment would affect the afflicted areas only and leave healthy tissues alone. This idea was termed the magic bullet concept.[84] A hundred years later, Dr. Ehrlich's dream is becoming a reality through the development of targeted drug delivery. Targeted drug delivery involves optimization of a drug delivery system's pharmacokinetics and pharmacodynamics in order to achieve selective accumulation and release of the drug at a specific site within a body.[8,9,32,35] There are two main methods of targeting tumor tissues.

The first method is known as passive targeting and is caused by the enhanced permeability and retention effect (EPR.)[8,9,39] This phenomenon is defined as the selective accumulation of macromolecules, with a mass of 40 to 800 kDa, within tumor tissues. The cause of EPR is the poorly formed vasculature of tumor tissues that can have pore sizes in the range of 100 – 1200 nm.[9] Nanoparticles with a diameter smaller than these pores while larger than the pore diameters of normal vascular tight junctions (usually 2 nm)[9] can permeate into the tumor tissue whereas the tight junctions of normal vasculature prevent this. The lack of a well-developed lymphatic system or even its entire absence within tumor tissues also prevents the clearance of the accumulated macromolecules. Thus the incorporation of chemotherapy drugs into nanoscale drug delivery systems allows for an inherently more selective therapy. The EPR effect seems to only be sensitive to the size of the drug delivery system rather than the composition and all types of materials have been exploited for delivering therapeutics or imaging agents. EPR arises in most types of tumors though it may be less expressed for heterogeneous tumors. In larger tumors, the vascular network does not cover the entire tissue resulting in hypoxic, acidic and necrotic regions forming. The chemotherapy drugs and their associated drug delivery systems have difficulty reaching those regions.[9,85] In order to augment the EPR effect in hypovascular regions, angiotensin II has been used to induce hypertension during the infusion process.[86-88] Nitric oxide releasing agents, which act as vasodilators, have also been used to augment EPR.[89,90] The role of nitric oxide as a tumor suppressor has also been demonstrated.[91,92] Other vascular modulators such as angiotensin II-converting enzyme/bradykinin inhibitors,[93] prostaglandin I2 agonists[94] and carbon monoxide[95] have been investigated for EPR augmentation.

Another obstacle that has been encountered for the EPR effect is the polyethylene glycol (PEG) dilemma.[9,96] The improved circulation time and EPR of PEGylated macromolecular drug delivery systems has been shown to be counteracted by the poor cellular uptake and endosomal escape due

to the polar, hydrated PEG layer impeding contact of the PEGylated particle to the cell surface receptors. In addition to this, it has been demonstrated that certain PEG-specific IgM antibodies are formed after several administrations of a PEGylated particle into a rat. These antibodies cause the rapid elimination of the particle from the blood by the formation of an IgM antibody complex that is cleared by the liver or macrophages.[97] A new method to increase the plasma half-life of small drugs, peptides or imaging agents with a size below the renal clearance threshold involves conjugating the compounds to serum albumin or Immunoglobulin G (or analogues that retain the FcRn-binding affinity at endosomal pH). Such fused compounds have shown superior circulation times due to FcRn-mediated recycling while still benefiting from the EPR effect.[98-102]

The second method of targeting tumors is known as active targeting. This involves the incorporation of rationally designed targeting ligands to a drug or drug delivery system. The targeting ligands bind with a certain selectivity and affinity to a specific target. The target may be a cell surface receptor, tumor endothelial cell surface receptor or a specific extracellular matrix. The ligands can be proteins,[103-106] peptides,[107-112] glycopeptides,[113] peptidomimetics,[114] small molecules[115] or nucleic acid aptamers.[116,117] Humanized and chimeric monoclonal antibodies are among the most promising of these candidates and have also been shown to induce chemotherapeutic effects.[9,93,103] The use of antibodies in antibody-directed enzyme prodrug therapy is an indirect method to actively target tumor tissues.[9] The procedure involves administration of an exogenous enzyme conjugated to a monoclonal antibody targeting ligand. It is allowed to accumulate into the tumor tissue by both passive and active targeting before a chemotherapy prodrug, with an enzymatic activation specific to that enzyme, is administered.

The major benefit of incorporating an active-targeting motif to a drug delivery system is that, in addition to improving the selectivity of the drug, the targeting ligands can act as agonists or antagonists in a certain biochemical process. Cytokines and monoclonal antibodies have been discovered and designed that can directly induce apoptosis or rally an immune response such as phagocytosis, complement dependent cytotoxicity or antibody-dependent cellular cytotoxicity.[103,104] Growth factor receptor ligands, such as those that target EGFR and VEGFR, can also act as antagonists providing a cytostatic action.[105,118] The targeting ligands can initiate active assimilation of the drug delivery systems into the target cells. For instance, certain arginine-glycine-aspartic acid (RGD) peptides have been shown to induce integrin-mediated endocytosis.[111,112]

There are limitations in developing targeting ligands for chemotherapy. To date, there are no distinct receptors on a cancer cell's surface that are exclusive to it. Hence there is always some inherent affinity of the targeting ligands for normal cells. It is only through targeting receptors that are

overexpressed or mutated at crucial sites in the primary structure that a higher affinity for cancer cells can be achieved.[9] The targeting ligands will have an induced toxicity if they can induce a toxic reaction or stimulate endocytosis. Genetic polymorphisms and mutations of a tumor cell receptor can also cause a reduced affinity of a specific targeting ligand in individual patients compared with results from clinical trials.[119] If the targeting ligand is composed of biological subunits, then it may be susceptible towards metabolic degradation and may need chemical modification to increase its lifetime within the body. Incorporation of smaller targeting ligands into an appropriate drug delivery system is often also necessary to improve their pharmacokinetics.

2.2.7) Cell-penetrating Peptides and Drug Delivery

Polycationic polymers have been used as non-viral gene transvectors due to their affinity for DNA and RNA.[35,43,120] Certain cationic amphipathic polypeptides have also shown antimicrobial capability.[121,122] The cell-penetrating peptides (CPPs) such as trans-activating transcriptional activator (Tat)[123] and penetratin are also polycationic peptides and their non-classical cell-penetrating ability usually depends on their degree of cationic residue functionalization as well as the basicity of the residue's conjugate base.[124] For instance, increasing the number of arginine residues on a CPP improves the cell-penetrating ability of the peptide more than adding lysine residues,[125] which in turn have a greater effect than adding histidine residues.[9,126] The multidentate and pi interaction of arginine residues with the cell membrane also plays a role. The addition of hydrophobic and aromatic residues can further improve the cell-penetrating ability of the peptide.[126] Tyrosine and tryptophan have shown the highest synergistic potential for increasing the cell-penetrating ability of the peptide. However, histidine is the only natural aromatic amino acid residue that displays pH-responsive behavior under physiological conditions.

The use of cell-penetrating peptides for drug delivery systems in chemotherapy has been investigated as a means to both sensitize multidrug resistant cancer cells to the drugs by counteracting drug efflux[9,127-132] as well as to aid in the dispersion of the drugs to the hypoxic and acidic regions of solid tumors.[9,128,129] Cell-penetrating peptides are able to transport chemotherapeutic drugs across the blood-brain barrier, making it possible to treat certain brain cancers that cannot be surgically removed or treated with conventional chemotherapy.[127,133] Some cell-penetrating peptides also have demonstrated intrinsic antineoplastic activity.[134-137]

In addition to conventional cytotoxic and cytostatic drugs, cell-penetrating peptides have also been conjugated with various other cargos. These include antibodies, peptides, fluorescent dyes and oligonucleotides as well as their analogs.[9]

2.3) Radical Polymerization

2.3.1) Overview of Radical Polymerization

Radical polymerization is a chain polymerization process whereby vinyl monomers are connected to each other sequentially to the end of a growing polymer chain. It is extensively used in industry for preparing commercial materials due to its robust nature. Unlike ionic chain polymerization, it is tolerant to a vast number of functional groups as well as impurities. Unlike condensation polymerization, high molecular weights can be achieved even at low monomer conversions. Reaction temperatures also play a less crucial role for radical polymerization than for ionic polymerization. Overall, less stringent reaction conditions are required. Due to the fact that the backbone is composed of carbon-carbon bonds, depolymerization is also seldom a problem. [138-140]

Like all chain reaction mechanisms, the kinetic model for radical polymerization involves three basic steps. These are initiation, propagation and termination.[138-140]

The initiation step involves the formation of an active radical species within the polymerization mixture, usually by the homolytic decomposition of a suitable initiator. There are many types of initiators and they are classed according to the stimulus by which they are induced to form radicals. Such stimuli include thermal, photolytic and electrochemical. Some initiation methods can act directly on a monomer present in the reaction mixture. These include thermal, ionizing radiation and ultrasound-stimulated self-initiation. Once the initiating radical is formed it can react with a monomer in the reaction mixture or it can undergo any number of side reactions that do not result in a growing polymer chain (propagating radical.) The initiator efficiency is the fraction of initiator-derived radicals that form a propagating radical.[138-140]

The propagation step is described as the successive addition of monomer units to the end of a propagating radical. With each addition, the propagating radical is retained at the propagating end of the polymer chain.[138-140]

The termination step involves the reaction of two radical species to form stable products. There are two ways in which the radicals can do this, via combination or via disproportionation. Termination

by combination results in the two radicals being bonded together by a sigma bond to form a single compound. Termination by disproportionation results in the formation of two separate, stable compounds.[138-140]

There is another step that can occur during radical polymerization and it can have pronounced effects on the product properties. This is known as a transfer step. It is a process whereby a radical is transferred from a propagating chain to another molecule. Hence one chain is terminated but no radicals are destroyed in the process. If the newly formed radical is capable of initiating polymerization, a new polymer chain is formed.[138-140]

The reaction of radicals with monomers and with each other during these steps depends on four factors. These are polar, steric, stabilization and thermodynamic effects. Polar effects are observed through nucleophilic radicals reacting more readily with electrophilic monomers and vice versa. Steric effects are observed by the almost complete incorporation of functional monomers in a head-to-tail manner. In other words, reaction between the propagating radical and monomer occurs at the less sterically hindered end on the vinyl group of the monomer. The much lower reactivity of 1,2-substituted vinyl monomers is also evidence of the contribution of steric effects in radical propagation. Stabilization effects arise when delocalization of the unpaired electron is possible within the radical. If the reactant radical is stabilized by delocalization, it will be less reactive than an analogous radical that does not exhibit delocalization. On the other hand, if a reaction were to result in the formation of a radical that is stabilized by delocalization, it will be more favorable than an analogous reaction that does not form a product radical that is stabilized by delocalization. Thermodynamic effects arise from differences in the relative energies of the reactants and products, which contribute to the magnitude of the reaction barrier. [139,140]

The kinetics of radical polymerization is not a trivial matter and has been the subject of much research. There are numerous coupled processes involved that can complicate things greatly. However, the overall process can be divided into a simplified set of fundamental reactions, with varying degrees of accuracy. These are initiator decomposition (if a chemical initiator is being used), chain initiation, chain propagation, chain transfer and chain termination. Each of these reactions can be described by an associated rate law. The real difficulty lies in the melding of the effects of chain length on the rates of these reactions into the fundamental equations. This is especially tricky for the propagation and termination rate coefficients as they tend to display non-linear changes with chain length that can also depend on parameters such as viscosity of the reaction mixture, polarity of the solvent, pressure and rigidity of the polymer backbone.[139,140]

Various polymers prepared by radical polymerization have been applied as biomedical materials. Some important examples include polyvinyl chloride, polytetrafluoroethylene, poly(methyl methacrylate), poly(methyl methacrylamide), poly(*N*-vinylpyrrolidone) (PVP) and polyvinylalcohol (prepared from polyvinylacetate).[138-140]

2.3.2) PVP as a Biomaterial

PVP is a hydrophilic polymer that has been used in the pharmaceutical industry for over a hundred years. Its main application in this regard is as an excipient and a disintegrant. It was used during the Second World War as a blood plasma enhancer. When mixed with iodine, the formulation better known as Betadine or Pyodine serves as a broad spectrum topical antiseptic. It has also been used as an adhesive, emulsifier and thickening agent, as well as a component of water purification membranes and as a liquid-phase dispersion-enhancing agent in DOSY NMR. The similar properties to PEG, when in aqueous solutions, make PVP and 2-(hydroxypropyl) methacrylamide (HPMA) suitable alternative hydrophilic polymers for drug delivery purposes. The fact that PVP and HPMA are synthesized by free radical polymerization, while PEG is prepared by anionic ring-opening polymerization, makes their large-scale production less stringent. They may require more stringent purification though. PVP bioconjugates have also shown longer circulation times compared to the analogous PEG conjugates.[141] However, the inherent lack of control associated with conventional radical polymerizations results in polymers with broad molecular weight distributions (*i.e*. large dispersity) and poorly defined end-groups.

PVP with a molecular weight above the renal clearance threshold accumulates in the patient permanently and can trigger an immune response over time.[142-144] Many components of nanoscale drug delivery systems also need to have low dispersities in order to achieve the desired architecture that exhibits the optimum pharmacokinetics. The use of a chain transfer agent can aid in controlling the molecular weight of the product, but does not lower its dispersity significantly. The use of a controlled radical polymerization process can provide control of both of these properties. Hence, the polymerization of PVP by controlled radical polymerization processes has been greatly studied.

Nitroxide-mediated polymerization of NVP was unsuccessful, yielding polymers with large dispersities.[145]

ATRP has also proven to be inadequate since the reversibility of the deactivation by the metal center depends on the stability of the propagating radical as well as the stabilizing ligands.[146] An unstable propagating radical would require a metal complex with highly stabilizing ligands for the reaction to

be significantly reversible but, under those conditions, propagation would dominate over deactivation. Regardless, PVP with dispersities between 1.2 and 1.4 and number-average molecular weights below 5000 g/mol have been prepared by ATRP.[147]

Organostibine-mediated polymerization of PVP has been investigated by Yamago *et al*.[148] as well as Ray *et al*.[149] The organostibine acts as a degenerative chain transfer agent during the polymerization process. The reaction times they published are substantially shorter than those published in the literature for other free radical polymerizations of NVP to similar conversions.[148,149] This was due to a higher concentration of initiator being used for the organostibine-mediated polymerization. Yamago *et al*. also polymerized NVP using analogous organotellurium chain transfer agents.[150] While these chain transfer agents show unprecedented control of the dispersity, they are limited in the sense of incorporating end-group functionality for the polymer chains and often require stringent purification protocols for the removal of antimony or tellurium from the product.

Reversible addition-fragmentation chain transfer (RAFT) polymerization has also been applied to control NVP polymerization with significant success as reported by Moad *et al*.,[151,152] Kowollik *et al.*[153] and Pound *et al.*[154,155] Though the conversion rates were slower and the dispersities slightly higher than those for organostibine and organotellurium-mediated polymerizations, the process is more tolerant to various functionalized monomers, and allows for greater control of the end-groups formed by these processes. Another perk of RAFT-mediated polymerization is that the synthesis of most RAFT agents is usually rather simple and, with a few exceptions, the products tend to be quite stable under general storage conditions.[153]

2.3.3) Controlled Radical Polymerization and RAFT Polymerization

One of the major drawbacks of radical polymerization is the lack of control of the rate of propagation relative to the rate of initiation. By approximating the formation of a polymer chain as a random walk process, a broad distribution of the polymer chain lengths is possoble even at low monomer conversions. Other issues include lack of control of functionality with respect to the chain ends and the rapid termination of propagating radicals, making the synthesis of block copolymers and other macromolecular architectures only achievable by grafting techniques. The chemical linkage of two macromolecules at their end groups is only efficient when click chemistry techniques are employed.[156,157] Grafting techniques employed for coupling macromolecules are problematic, mostly due to termination reactions and the difficulty in separating byproducts. The synthesis of

gradient copolymers is also not possible since the gradient will be distributed among the polymer chains produced at different monomer conversions.

These limitations spurred a large amount of research that began with the emergence of living vinyl polymerization techniques, such as anionic polymerization, almost 60 years ago[140] and has culminated in the development of controlled radical polymerization. One of the most notable of these early techniques is nitroxide-mediated polymerization (NMP.) [140,145] Another more recent example is atom transfer radical polymerization (ATRP.) [140,146,147] Both these techniques depend on the persistent radical effect to reduce the rate of propagation relative to initiation and minimize the rate of irreversible termination by allowing a reversible termination reaction to dominate. In 1998, the Commonwealth Scientific and Industrial Research Organization (CSIRO) introduced a newly invented controlled radical polymerization technique known as the reversible addition-fragmentation chain transfer (RAFT) polymerization.[151,153] What makes RAFT polymerization stand out from NMP and ATRP is that it does not rely on the persistent radical effect to achieve control of the polymerization kinetics, but rather it is a degenerative chain transfer of the propagating radical between the polymer chains that induces a means of controlling the polymerization. This means that the RAFT process displays quasi-identical rates of polymerization and any deviations are usually caused by the chain length dependence of the rate coefficients. Hence, synthesis time tends to be almost identical to the analogous conventional radical polymerization. The process itself is also relatively simple, usually only requiring the addition of a special transfer agent, known as a RAFT agent. The basis of a RAFT agent is a thiocarbonylthio functional group as depicted in Figure 2.2.

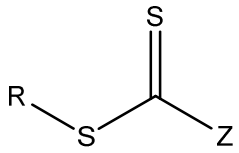

Figure 2.2: Fundamental Structure of a RAFT Agent.

Z in Figure2.2 represents a stabilizing group and plays a role in the reactivity of the RAFT agent. R is a leaving group. Its purpose is to re-initiate polymerization, making the number of polymer chains in the final product approximately equal to the number of RAFT agent molecules initially added to the reaction mixture. It can also be used to add functionality to the α-end of the polymer chains.

The mechanism of a general RAFT polymerization follows that of a conventional radical polymerization with two equilibrium reactions imposed during the propagation step. Scheme 2.1 illustrates this.

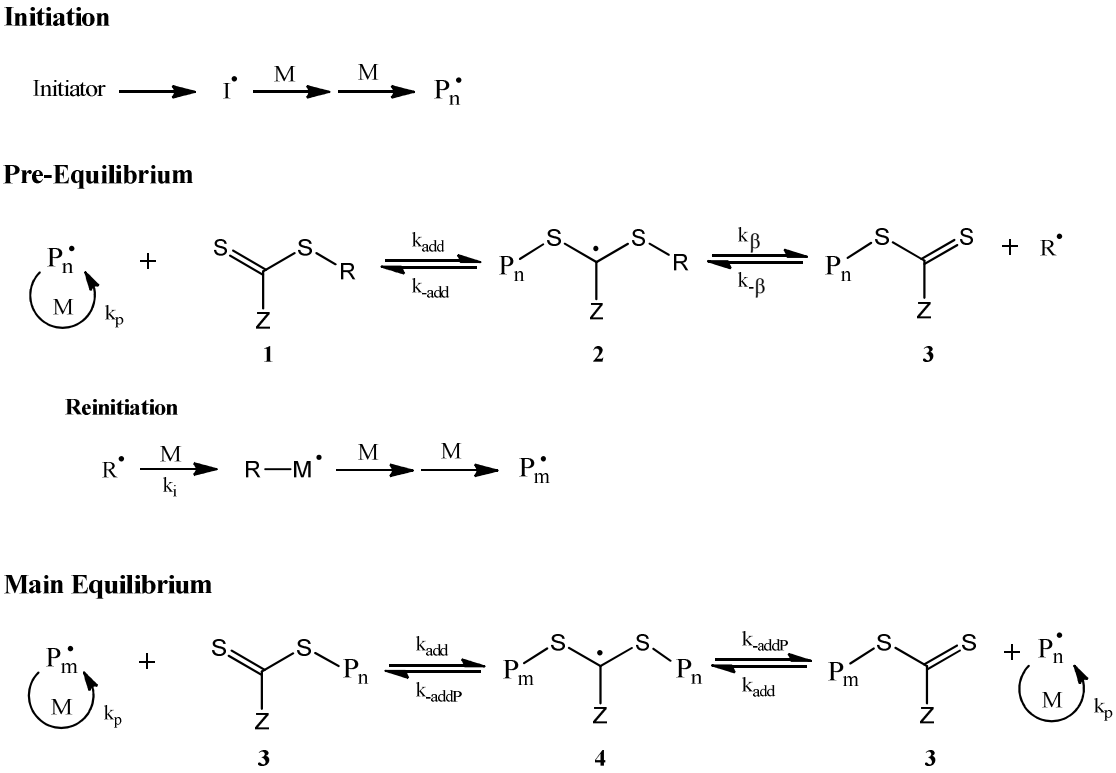

Scheme 2.1: General Mechanism for a RAFT Polymerization.

The first equilibrium, also known as the pre-equilibrium or initialization, involves the addition of the propagating radical to the RAFT agent to form the intermediate adduct radical **2.** This is followed by fragmentation of **2** into either the reactants or a thiocarbonylthio-terminated polymer chain **3** (poly-RAFT agent) and the leaving group radical ($R^{\bullet}$). The leaving group is usually chosen to be such that fragmentation of **2** favors the formation of products. Hence $R^{\bullet}$ needs to be more stable than the propagating radical but still able to reinitiate polymerization.

The second equilibrium is known as the main equilibrium and involves the degenerative transfer of the propagating radical between the dormant polymer chains **3**. No radicals are lost or formed by the RAFT equilibria though termination and initiation still occur as in a conventional radical polymerization. Hence, an initiator must be added to allow for polymerization to occur but the radical concentration must be kept low to minimize the rate of termination of the higher molecular weight radicals. [151,153]

There are four main classes of RAFT agents, based on the type of Z-group they have, each of which is capable of controlling a specific monomer class. Alkyl and aryl dithioesters are very reactive and hence are used for RAFT polymerization of more activated monomers such as acrylates, acrylamides, styrene and acrylonitrile. These RAFT agents cause inhibition if used for polymerization of less activated monomers as the adduct radical intermediate is more stable than the propagating radicals. Trithiocarbonates can also be used for more activated monomers and tend to cause retardation or inhibition during polymerization of less activated monomers. Dithiocarbonates, also known as xanthates, and dithiocarbamates are not reactive enough to provide sufficient control for the more activated monomers but work well for less activated monomers such as vinyl pyrrolidone and vinyl acetate. The switchable RAFT agents, such as *N*-(4-pyridinyl)-*N*-methyldithiocarbamates, have demonstrated control over polymerizations of both more-activated monomers, when protonated, and less-activated monomers, when deprotonated.[158] Fluorodithioformates have been proposed as universal RAFT agents though their applications and success has been limited so far.[153,158]

Thanks to the development of such controlled radical polymerization techniques, a vast array of polymer architectures can now be easily synthesized. These include block, star, gradient and brush copolymers. Controlling the dispersity of the polymer chains is also achievable even for high molecular weight polymers.

2.4) *N*-Carboxyanhydrides and their Ring-Opening Polymerization

2.4.1) Overview of Ring-Opening Polymerization

Ring-opening polymerization (ROP) is a form of chain-growth polymerization that involves the conjugation of cyclic monomers to the end of a propagating chain by breaking a bond that is part of the ring structure. The propagating center can be cationic, anionic or radical in nature. It has been used to prepare polymers from cyclic alkanes, alkenes, ethers, acetals, esters (lactones, lactides, and carbonates), anhydrides, polysulfur, sulfides, polysulfides, amines, amides (lactams), imides, *N*-carboxyanhydrides, 1,3 - oxaza derivatives, phosphates, phosphonates, phosphites, phosphines, phosphazenes, siloxanes, silaethers, carbosilanes and silanes.[159] Thus ring-opening polymerization provides a method to prepare polymers with functionality incorporated into the polymer backbone, similar to condensation polymerization. However, since it is a chain polymerization process, it allows for high molecular weight polymers to be prepared at lower monomer conversions as well as incorporating more control over the polymerization process than possible for condensation polymerizations - not taking into account sequential condensation polymerization as that is not

practical for high molecular weight polymer synthesis. To date, ROP is the most efficient way to prepare certain types of biopolymers and biodegradable polymers in large quantities.[159-161]

2.4.2) Overview of *N*-Carboxyanhydrides

Peptides and proteins are fundamental structural components of life due to their ability to form complex shapes and interactions under the appropriate conditions. For this reason, they have been extensively studied as biomaterials for biomedical engineering, drug delivery systems and therapeutic compounds. Traditional peptide synthesis techniques involve sequential addition of protected amino acid residues to one another in solution with isolation and deprotection steps in between. Solid phase peptide synthesis involves the immobilization of the initial amino acid residue onto an appropriate resin, optimizing the product isolation after each step. Solid phase peptide synthesis still becomes complicated and expensive for the preparation of significantly large peptide sequences.

2,5-Dioxo-1,3-oxazolidines, also known as *N*-carboxanhydrides (NCAs), were first discovered in 1906 by Hermann Leuchs when he tried to distill *N*-methoxycarbonyl amino acid chlorides.[160,162] NCAs have the general structure depicted in Figure 2.3.

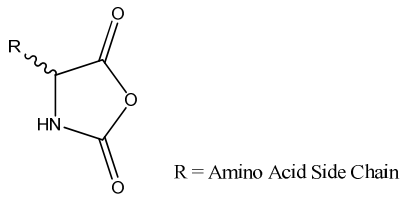

Figure 2.3: General Structure of α-Amino Acid *N*-Carboxyanhydrides.

These amino acid derivatives are unique as they are simultaneously protected at the α-nitrogen and activated at the α-carboxyl group. They can readily react with nucleophiles without isomerization.[160,163] However, they have a tendency to oligomerize since the carbamic acid intermediate that is formed after reaction with a nucleophile is unstable and decomposes to free the α-amino group, liberating carbon dioxide. They also tend to isomerize in the presence of bases such as trialkylamines and even in pyridine in high enough concentrations.[164] The mechanism involves deprotonation of the amino nitrogen in the heterocyclic ring. Another issue with NCAs is their competitive reactivity. More precisely, NCAs can act as electrophiles by adding a nucleophile at the α-carboxyl group. They can also act as acids, liberating a proton from their α-nitrogen to form an NCA anion that is a sufficiently strong nucleophile to react with NCAs. This makes their use in

peptide synthesis complicated as addition of more than one residue is difficult to control. Some success has been achieved using a biphasic aqueous buffer-acetonitrile system with rigorous control over the pH.[164,165] The preparation of urethane-protected NCAs (UNCAs) has improved their use in sequential peptide synthesis. However, UNCAs can still isomerize in the presence of a base.[163-165]

2.4.3) NCAs as Monomers for Ring-Opening Polymerization

NCAs are well suited for homopolymerization of amino acids. The mechanism by which they polymerize falls under the category of Ring-Opening Polymerization. There are two classical initiation mechanisms which can be active during their polymerization. They are known as the normal amine mechanism and the activated monomer mechanism. Scheme 2.2 depicts these initiation mechanisms for NCA polymerization.

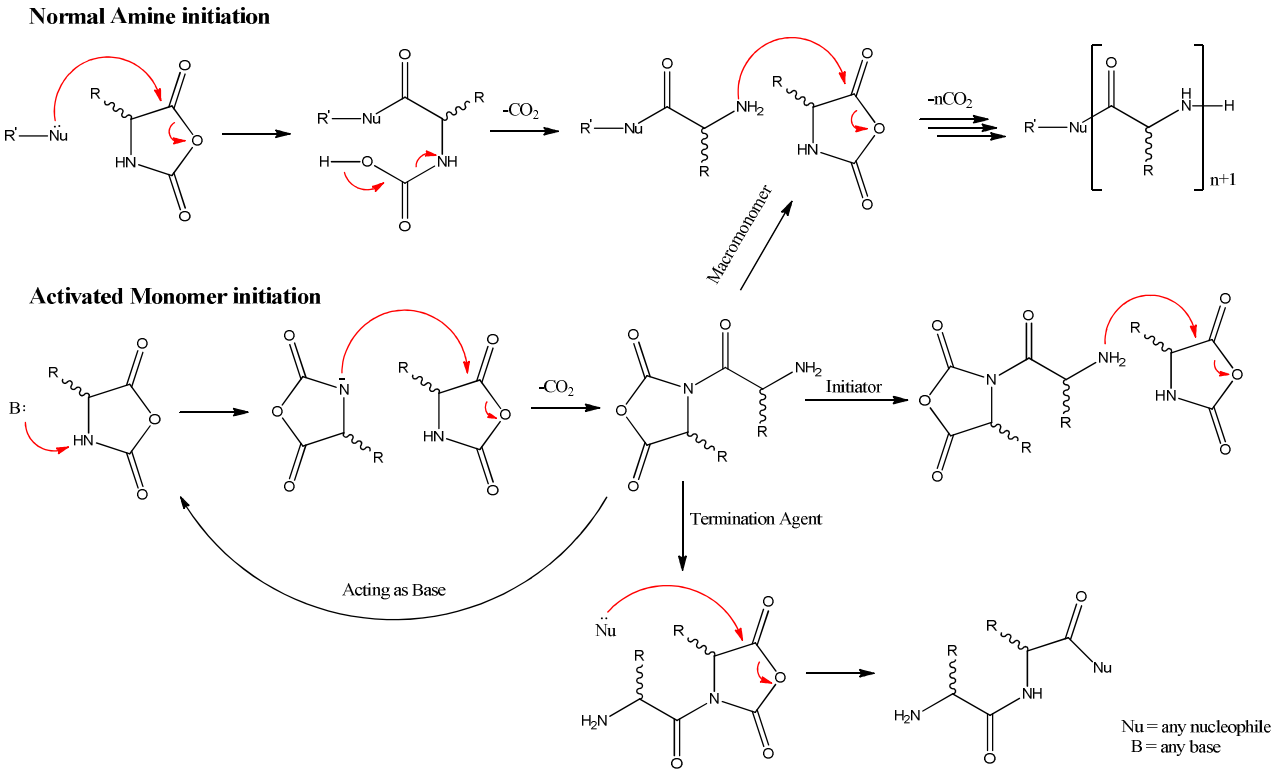

Scheme 2.2: Mechanisms of Initiating NCA Polymerization.

Looking at the two mechanisms for NCA initiation, it is evident that the normal amine mechanism has characteristics of a living polymerization while the activated monomer mechanism has many termination and transfer reactions that would suggest very little control is possible for the polymers formed when this mechanism is active. This is the major obstacle towards preparing well-structured polymeric materials from NCAs as both mechanisms are active under normal conditions.[167,168] To

complicate the process further, it has been shown that trace impurities in the reaction mixture can also have dire consequences for the products formed.[161,165,167,168]

Optimization of the conventional method that uses a primary amine as an initiator has been achieved by applying a high vacuum and low temperatures during the polymerization.[168-170] It is believed that the reduced concentration of impurities, especially water, under high vacuum conditions provides a better control of the polymerization by minimizing the possible termination reactions. A higher activation energy barrier for the Activated Monomer Mechanism as opposed to that for the Normal Amine Mechanism is what makes NCA polymerization more controlled at lower temperatures.[169]

Development of zerovalent transition metal initiators, most notably Co(0) and Ni(0) complexes, [171-173] has also allowed the living polymerization of NCAs without competing side reactions. This procedure has been employed in the synthesis of random, block and gradient copolypeptides as well as hybrid materials. The mechanism is illustrated by Scheme 2.3 and involves the consecutive formation of 5 metallocycle intermediates, starting with an oxidative addition of an NCA to the metal center. The forth intermediate essentially undergoes the first propagation step and the consecutive propagation steps occur in a similar manner, though they are better depicted as the fifth intermediate. [171]

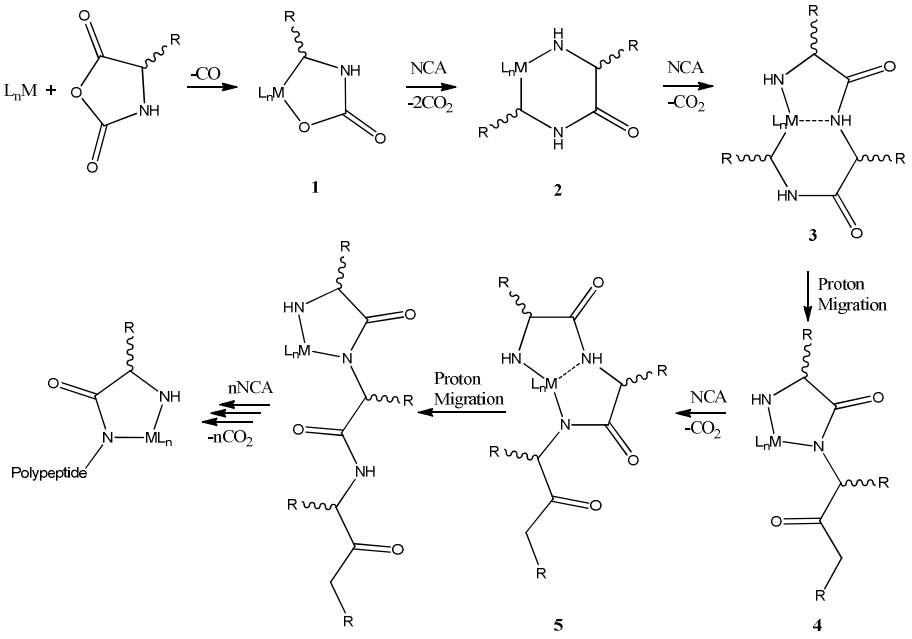

Scheme 2.3: NCA Polymerization Using Zerovalent Transition Metal Initiators.

The metallocycle can be removed easily by dialysis with mild acid.[173] In order to control the functionality at the *C*-terminus of the polypeptide, the appropriately functionalized amido-amidate

metallacycle intermediate **4** can be prepared by tandem oxidative addition of allyloxycarbonylaminoamides to the metal center as depicted by Scheme 2.4.[174]

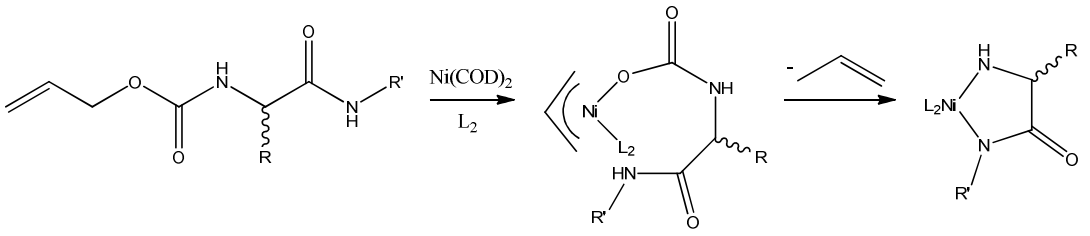

Scheme 2.4: Preparation of Functionalized Transition Metal Initiators.

The use of amine hydrochloride salts as initiators results in living polymerization of NCAs to be achieved by a reversible deactivation mechanism analogous to ATRP while also negating any side reactions caused by the formation of NCA anions.[168] The reaction is quite slow however and only the single monomer adduct is formed at ambient temperatures.

N-(Trimethylsilyl)amine (TMS-amine) initiators can control NCA polymerization via a ring-opening metathesis mechanism as shown in Scheme 2.5.[175]

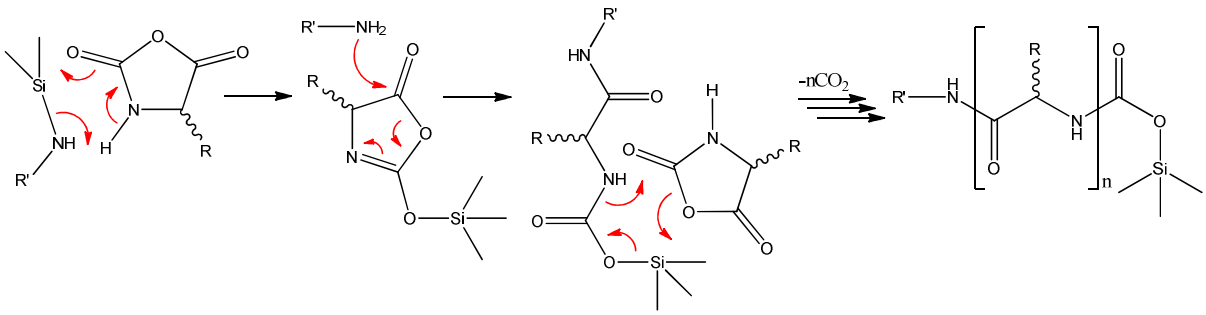

Scheme 2.5: Initiation Using TMS-amine Initiators.

The reaction proceeds with similar control as the other methods, but polymerization is faster than low temperature polymerization with amine initiators or polymerization at elevated temperatures with amine hydrochloride initiators. However, the TMS-carbamate intermediates are degraded in the presence of air or moisture.

Polypeptides prepared by NCA polymerization are attractive for use as biomedical materials since they are composed of biological building blocks that can be decomposed by the body. They can also adopt similar secondary or tertiary structures as those of natural proteins and exhibit stimuli-responsive behavior. For instance, polyglutamic acid shows a conformational change from α-helix to random coil in aqueous media when the pH is raised from below 5.5 to a higher value.[176,177] Polyglutamic acid hydrazone conjugates with hydrophobic drugs release their payload in an acidic

environment.[178] Polyhistidine is hydrophobic at physiological pH, but becomes soluble in water when the pH is below 7.[66] Poly(L-lysine) is a commercially important polypeptide, prepared by NCA polymerization.[165] It is used as an attachment factor that improves cell adherence in tissue culture[179] and in non-viral gene transvectors as it forms polyionic complexes with the phosphate groups of DNA and RNA.[43]

2.5) Brief Deduction of the Researched Literature

The incorporation of nanotechnology in medicine, coupled with state-of-the-art diagnostic and imaging techniques has improved our understanding of the pharmacokinetics and pharmacodynamics of chemotherapy drugs.[32,42,46] It has also provided a better description of the development, growth and spread of cancer within the body. This combined knowledge has indicated that many conventional chemotherapy regimens are unable to completely treat the afflicted tissue due to poor pharmacokinetics of the drugs throughout the body and their even poorer pharmacokinetics within a tumor.[9] The development of the multidrug resistance phenotype within tumor tissues intensifies this issue.[17,18,20] Since a drug's efficacy is strongly dependent on its selectivity for its intended target as well as its distribution within the body, modern chemotherapy research aims at improving drug delivery of existing chemotherapeutic compounds instead of developing novel drugs.

Most cancer drug delivery systems are nanostructures as these tend to accumulate within tumors by the Enhanced Permeability and Retention Effect.[39] Various targeting ligands have been attached to the drug delivery systems to further increase their selectivity for tumor tissue. However, this is difficult as most cell surface receptors of cancerous cells are identical or almost identical to those found in healthy tissues. Certain targets can stimulate synergistic responses, such as endocytosis.[111,112,118]

In order to achieve selective release of the drugs at the target site, various stimuli-responsive materials have been developed.[58-65,69-71,73] These can respond to either physical stimuli, such as heat and light, or chemical stimuli, such as pH or ionic strength. Various labile linkers have also been developed, which can be designed to cleave under conditions specific to the target region. There has been limited success for developing a reversibly labile linker for an amine that releases its payload under the mildly acidic conditions of an endosome or lysosome.[32,73,82,83,179] Imines can provide such a linker but they tend to be too labile in aqueous conditions. Confining the imine bond to a hydrophobic region within a drug delivery system can improve its stability by both reducing the

concentration of water available as well as decreasing the pKa of the protonated imine. There has been work done on PEG conjugates with hydrophobic drugs, via an imine bond, to form micelles.[83,180]

Such a linker could prove beneficial for preparing a prodrug based on poly(L-lysine). This polypeptide has shown cytotoxic activity, via membrane disruption, as well as a cell-penetrating ability[125] under acidic pH. It has been shown that cell-penetrating peptides can improve the penetration of chemotherapy drugs within a tumor and even aid them in crossing the blood-brain barrier.[9]

Many hydrophilic polymers are used as components in drug delivery systems, PEG being the most common. Their main purpose is to provide solubility to the drug delivery system. Their steric hindrance and inert composition also provides the system with stealth properties against the body's reticuloendothelial system (RES).[32,96,96,141] There are a few disadvantages to using PEG. Firstly, it is prepared by anionic ring-opening polymerization, which requires extremely stringent reaction conditions. Secondly, it gradually becomes detectable by the RES with time.[96] For these reasons, other hydrophilic polymers have been developed for drug delivery systems. Poly(*N*-(2-hydroxypropyl)methacrylamide) and poly(*N*-vinylpyrrolidone) are two such polymers. They can be prepared by radical polymerization or RAFT-mediated polymerization. PVP has been shown to have longer circulation times than PEG.[141]

No literature has been found for the preparation of PVP-*block*-poly(L-lysine) block copolymers, for their behavior in aqueous solutions, the conjugation of chemotherapeutic compounds to them via imine bonds or their cell-penetrating ability. There have been some papers dealing with PEG-poly(L-lysine) block copolymers though their focus was on polyionic complex micelles for gene delivery.[43,181,182] An article also mentioned the use of these copolymers as carriers for MRI contrast agents by modifying the lysine residues with chelating agents.[183] There is also the pioneering work of Ringsdorf *et al.* that involved functionalizing some of the lysine residues of a PEG-poly(L-lysine) block copolymer with palmitic acid, via amide bond formation, to imbue sufficient hydrophobicity to the block so as to form micelles in aqueous solutions. They loaded these micelles with a cyclophosphamide-sulfido derivative prodrug and were able to fine-tune its release rate from minutes to hours.[182,184] Current methodologies for formulating prodrugs of CPPs involve incorporation of the CPPs as an intermediate phase between the hydrophilic and hydrophobic phases of polymeric micelles or within the core of a nanoparticle.[9] The CPPs are exposed when a labile linker connecting the hydrophilic polymer to the CPPs is cleaved or when the nanoparticle disintegrates. However, such ternary block copolymers usually require stringent and complicated synthesis procedures and these are limited by the compatibility of the functional groups on the CPP

and polymer chains. The only reports found of imine bonds being used in prodrug formulations are for crosslinking chitosan microcapsules with terephthalaldehyde[73] and for the conjugation of Doxorubicin to an aldehyde end-functional PEG via its daunosamine residue[179] as well as to the benzaldehyde residues of poly(1,2:3,4-di-*O*-isopropylidene-6-*O*-(2'-formyl-4'-vinylphenyl)-D-galactopyranose-*co*-5,6-benzo-2-methylene-1,3-dioxepane).[184] Thus this work will incorporate imine bonds to both the ketone and amine functional groups of Doxorubicin in order to maximize its hydrophobicity and prevent its oligomerization via Schiff base linkages.

2.6) References

1. International Agency for Research on Cancer GLOBOCAN, Estimated Cancer Incidence, Mortality and Prevalence Worldwide in 2012*
*. *http://globocan.iarc.fr/Default.aspx*2012).

2. Ferlay, J.; Shin, H. R.; Bray, F.; Forman, D.; Mathers, C.; Parkin, D. M. Estimates of worldwide burden of cancer in 2008: GLOBOCAN 2008. *Int. J. Cancer* **2010***, 127*, 2893-2917.

3. Waugh, A.; Grant, A. *Ross & Wilson Anatomy and Physiology in Health and Illness;* Elsevier: Amsterdam, 2010.

4. Clark, W. H. Tumour progression and the nature of cancer. *Br. J. Cancer* **1991***, 64*, 631.

5. Ko, A. H.; Dollinger, M.; Rosenbaum, E. H. *Everyone's Guide to Cancer Therapy;* Andrews McMeel Publishing: Missouri, 2002.

6. World Health Organisation Cancer - Health Topics. *http://www.who.int/topics/cancer/en/*2012).

7. National Cancer Institute Cancer. *http://www.cancer.gov/*2012).

8. Skeel, R. T. *Handbook of Cancer Chemotherapy;* Lippincott Williams & Wilkins: Philadelphia, 2007.

9. Kratz, F.; Senter, P.; Steinhagen, H. *Drug Delivery in Oncology: From Basic Research to Cancer Therapy;* Wiley-VCH Verlag & Co. KGaA: Weinheim, Germany, 2012.

10. Chiappa, A.; Bertani, E.; Makuuchi, M.; Zbar, A. P.; Contino, G.; Viale, G.; Pruneri, G.; Bellomi, M.; Della Vigna, P.; Zampino, M. G.; Fazio, N.; Travaini, M. L.; Trifiro, G.; Corbellini, C.; Andreoni, B. Neoadjuvant chemotherapy followed by hepatectomy for primarily resectable colorectal cancer liver metastases. *Hepatogastroenterology* **2009***, 56*, 829-834.

11. Kent, E. C.; Hussain, M. H. Neoadjuvant Therapy for Prostate Cancer: An Oncologist's Perspective. *Rev. Urol.* **2003***, 5 Suppl 3*, S28-37.

12. Razzaq, A. A.; Cohen, A. R. Neoadjuvant chemotherapy for hypervascular malignant brain tumors of childhood. *Pediatr. Neurosurg.* **1997***, 27*, 296-303.

13. Schott, A. F.; Hayes, D. F. Defining the benefits of neoadjuvant chemotherapy for breast cancer. *J. Clin. Oncol.* **2012**, *30*, 1747-1749.

14. Thillai, K.; Allan, S.; Powles, T.; Rudman, S.; Chowdhury, S. Neoadjuvant and adjuvant treatment of renal cell carcinoma. *Expert Rev. Anticancer Ther.* **2012**, *12*, 765-776.

15. Oettle, H.; Neuhaus, P.; Hochhaus, A.; Hartmann, J. T.; Gellert, K.; Ridwelski, K.; Niedergethmann, M.; Zulke, C.; Fahlke, J.; Arning, M. B.; Sinn, M.; Hinke, A.; Riess, H. Adjuvant chemotherapy with gemcitabine and long-term outcomes among patients with resected pancreatic cancer: the CONKO-001 randomized trial. *JAMA* **2013**, *310*, 1473-1481.

16. Iwagaki, H.; Tanaka, N.; Esato, K.; Kaibara, N.; Sano, K.; Dohi, K.; Toge, T.; Nakamura, T.; Nakasato, H.; Orita, K. Post-operative adjuvant chemotherapy for colorectal cancer with 5-fluorouracil (5-FU) infusion combined with 1-hexylcarbamoyl-5-fluorouracil (HCFU) oral administration after curative resection. *Anticancer Res.* **2001**, *21*, 4163-4168.

17. Coley, H. M. Overcoming multidrug resistance in cancer: clinical studies of p-glycoprotein inhibitors. *Methods Mol. Biol.* **2010**, *596*, 341-358.

18. Dallas, S.; Miller, D. S.; Bendayan, R. Multidrug Resistance-Associated Proteins: Expression and Function in the Central Nervous System. *Pharmacol. Rev.* **2006**, *58*, 140-161.

19. Di Pietro, A.; Dayan, G.; Conseil, G.; Steinfels, E.; Krell, T.; Trompier, D.; Baubichon-Cortay, H.; Jault, J. P-glycoprotein-mediated resistance to chemotherapy in cancer cells: using recombinant cytosolic domains to establish structure-function relationships. *Braz. J. Med. Biol. Res.* **1999**, *32*, 925-939.

20. Milane, L.; Ganesh, S.; Shah, S.; Duan, Z.; Amiji, M. Multi-modal strategies for overcoming tumor drug resistance: Hypoxia, the Warburg effect, stem cells, and multifunctional nanotechnology. *J. Control. Release* **2011**, *155*, 237-247.

21. Munoz, M.; Henderson, M.; Haber, M.; Norris, M. Role of the MRP1/ABCC1 Multidrug Transporter Protein in Cancer. *IUBMB Life* **2007**, *59*, 752-757.

22. Natarajan, K.; Xie, Y.; Baer, M. R.; Ross, D. D. Role of breast cancer resistance protein (BCRP/ABCG2) in cancer drug resistance. *Biochem. Pharmacol.* **2012**, *83*, 1084-1103.

23. Staud, F.; Pavek, P. Breast cancer resistance protein (BCRP/ABCG2). *Int. J. Biochem. Cell Biol.* **2005**, *37*, 720-725.

24. Persidis, A. Cancer multidrug resistance. *Nat. Biotech.* **1999**, *17*, 94-95.

25. O'Brien, D. I.; Nally, K.; Kelly, R. G.; O'Connor, T. M.; Shanahan, F.; O'Connell, J. Targeting the Fas/Fas ligand pathway in cancer. *Expert Opin. Ther. Targets* **2005**, *9*, 1031-1044.

26. Igney, F.; Krammer, P. Tumor counterattack: fact or fiction? *Cancer Immunol. Immunother.* **2005**, *54*, 1127-1136.

27. Pharmaceutical Society of Australia *Australian Medicines Handbook 2013;* Australian Medicines Handbook Pty. Limited: 2013.

28. Beijnen, J. H.; van der Houwen, O. A. G. J.; Underberg, W. J. M. Aspects of the degradation kinetics of doxorubicin in aqueous solution. *Int. J. Pharm.* **1986**, *32*, 123-131.

29. Vetvicka, D.; Hruby, M.; Hovorka, O.; Etrych, T.; Vetrik, M.; Kovar, L.; Kovar, M.; Ulbrich, K.; Rihova, B. Biological Evaluation of Polymeric Micelles with Covalently Bound Doxorubicin. *Bioconjugate Chem.* **2009**, *20*, 2090-2097.

30. Chytil, P.; Etrych, T.; Koňák, Č; Šírová, M.; Mrkvan, T.; Říhová, B.; Ulbrich, K. Properties of HPMA copolymer–doxorubicin conjugates with pH-controlled activation: Effect of polymer chain modification. *J. Control. Release* **2006**, *115*, 26-36.

31. Sirova, M.; Mrkvan, T.; Etrych, T.; Chytil, P.; Rossmann, P.; Ibrahimova, M.; Kovar, L.; Ulbrich, K.; Rihova, B. Preclinical Evaluation of Linear HPMA-Doxorubicin Conjugates with pH-Sensitive Drug Release: Efficacy, Safety, and Immunomodulating Activity in Murine Model. *Pharm. Res.* **2010**, *27*, 200-208.

32. Wang, B.; Teruna, S.; Soltero, R. A. *Drug Delivery: Principles and Applications;* John Wiley & Sons: New Jersy, 2005.

33. Prentis, R. A.; Lis, Y.; Walker, S. R. Pharmaceutical innovation by the seven UK-owned pharmaceutical companies (1964-1985). *Brit. J. Clin. Pharmaco.* **1988**, *25*, 387-396.

34. Mavromoustakos, T.; Durdagi, S.; Koukoulitsa, C.; Simcic, M.; Papadopoulos, M. G.; Hodoscek, M.; Grdadolnik, S. G. Strategies in the rational drug design. *Curr. Med. Chem.* **2011**, *18*, 2517-2530.

35. De Villiers, M. M.; Aramwit, P.; Kwon, G. S. *Nanotechnology in Drug Delivery;* Springer: New York, 2009.

36. Rao, C. N. R.; Cheetham, A. K. Science and technology of nanomaterials: current status and future prospects. *J. Mater. Chem.* **2001**, *11*, 2887-2894.

37. Rao, C. N. R.; Kulkarni, G. U.; Thomas, P. J.; Edwards, P. P. Size-Dependent Chemistry: Properties of Nanocrystals. *Chem. Eur. J.* **2002**, *8*, 28-35.

38. Roduner, E. Size matters: why nanomaterials are different. *Chem. Soc. Rev.* **2006**, *35*, 583-592.

39. Greish, K. Enhanced permeability and retention (EPR) effect for anticancer nanomedicine drug targeting. *Methods Mol. Biol.* **2010**, *624*, 25-37.

40. Huang, X.; Jain, P. K.; El-Sayed, I.; El-Sayed, M. Gold nanoparticles: interesting optical properties and recent applications in cancer diagnostics and therapy. *Nanomedicine* **2007**, *2*, 681-693.

41. Neuberger, T.; Schöpf, B.; Hofmann, H.; Hofmann, M.; von Rechenberg, B. Superparamagnetic nanoparticles for biomedical applications: Possibilities and limitations of a new drug delivery system. *J. Magn. Magn. Mater.* **2005**, *293*, 483-496.

42. Shen, Y.; Tang, B. Z.; Abd-El-Aziz, A. S.; Craig, S.; Dong, J.; Masuda, T.; Weder, C. *Functional Polymers for Nanomedicine;* Royal Society of Chemistry: Cambridge, 2013.

43. Harada-Shiba, M.; Yamauchi, K.; Harada, A.; Takamisawa, I.; Shimokado, K.; Kataoka, K. Polyion complex micelles as vectors in gene therapy--pharmacokinetics and in vivo gene transfer. *Gene Ther.* **2002***, 9*, 407-414.

44. Saiz, E.; Zimmermann, E. A.; Lee, J. S.; Wegst, U. G. K.; Tomsia, A. P. Perspectives on the role of nanotechnology in bone tissue engineering. *Dent. Mater.* **2013***, 29*, 103-115.

45. Danie Kingsley, J.; Ranjan, S.; Dasgupta, N.; Saha, P. Nanotechnology for tissue engineering: Need, techniques and applications. *J. Pharm. Res.* **2013***, 7*, 200-204.

46. Shilo, M.; Reuveni, T.; Motiei, M.; Popovtzer, R. Nanoparticles as computed tomography contrast agents: current status and future perspectives. *Nanomedicine (Lond)* **2012***, 7*, 257-269.

47. Goldberg, M.; Langer, R.; Jia, X. Nanostructured materials for applications in drug delivery and tissue engineering. *Journal of Biomaterials Science, Polymer Edition* **2007***, 18*, 241-268.

48. Kanazawa, H.; Kashiwase, Y.; Yamamoto, K.; Matsushima, Y.; Kikuchi, A.; Sakurai, Y.; Okano, T. Temperature-responsive liquid chromatography. 2. Effects of hydrophobic groups in N-isopropylacrylamide copolymer-modified silica. *Anal. Chem.* **1997***, 69*, 823-830.

49. Hosoya, K.; Sawada, E.; Kimata, K.; Araki, T.; Tanaka, N.; Frechet, J. M. J. In situ Surface-Selective Modification of Uniform Size Macroporous Polymer Particles with Temperature-Responsive Poly-N-isopropylacrylamide. *Macromolecules* **1994***, 27*, 3973-3976.

50. Malmstadt, N.; Yager, P.; Hoffman, A. S.; Stayton, P. S. A smart microfluidic affinity chromatography matrix composed of poly(N-isopropylacrylamide)-coated beads. *Anal. Chem.* **2003***, 75*, 2943-2949.

51. Ayano, E.; Nambu, K.; Sakamoto, C.; Kanazawa, H.; Kikuchi, A.; Okano, T. Aqueous chromatography system using pH- and temperature-responsive stationary phase with ion-exchange groups. *J. Chromatogr. A* **2006***, 1119*, 58-65.

52. Gugliuzza, A. Intelligent Membranes: Dream or Reality? *Membranes* **2013***, 3*, 151-154.

53. Nicoletta, F. P.; Cupelli, D.; Formoso, P.; De Filpo, G.; Colella, V.; Gugliuzza, A. Light Responsive Polymer Membranes: A Review. *Membranes* **2012***, 2*, 134-197.

54. Mateescu, A.; Wang, Y.; Dostalek, J.; Jonas, U. Thin Hydrogel Films for Optical Biosensor Applications. *Membranes* **2012***, 2*, 40-69.

55. Kavanagh, A.; Byrne, R.; Diamond, D.; Fraser, K. J. Stimuli Responsive Ionogels for Sensing Applications - An Overview. *Membranes* **2012***, 2*, 16-39.

56. Castellanos, A.; DuPont, S. J.; Heim, A. J.,2nd; Matthews, G.; Stroot, P. G.; Moreno, W.; Toomey, R. G. Size-Exclusion "capture and release" separations using surface-patterned poly(N-isopropylacrylamide) hydrogels. *Langmuir* **2007***, 23*, 6391-6395.

57. Suedee, R.; Seechamnanturakit, V.; Canyuk, B.; Ovatlarnporn, C.; Martin, G. P. Temperature sensitive dopamine-imprinted (N,N-methylene-bis-acrylamide cross-linked) polymer and its potential application to the selective extraction of adrenergic drugs from urine. *J. Chromatogr. A* **2006***, 1114*, 239-249.

58. Bawa, P.; Pillay, V.; Choonara, Y. E.; du Toit, L. C. Stimuli-responsive polymers and their applications in drug delivery. *Biomed. Mater.* **2009**, *4*, 022001-022016.

59. Lee, S.; Nguyen, S. T. Smart Nanoscale Drug Delivery Platforms from Stimuli-Responsive Polymers and Liposomes. *Macromolecules* **2013**, *46*, 9169-9180.

60. Meng, F.; Zhong, Z.; Feijen, J. Stimuli-Responsive Polymersomes for Programmed Drug Delivery. *Biomacromolecules* **2009**, *10*, 197-209.

61. Yang, J. Stimuli-responsive drug delivery systems. *Adv. Drug Deliv. Rev.* **2012**, *64*, 965-966.

62. Gil, E. S.; Hudson, S. M. Stimuli-reponsive polymers and their bioconjugates. *Prog. Polym. Sci.* **2004**, *29*, 1173-1222.

63. Singh, V.; Bushetti, S. S.; Appala, R.; Shareef, A.; Imam, S. S.; Singh, M. Stimuli-sensitive hydrogels: a novel ophthalmic drug delivery system. *Indian J. Ophthalmol.* **2010**, *58*, 477-481.

64. Masteikova, R.; Chalupova, Z.; Sklubalova, Z. Stimuli-sensitive hydrogels in controlled and sustained drug delivery. *Medicina (Kaunas)* **2003**, *39 Suppl 2*, 19-24.

65. MacEwan, S. R.; Callahan, D. J.; Chilkoti, A. Stimulus-responsive macromolecules and nanoparticles for cancer drug delivery. *Nanomedicine (Lond)* **2010**, *5*, 793-806.

66. Lee, E. S.; Shin, H. J.; Na, K.; Bae, Y. H. Poly(l-histidine)–PEG block copolymer micelles and pH-induced destabilization. *J. Control. Release* **2003**, *90*, 363-374.

67. Batrakova, E. V.; Kabanov, A. V. Pluronic block copolymers: Evolution of drug delivery concept from inert nanocarriers to biological response modifiers. *J. Control. Release* **2008**, *130*, 98-106.

68. Chen, X.; Cheng, X.; Soeriyadi, A. H.; Sagnella, S. M.; Lu, X.; Scott, J. A.; Lowe, S. B.; Kavallaris, M.; Gooding, J. J. Stimuli-responsive functionalized mesoporous silica nanoparticles for drug release in response to various biological stimuli. *Biomater. Sci.* **2014**, *2*, 121-130.

69. Yin, Q.; Shen, J.; Zhang, Z.; Yu, H.; Li, Y. Reversal of multidrug resistance by stimuli-responsive drug delivery systems for therapy of tumor. *Adv. Drug Deliv. Rev.* **2013**, *65*, 1699-1715.

70. Schmaljohann, D. Thermo- and pH-responsive polymers in drug delivery. *Adv. Drug Deliv. Rev.* **2006**, *58*, 1655-1670.

71. Jeong, B.; Gutowska, A. Lessons from nature: stimuli-responsive polymers and their biomedical applications. *Trends Biotechnol.* **2002**, *20*, 305-311.

72. Patchornik, A.; Berger, A.; Katchalski, E. Poly-L-histidine. *J. Am. Chem. Soc.* **1957**, *79*, 5227-5230.

73. Liu, L.; Yang, J.; Ju, X.; Xie, R.; Liu, Y.; Wang, W.; Zhang, J.; Niu, C. H.; Chu, L. Monodisperse core-shell chitosan microcapsules for pH-responsive burst release of hydrophobic drugs. *Soft Matter* **2011**, *7*, 4821-4827.

74. Thomas, G. *Fundamentals of Medicinal Chemistry;* John Wiley & Sons: West Sussex, 2003.

75. Khandare, J.; Minko, T. Polymer-drug conjugates: Progress in polymeric prodrugs. *Prog. Polym. Sci.* **2006**, *31*, 359-397.

76. Haag, R.; Kratz, F. Polymer Therapeutics: Concepts and Applications. *Angew. Chem. Int. Ed.* **2006**, *45*, 1198-1215.

77. Ringsdorf, H. Structure and properties of pharmacologically active polymers. *Journal of Polymer Science: Polymer Symposia* **1975**, *51*, 135-153.

78. York, A. W.; Kirkland, S. E.; McCormick, C. L. Advances in the synthesis of amphiphilic block copolymers via RAFT polymerization: Stimuli-responsive drug and gene delivery. *Adv. Drug Deliv. Rev.* **2008**, *60*, 1018-1036.

79. Alvarez-Lorenzo, C.; Concheiro, A. *Smart Materials for Drug Delivery;* The Royal Society of Chemistry: Cambridge, 2013; Vol. 1.

80. Choi, S. K.; Verma, M.; Silpe, J.; Moody, R. E.; Tang, K.; Hanson, J. J.; Baker, J. R.,Jr A photochemical approach for controlled drug release in targeted drug delivery. *Bioorg. Med. Chem.* **2012**, *20*, 1281-1290.

81. Hu, X.; Liu, S.; Huang, Y.; Chen, X.; Jing, X. Biodegradable Block Copolymer-Doxorubicin Conjugates via Different Linkages: Preparation, Characterization, and In Vitro Evaluation. *Biomacromolecules* **2010**, *11*, 2094-2102.

82. Simplício, A. L.; Clancy, J. M.; Gilmer, J. F. Prodrugs for Amines. *Molecules* **2008**, *13*, 519-547.

83. Ohya, Y.; Kuroda, H.; Hirai, K.; Ouchi, T. Synthesis and Cytotoxic Activity of Conjugates of Monomethoxy-Poly(Ethylene Glycol) End-Capped with Doxorubicin via Ester, Amide, or Schiffs Base Bond. *J. Bioact. Compat. Pol.* **1995**, *10*, 51-66.

84. Strebhardt, K.; Ullrich, A. Paul Ehrlich's magic bullet concept: 100 years of progress. *Nat. Rev. Cancer* **2008**, *8*, 473-480.

85. Maki, S.; Konno, T.; Maeda, H. Image enhancement in computerized tomography for sensitive diagnosis of liver cancer and semiquantitation of tumor selective drug targeting with oily contrast medium. *Cancer* **1985**, *56*, 751-757.

86. Nagamitsu, A.; Greish, K.; Maeda, H. Elevating Blood Pressure as a Strategy to Increase Tumor-targeted Delivery of Macromolecular Drug SMANCS: Cases of Advanced Solid Tumors. *Jpn. J. Clin. Oncol.* **2009**, *39*, 756-766.

87. Suzuki, M.; Hori, K.; Abe, I.; Saito, S.; Sato, H. Functional characterization of the microcirculation in tumors. *Cancer Metastasis Rev.* **1984**, *3*, 115-126.

88. Suzuki, M.; Hori, K.; Abe, I.; Saito, S.; Sato, H. A New Approach to Cancer Chemotherapy: Selective Enhancement of Tumor Blood Flow with Angiotensin II. *J. Natl. Cancer Inst.* **1981**, *67*, 663-669.

89. Seki, T.; Fang, J.; Maeda, H. Enhanced delivery of macromolecular antitumor drugs to tumors by nitroglycerin application. *Cancer. Sci.* **2009**, *100*, 2426-2430.

90. Maeda, H. Nitroglycerin enhances vascular blood flow and drug delivery in hypoxic tumor tissues: Analogy between angina pectoris and solid tumors and enhancement of the EPR effect. *J. Control. Release* **2010**, *142*, 296-298.

91. Yasuda, H.; Nakayama, K.; Watanabe, M.; Suzuki, S.; Fuji, H.; Okinaga, S.; Kanda, A.; Zayasu, K.; Sasaki, T.; Asada, M.; Suzuki, T.; Yoshida, M.; Yamanda, S.; Inoue, D.; Kaneta, T.; Kondo, T.; Takai, Y.; Sasaki, H.; Yanagihara, K.; Yamaya, M. Nitroglycerin Treatment May Enhance Chemosensitivity to Docetaxel and Carboplatin in Patients with Lung Adenocarcinoma. *Clin. Cancer Res.* **2006**, *12*, 6748-6757.

92. Korde Choudhari, S.; Chaudhary, M.; Bagde, S.; Gadbail, A.; Joshi, V. Nitric oxide and cancer: a review. *World. J. Surg. Oncol.* **2013**, *11*, 118.

93. Noguchi, A.; Takahashi, T.; Yamaguchi, T.; Kitamura, K.; Noguchi, A.; Tsurumi, H.; Takashina, K.; Maeda, H. Enhanced Tumor Localization of Monoclonal Antibody by Treatment with Kininase II Inhibitor and Angiotensin II. *Cancer. Sci.* **1992**, *83*, 240-243.

94. Tanaka, S.; Akaike, T.; Wu, J.; Fang, J.; Sawa, T.; Ogawa, M.; Beppu, T.; Maeda, H. Modulation of Tumor-selective Vascular Blood Flow and Extravasation by the Stable Prostaglandin I2 Analogue Beraprost Sodium. *J. Drug Target.* **2003**, *11*, 45-52.

95. Fang, J.; Qin, H.; Nakamura, H.; Tsukigawa, K.; Shin, T.; Maeda, H. Carbon monoxide, generated by heme oxygenase-1, mediates the enhanced permeability and retention effect in solid tumors. *Cancer. Sci.* **2012**, *103*, 535-541.

96. Hatakeyama, H.; Akita, H.; Harashima, H. The polyethyleneglycol dilemma: advantage and disadvantage of PEGylation of liposomes for systemic genes and nucleic acids delivery to tumors. *Biol. Pharm. Bull.* **2013**, *36*, 892-899.

97. Ishida, T.; Ichihara, M.; Wang, X.; Yamamoto, K.; Kimura, J.; Majima, E.; Kiwada, H. Injection of PEGylated liposomes in rats elicits PEG-specific IgM, which is responsible for rapid elimination of a second dose of PEGylated liposomes. *J. Control. Release* **2006**, *112*, 15-25.

98. Miele, E.; Spinelli, G. P.; Miele, E.; Tomao, F.; Tomao, S. Albumin-bound formulation of paclitaxel (Abraxane ABI-007) in the treatment of breast cancer. *Int. J. Nanomedicine* **2009**, *4*, 99-105.

99. Petrelli, F.; Borgonovo, K.; Barni, S. Targeted delivery for breast cancer therapy: the history of nanoparticle-albumin-bound paclitaxel. *Expert Opin. Pharmacother.* **2010**, *11*, 1413-1432.

100. Kenanova, V.; Olafsen, T.; Williams, L. E.; Ruel, N. H.; Longmate, J.; Yazaki, P. J.; Shively, J. E.; Colcher, D.; Raubitschek, A. A.; Wu, A. M. Radioiodinated versus Radiometal-Labeled Anti–Carcinoembryonic Antigen Single-Chain Fv-Fc Antibody Fragments: Optimal Pharmacokinetics for Therapy. *Cancer Research* **2007**, *67*, 718-726.

101. Olafsen, T.; Kenanova, V. E.; Sundaresan, G.; Anderson, A.; Crow, D.; Yazaki, P. J.; Li, L.; Press, M. F.; Gambhir, S. S.; Williams, L. E.; Wong, J. Y. C.; Raubitschek, A. A.; Shively, J. E.; Wu, A. M. Optimizing Radiolabeled Engineered Anti-p185HER2 Antibody Fragments for In vivo Imaging. *Cancer Research* **2005**, *65*, 5907-5916.

102. Kenanova, V.; Olafsen, T.; Crow, D. M.; Sundaresan, G.; Subbarayan, M.; Carter, N. H.; Ikle, D. N.; Yazaki, P. J.; Chatziioannou, A. F.; Gambhir, S. S.; Williams, L. E.; Shively, J. E.; Colcher, D.;

Raubitschek, A. A.; Wu, A. M. Tailoring the Pharmacokinetics and Positron Emission Tomography Imaging Properties of Anti–Carcinoembryonic Antigen Single-Chain Fv-Fc Antibody Fragments. *Cancer Research* **2005**, *65*, 622-631.

103. Scott, A. M.; Wolchok, J. D.; Old, L. J. Antibody therapy of cancer. *Nat. Rev. Cancer.* **2012**, *12*, 278-287.

104. Dranoff, G. Cytokines in cancer pathogenesis and cancer therapy. *Nat. Rev. Cancer.* **2004**, *4*, 11-22.

105. Normanno, N.; De Luca, A.; Bianco, C.; Strizzi, L.; Mancino, M.; Maiello, M. R.; Carotenuto, A.; De Feo, G.; Caponigro, F.; Salomon, D. S. Epidermal growth factor receptor (EGFR) signaling in cancer. *Gene* **2006**, *366*, 2-16.

106. Sitohy, B.; Nagy, J. A.; Dvorak, H. F. Anti-VEGF/VEGFR Therapy for Cancer: Reassessing the Target. *Cancer Research* **2012**, *72*, 1909-1914.

107. Rasmussen, U. B.; Schreiber, V.; Schultz, H.; Mischler, F.; Schughart, K. Tumor cell-targeting by phage-displayed peptides. *Cancer Gene Ther.* **2002**, *9*, 606-612.

108. Aina, O. H.; Marik, J.; Liu, R.; Lau, D. H.; Lam, K. S. Identification of novel targeting peptides for human ovarian cancer cells using "one-bead one-compound" combinatorial libraries. *Mol. Cancer. Ther.* **2005**, *4*, 806-813.

109. Lopci, E.; Nanni, C.; Rampin, L.; Rubello, D.; Fanti, S. Clinical applications of 68Ga-DOTANOC in neuroendocrine tumours. *Minerva Endocrinol.* **2008**, *33*, 277-281.

110. Emons, G.; Sindermann, H.; Engel, J.; Schally, A. V.; Grundker, C. Luteinizing hormone-releasing hormone receptor-targeted chemotherapy using AN-152. *Neuroendocrinology* **2009**, *90*, 15-18.

111. Temming, K.; Schiffelers, R. M.; Molema, G.; Kok, R. J. RGD-based strategies for selective delivery of therapeutics and imaging agents to the tumour vasculature. *Drug Resist. Updat.* **2005**, *8*, 381-402.

112. Chen, K.; Chen, X. Integrin Targeted Delivery of Chemotherapeutics. *Theranostics* **2011**, *1*, 189-200.

113. Johansson, E. M. V.; Dubois, J.; Darbre, T.; Reymond, J. Glycopeptide dendrimer colchicine conjugates targeting cancer cells. *Bioorg. Med. Chem.* **2010**, *18*, 6589-6597.

114. Avendaño, C.; Menéndez, J. C. Peptidomimetics in cancer chemotherapy. *Clin. Transl. Oncol.* **2007**, *9*, 563-570.

115. Zwicke, G., Mansoori, G., Jeffery,C. Utilizing the folate receptor for active targeting of cancer nanotherapeutics. *Nano Reviews* **2012**, *3*.

116. Zhang, Y.; Hong, H.; Cai, W. Tumor-targeted drug delivery with aptamers. *Curr. Med. Chem.* **2011**, *18*, 4185-4194.

117. Fang, X.; Tan, W. Aptamers Generated from Cell-SELEX for Molecular Medicine: A Chemical Biology Approach. *Acc. Chem. Res.* **2010**, *43*, 48-57.

118. Shinkaruk, S.; Bayle, M.; Lain, G.; Deleris, G. Vascular endothelial cell growth factor (VEGF), an emerging target for cancer chemotherapy. *Curr. Med. Chem. Anticancer Agents* **2003**, *3*, 95-117.

119. Ma, Q.; Lu, A. Y. H. Pharmacogenetics, Pharmacogenomics, and Individualized Medicine. *Pharmacol. Rev.* **2011**, *63*, 437-459.

120. Lungwitz, U.; Breunig, M.; Blunk, T.; Göpferich, A. Polyethylenimine-based non-viral gene delivery systems. *Eur. J. Pharm. Biopharm.* **2005**, *60*, 247-266.

121. Wyrsta, M. D.; Cogen, A. L.; Deming, T. J. A Parallel Synthetic Approach for the Analysis of Membrane Interactive Copolypeptides. *J. Am. Chem. Soc.* **2001**, *123*, 12919-12920.

122. Wiradharma, N.; Khoe, U.; Hauser, C. A. E.; Seow, S. V.; Zhang, S.; Yang, Y. Synthetic cationic amphiphilic α-helical peptides as antimicrobial agents. *Biomaterials* **2011**, *32*, 2204-2212.

123. Frankel, A. D.; Pabo, C. O. Cellular uptake of the tat protein from human immunodeficiency virus. *Cell* **1988**, *55*, 1189-1193.

124. Copolovici, D. M.; Langel, K.; Eriste, E.; Langel, Ã Cell-Penetrating Peptides: Design, Synthesis, and Applications. *ACS Nano* **2014**, *8*, 1972-1994.

125. Han, K.; Jeon, M. J.; Kim, S. H.; Ki, D.; Bahn, J. H.; Lee, K. S.; Park, J.; Choi, S. Y. Efficient intracellular delivery of an exogenous protein GFP with genetically fused basic oligopeptides. *Mol. Cells* **2001**, *12*, 267-271.

126. Bechara, C.; Sagan, S. Cell-penetrating peptides: 20 years later, where do we stand? *FEBS Lett.* **2013**, *587*, 1693-1702.

127. Mazel, M.; Clair, P.; Rousselle, C.; Vidal, P.; Scherrmann, J.; Mathieu, D.; Temsamani, J. Doxorubicin-peptide conjugates overcome multidrug resistance. *Anticancer Drugs* **2001**, *12*.

128. Nakase, I.; Konishi, Y.; Ueda, M.; Saji, H.; Futaki, S. Accumulation of arginine-rich cell-penetrating peptides in tumors and the potential for anticancer drug delivery in vivo. *J. Control. Release* **2012**, *159*, 181-188.

129. Aroui, S.; Ram, N.; Appaix, F.; Ronjat, M.; Kenani, A.; Pirollet, F.; Waard, M. Maurocalcine as a Non Toxic Drug Carrier Overcomes Doxorubicin Resistance in the Cancer Cell Line MDA-MB 231. *Pharm. Res.* **2009**, *26*, 836-845.

130. Aroui, S.; Brahim, S.; Waard, M. D.; Kenani, A. Cytotoxicity, intracellular distribution and uptake of doxorubicin and doxorubicin coupled to cell-penetrating peptides in different cell lines: A comparative study. *Biochem. Biophys. Res. Commun.* **2010**, *391*, 419-425.

131. Castex, C.; Merida, P.; Blanc, E.; Clair, P.; Rees, A. R.; Temsamani, J. 2-Pyrrolinodoxorubicin and its peptide-vectorized form bypass multidrug resistance. *Anticancer Drugs* **2004**, *15*.

132. Nori, A.; Jensen, K. D.; Tijerina, M.; Kopečková, P.; Kopeček, J. Tat-Conjugated Synthetic Macromolecules Facilitate Cytoplasmic Drug Delivery To Human Ovarian Carcinoma Cells. *Bioconjugate Chem.* **2003**, *14*, 44-50.

133. Rousselle, C.; Clair, P.; Lefauconnier, J.; Kaczorek, M.; Scherrmann, J.; Temsamani, J. New Advances in the Transport of Doxorubicin through the Blood-Brain Barrier by a Peptide Vector-Mediated Strategy. *Molecular Pharmacology* **2000**, *57*, 679-686.

134. Laakkonen, P.; Åkerman, M. E.; Biliran, H.; Yang, M.; Ferrer, F.; Karpanen, T.; Hoffman, R. M.; Ruoslahti, E. Antitumor activity of a homing peptide that targets tumor lymphatics and tumor cells. *Proceedings of the National Academy of Sciences of the United States of America* **2004**, *101*, 9381-9386.

135. Midgley, C. A.; Desterro, J. M. P.; Saville, M. K.; Howard, S.; Sparks, A.; Hay, R. T.; Lane, D. P. An N-terminal $p14^{ARF}$ peptide blocks Mdm2-dependent ubiquitination *in vitro* and can activate p53 *in vivo*. *Oncogene* **2000**, *19*, 2312-2323.

136. Johansson, H. J.; El-Andaloussi, S.; Holm, T.; Mae, M.; Janes, J.; Maimets, T.; Langel, U. Characterization of a Novel Cytotoxic Cell-penetrating Peptide Derived From p14ARF Protein. *Mol. Ther.* **2007**, *16*, 115-123.

137. Vallespi, M. G.; Fernandez, J. R.; Torrens, I.; Garcia, I.; Garay, H.; Mendoza, O.; Granadillo, M.; Falcon, V.; Acevedo, B.; Ubieta, R.; Guillen, G. E.; Reyes, O. Identification of a novel antitumor peptide based on the screening of an Ala-library derived from the LALF32?51 region. *J. Pept. Sci.* **2010**, *16*, 40-47.

138. Nesvadba, P. *Radical Polymerization in Industry;* Encyclopedia of Radicals in Chemistry, Biology and Materials; John Wiley & Sons, Ltd, 2012.

139. Odian, G. *Principles of Polymerization;* John Wiley & Sons, Inc.: Hoboken, New Jersey, 2004.

140. Matyjaszewski, K.; Davis, T. P. *Handbook of Radical Polymerization;* John Wiley and Sons.inc: Hoboken, New Jersey, 2002.

141. Kaneda, Y.; Tsutsumi, Y.; Yoshioka, Y.; Kamada, H.; Yamamoto, Y.; Kodaira, H.; Tsunoda, S.; Okamoto, T.; Mukai, Y.; Shibata, H.; Nakagawa, S.; Mayumi, T. The use of PVP as a polymeric carrier to improve the plasma half-life of drugs. *Biomaterials* **2004**, *25*, 3259-3266.

142. Ranucci, E.; Macchi, L.; Annunziata, R.; Ferruti, P.; Chiellini, F. End-Functionalised 1-Vinyl-2-Pyrrolidinone Oligomers Bearing Lactate Functions at One End. *Macromol. Biosci.* **2004**, *4*, 706-713.

143. Gärtner, K.; Vogel, G.; Ulbrich, M. Untersuchungen zur Penetration von Makromolekülen (Polyvinylpyrrolidon) durch glomeruläre und postglomeruläre Capillaren in den Harn und die Nierenlymphe und zur Größe der extravasalen Umwälzung von 131J-Albumin im Interstitium der Niere. *Pflüger's Archiv* **1968**, *298*, 305-321.

144. Wessel, W.; Schoog, M.; Winkler, E. Polyvinylpyrrolidone (PVP), its diagnostic, therapeutic and technical application and consequences thereof. *Arzneimittel-Forschung* **1971**, *21*, 1468-1482.

145. Bilalis, P.; Pitsikalis, M.; Hadjichristidis, N. Controlled nitroxide-mediated and reversible addition-fragmentation chain transfer polymerization of N-vinylpyrrolidone: Synthesis of block copolymers with styrene and 2-vinylpyridine. *J. Polym. Sci. A Polym. Chem.* **2006**, *44*, 659-665.

146. Matyjaszewski, K. Atom Transfer Radical Polymerization (ATRP): Current Status and Future Perspectives. *Macromolecules* **2012**, *45*, 4015-4039.

147. Lu, X.; Gong, S.; Meng, L.; Li, C.; Yang, S.; Zhang, L. Controllable synthesis of poly(N-vinylpyrrolidone) and its block copolymers by atom transfer radical polymerization. *Polymer* **2007**, *48*, 2835-2842.

148. Yamago, S.; Ray, B.; Iida, K.; Yoshida, J.; Tada, T.; Yoshizawa, K.; Kwak, Y.; Goto, A.; Fukuda, T. Highly Versatile Organostibine Mediators for Living Radical Polymerization. *J. Am. Chem. Soc.* **2004**, *126*, 13908-13909.

149. Ray, B.; Kotani, M.; Yamago, S. Highly Controlled Synthesis of Poly(N-vinylpyrrolidone) and Its Block Copolymers by Organostibine-Mediated Living Radical Polymerization. *Macromolecules* **2006**, *39*, 5259-5265.

150. Yusa, S.; Yamago, S.; Sugahara, M.; Morikawa, S.; Yamamoto, T.; Morishima, Y. Thermo-Responsive Diblock Copolymers of Poly(N-isopropylacrylamide) and Poly(N-vinyl-2-pyrroridone) Synthesized via Organotellurium-Mediated Controlled Radical Polymerization (TERP). *Macromolecules* **2007**, *40*, 5907-5915.

151. Moad, G.; Rizzardo, E.; Thang, S. H. Living Radical Polymerization by the RAFT Process. *Aust. J. Chem.* **2005**, *58*, 379-410.

152. Postma, A.; Davis, T. P.; Li, G.; Moad, G.; O'Shea, M. S. RAFT Polymerization with Phthalimidylmethyl Trithiocarbonates or Xanthates. On the Origin of Bimodal Molecular Weight Distributions in Living Radical Polymerization. *Macromolecules* **2006**, *39*, 5307-5318.

153. Kowollik, C. B. *Handbook of RAFT Polymerization;* WILEY-VCH Verlag GmbH & Co. KGaA: Weinheim, Baden-Württemberg, 2008.

154. Pound, G.; McLeary, J. B.; McKenzie, J. M.; Lange, R. F. M.; Klumperman, B. In-Situ NMR Spectroscopy for Probing the Efficiency of RAFT/MADIX Agents. *Macromolecules* **2006**, *39*, 7796-7797.

155. Pound, G.; McKenzie, J. M.; Lange, R. F. M.; Klumperman, B. Polymer-protein conjugates from small omega]-aldehyde endfunctional poly(N-vinylpyrrolidone) synthesised via xanthate-mediated living radical polymerisation. *Chem. Commun.* **2008**, 3193-3195.

156. Smith, K. A.; Lin, Y.; Dement, D. B.; Strzalka, J.; Darling, S. B.; Pickel, D. L.; Verduzco, R. Synthesis and Crystallinity of Conjugated Block Copolymers Prepared by Click Chemistry. *Macromolecules* **2013**, *46*, 2636-2645.

157. Quemener, D.; Davis, T. P.; Barner-Kowollik, C.; Stenzel, M. H. RAFT and click chemistry: A versatile approach to well-defined block copolymers. *Chem. Commun.* **2006**, 5051-5053.

158. Benaglia, M.; Chiefari, J.; Chong, Y. K.; Moad, G.; Rizzardo, E.; Thang, S. H. Universal (Switchable) RAFT Agents. *J. Am. Chem. Soc.* **2009**, *131*, 6914-6915.

159. Dubois, P.; Coulembier, O.; Raquez, J. M. *Handbook of Ring-Opening Polymerization;* Wiley: 2009.

160. Kricheldorf, H. R. Polypeptides and 100 Years of Chemistry of α-Amino Acid N-Carboxyanhydrides. *Angew. Chem. Int. Ed.* **2006**, *45*, 5752-5784.

161. Chiellini, E. *Biomedical Polymers and Polymer Therapeutics;* Springer: 2001.

162. Leuchs, H. Ueber die Glycin-carbonsäure. *Ber. Dtsch. Chem. Ges.* **1906**, *39*, 857-861.

163. Kricheldorf, H. R.; Fehrle, M. N-(2-Nitrophenylsulfenyl)-α-amino Acid N-Carboxy Anhydrides (NPS-α-NCAs). *Chem. Ber.* **1974**, *107*, 3533-3547.

164. Benoiton, N. L. *Chemistry of Peptide Synthesis;* Taylor & Francis Group, LLC: United States of America, 2006.

165. Xue, C. B.; Naider, F. Application of N-(tert-butyloxycarbonyl)amino acid N-carboxyanhydrides in solid-phase peptide synthesis. *J. Org. Chem.* **1993**, *58*, 350-355.

166. Fuller, W. D.; Cohen, M. P.; Shabankareh, M.; Blair, R. K.; Goodman, M.; Naider, F. R. Urethane protected amino acid N-carboxyanhydrides and their use in peptide synthesis. *J. Am. Chem. Soc.* **1990**, *112*, 7414-7416.

167. Cheng, J.; Deming, T. J. In *Synthesis of Polypeptides by Ring-Opening Polymerization of α-Amino Acid N-Carboxyanhydrides;* Deming, T., Ed.; Peptide-Based Materials; Springer Berlin Heidelberg: 2012; Vol. 310, pp 1-26.

168. Habraken, G. J. M.; Peeters, M.; Dietz, C. H. J. T.; Koning, C. E.; Heise, A. How controlled and versatile is N-carboxy anhydride (NCA) polymerization at 0°C? Effect of temperature on homo-, block- and graft (co)polymerization. *Polym. Chem.* **2010**, *1*, 514-524.

169. Habraken, G. J. M.; Wilsens, K. H. R. M.; Koning, C. E.; Heise, A. Optimization of N-carboxyanhydride (NCA) polymerization by variation of reaction temperature and pressure. *Polym. Chem.* **2011**, *2*, 1322-1330.

170. Deming, T. J. Facile synthesis of block copolypeptides of defined architecture. *Nature* **1997**, *390*, 386-389.

171. Deming, T. J. Cobalt and Iron Initiators for the Controlled Polymerization of α-Amino Acid-N-Carboxyanhydrides. *Macromolecules* **1999**, *32*, 4500-4502.

172. Deming, T. J. Amino Acid Derived Nickelacycles: Intermediates in Nickel-Mediated Polypeptide Synthesis. *J. Am. Chem. Soc.* **1998**, *120*, 4240-4241.

173. Curtin, S. A.; Deming, T. J. Initiators for End-Group Functionalized Polypeptides via Tandem Addition Reactions. *J. Am. Chem. Soc.* **1999**, *121*, 7427-7428.

174. Lu, H.; Wang, J.; Lin, Y.; Cheng, J. One-Pot Synthesis of Brush-Like Polymers via Integrated Ring-Opening Metathesis Polymerization and Polymerization of Amino Acid N-Carboxyanhydrides. *J. Am. Chem. Soc.* **2009**, *131*, 13582-13583.

175. Li, C. Poly(l-glutamic acid)–anticancer drug conjugates. *Adv. Drug Deliv. Rev.* **2002**, *54*, 695-713.

176. Tsutsumi, A.; Perly, B.; Forchioni, A.; Chachaty, C. A Magnetic Resonance Study of the Segmental Motion and Local Conformations of Poly(L-glutamic acid) in Aqueous Solutions. *Macromolecules* **1978**, *11*, 977-986.

177. Hurwitz, E.; Wilchek, M.; Pitha, J. Soluble Macromolecules as Carriers for Daunorubicin. *J. Appl. Biochem.* **1980**, *2*, 25-35.

178. Dumitrui, S. *Polymeric Biomaterials;* Marcel Dekker, Inc.: United States of America, 2002.

179. Saito, H.; Hoffman, A. S.; Ogawa, H. I. Delivery of Doxorubicin from Biodegradable PEG Hydrogels Having Schiff Base Linkages. *J. Bioact. Compat. Pol.* **2007**, *22*, 589-601.

180. Toncheva, V.; Wolfert, M. A.; Dash, P. R.; Oupicky, D.; Ulbrich, K.; Seymour, L. W.; Schacht, E. H. Novel vectors for gene delivery formed by self-assembly of DNA with poly(L-lysine) grafted with hydrophilic polymers. *Biochim. Biophys. Acta* **1998**, *1380*, 354-368.

181. Lavasanifar, A.; Samuel, J.; Kwon, G. S. Poly(ethylene oxide)-block-poly(l-amino acid) micelles for drug delivery. *Adv. Drug Deliv. Rev.* **2002**, *54*, 169-190.

182. Shiraishi, K.; Kawano, K.; Minowa, T.; Maitani, Y.; Yokoyama, M. Preparation and in vivo imaging of PEG-poly(L-lysine)-based polymeric micelle MRI contrast agents. *J. Control. Release* **2009**, *136*, 14-20.

183. Finch, C. A. Book Review: Bioactive polymeric systems-an overview. *Brit. Polym. J.* **1988**, *20*, 166-166.

184. Xiao, N.; Liang, H.; Lu, J. Degradable and biocompatible aldehyde-functionalized glycopolymer conjugated with doxorubicinvia acid-labile Schiff base linkage for pH-triggered drug release. *Soft Matter* **2011**, *7*, 10834-10840.

CHAPTER 3

RAFT-Mediated Polymerization of *N*-vinylpyrrolidone with *O*-ethyl-*S*-(phthalimidylmethyl)xanthate Performed in Batch-Mode

3.1) Introduction

This chapter focuses on the preparation of PVP with a low dispersity (*Đ*) and a free primary amine α-end-group by a RAFT-mediated polymerization. Amines are not compatible with RAFT agents as they readily attack the thiocarbonyl carbon, resulting in elimination of the R-group thiol and, in the case of xanthates, formation of an *O*-thiocarbamate.[1] By using a protecting group that masks the nucleophilicity of the amine, the RAFT-mediated polymerization with a protected amine-functionalized RAFT agent is feasible and the desired amine-functionalized polymer could be obtained by removal of the protecting group. This was attempted using a RAFT-mediated polymerization of NVP with *O*-ethyl-*S*-(phthalimidylmethyl)xanthate (XA2).[2] The phthalimide-functionalized R-group of this RAFT agent can be converted to a primary amine by reacting with hydrazine in methanol.[3,4] Alternatively, it can be removed by a two-step process that involves reduction with sodium borohydride and subsequent acidic or basic hydrolysis of the *O*-hydroxymethylbenzamide.[4-6] The amine α-end-group functionalized PVP was intended for use as a macroinitiator during the ring-opening polymerization of N^{ϵ}-(benzyloxycarbonyl)-L-lysine *N*-carboxyanhydride.

In order to get a fundamental idea of the kinetic parameters for the XA2-mediated polymerization of NVP, several trials were performed at different monomer to RAFT agent ratios. An *in-situ* ^{1}H-NMR polymerization was carried out for the trial with the lowest monomer to RAFT agent ratio.

The RAFT-mediated polymerization of NVP with XA2 was first described by Postma *et al.*[2] Polymers with number-average molecular weights (M_n) over 13,000 g/mol were obtained using a monomer to RAFT agent ratio ($\frac{[NVP]}{[XA2]}$ = R) of 517. These had a dispersity (*Đ*) around 1.5, indicating inadequate control of the polymerization. Their second highest monomer to RAFT agent ratio was 92. The polymers obtained by these trials had M_n between 5,000 g/mol and 9,000 g/mol with *Đ* around 1.2.

Two trials, using R = 117 and R = 196, were performed by our group in order to better assess if PVP with M_n above 10,000 g/mol and *Đ* < 1.3 could be obtained by a RAFT-mediated polymerization of NVP with XA2.

3.2) Materials and Experimental Methods

N-Vinylpyrrolidone (NVP) was purchased from Merck and vacuum distilled over 5% ground potassium hydroxide before use. Azobisisobutyronitrile (AIBN) was purchased from Merck and recrystallized from methanol before use. Potassium *O*-ethyldithiocarbonate, anhydrous calcium chloride, anhydrous magnesium sulfate, anhydrous calcium sulfate, potassium hydroxide pellets, concentrated sulfuric acid (95 – 97%) and sodium metal were purchased from Merck and used as received. A seven inch Wilmad® quick pressure valve medium wall NMR tube with a 5 mm diameter, *N*-(bromomethyl)phthalimide, benzophenone, *N,N*-dimethylacetamide (DMAC, Chromosolv® Plus, for HPLC ≥ 99.9%), butylated hydroxytoluene (BHT) 99% (GC) and chloroform-d 99.8 atom % were purchased from Sigma Aldrich and used as received. Benzene-d6 (99.6 atom %) was purchased from ACROS Organics and used as received. Methanol, chloroform ($CHCl_3$), dichloromethane (DCM) and diethyl ether were purchased from KIMIX. Methanol was fractionally distilled before use. Chloroform and dichloromethane were washed with concentrated sulfuric acid followed by 5% sodium bicarbonate solution and finally water before being dried over calcium chloride and fractionally distilled from calcium sulfate. Diethyl ether was distilled from sodium and benzophenone. Lithium chloride ≥ 98% was purchased from Riedel-de Haën and used as is. 0.45 µm Glass fiber prefilters were purchased from PALL Life Sciences.

3.2.1) Synthesis of XA2

XA2 was synthesized as published by Postma *et al.*[2] Potassium *O*-ethyldithiocarbonate (5.15 g, 3.21×10^{-2} mol) was suspended in 200 mL chloroform and *N*-(bromomethyl)phthalimide (5.00 g, 2.08×10^{-2} mol) was added. The solution was stirred at room temperature for 14 hours overnight. The solution was then filtered, washed with 2×50 mL de-ionized water followed by 50 mL saturated calcium chloride solution and dried over magnesium sulfate. After filtering the solution, the solvent was removed by rotary evaporation. Product yield: 5.56 g (95%). ^{1}H-NMR (300 MHz, $CDCl_3$): δ = 1.46 (tr, 7.1 Hz, 3H), 4.68 (q, 7.1 Hz, 2H), 5.33 (s, 2H), 7.75 (m, 2H), 7.85 (m, 2H).

3.2.2) RAFT-Mediated Polymerization of NVP with XA2 – R = 196

NVP (2.0 g, 1.8×10^{-2} mol), XA2 (0.025 g, 8.89×10^{-5} mol) and AIBN (0.003 g, 1.83×10^{-5} mol) were placed in a Schlenk tube which was capped with a rubber septum. This ratio should give a monomer to XA2 ratio (R) of 202. R was confirmed by ^{1}H-NMR to be 196. Three freeze-pump-thaw cycles were

performed. The Schlenk tube was back-filled with argon and placed in an oil bath which was regulated at 65 °C by a thermocouple. Samples for NMR and SEC were taken using a syringe that had been purged with argon. The samples were taken after reaction times of 120 minutes, 240 minutes and 345 minutes.

The polymer was isolated from the reaction mixture by precipitation in diethyl ether. Dichloromethane was used as a solvent to aid in the precipitation process. The precipitate was separated by centrifugation at 2500 rpm for 3 minutes, washed with a small portion of diethyl ether, separated again by centrifugation and dried under vacuum.

3.2.3) RAFT-Mediated Polymerization of NVP with XA2 – R = 117

NVP (2.000 g, 1.80×10^{-2} mol), XA2 (0.042 g, 1.49×10^{-4} mol) and AIBN (0.0034 g, 2.07×10^{-5} mol) were placed in a Schlenk tube which was capped with a rubber septum. R = 117 according to NMR. Three freeze-pump-thaw cycles were performed. The Schlenk tube was back-filled with argon and placed in an oil bath which was regulated at 65 °C by a thermocouple. Samples were taken for NMR and SEC analysis after 50 minutes, 110 minutes, 185 minutes and 245 minutes. Isolation of the polymer from the reaction mixture was performed as described in Section 3.2.2.

3.2.4) ^{1}H-NMR *In-situ* Polymerization of NVP with XA2 – R = 5

NVP (0.300 g, 2.7×10^{-3} mol), XA2 (0.152 g, 5.4×10^{-4} mol) and AIBN (0.009 g, 5.48×10^{-5} mol) were added to 0.5 mL benzene-d6. R = 5 for this reaction. The volume of the solution was measured (0.89 mL.) 0.7 mL of the solution was placed in a Wilmad® quick pressure valve NMR tube and three freeze-pump-thaw cycles were performed on the sample. The tube was back-filled with argon and placed in a Varian 400 MHz Inova NMR spectrometer. A spectrum of the initial conditions was taken at 25 °C before switching the variable temperature flow gas to nitrogen, removing the sample from the spectrometer and raising the temperature to 65 °C. The polymerization was performed at 65 °C as this was the temperature at which the calculated half-life of AIBN was 10 hours (see Section 4.2). Once the temperature had stabilized, the sample was inserted. The time required for shimming the magnetic field and adjusting the deuterium feedback loop was recorded.

The spectrometer was programmed to take an array of spectra, recording a scan every 5 minutes for 10 hours. Each scan was taken using 4 transients, with an acquisition time of 4 seconds and relaxation delay of 1 second. The pre-acquisition delay between scans was set to 280 seconds.

3.2.5) SEC Analysis

Each SEC sample was prepared by dissolving approximately 2 mg of the isolated polymer in 1.5 mL of dimethylacetamide (HPLC grade) containing 0.05% (w/v) BHT and 0.03% (w/v) lithium chloride. The samples were filtered through a 0.45 µm glass fiber prefilter before analysis. A Waters 717 Plus autosampler connected to a Shimadzu LC-10AT pump was used with the following column configuration: 1×PSS GRAM analytical precolumn (10 µm particle size, 8.0×50 mm), 1×PSS GRAM analytical column (10 µm particle size, 100 Å pore size, 8.0×300 mm), 2×PSS GRAM analytical columns (10 µm particle size, 3000 Å pore size, 8.0×300 mm.) A Waters 2487 dual wavelength absorbance detector and a Waters 410 differential refractometer were connected in series. The dwell time between the detectors was 18 seconds. The temperature of the column oven was set to 40 °C and the flow rate was 1 mL per minute. The instrument was calibrated using peak position calibration with narrow, linear poly(methyl methacrylate) (PMMA) standards.

3.2.6) NMR Analysis

Unless otherwise stated, both the reaction mixture and the isolated polymer samples were analyzed using ^{1}H-NMR spectroscopy. $CDCl_3$ was used as the solvent. All NMR spectra were taken using a Varian 300 MHz VNMRS, Varian 400 MHz Inova or Varian 600 MHz Unity spectrometer. ^{1}H-NMR analysis of the reaction mixtures taken at different time intervals was used to determine the NVP and XA2 conversions with reaction time. ^{1}H-NMR analysis of the isolated polymer samples was used to confirm that the phthalimide and xanthate functionalities were incorporated into the polymer as well as compare their relative abundance. Unless otherwise stated, all PVP samples were dissolved in $CDCl_3$, with a concentration of approximately 15 mg per mL.

3.3) Results and Discussion

3.3.1) Analysis of Polymers Prepared in Sections 3.2.2 and 3.2.3

NMR Analysis

Figure 3.1 shows the ^{1}H-NMR spectra of the reaction mixture at A) 0% and B) 50% monomer conversion for the trial with R = 196.

By normalizing the peaks for the aromatic phthalimide protons of XA2 (a and b) to 4.00, the change in signal intensity could be computed for the vinyl protons of the monomer (f) as well as for the methylene protons on XA2 (d).

[NVP] at each time interval was calculated using Equation 3.1:

$$\frac{[NVP]_t}{[NVP]_0} = \frac{2\times\int_{\delta=4.21}^{\delta=4.56} F(\delta)d\delta}{R\times\int_{\delta=7.68}^{\delta=7.89} F(\delta)d\delta} \tag{3.1}$$

[XA2] at each time interval was computed using Equation 3.2:

$$\frac{[XA2]_t}{[XA2]_0} = \frac{2\times\int_{\delta=5.29}^{\delta=5.37} F(\delta)d\delta}{\int_{\delta=7.68}^{\delta=7.89} F(\delta)d\delta} \tag{3.2}$$

Figure 3.2 shows the ^{1}H-NMR spectrum for the polymer isolated from the sample taken at 50 percent monomer conversion for the trial with R = 196. Since the phthalimide protons of the R-group could only be present after isolation of the polymer if they were part of the polymer chain, they could be used as an internal reference for the number of polymer chains. However, isolation of the polymer from the reaction mixture could affect M_n by partial fractionation of the low molecular weight chains into the non-solvent. Hence, $M_{n,NMR}$ was calculated from the crude polymer samples. The conversion of XA2 had to be taken into account.

The degree of polymerization (DP) in the samples of the reaction mixture was calculated using Equation 3.3.

$$DP = \frac{4\times\left(\int_{\delta=2.90}^{\delta=4.20} F(\delta)d\delta - \int_{\delta=4.26}^{\delta=4.56} F(\delta)d\delta\right)}{3\times\int_{\delta=7.68}^{\delta=7.89} F(\delta)d\delta\times\left(1-0.5\times\int_{\delta=5.32}^{\delta=5.38} F(\delta)d\delta\right)} \tag{3.3}$$

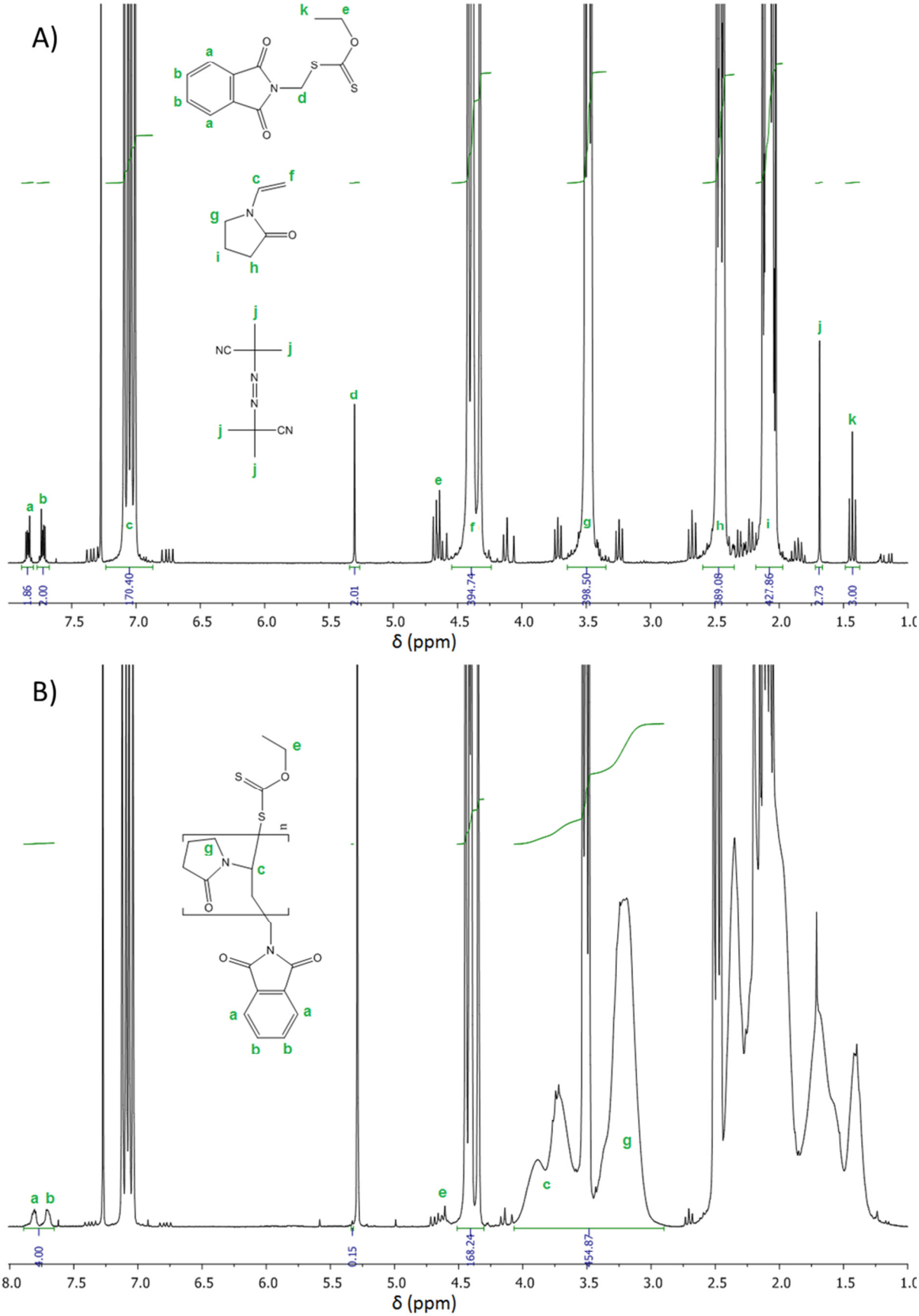

Figure 3.1: ^{1}H-NMR Spectra for the Reaction Mixture of the Trial with R = 196. A) Initial Conditions. B) 50% Monomer Conversion.

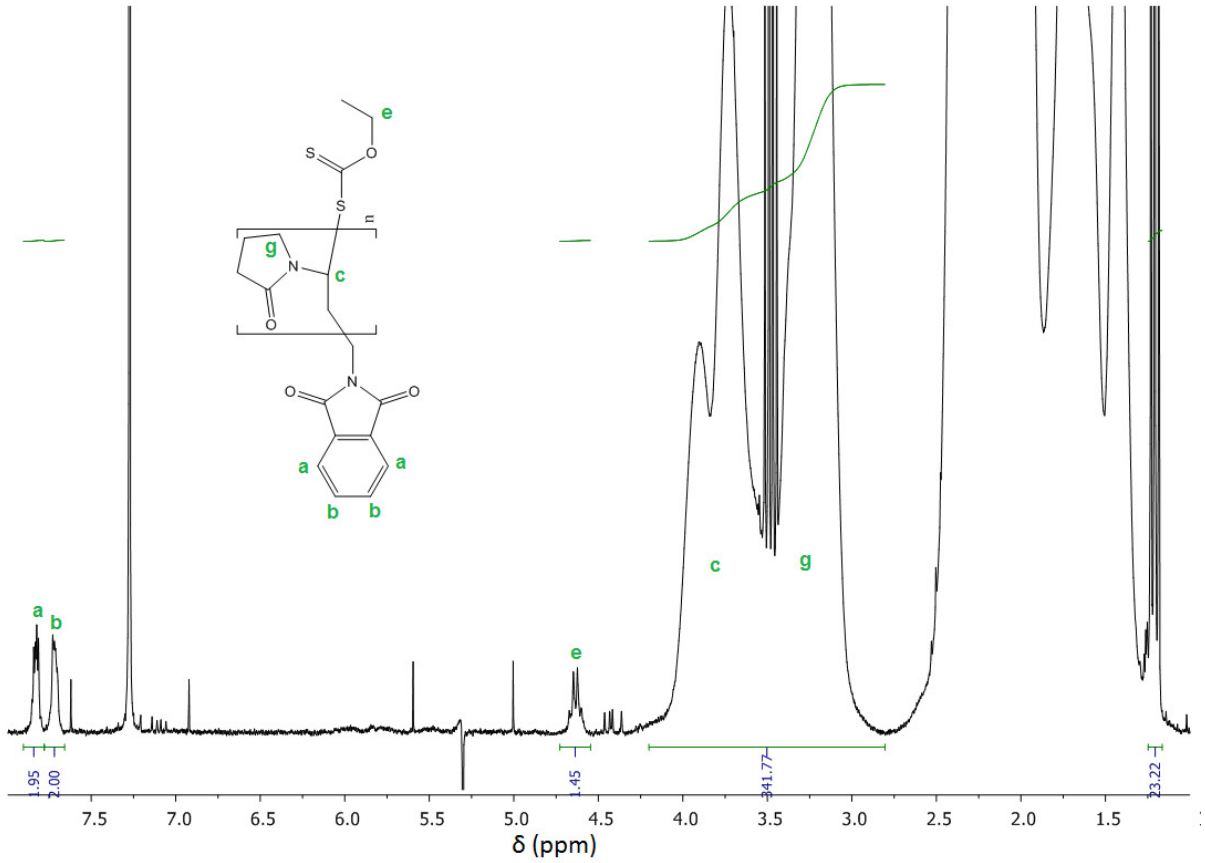

Figure 3.2: ^{1}H-NMR Spectrum for the Isolated Polymer from the Trial with R = 196 at 50% Monomer Conversion (Presaturation of the DCM Solvent Peak at δ = 5.31 ppm).

The backbone protons peak at δ = 2.9 - 4.2 ppm in Figure 3.1.B is overlapped with the NVP protons peak at δ = 3.47 - 3.60 ppm. The intensity of this peak should however be equal (or very close) to that for the vinyl protons peak at d = 4.26 - 4.56 ppm. Hence, by subtracting the integral for the vinyl protons from the integral for d = 2.9 - 4.2 ppm, the interference from the NVP protons is removed.

$M_{n,NMR}$ could then be calculated using Equation 3.4.

$$M_{n,NMR} = DP \times 111.14 g.mol^{-1} + 281.34 g.mol^{-1} \quad (3.4)$$

The theoretical M_n ($M_{n,theory}$) for an ideal RAFT-mediated polymerization could also be calculated by using Equation 3.5.

$$M_{n,theory} = R \times \left(1 - \frac{[NVP]_t}{[NVP]_0}\right) \times 111.14 g.mol^{-1} + 281.34 g.mol^{-1} \quad (3.5)$$

NVP conversion, XA2 conversion M_n and $M_{n,theory}$ for the samples obtained by the experiments described in Sections 3.2.2 and 3.2.3 are given in Table 3.1.

There were still traces of XA2 detected in the reaction mixture at the end of both reactions. The singlet at δ = 5.27 ppm in Figure 3.1.B was from DCM, most likely introduced by vapors from a contaminated pipette bulb. The number-average molecular weights (M_n) for the samples taken at low monomer conversions were significantly larger than predicted for an ideal RAFT-mediated polymerization. These properties are characteristic of hybrid behavior.[7,8] This suggests that the phthalimidylmethyl radical is a poor leaving group relative to the PVP propagating radical.

Table 3.1: Results for RAFT-mediated Polymerizations of NVP with XA2 as described in Section 3.2.2 and 3.2.3. (a) – Measured using the isolated polymer samples.

$\frac{[NVP]}{[XA2]}$	Time (Minutes)	NVP Conversion (%)	XA2 Conversion (%)	%Xanthate Retained	$M_{n,theory}$ (g/mol)	$M_{n,NMR}$ (g/mol)	$M_{n,SEC}$ (g/mol)	$Đ$ (SEC)
196	120	25	72	87[a]	5900	7800	17900	1.54
196	240	46	93	82[a]	10300	10300	17600	1.26
196	345	53	ca. 99	73[a]	11800	10900	18700	1.24
117	50	23	55	ca. 100	3300	5600	8200	1.30
117	110	42	84	ca. 100	5700	6800	9600	1.27
117	185	61	95	ca. 100	8200	8700	11100	1.24
117	245	71	97	ca. 100	9900	9500	12900	1.24

A large increase in viscosity of the reaction mixture was noted when the monomer conversion was over 60%. A loss of xanthate functionality relative to phthalimide functionality was noted for the isolated polymer samples, as noted by the data in Table 3.1 for the trial with R = 196. Some alkene-terminated polymer chains also began to form (δ = 6.88 – 7.07 ppm in $CDCl_3$ – only detectable in isolated samples), though their quantification proved difficult by NMR alone. The relatively low concentration (compared to the sensitivity of the instrument), residual monomer in the isolated samples, the broad nature of the peak and a relatively long longitudinal relaxation time (T1) of vinyl protons in general were the major interferences. It was unclear what was causing the loss of xanthate chain ends but the formation of alkene-functionalized chains would suggest a slow thermolytic β-scission of the xanthate-functionalized polymer was occurring.[1-3] Termination by disproportionation could also be the cause of alkene-functionalized chain ends. However, this has not been observed during the NRP of NVP.[9] Hydrolysis of the xanthate end-group into a thiol (and its subsequent oxidation into a disulfide) or a hydroxyl end-group (see Chapter 6 for more information) could also cause the relative abundance of xanthate end-groups to decrease. The resonance of the α-proton of the disulfide is overlapped by the polymer backbone resonance in the ^{1}H-NMR spectrum, making it impossible to confirm this by NMR alone. The hydroxyl end-group also cannot

be detected by NMR though the α-proton resonates at δ = 5.21 – 5.54 ppm in $CDCl_3$. This is a very broad peak and is difficult to detect at low concentrations. It is only clearly detected for low molecular weight polymers with a high degree of end-group conversion.

To be able to make a more accurate assessment of the situation, the number of alkene end-groups as well as the presence of disulfides, thiols or hydroxyl end-groups needs to be quantified. A more accurate measurement of the xanthate end-groups is unfortunately not possible with MALDI-TOF MS as they are photolytically labile even when embedded in the matrix. Gruendling *et al.*[10] used ESI MS to study the end-group degradation of poly(methyl methacrylate) and polystyrene prepared by RAFT-mediated polymerization. This type of analysis could prove useful in this case but, due to time constraints, it was not performed.

The thermolysis of RAFT agents by β-scission has been documented[1,7] and its mechanism is depicted in Scheme 3.1.

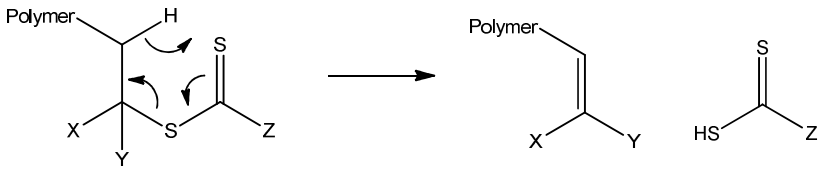

Scheme 3.1: Thermolysis of a RAFT agent from a Polymer Chain.

According to the literature, this can be a problem for xanthates at temperatures below 100 °C, but it depends on the R-group of the RAFT agent as well as on the polarity of the surrounding solution.[7] It was shown that acrylate R-groups seem to confer the most destabilizing effect while phenylacetate R-groups stabilize the thiocarbonyl thio group against thermolysis. As a general rule, the carbon–sulfur single bond is the most labile bond and factors that affect its strength include strongly electron-donating Z-groups, such as dithiobenzoates, as well as a high-energy penalty for the formation of breakdown products, like methylbenzene carbocations.

Thus to avoid excessive loss of the xanthate end-groups during polymerization, the reaction temperature should be kept as low as possible. This can be achieved by substituting AIBN with an initiator that has a 10-hour half-life at a lower temperature. In our work however, we simply applied rigorous control of the reaction temperature to ensure that the amount of xanthate functionality that was lost was kept sufficiently low.

Determination of the fraction of xanthate-functionalized chains relative to phthalimide-initiated chains by using the ^{1}H-NMR spectrum of the crude reaction mixture was difficult due to the presence of multiple interferences. The most significant interference came from the carbon satellite peaks for

the vinyl protons (f - Figure 3.1.A) overlapping with the methylene protons (e - Figure 3.2) of the xanthate-functionalized chains. This was accounted for by subtracting 0.55% (natural abundance of ^{13}C = 1.1%) of the integral value for the vinyl protons peak (f) from the integral of the methylene protons peak (e) (Figure 3.1.B). This proved difficult for high concentrations of monomer and polymer coupled with low concentrations of xanthate as the base of the vinyl protons peak (f - Figure 3.1.A) and the polymer backbone peak (c - Figure 3.1.B) also began to overlap with the xanthate methylene protons peak. This made baseline correction difficult in that region. This analysis proved most difficult for the samples from the polymerization with R = 196. Optimized shimming of the axial and radial shims as well as presaturation of the ^{13}C nuclei could improve the analysis conditions. Using an instrument with a larger static magnetic field strength would also aid in providing better resolution between the monomer peak's carbon satellites as well as the polymer backbone peak from the methylene protons peak of the xanthate.

SEC Analysis

SEC was performed for the isolated polymer samples obtained as described in Sections 3.2.2 and 3.2.3. The instrument was calibrated using peak position calibration with narrow, linear poly(methyl methacrylate) (PMMA) standards. Thus the distribution measurements for PVP on this system are relative to PMMA. Fortunately, both PVP and PMMA are linear polymers. That means the major divergences in the measured distribution parameters of the PVP samples from their actual values when using the PMMA calibration curve will be due to the differences in the hydrodynamic volume of the polymers in the mobile phase. Einstein's viscosity law states that the product of a polymer chain's molecular weight and intrinsic viscosity in a solution is directly proportional to the hydrodynamic volume of an equivalent sphere.[11] Thus the solvation properties of a polymer chain in a solution can affect its hydrodynamic volume, the key parameter controlling the separation process in SEC. One relation between the intrinsic viscosity of a polymer and its molecular weight (MW) is given by the Mark-Houwink equation.[11]

$$[\eta] = KMW^{a} \tag{3.6}$$

Where K and a are the Mark-Houwink parameters that vary with polymer chemistry, architecture, solvent and temperature. This means that as long as the differences in hydrodynamic volume between the calibrant and the analyte are only due to their different solvation properties, the differences between their intrinsic viscosities in a particular solution can be calculated. There is a large collection of Mark-Houwink constants for many different polymers in various solutions[11,12]

though caution is advised when using these values to attempt a universal calibration without an on-line viscometer. For more information on the caveats of Mark-Houwink calibrations, the reader is referred to Striegel.[11] The main causes for inaccuracies in Mark-Houwink calibrations include the great uncertainty in the published Mark-Houwink parameters, the necessity for corresponding architectures as well as molecular weight range of the two polymers being compared.[11,12] A much simpler approach would be to recalibrate the system using PVP standards, to directly determine the absolute molecular weight of the eluting fractions using a light scattering detector or to use universal calibration by connecting an on-line viscometer.[11]

The SEC traces were normalized according to the method described in Appendix A1 and plotted according to molecular weight in Figure 3.3.

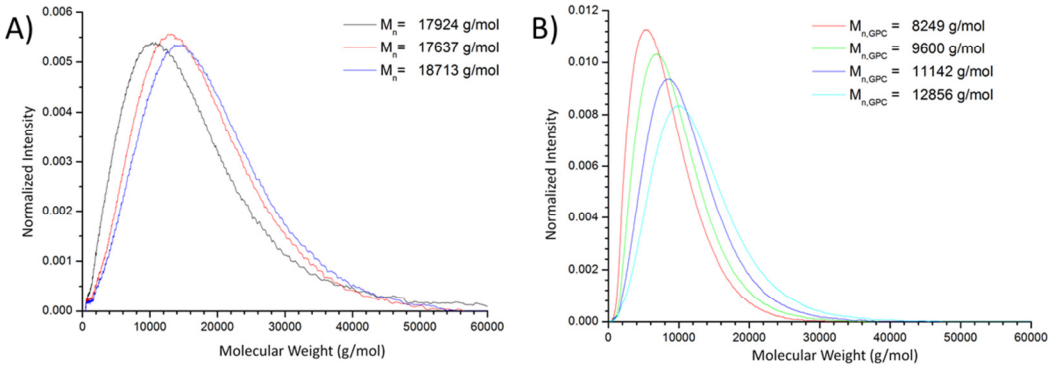

Figure 3.3: Normalized Molar Mass Distributions for RAFT-mediated Polymerizations with A) R = 196, B) R = 117 at Different Monomer Conversions.

$M_{n,SEC}$ and $Đ_{SEC}$ for each sample were calculated from the results in Figure 3.3 and are displayed in Table 3.1. Generally, $M_{n,SEC}$ was larger than $M_{n,theory}$ or $M_{n,NMR}$. However, the trend did not seem to follow an exponential deviation with molecular weight, as predicted by the Mark-Houwink equation, and was larger than predicted for the samples isolated at low monomer conversions. A universal calibration based on the Mark-Houwink parameters could help determine the magnitude of this deviation and it could be performed post-analysis. Unfortunately, the Mark Houwink parameters for either polymer in DMAC could not be found nor was there access to an on-line viscometer. Comparison of the published Mark-Houwink parameters for PMMA[13] and PVP[14] in DMF indicated that PMMA has a smaller hydrodynamic volume compared to PVP in mobile phases similar to DMAC. This would result in a positive error when calculating the molecular weight of PVP using PMMA standards but this does not help to account for the deviation from the expected values of $M_{n,SEC}$ at low monomer conversion.

The larger than expected $M_{n,SEC}$ for the polymerizations with R = 117 and R = 196 at low conversions could be explained by the theory that there is an inefficient pre-equilibrium phase for the RAFT-mediated polymerization of NVP with XA2, as indicated by the NMR data. The larger dispersity of the synthesized polymers would result in a greater weight fraction of higher molecular weight polymer chains. This would cause a greater positive error when calculating $M_{n,SEC}$ and $M_{w,SEC}$ due to the greater difference in hydrodynamic volume of the calibrant and the analyte at larger molecular weights. One reason for a slow pre-equilibrium phase can be that the leaving group (R-group) radical of the RAFT agent is less stable than the propagating radical. Fragmentation of the adduct radical would then favor formation of the propagating radical and propagation of the polymer chains would be significant before complete conversion of RAFT agent is achieved. Calculating the apparent transfer constant (C_{tr}) for XA2 with a monomer to RAFT agent ratio of 196, as described by Kowollik *et al*.,[7] gave a value of 3.26. This signifies that XA2 is not a very efficient RAFT agent for the polymerization of NVP.

3.3.2) Pre-Equilibrium Kinetics Study by *In-Situ* ^{1}H-NMR

Since *O*-ethyl xanthates are sufficient stabilizing groups for RAFT agents intended to control the polymerization of less activated monomers such as NVP and vinyl acetate,[7,15-20] the low apparent C_{tr} for XA2 may be due to the phthalimidylmethyl radical being less stable than the propagating radical. This would make it less likely to fragment from the adduct-radical intermediate compared to the propagating radical. The resulting lower rate of RAFT agent consumption would affect $Đ$ for the final product since new dormant chains would be formed for a longer period during the polymerization while the pre-existing dormant chains would be able to propagate.

In order to accurately assess the pre-equilibrium kinetics for the RAFT-mediated polymerization of NVP with XA2, ^{1}H-NMR *in-situ* polymerization was performed. The kinetic data obtained was used to calculate the probability of radical transfer from a propagating radical to the R-group on the RAFT agent as a function of reaction time and composition. This would help to quantify the relative rates of fragmentation of the R-group radical and the propagating chain radicals from the adduct-radical intermediate during the pre-equilibrium phase of the reaction.

A relatively high concentration of RAFT agent to monomer was used for the kinetic study in order to extend the pre-equilibrium phase of the RAFT process as well as to be able to accurately quantify the relative amount of monomer and RAFT agent in the reaction mixture by NMR. The spectral array, obtained as described in Section 3.2.4, was used to calculate the change in [NVP] and [XA2] during

the reaction. Figure 3.4 is a plot of [NVP] and [XA2] with respect to reaction time during the *in-situ* NMR experiment.

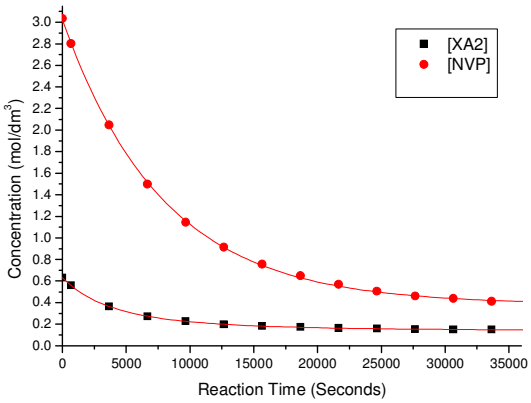

Figure 3.4: Plot of [XA2] and [NVP] During *In-situ* ^{1}H-NMR Polymerization with R = 5.

An exponential function was fitted from the data using least squares approximation to give [XA2] and [NVP] as functions of time. The least squares approximations for [NVP] and [XA2] were obtained using OriginPro 8. These functions are given in Appendix A2.1.

The probability that a propagating radical or initiator-derived radical would transfer their radicals to the phthalimidylmethyl leaving group of XA2 instead of continuing to propagate at a specific time during the reaction could be calculated using Equation 3.7.

$$\mathrm{P(T)} = \frac{\frac{d[XA2]}{dt}}{\frac{d[XA2]}{dt}+\frac{d[NVP]}{dt}} \tag{3.7}$$

$\mathrm{P(T)}$ for the ^{1}H-NMR *in-situ* polymerization was plotted in Figure 3.5:

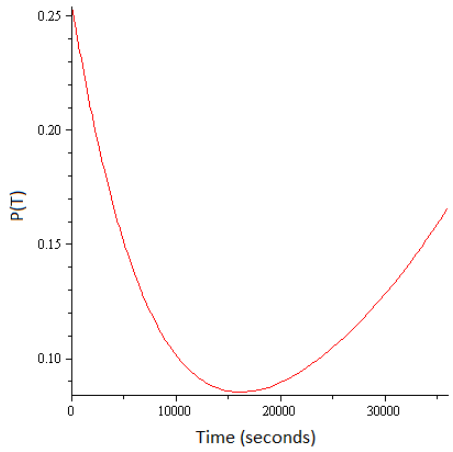

Figure 3.5: $\mathrm{P(T)}$ for the ^{1}H-NMR *In-situ* Polymerization with R = 5.

There was an increase in $P(T)$ after 16700 seconds that correlated with an increase in [XA2]/[NVP] to a value greater than the initial value of 0.2. However, $\frac{d[X]}{dt}$ was close to 0 from that time onwards, meaning that there may be large errors involved with its approximation in this region. Also, the reaction of initiator-derived radicals with XA2 may be significantly affecting $P(T)$ at this stage. Figure 3.6 is a plot of [XA2]/[NVP] as a function of reaction time:

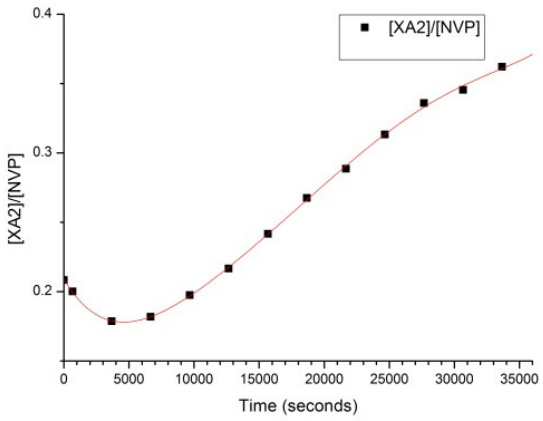

Figure 3.6: [XA2]/[NVP] as a Function of Time for the ^{1}H-NMR *In-situ* Polymerization.

$P(T)$ less than 0.5 suggests that propagation is favored over radical transfer to the R-group. A decrease in $P(T)$ can be ascribed to the cumulative effects of the decreasing RAFT agent concentration as well as an increase in poly-RAFT agent concentration. Pound *et al.*[17] performed a similar kinetic study for the RAFT-mediated polymerization of NVP with *O*-ethyl-*S*-(cyanoisopropyl)xanthate (X1). They reported on the quantitative conversion of the RAFT agent to a single-monomer adduct before any further propagation of the dormant polymer chains took place. They claimed this effect was due to the greater stability of the cyanoisopropyl radical compared to the propagating radical of PVP. By comparing the change in $P(T)$ as a function of RAFT agent conversion for the two experiments, the effect that the poly-RAFT agent concentration has on $P(T)$ for each leaving group could be assessed. The calculations are given in Appendix A2.3. $P(T)$ for X1 was found to be 0.484 and did not change significantly until all of X1 was consumed. This indicated that the concentration of poly-RAFT agent did not affect $P(T)$ and hence fragmentation of the cyanoisopropyl R-group was greatly favored over that for the propagating radical. The monomer conversion was only 17% after all the detectable RAFT agent was converted to a poly-RAFT agent. In contrast, despite having a higher initial RAFT agent concentration, $P(T)$ for XA2 was only 0.254 initially and decreased to 0.085 at 72% XA2 conversion. The monomer concentration was only 0.6 M (77% conversion) at this stage, drastically reducing the rate of propagation.

Even though the lower stability of the phthalimidylmethyl radical relative to the PVP propagating radical makes it a poor choice as a leaving group for a RAFT-mediated polymerization of NVP, this issue seems to only be a problem at low monomer conversions and low initial RAFT agent concentrations, as noted by the results of the polymerization with R = 196 in Table 3.1. The RAFT-mediated polymerization with R = 117 in Section 3.2.2 gave a polymer with $M_{n,NMR}$ = 9500 g/mol and a dispersity of 1.24. While this is within the bounds for a controlled polymerization, decreasing the dispersity of the product as much as possible would be beneficial. It would not only allow for a greater control of the aggregate architecture of the drug delivery system but it would also decrease the mole fraction of high molecular weight polymer chains. Since PVP is not biodegradable, it is essential that the polymer used for parenteral infusions does not have any polymer chains with a molar mass greater than the renal excretion threshold.[21,22] This has been estimated to a value of 25,000 g/mol by Gärtner *et al.*[21] and, in practice, pharmaceutical grade PVP with a K-value of 17 (M_w = 10,000 g/mol) is the limit allowed for parenteral formulations.[23]

The probability of adduct radical formation depends on the frequency of collision of a propagating radical with a RAFT agent as well as the relative stability of the adduct radical compared to the propagating radical, an increase in the probability of transfer can be obtained by using a higher initial RAFT agent concentration.

$P(T)$ for the polymerizations described in Sections 3.2.2 and 3.2.3 was calculated in order to measure the change in $P(T)$ with initial RAFT agent concentration. The least squares approximations for [NVP] and [XA2] for the trials in Section 3.2.2 and 3.2.3 were obtained using OriginPro 8. These functions are given in Appendix A2.2. $P(T)$ was parameterized with respect to monomer conversion in each case and the results were plotted in Figure 3.7.

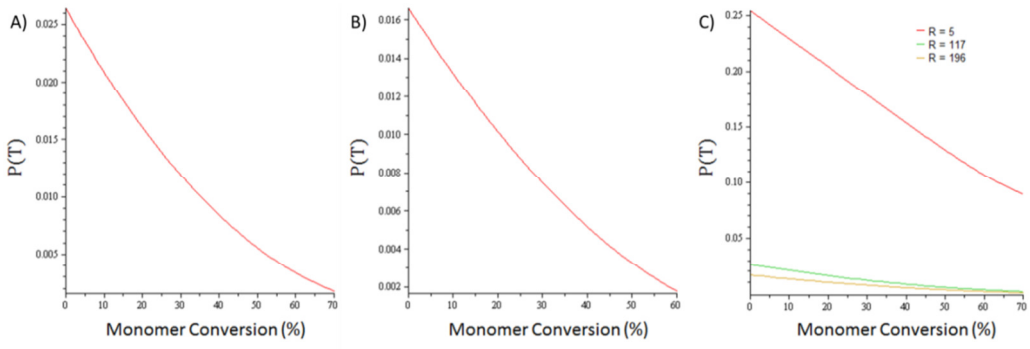

Figure 3.7: $P(T)$ for the Polymerizations with Different Initial Monomer to RAFT Agent Ratios (R). A) R = 117 and B) R = 196. C) Comparison of $P(T)$ for the Polymerizations with R = 5, 117 and 196.

Since the approximations were made with only one data set for each monomer to RAFT agent ratio, nothing can be said about their accuracy. Also, the data sets for the polymerizations with R = 117

and R = 196 consisted of only 5 and 4 data points, respectively. Thus the accuracy of these approximations is more questionable. Some qualitative information could still be extracted from the results though.

From Figure 3.7.C, it is clear that $\mathrm{P(T)}$ tends to be greater throughout the reaction for lower initial monomer to RAFT agent ratios. Thus $\mathrm{P(T)}$ for the RAFT-mediated polymerization of NVP with XA2 could be maximized by performing the polymerization with a high initial concentration of XA2. These conditions should also increase the concentration of poly-RAFT agent forming during the reaction. That would improve the probability of radical transfer between the propagating and dormant polymer chains of a specific molecular weight during the main equilibrium. However, in order to prepare polymers with a larger molecular weight the ratio of monomer to RAFT agent has to be increased.

3.4) Conclusions

Polymerization of NVP with XA2 to prepare heterotelechelic linear polymers with a phthalimide α-end-group and a xanthate ω-end-group was achieved as described by Postma *et al.*[2] Analysis by ^{1}H-NMR and SEC revealed that the polymerization was well controlled in terms of α-end-group functionality, but there was a substantial loss of xanthate functionality in the isolated polymers. This was as high as 21% in some cases. There was also hybrid behavior observed due to the relatively poor radical stability of the phthalimidylmethyl radical compared to the propagating radicals of PVP. This caused the probability of a successful radical transfer from a propagating radical to a phthalimidylmethyl radical to decrease with poly-RAFT agent concentration. However, it was confirmed experimentally that this probability increased with an increase in the ratio of RAFT agent to monomer. The apparent C_{tr} was calculated to be 3.26 when R = 196.

3.5) References

1. Moad, G.; Chong, Y. K.; Postma, A.; Rizzardo, E.; Thang, S. H. Advances in RAFT polymerization: the synthesis of polymers with defined end-groups. *Polymer* **2005***, 46*, 8458-8468.

2. Postma, A.; Davis, T. P.; Li, G.; Moad, G.; O'Shea, M. S. RAFT Polymerization with Phthalimidylmethyl Trithiocarbonates or Xanthates. On the Origin of Bimodal Molecular Weight Distributions in Living Radical Polymerization. *Macromolecules* **2006***, 39*, 5307-5318.

3. Postma, A.; Davis, T. P.; Evans, R. A.; Li, G.; Moad, G.; O'Shea, M. S. Synthesis of Well-Defined Polystyrene with Primary Amine End Groups through the Use of Phthalimidyl-Functional RAFT Agents. *Macromolecules* **2006***, 39*, 5293-5306.

4. Wuts, P. G. M.; W. Greene, T. W. *Greene's Protective Groups in Organic Synthesis;* John Wiley and Sons, Inc.: Hoboken, New Jersey, 2012.

5. Osby, J. O.; Martin, M. G.; Ganem, B. An exceptionally mild deprotection of phthalimides. *Tetrahedron Lett.* **1984***, 25*, 2093-2096.

6. Horii, Z.; Iwata, C.; Tamura, Y. Reduction of Phthalimides with Sodium Borohydride. *J. Org. Chem.* **1961***, 26*, 2273-2276.

7. Kowollik, C. B. *Handbook of RAFT Polymerization;* WILEY-VCH Verlag GmbH & Co. KGaA: Weinheim, Baden-Württemberg, 2008.

8. Pietsch, C.; Fijten, M. W. M.; Lambermont-Thijs, H. M. L.; Hoogenboom, R.; Schubert, U. S. Unexpected reactivity for the RAFT copolymerization of oligo(ethylene glycol) methacrylates. *J. Polym. Sci. A Polym. Chem.* **2009***, 47*, 2811-2820.

9. Senogles, E.; Thomas, R. Polymerization kinetics of N-vinyl pyrrolidone. *J. Polymer Sci.: Symposium* **1975***, 49*, 203-210.

10. Gruendling, T.; Pickford, R.; Guilhaus, M.; Barner-Kowollik, C. Degradation of RAFT polymers in a cyclic ether studied via high resolution ESI-MS: Implications for synthesis, storage, and end-group modification. *J. Polym. Sci. A Polym. Chem.* **2008***, 46*, 7447-7461.

11. Striegel, A. M.; Yau, W. W.; Kirkland, J. J.; Bly, D. D. *Modern Size-Exclusion Liquid Chromatography: Practice of Gel Permeation and Gel Filtration Chromatography.* John Wiley & Sons, Inc.: Hoboken, New Jersey, 2009.

12. Brandrup, J.; Immergut, E. H.; Abe, A.; Grulke, E. A.; Bloch, D. R. *Polymer Handbook;* John Wiley & Sons, Incorporated: 2003.

13. Wagner, H. L. The Mark–Houwink–Sakurada Relation for Poly(Methyl Methacrylate). *J. Phys. Chem. Ref. Data* **1987***, 16*, 165-173.

14. Mori, S. Calibration of size exclusion chromatography columns for molecular weight determination of polyacrylonitrile and poly(vinylpyrrolidone) in N,N-dimethylformamide. *Anal. Chem.* **1983***, 55*, 2414-2416.

15. Moad, G.; Rizzardo, E.; Thang, S. H. Living Radical Polymerization by the RAFT Process. *Aust. J. Chem.* **2005**, *58*, 379-410.

16. Pound, G.; McKenzie, J. M.; Lange, R. F. M.; Klumperman, B. Polymer-protein conjugates from small omega]-aldehyde end-functional poly(N-vinylpyrrolidone) synthesised via xanthate-mediated living radical polymerisation. *Chem. Commun.* **2008**, 3193-3195.

17. Pound, G.; McLeary, J. B.; McKenzie, J. M.; Lange, R. F. M.; Klumperman, B. In-Situ NMR Spectroscopy for Probing the Efficiency of RAFT/MADIX Agents. *Macromolecules* **2006**, *39*, 7796-7797.

18. Jacobs, J.; Pound-Lana, G.; Klumperman, B. Poly(N-vinylpyrrolidone-b-(gamma]-benzyl-l-glutamate)) - synthesis and self-assembly into pH-sensitive micelles. *Polym. Chem.* **2012**, *3*, 2551-2560.

19. Bailly, N.; Thomas, M.; Klumperman, B. Poly(N-vinylpyrrolidone)-block-poly(vinyl acetate) as a drug delivery vehicle for hydrophobic drugs. *Biomacromolecules* **2012**, *13*, 4109-4117.

20. Wan, D.; Satoh, K.; Kamigaito, M.; Okamoto, Y. Xanthate-Mediated Radical Polymerization of N-Vinylpyrrolidone in Fluoroalcohols for Simultaneous Control of Molecular Weight and Tacticity. *Macromolecules* **2005**, *38*, 10397-10405.

21. Gärtner, K.; Vogel, G.; Ulbrich, M. Untersuchungen zur Penetration von Makromolekülen (Polyvinylpyrrolidon) durch glomeruläre und postglomeruläre Capillaren in den Harn und die Nierenlymphe und zur Größe der extravasalen Umwälzung von 131J-Albumin im Interstitium der Niere. *Pflüger's Archiv* **1968**, *298*, 305-321.

22. Wessel, W.; Schoog, M.; Winkler, E. Polyvinylpyrrolidone (PVP), its diagnostic, therapeutic and technical application and consequences thereof. *Arzneimittel-Forschung* **1971**, *21*, 1468-1482.

23. Pramanick, S.; Singodia, D.; Vikas, C. Excipient Selection in Parenteral Formulation Development. *Pharma Times* **2013**, *45*, 65-77.

CHAPTER 4

Designing a Semi-Batch RAFT-Mediated Polymerization of *N*-vinylpyrrolidone with *O*-ethyl-*S*-(phthalimidylmethyl)xanthate

4.1) Introduction

For the preparation of high molecular weight polymers by RAFT-mediated polymerization in a batch reactor, the ratio of monomer to RAFT agent has to be sufficiently large. On the other hand, the probability of radical transfer from a propagating chain to the R-group of the RAFT agent at any given moment during the pre-equilibrium ($P(T)$) is inversely proportional to the ratio of NVP to RAFT agent for XA2. In Chapter 3, the dispersity of the polymer formed during the batch-mode RAFT-mediated polymerization of NVP with XA2 decreased with an increase in $P(T)$ for a particular molecular weight. Thus in order to synthesize PVP with a high molecular weight and the lowest possible dispersity by RAFT-mediated polymerization with XA2, the ratio of NVP to XA2 should be kept as low as possible during the polymerization. This can be achieved by performing the RAFT-mediated polymerization in a semi-batch reactor. By this methodology, an initially large concentration of RAFT agent will ensure a high $P(T)$ for the initial stages of the polymerization. $P(T)$ can be optimized by gradually feeding more monomer and initiator into the reactor at a rate that keeps the monomer concentration at a level that allows propagation to take place, while maintaining a relatively high ratio of (poly)RAFT agent to monomer throughout the polymerization in order to end up with a narrow molecular weight distribution.

The monomer concentration should also not be too low in order to avoid the rate of propagation from becoming diffusion controlled[1-3] as well as to keep other parameters such as solution viscosity and reaction time in check. The initial RAFT agent concentration should not be too high so as to avoid any retardation or inhibition periods. During the initial stages of a RAFT-mediated polymerization, a larger fraction of propagating radicals are oligomeric in size than is the case during the initial stages of an NRP. Since termination is diffusion-controlled, the rate of termination during the initial stages of a RAFT-mediated polymerization is abnormally high.[4] This could lower the fraction of phthalimide-functionalized dormant polymer chains present at the later stages of the polymerization unnecessarily as well as affect the polymer dispersity.

In order to optimize the semi-batch process we first need to describe how the monomer should be fed into the reactor in order to control the monomer conversion profile for a particular set of initial conditions. It would also be helpful to deduce the evolution of M_n with reaction time. The concentration profile for the monomer in a semi-batch process can be calculated by solving Equation 4.1.

$$\frac{d[M]}{dt} = -\frac{M_0}{(V_0+v)^2}\frac{dv}{dt} + \frac{C_m(t)}{(V_0+v)}\frac{dv}{dt} - k_p[M]\sqrt{\frac{fk_dI_0e^{(-k_dt)}}{k_t(V_0+v)}} \quad (4.1)$$

Where

$[M]$ = monomer concentration (mol.dm^{-3})

M_0 = initial number of moles of monomer in the reaction mixture (mol)

V_0 = initial volume of the reaction mixture (dm^3)

v = total volume added to the reaction mixture from t_0 to t (dm^3)

$C_m(t)$ = concentration of monomer in the feed at time t (mol.dm^{-3})

k_p = propagation rate constant (mol^{-1}.dm^3.s^{-1})

f = efficiency factor for the thermal initiator used (-)

k_d = rate constant for initiator decomposition (s^{-1})

I_0 = initial number of moles of initiator in the reaction mixture (mol)

k_t = termination rate constant (mol^{-1}. dm^3.s^{-1})

The derivation for Equation 4.1 can be found in Appendix A3.

This is a non-linear first-order ordinary differential equation of three functions ($[\mathrm{M}](\mathrm{t})$, $C_m(t)$ and $v(t)$) of one variable (t). Hence two more equations are required to be able to simultaneously solve the system of differential equations. For instance, if the monomer concentrations in the reactor and the monomer feed are kept constant, the equation becomes:

$$\frac{dv}{dt} = \frac{k_pC}{\left(C_m - \frac{M_0}{(V_0+v)}\right)}\sqrt{\frac{fk_dI_0e^{(-k_dt)}(V_0+v)}{k_t^*}}\,;\, v(0) = 0 \quad (4.2)$$

Where

C = the constant concentration of monomer in the reaction mixture

Equation 4.2 provides the rate at which the monomer feed needs to be added to the reactor during the reaction.

Approximate solutions to the initial value problem can be obtained via numerical methods such as Euler's Method, Predictor-Corrector or Runge-Kutta Methods. This will be useful in order to determine the total volume of the reaction mixture, and thus the concentration of the RAFT agent, with time. Knowing that would allow us to use Equation 3.5 to calculate $M_{n,theory}$. For a more accurate approximation of M_n, the RAFT agent conversion needs to be taken into account. However, the RAFT agent conversion in a semi-batch process should occur more rapidly due to the increase in $\mathrm{P(T)}$ hence any deviations of $M_{n,theory}$ from M_n should only occur in the early stages of the polymerization.

Evaluation of Equation 4.2 suggests that the rate at which the volume of monomer is fed into the reactor with time is directly proportional to the rate of propagation, the concentration of monomer in the feed and the desired concentration to be maintained in the reactor. This means that if a higher monomer conversion (lower monomer concentration) is maintained, the rate of monomer addition will be slower. This is intuitive since a lower monomer concentration would result in a slower rate of propagation. Also, the concentration of monomer in the feed must be greater than the maintained concentration in the reactor in order to overcome the dilution effect.

The rate of chain growth in the reaction mixture can be approximated by Equation 4.3.

$$\frac{dDP}{dt} \approx \frac{1}{[poly\text{-}X]} \times \left(-\frac{d}{dt}\left(\frac{M_r}{V}\right)\right) \tag{4.3}$$

The concentration of poly-RAFT agent in the reactor with time depends on the total volume of the reaction mixture as well as the initial concentration of RAFT agent used. Since the concentration of poly-RAFT agent in a semi-batch RAFT-mediated polymerization will be greater than that for a conventional batch-mode synthesis until near the end of the reaction, the rate of chain growth of a polymer by a dead-end continuous semi-batch process (d-CSB) will be slower. The term "dead-end" implies that the loss of initiator with time will impose an upper limit for M_n. The rate of decomposition of the initiator is only dependent on the amount of initiator in the reactor and the initiator decomposition rate constant. It is not dependent on the volume of the reaction mixture

hence it can be easily calculated and compensated for by adding more initiator with the feed, at a rate equal to the initial rate of initiator decomposition. This steady continuous semi-batch process (s-CSB) would not only be faster than a d-CSB but it also enables the synthesis of polymers with M_n larger than the upper limit for the d-CSB, provided that the rate of termination is kept sufficiently low.

The real issue is that competing side-reactions of the xanthate (such as Chugaev elimination,[5] thermolysis[4,6,7] or hydrolysis[4,7-9]) as well as the continuous initiation and termination of the propagating radicals during the reaction would affect the composition of end-groups in the final product as well as *Đ*. Thus an optimization of the semi-batch process that accounts for reaction time, composition and $\mathrm{P(T)}$ is necessary in order to achieve a product with the most desirable properties.

From Equation 4.2, increasing $\frac{dv}{dt}$ would increase [M], provided $C_m > C$. The concentration profile of poly-RAFT agent in the reactor can be determined by Equation 4.4, provided that the poly-RAFT agent and the initial RAFT agent do not undergo any side reactions.

$$[PX] = \frac{[X]_0 V_0}{(V_0+v)} - [X]_t \tag{4.4}$$

The change in [PX] with time can be calculated using Equation 4.5.

$$\frac{d[PX]}{dt} = -\frac{[X]_0 V_0}{(V_0+v)^2}\frac{dv}{dt} - \frac{d}{dt}\left(\frac{X}{V_0+v}\right) = -\frac{[X]_0 V_0}{(V_0+v)^2}\frac{dv}{dt} - \frac{1}{(V_0+v)}\frac{dX}{dt} + \frac{X}{(V_0+v)^2}\frac{dv}{dt} \tag{4.5}$$

From Equation 4.5, increasing $\frac{dv}{dt}$ causes [PX] and [X] to decrease more rapidly. This would result in a more rapid decrease in the probability of transfer for the pre-equilibrium phase. Thus, to avoid unnecessary dilution, C_m should be as high as possible *i.e.* neat monomer should be used as the feed. This may cause viscosity and mixing problems, limiting the maximum monomer conversion achievable between intervals. Also, the polarity of the reaction medium can affect the propagation rate constant beneficially.[10] Knowledge about the change in $\mathrm{P(T)}$ with a change in RAFT agent, poly-RAFT agent and monomer concentrations is required in order to balance the increase in reaction rate with the decrease in $\mathrm{P(T)}$. Obtaining this information would require several experiments with varying initial monomer, RAFT agent and poly-RAFT agent concentrations. A simpler approach for gauging the behavior of $\mathrm{P(T)}$ with respect to these parameters would be to perform semi-batch polymerizations that vary the dilution profile for [PX] and assess the differences in the composition of end-groups as well as *Đ* in the final products. The initial RAFT agent concentration was another variable parameter considered and its effect on the reaction time as well as the end-group composition was calculated. In order to avoid solvent effects as well as reduce the reaction times,

the initial monomer concentrations in the reactor as well as in the feed were those for the undiluted monomer. The monomer conversion in the reactor was kept below 60% for the trials as large increases in viscosity began to occur beyond this conversion. A discrete semi-batch process was considered for the experiments since automated machinery was not required for the monomer additions, making the process mechanically simpler than a continuous semi-batch process. This process allows propagation to take place in batch mode until a specific monomer conversion is reached. The reaction is then stopped, a discrete amount of monomer and initiator is added and the reaction is continued. If *Đ* does not decrease significantly with a decrease in the rate of dilution of [PX], it would indicate that a continuous semi-batch process may have little noticeable effect other than increasing the reaction time.

4.2) Simulating the Convergent Discrete Semi-Batch Process

The rate of propagation for the time interval $t_i \leq t < t_{i+1}$, between monomer additions, can be described by the kinetics for a batch process. Hence the concentration of monomer at any given time during the intervals can be determined by the piecewise function in Equation 4.6.

$$ln[M] = \frac{2k_p}{k_d}\sqrt{\frac{fk_dI_i}{k_t^*V}}\left(e^{\left(-\frac{k_d(t-t_i)}{2}\right)} - 1\right) + ln[M]_i \quad for\ t_i \leq t < t_{i+1} \tag{4.6}$$

The derivation of Equation 4.6 can be found in Appendix A4.

By rearranging Equation 4.6 to Equation 4.7, the reaction time required to reach a certain monomer conversion can be calculated.

$$t_{i+1} - t_i = -\frac{2}{k_d} ln\left(1 + \frac{k_d}{2k_p}\sqrt{\frac{k_t^*V_i}{fk_dI_i}} ln\frac{[M]_{i+1}}{[M]_i}\right) \tag{4.7}$$

Ideally, the length of each time interval does not depend on the absolute values of $[M]_i$ and $[M]_{i+1}$ but rather the desired monomer conversion as well as $[I]_i$. However, $[M]_i$ and $[M]_{i+1}$ should not be lower than certain critical values since k_p becomes greatly affected by monomer concentration at high monomer conversions or high solution viscosities. This is due to the rate of propagation becoming diffusion controlled.[1,2] From the experiments in Section 3.2, a distinct increase in viscosity of the reaction mixture was noted as the monomer conversion passed 60%.

In order to find the fraction of R-group initiated chains as well as xanthate-functionalized chains at the end of the discrete semi-batch polymerization, various parameters need to be given. Firstly, it is

assumed that the thiocarbonylthio end-group doesn't undergo any side reactions. The amount of initiator that decomposed during the reaction interval will be replenished, keeping the RAFT agent to monomer concentration at 10:1. This way, the propagation rate will only decrease due to the dilution of initiator and will not be significantly affected by the initiator decomposition during each interval. The limit of monomer conversion for each reaction interval will be 60% in order to optimize P(T) for each interval while avoiding excessive viscosity increases. If the amount of monomer added at the end of each interval is kept constant, this discrete semi-batch process will converge to a continuous semi-batch process as the number of reaction intervals approaches infinity. This process will be referred to as a convergent discrete semi-batch process (CDSB.)

The length of each time interval can be calculated using Equation 4.8.

$$t_{i+1} - t_i = -\frac{2}{k_d}\ln\left(1 + \frac{k_d}{2k_p}\sqrt{\frac{k_t^*\left(1+\frac{i}{b}\right)V_0}{fk_dI_i}}\,ln\left(\frac{\left(1+\frac{i}{b}\right)}{\left(1+\frac{3+2i}{2b}\right)}\right)\right) \tag{4.8}$$

The derivation of Equation 4.8 can be found in Appendix A6.

The number of initiator-derived chain ends that form during the interval t_i to t_{i+1} can be calculated by equation 4.9.

$$N_{Ii} = 2fI_i(1 - e^{(-k_d(t_{i+1}-t_i)})) \tag{4.9}$$

If it is assumed that the RAFT agent was completely converted to poly-RAFT agent at the end of the reaction and no side reactions took place, the mole fraction of R-group-functionalized polymer chains can be calculated using Equation 4.10.

$$\chi_{\alpha_R} = \frac{X_0}{(\sum_{i=0}^{n} N_{Ii}) + X_0} \tag{4.10}$$

Where

X_0 = Number of moles of RAFT agent used

If the RAFT agent conversion is known, the fraction of R-group-functionalized polymer chains for each interval can be calculated by multiplying Equation 4.10 by the fraction of RAFT agent conversion. The number of polymer chains that underwent termination by combination during each reaction interval can be calculated by Equation 4.11. Its derivation is in Appendix A7.

$$PT_i = fI_0(1 - e^{(-k_d(t_{i+1}-t_i))}) \tag{4.11}$$

Thus the fraction of dormant chains after n intervals (χ_{ω_X}) can be computed by Equation 4.12.

$$\chi_{\omega_X} = \frac{X_0}{(\sum_{i=0}^{n} PT_i)+X_0} \tag{4.12}$$

Where

PT_i = the number of terminated chains formed during interval i

If it is assumed that all of the RAFT agent is consumed after interval i, the theoretical M_n of the dormant polymer chains can be approximated by a modified version of Equation 3.5.

$$M_{n,theory} = \frac{[M]_0 V_0 + \frac{i}{b}[M]_{add} V_0}{[X]_0} \times 0.6 \times 111.14 g.mol^{-1} + 281.34 g/mol \tag{4.13}$$

After extensive evaluation of the literature, very few publications were found which contained the propagation and termination rate constants for NVP at 65 °C in the bulk phase.[10-13] The variation in the values for the reported rate constants was quite broad, making it difficult to determine which of these values were accurate. The work by Stach *et al.*[12] appears to be the most accurate as they worked with pulsed-laser polymerization and repeated their measurements for each parameter many times. They report an average k_p = 2536 L.mol^{-1}.s^{-1} for polymerization of neat NVP at 60 °C. No reports on the efficiency factor of AIBN in NVP could be found. To simplify our computations and remove the necessity for assumptions, the observed rate constant (φ) at 65 °C in neat NVP was calculated from the polymerization data.

This was done by rearranging Equation 4.6 to the following form:

$$ln\left(\frac{[M]}{[M]_0}\right) = \sqrt{\frac{4{k_p}^2 f}{k_t^*}}\sqrt{\frac{I_0}{k_d V}}\left(e^{\left(-\frac{k_d(t-t_0)}{2}\right)} - 1\right)$$

$$= \varphi\sqrt{\frac{I_0}{k_d V}}\left(e^{\left(-\frac{k_d(t-t_0)}{2}\right)} - 1\right) \tag{4.14}$$

$k_d = 2.1 \times 10^{-5} s^{-1}$ for AIBN at 65 °C was determined by least squares approximation of the data published in the Polymer Handbook[14] to obtain an Arrhenius plot. The observed rate constant (φ) was calculated from the slope of $ln\left(\frac{[M]}{[M]_0}\right)$ versus $\sqrt{\frac{I_0}{k_d V}}\left(e^{\left(-\frac{k_d(t-t_0)}{2}\right)} - 1\right)$, for each of the polymerizations performed in Section 3.2, as well as 4.5.1.

The fraction of phthalimide-functionalized chain ends (χ_{α_R}) and dormant polymer chains (χ_{ω_X}) during a CDSB were plotted as functions of $M_{n,theory}$ for different initial monomer to RAFT agent ratios (R_0) in Figures 4.1.A and 4.1.B, respectively. The observed rate constant was parameterized to φ = 0.250 $L^{0.5}.mol^{-0.5}.s^{-0.5}$ (See Section 4.6.1 and Appendix A5 for the calculation.) The reaction time required to reach a particular $M_{n,theory}$ for the different initial RAFT agent concentrations is plotted in Figure 4.2.

From Figure 4.2, a higher initial RAFT agent concentration results in a longer reaction time required to reach a desired M_n. A longer reaction time would result in more initiator-derived chains as well as more terminated chains forming, as illustrated in Figure 4.1. However, this difference was not more than 7% for for χ_{α_R} and 5.5% for χ_{ω_X}.

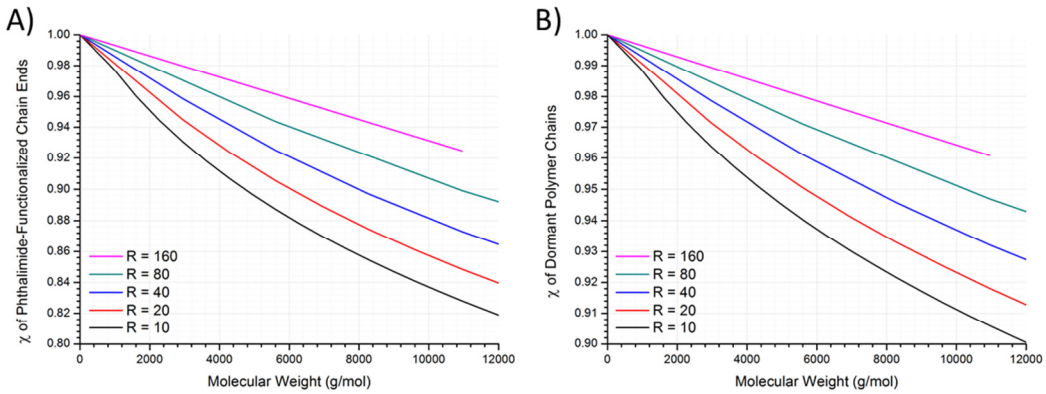

Figure 4.1: Calculated Mole Fractions of A) Phthalimide-Functionalized Chain Ends and B) Dormant Polymer Chains for the RAFT-Mediated Polymerization of NVP with XA2 by the CDSB.

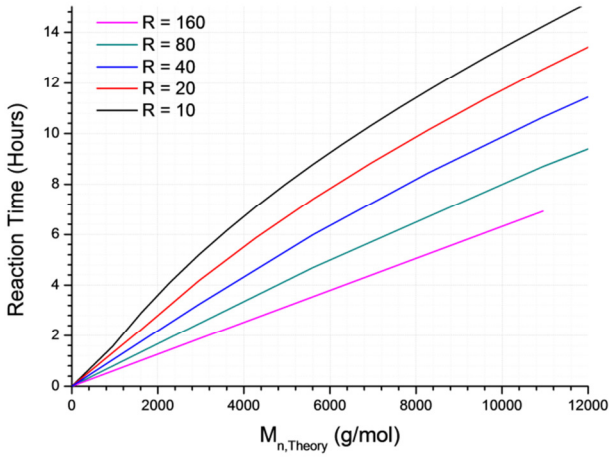

Figure 4.2: Reaction Time Required to Reach a Specific M_n During the CDSB.

4.3) Simulating the Steady Discrete Semi-Batch Process

Another discrete semi-batch process was considered. In this process, the degree of dilution of the thiocarbonyl thio functionality was kept constant. This was achieved by keeping $\frac{[M]_f}{[M]_i}$ for each interval constant. This process will be referred to as a steady discrete semi-batch process (SDSB) as it does not converge to a continuous semi-batch process.

The initial parameters, including the initial rate of dilution, were kept identical to those for the CDSB. Hence, the first two reaction intervals were identical. The length of each reaction interval, after the first, could be determined by Equation 4.15. Its derivation can be found in Appendix A8.

$$t_{i+1} - t_i = -\frac{2}{k_d} ln\left(1 + \frac{1}{\varphi}\sqrt{\frac{k_d V_i}{I_0}} ln(0.5714)\right) \tag{4.15}$$

Where

$$V_i = V_0 + \sum_{n=1}^{i} x_n \tag{4.16}$$

$$x_{i+1} = 2x_i \quad \forall\, i > 1, i \in \mathbb{N} \quad (x_1 = V_0) \tag{4.17}$$

χ_{α_R}, χ_{ω_X} and $M_{n,Theory}$ at the end of each reaction interval can be calculated by using Equations 4.10 to 4.13 and 4.15.

χ_{α_R} and χ_{ω_X} for different R_0 during the SDSB were plotted as functions of $M_{n,theory}$ in Figures 4.3.A and 4.3.B, respectively. The reaction time required to reach a particular $M_{n,theory}$ for the different R_0 is plotted in Figure 4.4.

The results in Figures 4.1 – 4.4 indicate that there is only a maximum difference of 3% for χ_{α_R} of the CDSB compared to the SDSB at a specific R_0. The difference in χ_{ω_X} between the two processes is only 2% at most. Their main difference is in the reaction times required to reach a specific molecular weight. The SDSB is less affected by the initial RAFT agent concentration as well as the desired molecular weight.

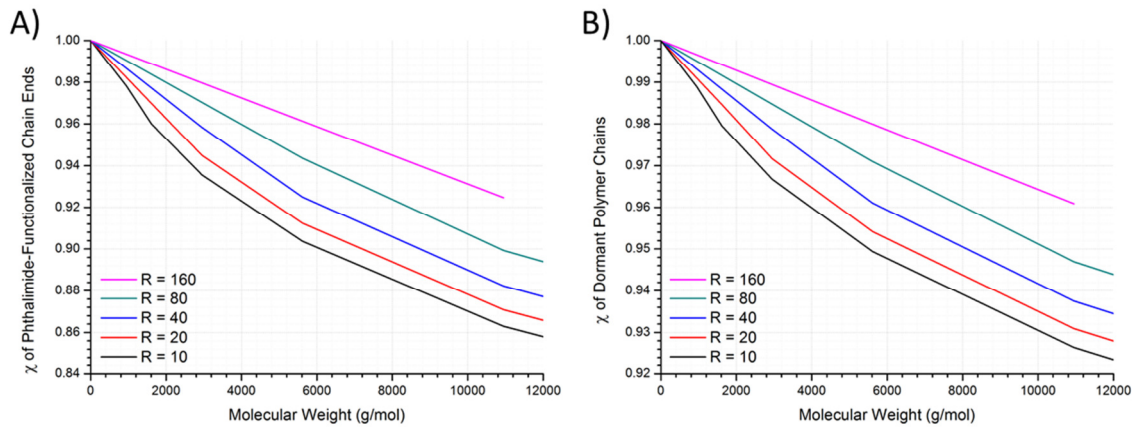

Figure 4.3: Calculated Mole Fractions of A) Phthalimide-Functionalized Chain Ends and B) Dormant Polymer Chains for the RAFT-Mediated Polymerization of NVP with XA2 by the SDSB.

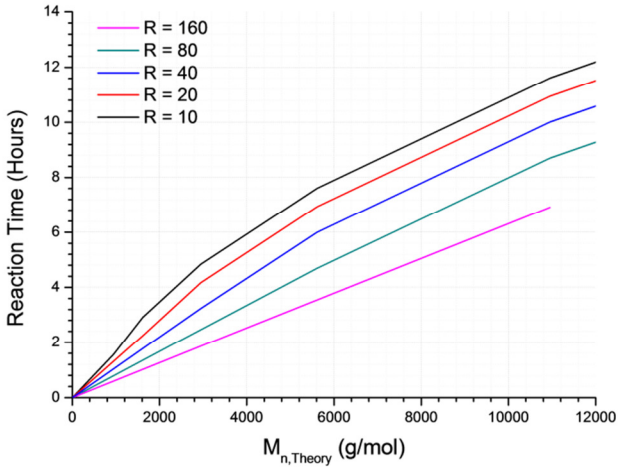

Figure 4.4: Reaction Time Required to Reach a Specific M_n During the SDSB.

The CDSB would take fourteen hours to reach $M_{n,Theory}$ = 10,000 g/mol if R_0 = 10 while the SDSB would only take eleven and a half hours. The difference in $Đ$ for the polymers prepared by a CDSB and a SDSB would indicate if a significant improvement in the transfer probability during the main equilibrium would be achieved by a continuous semi-batch process or if the reaction time would be unnecessarily extended after the pre-equilibrium phase is complete. In order to determine if there is a significant difference in χ_{α_R}, χ_{ω_X} and reaction time for a particular $M_{n,Theory}$, these parameters were calculated for a d-CSB as well as an s-CSB.

4.4) Simulating the Continuous Semi-Batch Process

For a d-CSB with the monomer conversion being kept constant at 60%, the rate of monomer addition for the RAFT-mediated polymerization of NVP with XA2 at 65 °C can be calculated by modification of Equation 4.2 to use the observed rate constant φ. This is illustrated in Equation 4.18. The reaction time required for the monomer conversion to reach 60% was calculated using Equation 4.19.

$$\frac{dv}{dt} = \frac{\varphi C}{2\left(C_m - \frac{M_0}{(V_0+v)}\right)} \sqrt{k_d I_0 e^{(-k_d t - t_0)}(V_0 + v)} \; ; v(0) = 0 \tag{4.18}$$

$$t_0 = -\frac{2}{k_d} \ln\left(1 + \ln(0.4)\frac{k_d}{\varphi}\sqrt{\frac{1}{k_d[I]_0}}\right) \tag{4.19}$$

In order to improve the limiting molar mass plateau for the d-CSB, the amount of initiator consumed to reach 60% monomer conversion was replenished at the beginning monomer feeding stage.

$M_{n,theory}$ can be calculated by Equation 4.20.

$$M_{n,theory} = \frac{X_0}{M_0} \times (V_0 + v) \times 0.6 \times 111.14 g.mol^{-1} + 281.34 g/mol \tag{4.20}$$

χ_{α_R} can be calculated by Equation 4.21.

$$\chi_{\alpha_R} = \frac{X_0}{X_0 + 2fI_0\left(1 - e^{-k_d t_0}\right) + 2fI_0\left(1 - e^{-k_d(t - t_0)}\right)} \tag{4.21}$$

χ_{ω_X} can be calculated by Equation 4.22.

$$\chi_{\omega_X} = \frac{X_0}{X_0 + fI_0(1 - e^{-k_d t_0}) + fI_0(1 - e^{-k_d(t - t_0)})} \tag{4.22}$$

χ_{α_R} and χ_{ω_X} for different R_0 during the d-CSB were plotted as functions of $M_{n,theory}$ in Figures 4.5.A and 4.5.B, respectively. The reaction time required to reach a particular $M_{n,theory}$ for different R_0 is plotted in Figure 4.6.

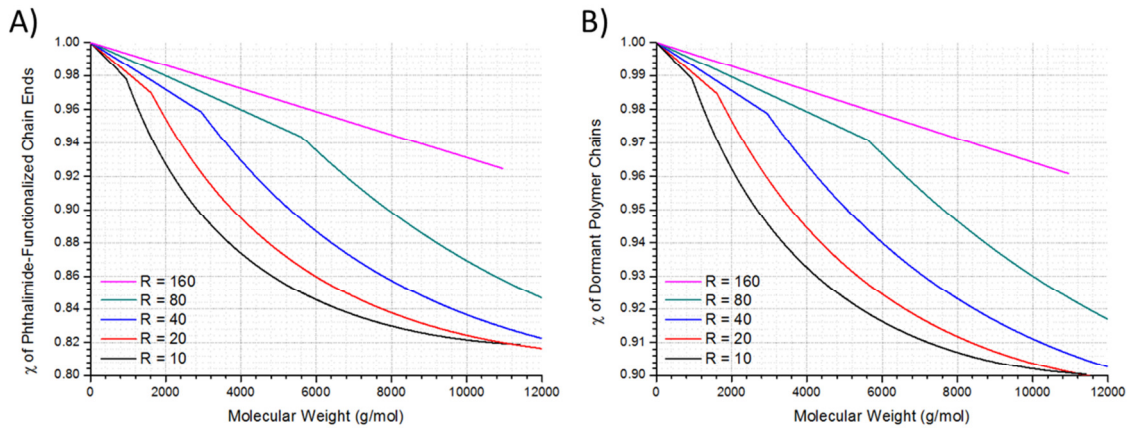

Figure 4.5: Calculated Mole Fractions of A) Phthalimide-Functionalized Chain Ends and B) Dormant Polymer Chains for the RAFT-Mediated Polymerization of NVP with XA2 by the d-CSB.

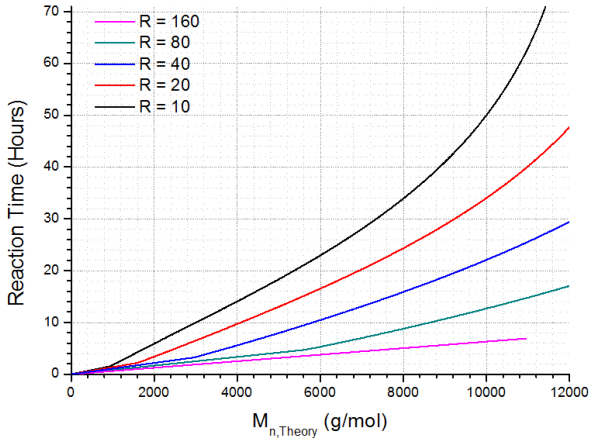

Figure 4.6: Reaction Time Required to Reach a Specific M_n During the d-CSB.

For an s-CSB, the amount of initiator is kept constant during the monomer feeding stage. Thus the rate of monomer addition can be calculated using Equation 4.23.

$$\frac{dv}{dt} = \frac{\varphi C}{2\left(C_m - \frac{M_0}{(V_0+v)}\right)}\sqrt{k_d I_0 (V_0 + v)}\,;\, v(0) = 0 \tag{4.23}$$

Equations 4.19 and 4.20 still hold for the SDSB and once the volume v required to reach $M_{n,theory}$ = 10,000 g/mol is known, the time required for the reaction to be completed can be calculated from Equation 4.23.

χ_{α_R} can be calculated by Equation 4.24 and χ_{ω_X} can be calculated by Equation 4.25. Their derivation can be found in Appendix A9.

$$\chi_{\alpha_R} = \frac{X_0}{X_0 + 2fk_d I_0 (t_0 + t)} \tag{4.24}$$

$$\chi_{\omega_X} = \frac{X_0}{X_0 + f k_d I_0 (t_0 + t)} \tag{4.25}$$

χ_{α_R} and χ_{ω_X} for different R_0 during the s-CSB were plotted as functions of $M_{n,theory}$ in Figures 4.7.A and 4.7.B, respectively. The reaction time required to reach a particular $M_{n,theory}$ for the different R_0 is plotted in Figure 4.8.

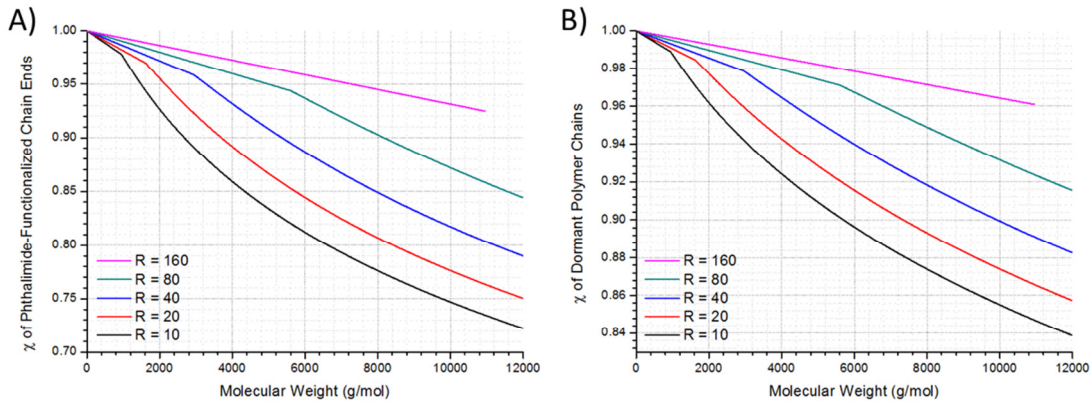

Figure 4.7: Calculated Mole Fractions of A) Phthalimide-Functionalized Chain Ends and B) Dormant Polymer Chains for the RAFT-Mediated Polymerization of NVP with XA2 by the s-CSB.

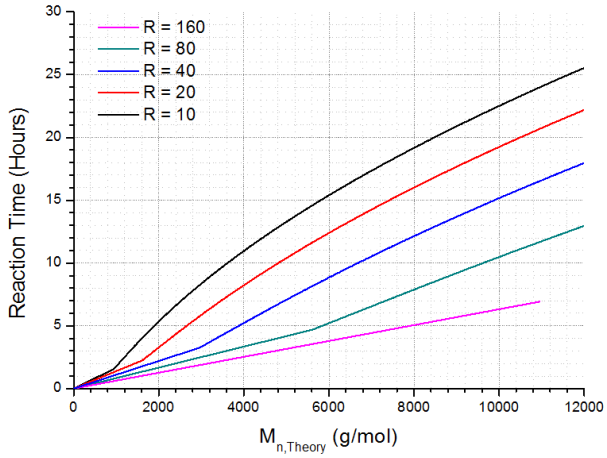

Figure 4.8: Reaction Time Required to Reach a Specific M_n During the s-CSB.

Comparing the results for the simulations of the continuous semi-batch processes to the discrete semi-batch processes, two important observations were made. χ_{α_R} and χ_{ω_X} for the d-CSB were similar to the CDSB for R_0 = 10 and R_0 = 20, the s-CSB had the lowest χ_{α_R} and χ_{ω_X}. These were more than 10% lower for R_0 = 10. Also both the continuous semi-batch processes would take considerably longer to reach the desired molecular weight than the discrete semi-batch processes. The d-CSB taking days longer for R_0 = 10 and R_0 = 20.

4.5) Materials and Experimental Methods

N-Vinylpyrrolidone was purchased from Merck and vacuum distilled from 5% ground potassium hydroxide before use. Azobisisobutyronitrile (AIBN) was purchased from Merck and recrystallized from methanol before use. Sodium metal, concentrated sulfuric acid (95 - 97%), anhydrous calcium chloride, potassium hydroxide pellets, sodium hydrogen carbonate (ACS reagent grade) and anhydrous calcium sulfate were purchased from Merck and used as received. Benzophenone, butylated hydroxytoluene (BHT) 99% (GC), dimethylacetamide (Chromosolv® Plus, for HPLC ≥ 99.9%) and chloroform-d 99.8 atom % were purchased from Sigma Aldrich and used as received. 4Å molecular sieves (8 – 12 mesh) were also purchased from Sigma Aldrich, dried in a vacuum oven at 165 °C for 5 hours and allowed to cool to room temperature under vacuum before use. Methanol, dichloromethane and diethyl ether were purchased from KIMIX. Methanol was fractionally distilled before use. Dichloromethane was washed with concentrated sulfuric acid followed by 5% sodium bicarbonate solution and finally water before being dried over calcium chloride and fractionally distilled from calcium sulfate before use. Diethyl ether was distilled from sodium and benzophenone. Lithium chloride ≥ 98% was purchased from Riedel-de Haën and used as is. 0.45 µm Glass fiber prefilters were purchased from PALL Life Sciences. *O*-Ethyl-*S*-(phthalimidylmethyl)xanthate (XA2) was prepared as described in Section 3.2.1.

4.5.1) Determining the Observed Rate Constant for the Polymerization of NVP with XA2

The data from the polymerizations in Sections 3.2.2 to 3.2.4 were used to determine φ for R = 196, R= 117 and R = 5 respectively. For R = 20, the data from the first reaction interval of the CDSB and SDSB in Sections 4.5.2 and 4.5.3 was used. The first measurement was performed as described below. Degassed NVP (1 g, 9.0×10^{-3} mol) was transferred to a Schlenk tube along with XA2 (0.1265 g, 4.5×10^{-4} mol) and AIBN (9.0×10^{-3} g, 5.5×10^{-5} mol). A magnetic stirrer bar was added and 3 freeze-pump-thaw cycles were performed before back-filling with nitrogen. The sample was polymerized at 65 °C for 1 hour and 50 minutes. Another two trials were performed though the reaction time was increased to 2 hours and 5 minutes in each case.

4.5.2) Polymerization of NVP with XA2 by the Convergent Discrete Semi-Batch Process

Degassed NVP (1 g, 9.0×10^{-3} mol) was transferred to a Schlenk tube (reactor) along with XA2 (0.1265 g, 4.5×10^{-4} mol) and AIBN (9.0×10^{-3} g, 5.5×10^{-5} mol). A magnetic stirrer bar was added and 3 freeze-

pump-thaw cycles were performed before back-filling with nitrogen. The sample was polymerized at 65 °C for 2 hours and 5 minutes. A sample of the crude reaction mixture was taken for NMR analysis. The reaction mixture was degassed by three freeze-pump-thaw cycles, before back-filling with nitrogen. The polymerization was re-initiated and polymerized for 10 hours and 5 minutes in total, with the reaction being stopped to take a sample and add more monomer at specific times. The reactant feed times and quantities are tabulated in Table 4.1. Crude and isolated polymer samples were taken at the end of each reaction interval and prepared as described in Section 3.2.2. From the third interval onwards, the reaction mixture became too viscous to be stirred by a magnetic stirrer alone. From then on, the reaction was stopped between intervals and the monomer feed was mixed in by hand using a Pasteur pipette. The reaction mixture was degassed by 3 freeze-pump-thaw cycles and back-filled with nitrogen before the polymerization was continued.

Table 4.1: Monomer and AIBN Feed Profile for CDSB.

Time (minutes)	Volume of NVP added (mL)	Mass of AIBN Added (mg)
125	1.0	0
245	1.0	0
355	1.0	2.8
435	1.0	0
515	1.0	0

4.5.3) Polymerization of NVP with XA2 by the Steady Discrete Semi-Batch Process

10 mL of NVP was distilled. Degassed NVP (1 g, 9.0×10^{-3} mol), XA2 (0.1265 g, 4.5×10^{-4} mol) and AIBN (9.0×10^{-3} g, 5.5×10^{-5} mol) were placed in a Schlenk tube. A magnetic stirrer bar was added and 3 freeze-pump-thaw cycles were performed. The Schlenk tube was back-filled with nitrogen and a drop was taken for NMR analysis of the initial conditions. The reaction mixture was polymerized at 65 °C for 8 hours and 50 minutes. The reaction was stopped at specific time intervals, a sample of the reaction mixture was taken for analysis and a specific amount of degassed monomer as well as AIBN were carefully transferred to the reaction mixture. The reaction mixture was then degassed by three freeze-pump-thaw cycles and back-filled with nitrogen before continuing the polymerization. The reactant feed times are given in Table 4.2. SEC samples were prepared as described in Section 3.2.2.

Table 4.2: Monomer and AIBN Feed Times for SDSB.

Time (minutes)	Volume of NVP added (mL)	Mass of AIBN added (mg)
125	1.0	0
245	2.0	2.5
380	4.0	0

4.6) Results and Discussion

4.6.1) Calculating the Observed Rate Constant for the Polymerization of XA2 with NVP

The observed rate constant (φ) was calculated from the slope of $ln\left(\frac{[M]}{[M]_0}\right)$ as a function of $\sqrt{\frac{I_0}{k_d V}}\left(e^{\left(-\frac{k_d(t-t_0)}{2}\right)}-1\right)$, for each of the polymerizations performed in Section 3.2, as well as 4.5.

The slope between each adjacent data pair was calculated to check for a linear correlation. This was equal to φ for that time interval. The data for the trial with R = 5 had a non-linear correlation (see Figure A5.1 in Appendices) indicating that the observed rate constant decreases at high monomer conversions. The other experiments all showed a linear correlation, hence a least-squares approximation of the data was used. φ for the first interval of the CDSB and the SDSB was also calculated, as described in Section 4.5.1. Since there were only two data points available for each analysis, the average of three trials was taken. The results of the observed rate constant calculations were tabulated in Table 4.3. The calculations for φ for each of the trials can be found in Appendix A5.

Table 4.3: Observed Rate Constant (φ) during RAFT-mediated Polymerization of NVP with XA2 at Different Initial Monomer to RAFT agent Ratios. (a) Obtained by Linear Least Squares approximation of All the Data. $k_d = 2.1 \times 10^{-5} s^{-1}$

$\frac{[M]_0}{[X]_0}$	φ ($L^{0.5}.mol^{-0.5}.s^{-0.5}$)
5	0.210
20	0.261
20	0.231
20	0.258
117	0.390[a]
196	0.218[a]

It would appear that the addition of benzene did not affect the initial observed rate constant significantly, as noted for the results of the trial with R = 5. Interestingly, the observed rate constant for the polymerization where R = 196 correlated well with the polymerizations where R = 20 while the polymerization where R = 117 had a much greater observed rate constant. The temperature was regulated in all cases by a thermocouple as well as a mercury thermometer and a large oil bath was used to dampen temperature fluctuations. The oil bath was allowed to stabilize until the temperature remained stable for an hour of frequent, periodic observation. It is unclear why there was an increase in the rate of polymerization for the trial with R = 117 but it was suspected that adventitious water present during the reaction may have increased k_p.[12] Repeating the trial gave a similar observed rate constant which stands to question the theory of adventitious water being the cause. If it were the case, then it should not only occur for the batch polymerization with R = 117. The presence of water was detected during NMR analysis of the reaction mixture for the batch polymerizations with R = 117 but its concentration could not be quantified. It was also detected in the reaction mixtures during all the other trials.

4.6.2) Polymerization of NVP with XA2 by the Convergent Discrete Semi-Batch Process

NMR Analysis

^{1}H-NMR analysis of the crude reaction mixture was used to determine the conversion of monomer with time at each interval as well as $M_{n,NMR}$ as described in Section 3.3.1. Figure 4.9 shows both the calculated and experimental monomer conversion profiles for the CDSB. The results fit well with the calculations for the first two intervals. A decrease in the rate of propagation was noted for the third interval. This could be due to adventitious oxygen being introduced during the reaction sampling and reactant feeding without stopping the reaction. From the third interval onwards, there was also a consistent increase in the total monomer to RAFT agent ratio by a factor of 1.5 more than the amount of monomer that was added. This could not be accounted for as the samples taken for analysis were minute and would have less of an effect on the concentrations of the reactants at later stages of the polymerization. There was also a noted increase in reaction rate from the third interval. The increase in the expected reaction rate could be due to the volume contraction as higher molecular weight polymer chains began to form. Another cause could be due to a decrease in k_t as the viscosity increases. Another reason for this increase could be due to the addition of more AIBN than intended due to an error during the weighing of the reagent.

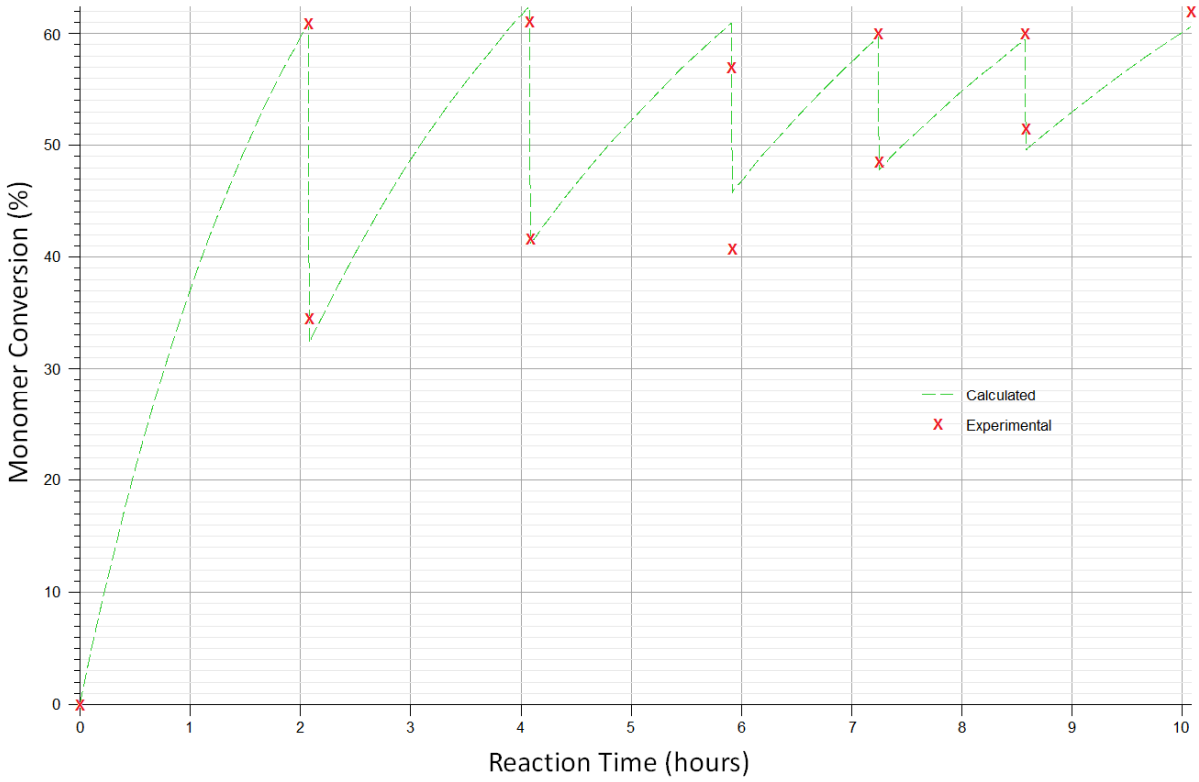

Figure 4.9: Monomer Conversion Profile for CDSB.

The fraction of xanthate functionality retained relative to phthalimide functionality was determined by ^{1}H-NMR analysis of the crude reaction mixture. However, when the concentration of monomer relative to xanthate became too great, the base of the vinyl protons peak became a problem. Optimized shimming, presaturation of the ^{13}C nuclei and using a higher field strength instrument could have improved the analysis conditions.

The results of the CDSB analysis are given in Table 4.4.

Table 4.4: Results for CDSB Polymerization. (a) – Measured for the isolated polymer sample.

Time (Minutes)	NVP Conversion (%)	XA2 Conversion (%)	%Xanthate Retained	$\frac{NVP_{total}}{XA2_0}$	$M_{n,theory}$ (g/mol)	$M_{n,NMR}$ (g/mol)	$M_{n,SEC}$ (g/mol)	Đ (SEC)
125	61%	80%	100	20.7	1700	2000	2200	1.23
245	61%	95%	100	39.0	2900	3000	2900	1.19
355	57%	100%	ca. 100	59.6	4100	4000	4300	1.21
435	60%	100%	ca. 100	90.1	6300	6300	5800	1.16
515	60%	100%	ca. 100	118.6	8200	8200	7900	1.16
605	62%	100%	79[a]	148.2	10500	10100	10600	1.17

The total monomer to initial RAFT agent ratio could be calculated from the NMR data which allowed the accurate determination of $M_{n,theory}$ at the end of each interval. $M_{n,theory}$ correlated well with $M_{n,NMR}$ indicating that XA2 had indeed been completely converted to poly-RAFT agent before any significant propagation took place.

SEC Results

SEC analyses of the samples from the CDSB were performed as described in Section 3.2.5. The SEC traces were normalized as described in Appendix A1 and plotted according to molecular weight in Figure 4.10.A.

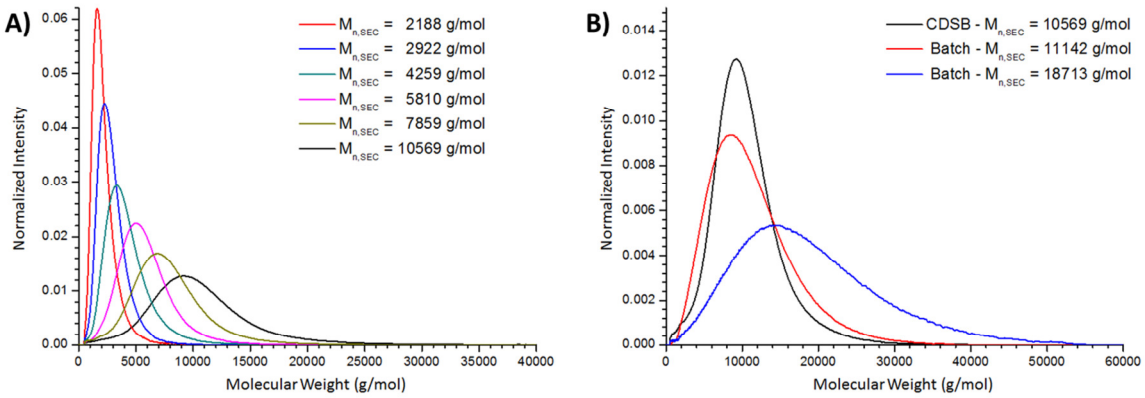

Figure 4.10: A) Molar Mass Distributions for the CDSB. B) Comparison of Molar Mass Distributions for the Final Product of the CDSB to those for the Batch-Mode Polymerizations Performed in Section 3.2.2 and 3.2.3.

Figure 4.10.B compares the normalized SEC results for the final product of the CDSB with the SEC results for the batch polymerizations described in Sections 3.2.2 and 3.2.3. From Figure 4.10.B, it is clear that the product of the CDSB had the lowest *Đ*. It was 0.07 less for the CDSB than for the batch polymerizations at a similar monomer conversion.

4.6.3) Polymerization of NVP with XA2 by the Steady Discrete Semi-Batch Process

NMR Analysis

^{1}H-NMR analysis of the crude reaction mixture was used to determine the conversion of NVP and XA2 with time as well as $M_{n,NMR}$ as described in Section 3.3.1. The amount of xanthate relative to phthalimide present in the reaction mixture at the end of each interval was also measured using this

data. The crude reaction mixture samples from the third and fourth intervals were analyzed using a 600 MHz Unity NMR spectrometer. The higher magnetic field strength provided spectra with better resolution between the methylene protons peak of the xanthate end group and the carbon satellites of the vinyl protons peak. However, half of the carbon satellite peak still overlapped with the methylene protons peak of the xanthate. The results of the SDSB are given in Table 4.5. Figure 4.11 shows the monomer conversion profile for the SDSB polymerization of NVP with XA2. It appeared as though the observed rate constant had increased considerably for the later stages. This could have arisen from adventitious water in the reaction mixture, temperature spikes in the oil bath or the inaccurate weighing of the initiator added to the reaction at the end of the second interval.

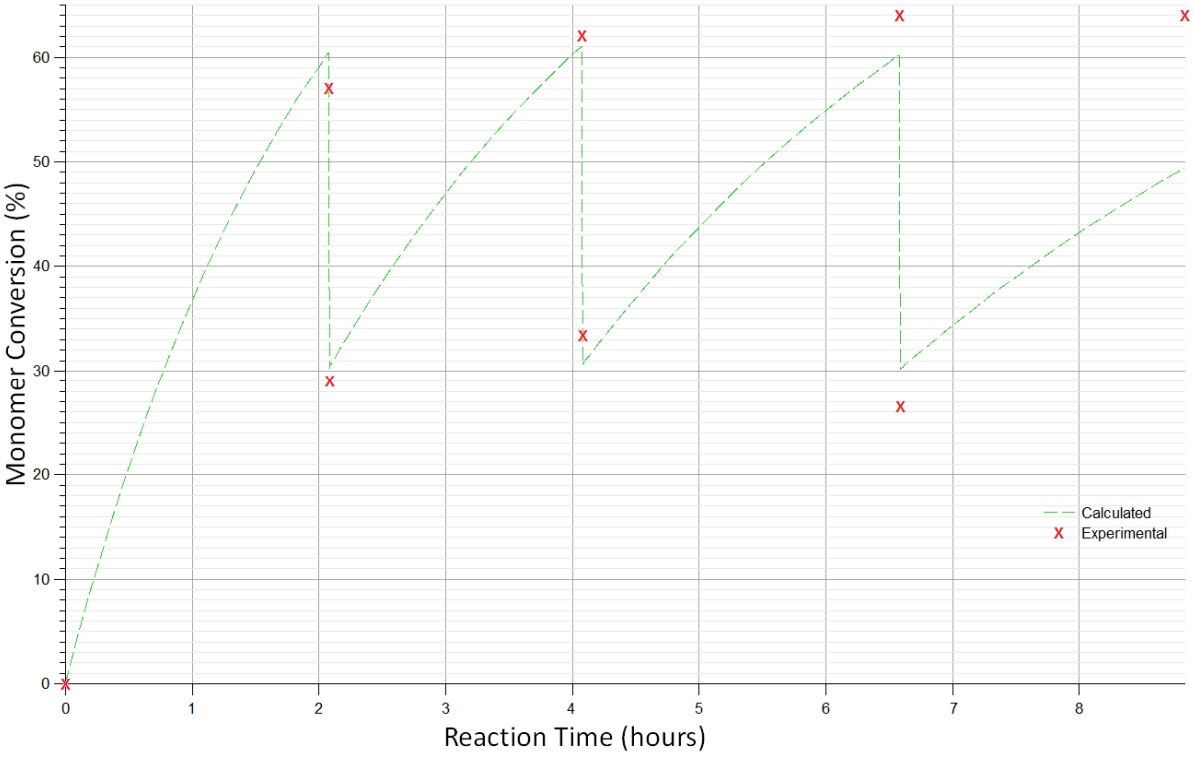

Figure 4.11: Monomer Conversion Profile for SDSB.

The 600 MHz ^{1}H-NMR spectra of the samples taken for the third and fourth intervals of the SDSB are superimposed on each other in Figure 4.12. The spectra were normalized by setting the integral for the phthalimide protons peak at δ = 7.67 – 7.74 ppm to 2.00. Only half of the carbon satellite of the vinyl protons peak (e) overlapped with the methylene protons peak of the xanthate (d). Its interference was accounted for by subtracting 0.5×0.55% of the integral intensity of the vinyl protons peak (e) from that of the methylene protons peak (d) of the xanthate.

Table 4.5: Results for SDSB Polymerization. (a) – Measured using a 600 MHz Spectrometer.

Time (Minutes)	NVP Conversion(%)	XA2 Conversion(%)	%Xanthate Retained	$\frac{NVP_{total}}{XA2_0}$	$M_{n,theory}$ (g/mol)	$M_{n,NMR}$ (g/mol)	$M_{n,SEC}$ (g/mol)	$Đ_{(SEC)}$
125	57%	82%	ca. 100	20.9	1450	1900	2800	1.12
245	62%	95%	ca. 100	41.0	3000	3300	3300	1.15
380	64%	99%	85[a]	76.5	6200	5700	7000	1.19
530	64%	100%	85[a]	184.4	14600	13400	16000	1.19

Strangely, there was no change in the fraction of xanthate compared to phthalimide between the two 600 MHz NMR spectra – both had an integration intensity of 1.7 after normalization and interference subtraction. One reason for this could be that there was no change in the amount of xanthate but rather that the longitudinal relaxation time (T1) for the methylene protons of the xanthate is longer than that for the phthalimide protons. This would result in a steady state forming at a lower relative population for the methylene protons, provided the transient scan time is sufficiently short. However, the spectra were recorded with a four second acquisition time and a 2 second relaxation delay. This is a generally long transient time and most protons should relax to their equilibrium population difference. However, T1 has been shown to be dependent on molecular size as larger molecules tumble more slowly.

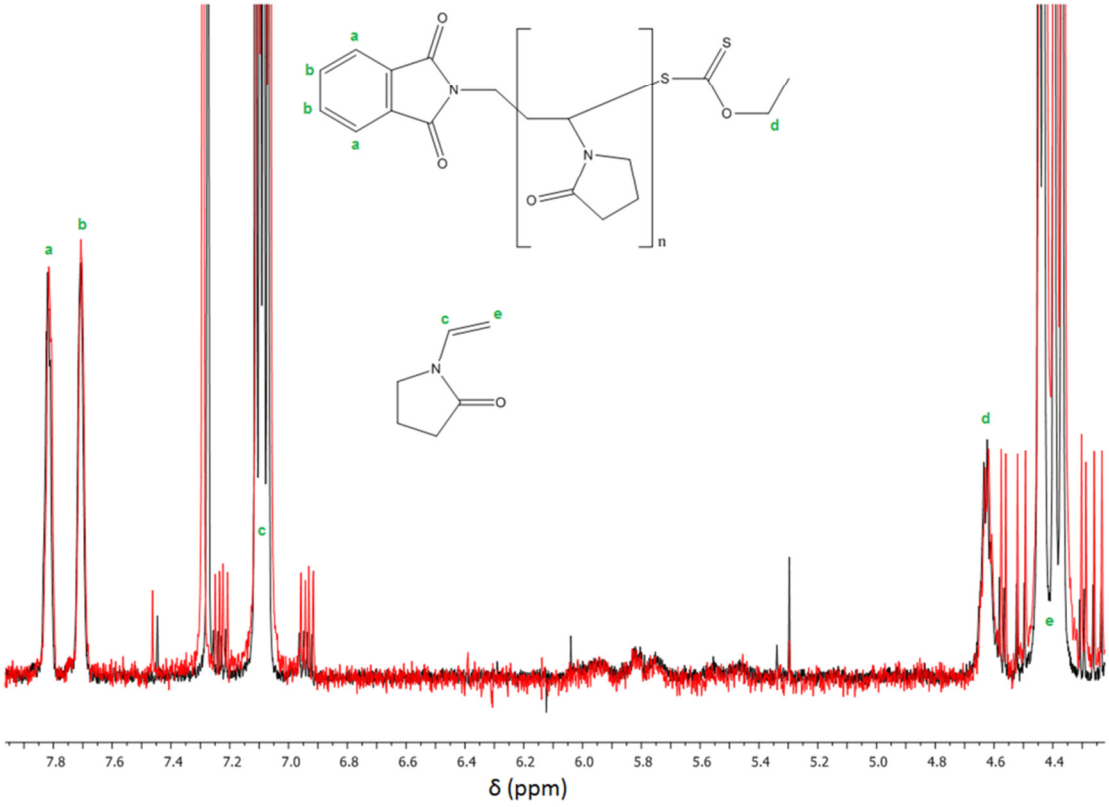

Figure 4.12: 600 MHz ^{1}H-NMR Spectrum of Reaction Mixture in $CDCl_3$ for (-) 3rd Interval of SDSB and (-) 4th Interval of SDSB.

SEC Results

SEC analyses of the samples obtained from the SDSB was performed as described in Section 3.2.5. The SEC traces were normalized as described in Appendix A1 and plotted according to molecular weight in Figure 4.13.A:

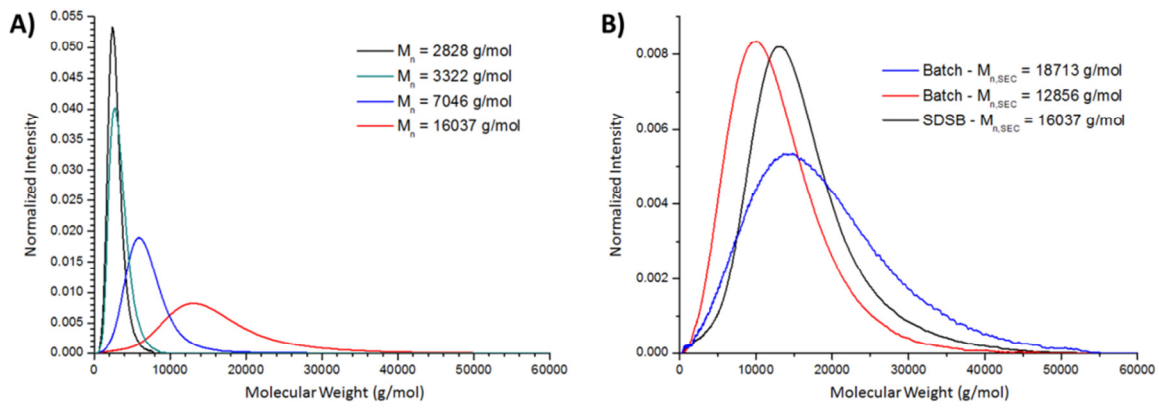

Figure 4.13: A) Molar Mass Distributions for SDSB. B) Comparison of Molar Mass Distributions for the Product of the SDSB with those for the Polymerizations Performed in Batch-Mode with R = 117 and R = 196 that had a Similar $M_{n,SEC}$.

Figure 4.13.B is a comparison of the normalized molar mass distributions for the final product of the SDSB with those for the batch-mode polymerizations described in Section 3.2.2 and 3.2.3. A comparison between the CDSB and SDSB results indicated that there was not much difference between the two products in terms of their distribution though an accurate comparison could not be made due to the differences in $M_{n,SEC}$ between the two products. It was much simpler to prepare a polymer with the desired molecular weight by the CDSB. Optimizing the stabilizing group on the RAFT agent combined with polymerization in semi-batch mode may improve the distribution of the products further.

4.7) Conclusions

The poor pre-equilibrium kinetics for the RAFT-mediated polymerization of NVP with XA2 were improved by optimizing the probability of radical transfer to the phthalimidylmethyl leaving group of XA2 from a propagating radical. This was achieved by performing the polymerization using a discrete semi-batch process. This process was modelled for two different monomer addition profiles. The first profile converged to a continuous semi-batch process and hence was called the convergent discrete semi-batch polymerization (CDSB). It resulted in a product with the lowest *Đ* for a particular M_n. It was also the easiest way to prepare a product with a specific M_n. The second process kept the dilution rate of the xanthate functionality constant and did not converge to a continuous semi-batch process. This process, called the steady discrete semi-batch process (SDSB), had products with only slightly larger *Đ* than those prepared by the convergent discrete semi-batch polymerization. The reaction time was significantly shorter for the SDSB. Also, both the fraction of phthalimide-functionalized chain ends as well as the fraction of dormant polymer chains were calculated to be larger for the SDSB than for the CDSB. The loss of xanthate end-groups compared to phthalimide end-groups was found to not increase with time. This suggested that the decomposition was caused by a reaction with a trace impurity rather than by a spontaneous decomposition such as thermolytic scission, disproportionation or hydrolysis.

4.8) References

1. Tefera, N.; Weickert, G.; Westerterp, K. R. Modeling of free radical polymerization up to high conversion. I. A method for the selection of models by simultaneous parameter estimation. *J. Appl. Polym. Sci.* **1997***, 63*, 1649-1661.

2. Tefera, N.; Weickert, G.; Westerterp, K. R. Modeling of free radical polymerization up to high conversion. II. Development of a mathematical model. *J. Appl. Polym. Sci.* **1997***, 63*, 1663-1680.

3. Matyjaszewski, K.; Davis, T. P. *Handbook of Radical Polymerization;* John Wiley and Sons.inc: Hoboken, New Jersey, 2002.

4. Kowollik, C. B. *Handbook of RAFT Polymerization;* WILEY-VCH Verlag GmbH & Co. KGaA: Weinheim, Baden-Württemberg, 2008.

5. Nace, H. R. In *The Preparation of Olefins by the Pyrolysis of Xanthates. The Chugaev Reaction;* Organic Reactions; John Wiley & Sons, Inc.: 2004.

6. Moad, G.; Chong, Y. K.; Postma, A.; Rizzardo, E.; Thang, S. H. Advances in RAFT polymerization: the synthesis of polymers with defined end-groups. *Polymer* **2005***, 46*, 8458-8468.

7. Willcock, H.; O'Reilly, R. K. End group removal and modification of RAFT polymers. *Polym. Chem.* **2010***, 1*, 149-157.

8. Jacobs, J.; Pound-Lana, G.; Klumperman, B. Poly(N-vinylpyrrolidone-b-(gamma]-benzyl-l-glutamate)) - synthesis and self-assembly into pH-sensitive micelles. *Polym. Chem.* **2012***, 3*, 2551-2560.

9. Pound, G.; McKenzie, J. M.; Lange, R. F. M.; Klumperman, B. Polymer-protein conjugates from small omega]-aldehyde end-functional poly(N-vinylpyrrolidone) synthesised via xanthate-mediated living radical polymerisation. *Chem. Commun.* **2008**, 3193-3195.

10. Santanakrishnan, S.; Hutchinson, R. A.; Učňová, L.; Stach, M.; Lacík, I.; Buback, M. Polymerization Kinetics of Water-Soluble N-Vinyl Monomers in Aqueous and Organic Solution. *Macromol. Symp.* **2011***, 302*, 216-223.

11. Hesse, P. *Radical Polymerization Kinetics in Aqueous Solution and in Systems with Secondary and Tertiary Radicals Studied by Novel Pulsed-Laser Techniques;* Cuvillear Verlag: Göttingen, 2008.

12. Stach, M.; Lacík, I.; Chorvát, D.; Buback, M.; Hesse, P.; Hutchinson, R. A.; Tang, L. Propagation Rate Coefficient for Radical Polymerization of N-Vinyl Pyrrolidone in Aqueous Solution Obtained by PLP-SEC. *Macromolecules* **2008***, 41*, 5174-5185.

13. Senogles, E.; Thomas, R. Polymerization kinetics of N-vinyl pyrrolidone. *J. Polymer Sci.: Symposium* **1975***, 49*, 203-210.

14. Brandrup, J.; Immergut, E. H.; Abe, A.; Grulke, E. A.; Bloch, D. R. *Polymer Handbook;* John Wiley & Sons, Incorporated: 2003.

CHAPTER 5

Deprotection of the Primary Amine α-End-Group on PVP

5.1) Introduction

As mentioned in Section 3.1, the thiocarbonylthio functional group reacts with amines to form a thiol and an *O*-thiocarbamate. This means that any free amine that forms by deprotection of the phthalimide-functionalized chains would react with any xanthate present in the reaction mixture. Also, the deprotection methods for the phthalimide group involve either reaction with hydrazine in methanol[1-4] or borohydride reduction followed by hydrolysis. Hydrazine is more nucleophilic than primary amines thus it would react rapidly with thiocarbonylthio groups. Sodium borohydride also acts as a nucleophile and attacks the xanthate end-group, converting it to a thiol in most cases. Since thiols can undergo oxidation to form disulfides under atmospheric conditions, it is necessary to end-cap these functional groups to avoid increasing M_n and *Đ* of the PVP block. While some thiol-functionalized PVP would be useful for coupling a targeting ligand to the surface of the micelle drug delivery system, most of it is not required and should be removed rather than capped. This is especially the case if any synthesis steps later on require catalytic hydrogenation because sulfur is generally not compatible with noble metal catalysts. Luckily, the xanthate end-group can be converted to a variety of different functional groups.[5-9]

To determine the amount of amine-functionalized polymer present after deprotection, derivatization with 3,5-bis(trifluoromethyl)benzaldehyde (TFBA) in a deuterated solvent (except water) and analyzing the sample by ^{1}H-NMR and ^{19}F-NMR was performed as described by Ji *et al.*[10] α, α, α-trifluorotoluene (TFT) was used as an internal standard. TFBA reacts with primary amines to form an imine, as depicted in Scheme 5.1. The fluorine nuclei of the TFBA imine conjugate have a different ^{19}F-NMR resonance frequency compared to those of free TFBA and the two peaks are resolved even for derivatized polymers.

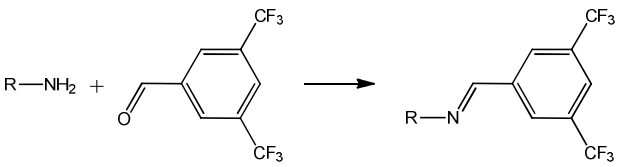

Scheme 5.1: Imine Formation of TFBA with Primary Amines.

Derivatization with pentafluorobenzaldehyde was also attempted.

5.2) Materials and Experimental Methods

Sodium hydrogen carbonate ($NaHCO_3$, ACS reagent grade), anhydrous calcium chloride, anhydrous calcium sulfate, concentrated sulfuric acid (95 – 97%), sodium metal and concentrated hydrochloric acid were purchased from Merck and used as received. Benzophenone, hydrazine hydrate (50 – 60%), 3,5-bis(trifluoromethyl)benzaldehyde (TFBA), pentafluorobenzaldehyde (PFBA), α,α,α-trifluorotoluene (TFT) and chloroform-d 99.8 atom % were purchased from Sigma Aldrich and used as received. 4Å molecular sieves (8 – 12 mesh) were also purchased from Sigma Aldrich, dried in a vacuum oven at 165 °C for 5 hours and allowed to cool to room temperature under vacuum before use. Methanol, dichloromethane and diethyl ether were purchased from KIMIX. Methanol was fractionally distilled before use. Dichloromethane was washed with concentrated sulfuric acid followed by 5% sodium bicarbonate solution and finally water before being dried over calcium chloride and fractionally distilled from calcium sulfate. Diethyl ether was distilled from sodium and benzophenone. Dimethylacetamide (Chromosolv® Plus, for HPLC ≥ 99.9%) was purchased from Sigma Aldrich and used as received. Butylated hydroxytoluene (BHT) 99% (GC) was purchased from Sigma Aldrich and used as received. Lithium chloride ≥ 98% was purchased from Riedel-de Haën and used as is. 0.45 µm Glass fiber prefilters were purchased from PALL Life Sciences. SnakeSkin® Dialysis tubing (3500 g/mol nominal molecular weight cutoff) was purchased from Thermo Scientific and used as is.

5.2.1) Thermolysis of the Xanthate End-Group

The general procedure for removal of the xanthate end-group by thermolysis was performed as follows. Isolated PVP to be thermolyzed was placed in a petri dish and covered with aluminium foil. A few small holes were punched in each cover using a fine needle. The samples were loaded into a vacuum oven along with a vial containing about 20 mL of liquid nitrogen and the pressure in the oven was dropped to below 1 mbar. Heating was then initiated and the samples were heated at 140 °C for 8 hours while keeping the pressure below 1 mbar. Afterwards, the heating was stopped and the oven was allowed to cool before the pressure was returned to atmospheric pressure. The samples were then retrieved and ^{1}H-NMR in $CDCl_3$ was performed to determine the degree of xanthate removal.

5.2.2) Deprotection of the Primary Amine End-Group

Thermolyzed PVP (0.3 g, 2.1×10^{-5} mol, M_n = 14,000 g/mol) was placed in three separate vials. The vials were labeled 1, 2 and 3. A 2.0 M stock solution of hydrazine in methanol was prepared by adding hydrazine hydrate (1.3037 g, 2.03×10^{-2} mol) to 8.7 mL of methanol. Specific aliquots of this solution were added to each vial and diluted with methanol. The amount of methanol and hydrazine solution added to each vial is depicted in Table 5.1.

Table 5.1: Hydrazine Stock Solution Dilution with Methanol for the 3 Trials.

Vial	Volume of Hydrazine Solution added (mL)	Volume of Methanol added (mL)	Molar Excess of Hydrazine
1	1	0	93
2	0.5	0.5	47
3	0.1	0.9	9

The vials were closed and left to react for 16 hours at 25 °C. The samples were then precipitated from diethyl ether three times, using dichloromethane as a solvent, and dried under vacuum. The isolated products were analyzed by ^{1}H-NMR to determine the degree of phthalimide deprotection.

5.2.3) Dialysis of the Deprotected PVP

Three samples of deprotected polymer, prepared as described in Section 5.2.2 with a 10 times molar excess of hydrazine, were each dissolved in 5 mL methanol. Each sample was placed in a separate 3,500 molecular weight cut-off (MWCO) dialysis tube and dialyzed with a different solvent. Sample 1 was dialyzed with three portions of 100 mL methanol, changed every 8 hours. Sample 2 was dialyzed with 3 portions of 100 mL de-ionized water followed by 2 portions of 100 mL methanol, changed every 8 hours. Sample 3 was dialyzed with 1 portion of 100 mL 0.1 M HCl followed by 3 portions of 100 mL de-ionized water and finally 2 portions of 100 mL methanol, changed every 8 hours. The polymers were isolated from solution by evaporation of the methanol under vacuum followed by dissolving the residue in DCM and precipitation from diethyl ether. ^{1}H-NMR spectra of Sample 2 and Sample 3 in $CDCl_3$ were recorded.

5.2.4) Derivatization with 3,5-Bis(trifluoromethyl)Benzaldehyde

0.024 g TFBA (9.9×10^{-5} mol) and 0.018 g TFT (1.23×10^{-4} mol) were added to 10 mL $CDCl_3$ to prepare a TFBA stock solution. 0.0193 g of the isolated polymer from Sample 2, prepared in Section 5.2.3, was

added to 1 mL of the TFBA stock solution. 5 beads of 4Å molecular sieves and 0.01 g $NaHCO_3$ were added to the sample and it was left to react in a 2 mL amber vial with a Teflon lid for 24 hours. The sample was filtered using a Pasteur pipette with a glass wool plug before being placed in an NMR tube for analysis. Both ^{1}H as well as ^{19}F NMR spectra were recorded for the sample and the stock solution. An acquisition time of 4 seconds and a relaxation delay of 16 seconds were used for acquiring the ^{19}F-NMR spectra. These were set to 4 seconds and 1 second, respectively, for the ^{1}H-NMR spectra.

5.2.5) Derivatization with Pentafluorobenzaldehyde

0.03 g (2.0×10^{-6} mol) deprotected PVP ($M_{n,NMR}$ = 13,400 g/mol), isolated as described for Sample 1 in Section 5.2.3, was dissolved in 1.00 mL $CDCl_3$. 0.007 g (3.6×10^{-5} mol) PFBA was added along with 0.02 g (2.4×10^{-4} mol) $NaHCO_3$ and a few beads of 4 Å molecular sieves. The sample was sealed and left in a cool, dark cupboard overnight. The solution was filtered through glass wool before ^{1}H-NMR analysis.

5.3) Results and Discussion

5.3.1) Themolysis of the Xanthate End-Group

NMR Analysis

The thermolyzed polymer samples were analyzed by ^{1}H-NMR in $CDCl_3$ in order to determine the degree of xanthate removal. Figure 5.1 shows the ^{1}H-NMR spectrum of the isolated polymer product from the CDSB superimposed on that for the thermolyzed product. The peaks at δ = 4.85 ppm and 6.95 ppm are characteristic of the internal and terminal vinyl protons of the alkene end-group on the thermolyzed product. Using the phthalimide proton peaks as an internal reference, the two spectra were normalized. Integration of the region in the ^{1}H-NMR spectrum of the thermolyzed product, where the methylene protons of the xanthate should be, indicated that the concentration of xanthate in the thermolyzed product was too low to be detected by ^{1}H-NMR. UV analysis could be used to get a more accurate measurement as it is a more sensitive technique.[9,11] However, due to time constraints, further analysis of the thermolysis efficiency was suspended. No byproducts of polymer degradation could be detected.

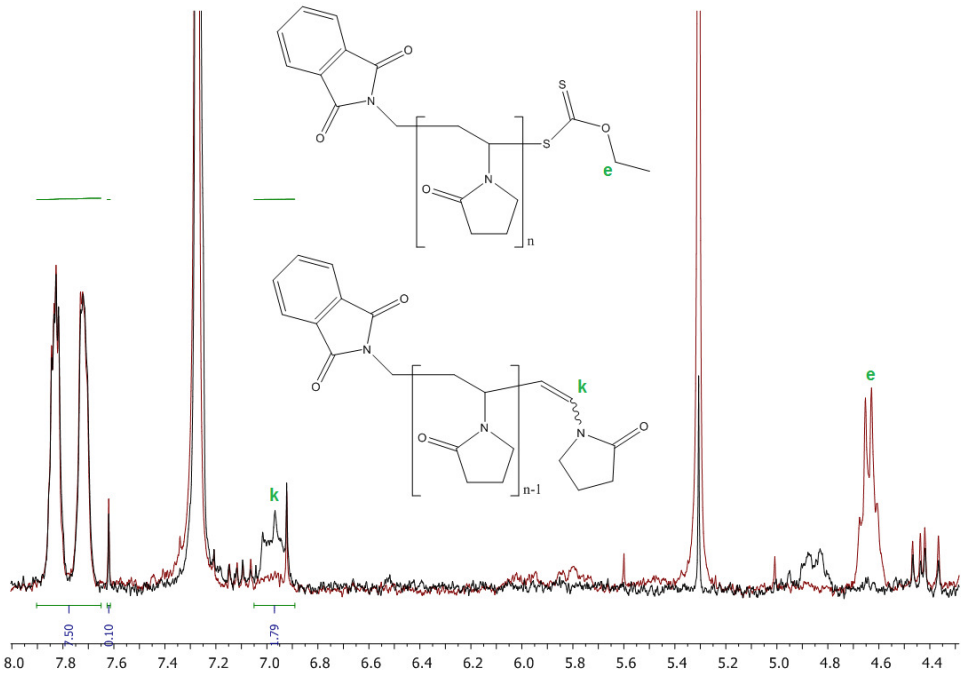

Figure 5.1: ^{1}H-NMR Spectra for (-) Xanthate-Functionalized PVP Starting Material and (-) Thermolyzed Product.

SEC Analysis

The thermolyzed PVP was analyzed by SEC in order to ensure that the polymer chains did not undergo any degradation during the thermolysis. Samples were prepared as described in Section 3.2.5. The SEC traces of the initial polymer and the thermolyzed product were baseline corrected and normalized as described in Appendix A1. The normalized distributions were plotted as functions of molecular weight in Figure 5.2.

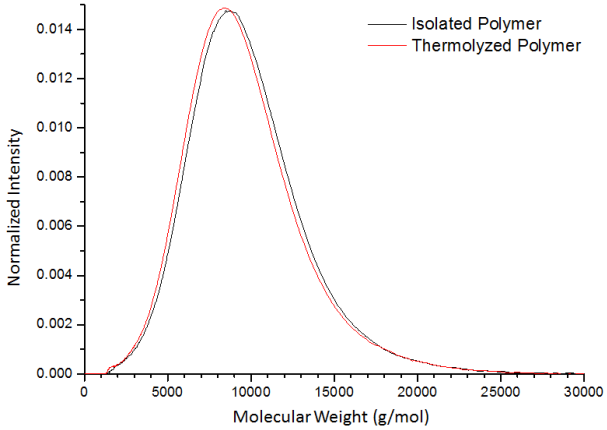

Figure 5.2: Comparison of the Normalized Molecular Weight Distributions for the Xanthate-Functionalized PVP and the Thermolyzed Product.

The almost identical molecular weight distributions indicate that there was indeed no degradation of the polymer chains. The slight shift in the peak positions could be due to non-linear baseline variations that could not be accounted for or a change in the hydrodynamic volume of the PVP due to the different end-group.

5.3.2) Deprotection of the Primary Amine α-End-Group and Isolation of the Product by Dialysis

NMR Analysis

The ^{1}H-NMR spectrum for vial 3 prepared in Section 5.2.2, with a 10-fold molar excess of hydrazine, is illustrated in Figure 5.3. The NMR spectrum of the thermolyzed polymer starting material was superimposed on it. The singlet at δ = 4.7 ppm could be due to some adsorbed molecular hydrogen that may have formed as a byproduct of hydrazine decomposition.[12,13] However, high temperatures are required for autothermal decomposition.[13] It could also be due to residual hydrazine although no references for the chemical shift of hydrazine in $CDCl_3$ could be found.

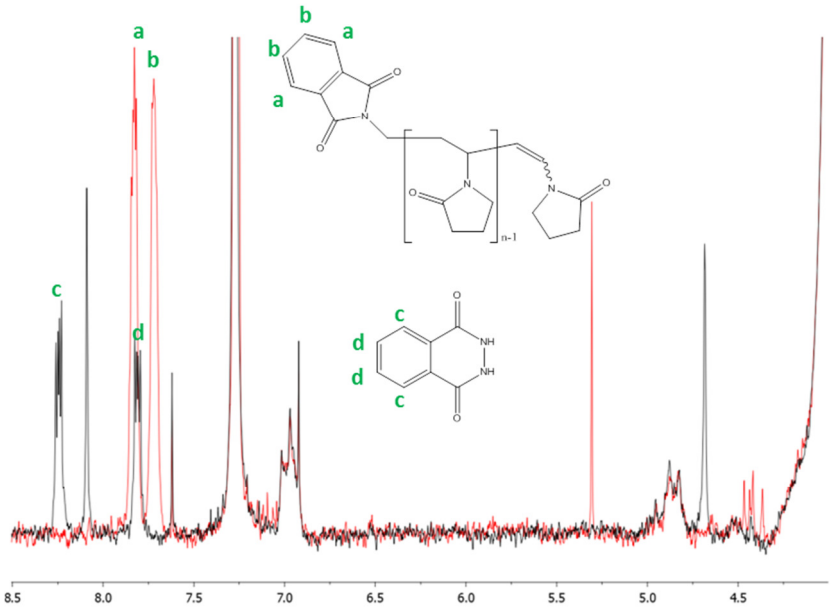

Figure 5.3: ^{1}H-NMR Spectra for (-) Thermolyzed Polymer. (-) Deprotected Polymer.

The absence of the phthalimide protons peaks at δ = 7.73 and 7.83 ppm indicated that the deprotection was quantitative even with only a 10-fold molar excess of hydrazine (equivalent to 0.2 M hydrazine and 0.02 M polymer solution). The peaks at δ = 7.81 and 8.25 ppm indicate that some residual 2,3-dihydro-1,4-phthalazinedione remained in the sample after precipitation. The spectrum

also indicated that the alkene end-group was not affected during the deprotection (δ = 6.91 – 7.06 ppm).

The ^{1}H-NMR spectra for Sample 2 and Sample 3, prepared in Section 5.2.3, were normalized by adjusting the integral for the polymer backbone peak at δ = 2.9 – 4.2 to equal that for the normalized thermolyzed polymer backbone peak with the same resonance frequency. Any changes in the fraction of alkene end-group between the thermolyzed PVP starting material and the dialyzed product was determined by measuring the change in the integral for the vinyl protons at δ = 6.95 ppm. For Sample 2, the integral intensity of the alkene end-groups changed from 0.81 to 0.74. This indicated that 9% of the alkene-terminal PVP chains had lost their alkene functionality, corresponding to approximately 7% of all the PVP chains in the sample. This change for Sample 3 was from 0.79 to 0.67, corresponding to 15% of the alkene-terminal PVP chains and approximately 12% of all the PVP chains in the sample. These results indicated that the presence of a strong acid increases the rate of alkene decomposition. The product formed could be an alkyl halide end-group, a hydroxyl end-group or an aldehyde end-group. A deeper investigation of the xanthate and alkene end-group hydrolysis is covered in Chapter 6.

SEC Analysis

The deprotected polymer was isolated from the excess hydrazine, as well as any byproducts of the deprotection, by the dialysis procedures described in Section 5.2.3. Figure 5.4.A shows the normalized molecular weight distribution for the deprotected polymer isolated from Sample 1 in Section 5.2.3. The normalized molecular weight distribution of the thermolyzed polymer starting material was superimposed on it. The comparison indicated that the $M_{n,SEC}$ decreased by 1,900 g/mol and *Đ* increased by 0.03. This would suggest decomposition of the polymer chains by the hydrazine. However, it is unlikely that hydrazine could cleave the hydrocarbon backbone. The unstable baseline made accurate correction impossible. A change in the hydrodynamic volume for PVP due to the different end-group could also play a role. Most likely however, the SEC chromatogram of the thermolyzed polymer was inaccurately taken. The SEC trace for this sample is illustrated in Figure 5.4.B.

The close correspondence of peak intensities in the high molecular weight region indicated that no coupling reactions, such as disulfide coupling or imine formation between an aldehyde-functionalized PVP and the amine-functionalized PVP, had occurred.

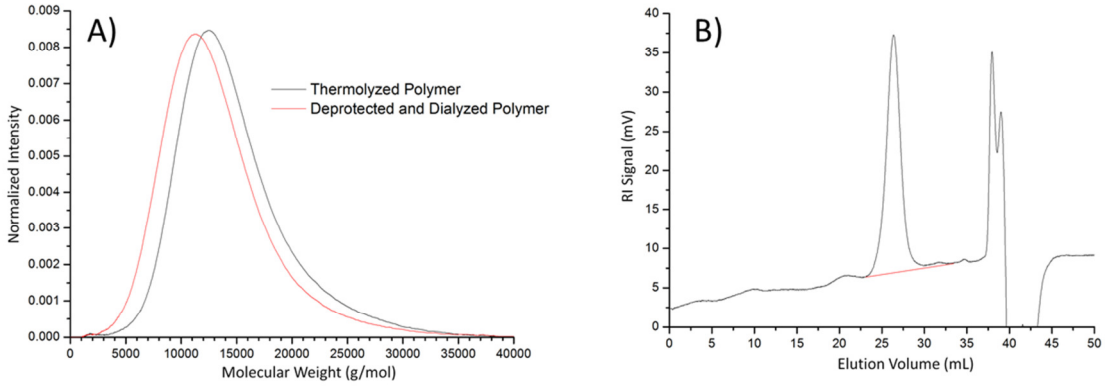

Figure 5.4: A) Normalized Molecular Weight Distribution for the (-) Polymer Isolated from Sample 1 in Section 5.2.3 Superimposed with those for the (-) Thermolyzed Polymer. B) SEC Trace for the Thermolyzed Polymer.

Figure 5.5.A shows the normalized molecular weight distribution of the deprotected polymer isolated from Sample 2 in Section 5.2.3 superimposed with that for its starting material. An increase in $M_{n,SEC}$ by 1,700 g/mol as well as an increase in *Đ* by 0.05 indicated that some of the polymer chains had undergone coupling reactions. A possible mechanism for coupling would be the partial hydrolysis of the alkene end-groups of the thermolyzed polymer to aldehydes followed by imine formation between the free amine end-groups and the aldehyde end-groups. This deduction is complemented by the results of Figure 5.5.A as the original distribution did not broaden but rather just decreased in intensity while a high molecular weight shoulder formed. Formation of disulfide linkages is unlikely to occur to a significant extent as the xanthate end-group was reduced to a level below the detection limit for NMR. Further evidence of conjugation by imine formation was noted for the results of Sample 3. Figure 5.5.B shows the normalized molecular weight distribution of the deprotected polymer isolated from Sample 3 as well as that for the thermolyzed PVP starting material. Comparing the normalized molecular weight distribution for Sample 3 with those for Sample 2, it is evident that a larger fraction of polymer chains had undergone coupling for Sample 3. For sample 3, $M_{n,SEC}$ increased by 3,500 g/mol and *Đ* increased by 0.13. The fact that the major peak for the molecular distributions of Sample 2 and Sample 3 did not shift significantly further indicated that the change in the molecular weight distribution for Sample 1 was due to an error in the measurement caused by the unstable baseline rather than by end-group effects.

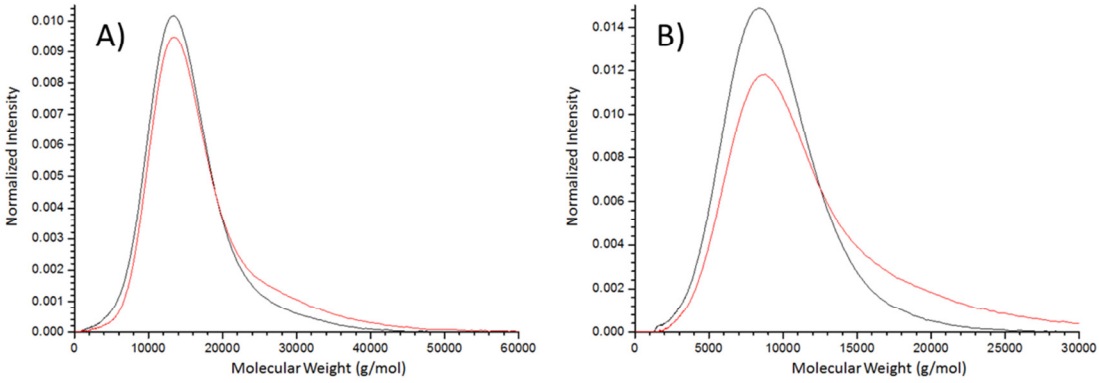

Figure 5.5: Normalized Molecular Weight Distributions of the Deprotected Polymer Samples (-) Isolated from A) Sample 2 and B) Sample 3, prepared in Section 5.2.3. (-) Thermolyzed Polymer.

5.3.3) Derivatization with 3,5-Bis(trifluoromethyl)Benzaldehyde

NMR Analysis

The ^{19}F-NMR spectrum of the TFBA stock solution, illustrated in Figure 5.6, was used to determine the ratio of TFBA relative to TFT. This ratio was 0.795 : 1.

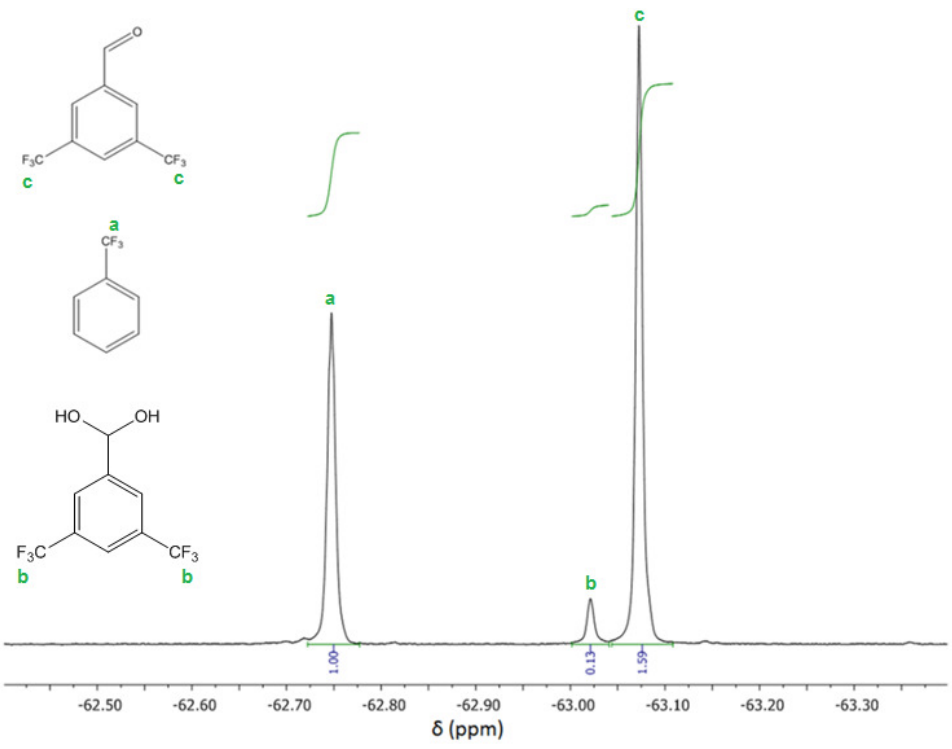

Figure 5.6: Normalized ^{19}F-NMR Spectrum of TFBA Stock Solution Prepared in Section 5.2.4.

There was an unassigned peak at δ = -63.02 ppm. It was unclear what impurity was responsible for this peak but it was suspected that it was the TFBA hydrate. The ^{1}H-NMR spectrum of the stock solution, illustrated in Figure 5.7, contained a broad resonance signal at δ = 3.8 ppm. It had the same integration intensity, relative to TFBA, as the fluorinated impurity. A resonance in this region is characteristic of the carbonyl proton of a hydrate. The electron-withdrawing effect of the meta-trifluoromethyl functional groups could cause the hydrate of TFBA to be more stable than that for benzaldehyde.

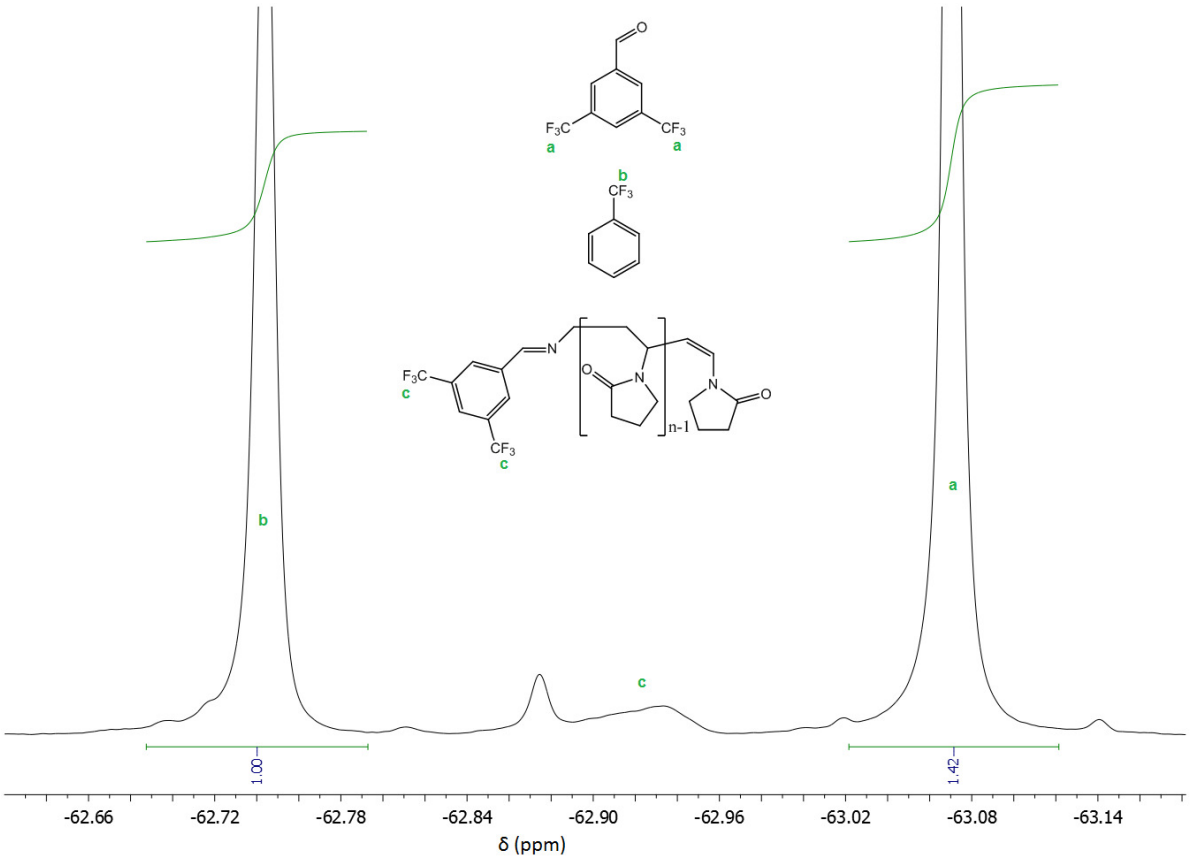

Figure 5.7: Normalized ^{1}H-NMR Spectrum of TFBA Stock Solution Prepared in Section 5.2.4.

The ^{1}H-NMR spectrum of the TFBA-derivatized sample, prepared in Section 5.2.4, is illustrated in Figure 5.8. The peaks downfield of δ = 8 ppm are from the excess TFBA. It was used to determine the amount of TFT relative to PVP. The spectrum was normalized with respect to the number of PVP chains in the sample by adjusting the integral for δ = 2.9 – 4.2 ppm to 393.68. This value is equal to the integral for the same region in the ^{1}H-NMR spectrum of the thermolyzed PVP starting material, illustrated in Figure 5.9. The difference in the amount of residual diethyl ether absorbed in the separate samples was accounted for using a numerical procedure that is described in Appendix A10.

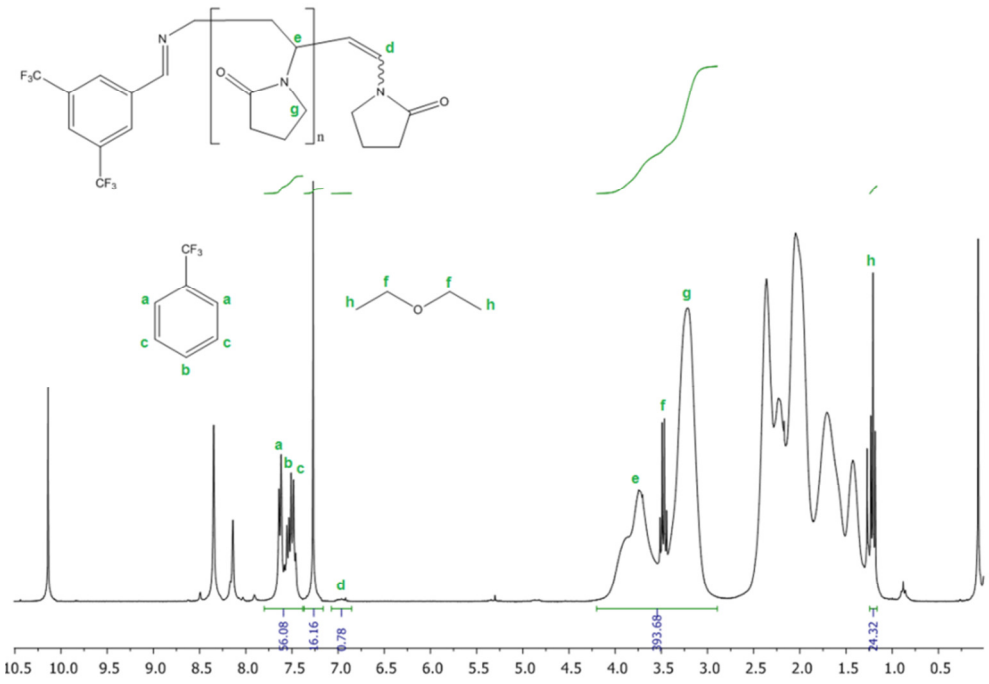

Figure 5.8: ^{1}H-NMR Spectrum of TFBA-Derivatized PVP Prepared in Section 5.2.4.

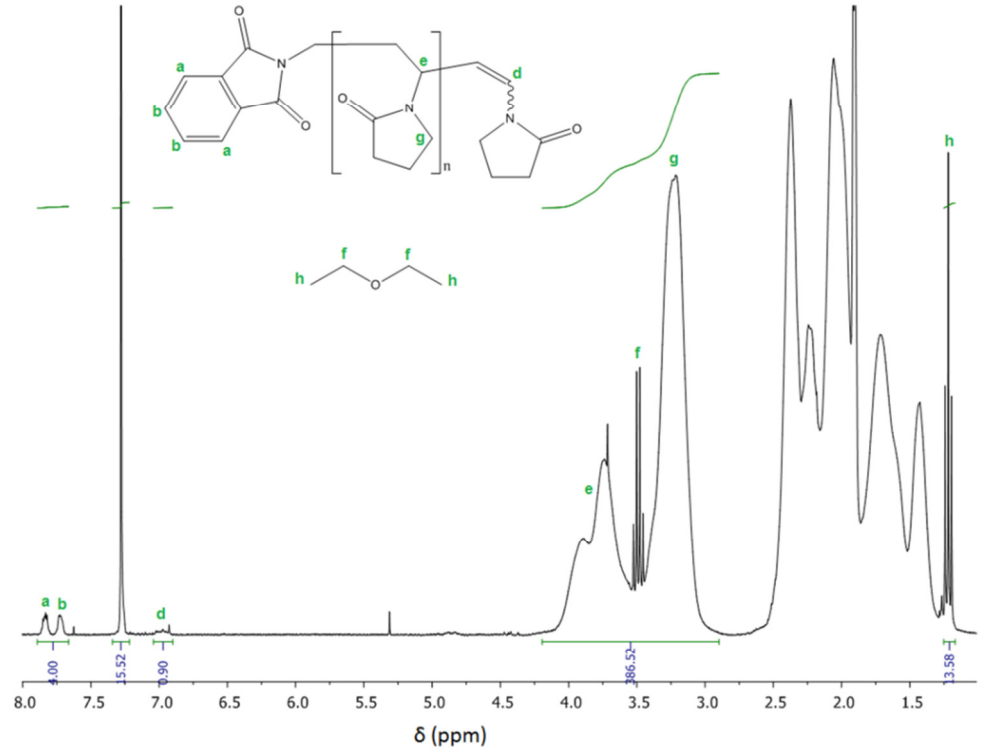

Figure 5.9: ^{1}H-NMR Spectrum of Thermolyzed Polymer used as the Starting Material for the Preparation of Sample 2 in Section 5.2.3.

Once the ^{1}H-NMR spectrum of the TFBA-derivatized polymer sample was normalized, the amount of TFT relative to the phthalimide-initiated PVP chains in the sample could be determined by dividing the integral for the aromatic TFT protons by 5. This gave a value of 11.22.

The change in the intensity of the TFBA peak in the ^{19}F-NMR spectrum of the TFBA-derivatized PVP sample, illustrated in Figure 5.10, could be used to determine the fraction of TFBA that reacted with the amine end-groups of PVP. This was calculated according to Equation 5.1.

$$\frac{\int_{\delta=-63.11}^{\delta=-63.04} f_1(\delta)d\delta - \int_{\delta=-63.11}^{\delta=-63.04} f_2(\delta)d\delta}{\int_{\delta=-63.11}^{\delta=-63.04} f_1(\delta)d\delta} = \frac{1.59-1.42}{1.59} = 0.107 \quad (5.1)$$

Where

$f_1(\delta)$ = ^{19}F-NMR spectrum of TFBA stock solution

$f_2(\delta)$ = ^{19}F-NMR spectrum of TFBA-derivatized PVP sample

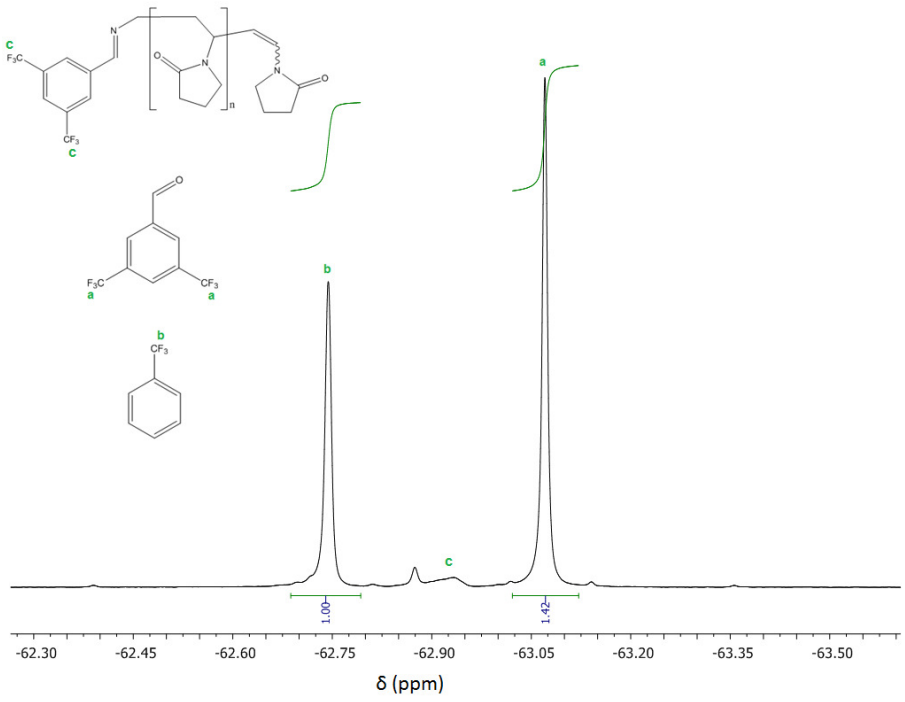

Figure 5.10: ^{19}F-NMR Spectrum of TFBA-Derivatized PVP Prepared in Section 5.2.4.

The fraction of phthalimide-functionalized PVP that had been successfully deprotected and derivatized was calculated according to the Equation 5.2.

$$\frac{\int_{\delta=-63.11}^{\delta=-63.04} f_3(\delta)d\delta - \int_{\delta=-63.11}^{\delta=-63.04} f_4(\delta)d\delta}{\int_{\delta=-63.11}^{\delta=-63.04} f_3(\delta)d\delta} \times 0.795 \times 11.22 = 0.95 \quad (5.2)$$

This indicated that at least 95% of the phthalimide functionalized chains were successfully deprotected and derivatized. This is in close agreement with the lack of any detectable phthalimide in the NMR spectra for the deprotected polymer samples as well as the theory that a few percent of the PVP chains underwent coupling by imine formation with aldehyde-functionalized PVP.

5.3.4) Derivatization with Pentafluorobenzaldehyde

NMR Analysis

In order to normalize the ^{1}H-NMR spectrum of the PFBA-derivatized PVP, the integral for the alkene protons in the ^{1}H-NMR spectrum was adjusted to 0.85 – the integral value for this peak after normalizing the thermolyzed sample. The interference from the carbon satellite of the chloroform peak was taken into account as described in Appendix A11. This was the fraction of xanthate end-groups in the starting material relative to phthalimide end-groups, as illustrated in Figure 4.12. The fraction of PFBA-derivatized PVP relative to phthalimide could then be measured directly from the integral of the imine protons at δ = 8.20 to 8.47 ppm, as illustrated in Figure 5.11.

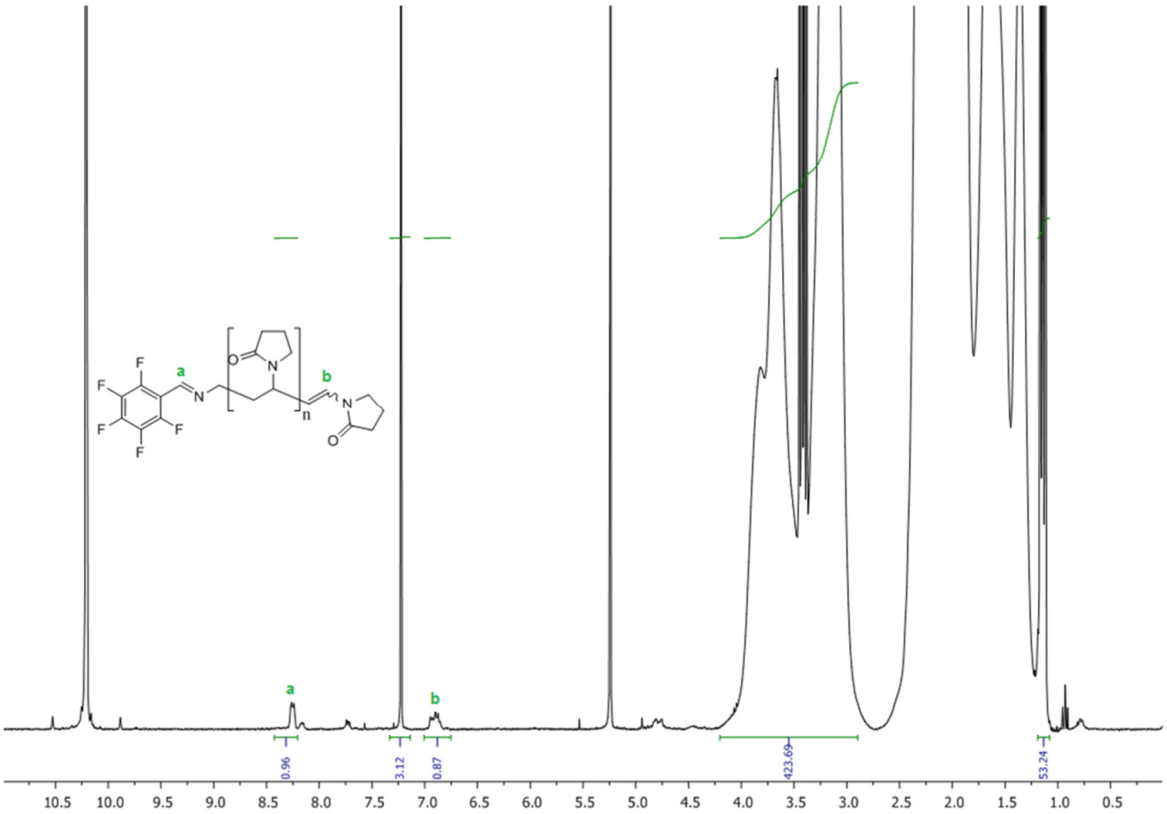

Figure 5.11: ^{1}H-NMR Spectrum for the PFBA-derivatized PVP.

This gave a value of 0.96, indicating that this procedure is as good as the TFBA derivatization analysis for polymers with a molecular weight range around 14,000 g/mol. For higher molecular weight polymers, the TFBA derivatization may be preferable as there are 6 equivalent fluorine nuclei per molecule as opposed to the single carbonyl hydrogen on PFBA. ^{19}F nuclei have a relative sensitivity of 83% compared to ^{1}H thus the TFBA derivatization should provide greater sensitivity by a factor of 0.83 × 6 = 4.98. However, the high chemical shift anisotropy effect for fluorine nuclei causes their transverse relaxation to decrease with the magnetic field strength of the instrument.[14] This can result in a reduced sensitivity from broadening signals when high field strength instruments are used. Also, the analysis time for the TFBA derivatization is greater than for the PFBA derivatization as three NMR spectra need to be taken and the longitudinal relaxation time of fluorine nuclei is usually considerably longer than for hydrogen nuclei.[15,16] Hence, the greater sensitivity of the TFBA derivatization may only be necessary for analyzing polymers with a much higher molecular weight.

5.4) Conclusions

The quantitative removal of the phthalimide protecting group from PVP prepared by RAFT-mediated polymerization with XA2 was achieved by reacting with hydrazine in methanol. This was confirmed by ^{1}H-NMR. The presence of free primary amines on the deprotected, isolated PVP was quantified using TFBA and PFBA derivatization procedures. Both showed over 90% of the phthalimide chain ends had been converted to phthalimide chain ends. PFBA derivatization proved to be effective and simpler for analyzing polymers with a molecular weight range of up to 14,000 g/mol. The xanthate end-group had to be removed beforehand as it would react with the hydrazine in solution as well as the free amine end-groups. This was quantitatively achieved by thermolysis of PVP in a vacuum oven at 140 °C and at a pressure of less than 1 mbar. There was an increase in $M_{n,SEC}$ and $Đ$ for the deprotected PVP compared to the thermolyzed PVP. It was considered that this was occurring due to hydrolysis of the alkene end-groups to aldehyde end-groups during dialysis and their subsequent conjugation with the amine end-groups to form imine bonds. Dialysis with 0.1 M HCl resulted in a greater increase in both $M_{n,SEC}$ and $Đ$.

5.5) References

1. Osby, J. O.; Martin, M. G.; Ganem, B. An exceptionally mild deprotection of phthalimides. *Tetrahedron Lett.* **1984**, *25*, 2093-2096.

2. Horii, Z.; Iwata, C.; Tamura, Y. Reduction of Phthalimides with Sodium Borohydride. *J. Org. Chem.* **1961***, 26*, 2273-2276.

3. Wuts, P. G. M.; W. Greene, T. W. *Greene's Protective Groups in Organic Synthesis;* John Wiley and Sons, Inc.: Hoboken, New Jersey, 2012.

4. Gibson, M. S.; Bradshaw, R. W. The Gabriel Synthesis of Primary Amines. *Angew. Chem. Int. Ed.* **1968***, 7*, 919-930.

5. Moad, G.; Chong, Y. K.; Postma, A.; Rizzardo, E.; Thang, S. H. Advances in RAFT polymerization: the synthesis of polymers with defined end-groups. *Polymer* **2005***, 46*, 8458-8468.

6. Kowollik, C. B. *Handbook of RAFT Polymerization;* WILEY-VCH Verlag GmbH & Co. KGaA: Weinheim, Baden-Württemberg, 2008.

7. Jacobs, J.; Pound-Lana, G.; Klumperman, B. Poly(N-vinylpyrrolidone-b-(gamma]-benzyl-l-glutamate)) - synthesis and self-assembly into pH-sensitive micelles. *Polym. Chem.* **2012***, 3*, 2551-2560.

8. Pound, G.; McKenzie, J. M.; Lange, R. F. M.; Klumperman, B. Polymer-protein conjugates from small omega]-aldehyde end-functional poly(N-vinylpyrrolidone) synthesised via xanthate-mediated living radical polymerisation. *Chem. Commun.* **2008**, 3193-3195.

9. Willcock, H.; O'Reilly, R. K. End group removal and modification of RAFT polymers. *Polym. Chem.* **2010***, 1*, 149-157.

10. Ji, S.; Hoye, T. R.; Macosko, C. W. Primary Amine (-NH2) Quantification in Polymers: Functionality by 19F NMR Spectroscopy. *Macromolecules* **2005***, 38*, 4679-4686.

11. Postma, A.; Davis, T. P.; Li, G.; Moad, G.; O'Shea, M. S. RAFT Polymerization with Phthalimidylmethyl Trithiocarbonates or Xanthates. On the Origin of Bimodal Molecular Weight Distributions in Living Radical Polymerization. *Macromolecules* **2006***, 39*, 5307-5318.

12. Fulmer, G. R.; Miller, A. J. M.; Sherden, N. H.; Gottlieb, H. E.; Nudelman, A.; Stoltz, B. M.; Bercaw, J. E.; Goldberg, K. I. NMR Chemical Shifts of Trace Impurities: Common Laboratory Solvents, Organics, and Gases in Deuterated Solvents Relevant to the Organometallic Chemist. *Organometallics* **2010***, 29*, 2176-2179.

13. Pakdehi, S. G.; Salimi, M.; Rasoolzadeh, M. A Review on Decomposition of Hydrazine and Its Kinetics as a Novel Approach for CO-Free H_2 Production. *RAME* **2014***, 3*, 21-25.

14. Gerig, J. T. Fluorine nuclear magnetic resonance of fluorinated ligands. *Meth. Enzymol.* **1989***, 177*, 3-23.

15. Sarkouhi, M.; Hassan, J.; Shamsipur, M. 19F-NMR Analysis of Primary and Secondary Amines Following Chemical Derivatization with Trifluoroacetic Anhydride. *Appl. Magn. Reson.* **2012***, 43*, 377-384.

16. Shi, P.; Wang, H.; Xi, Z.; Shi, C.; Xiong, Y.; Tian, C. Site-specific 19F NMR chemical shift and side chain relaxation analysis of a membrane protein labelled with an unnatural amino acid. *Protein Science* **2011***, 20*, 224-228.

CHAPTER 6

Hydrolysis of the Xanthate and Alkene End-Groups on PVP

6.1) Introduction

In Section 5.3.2, it was proposed that alkene end-groups of the thermolyzed PVP tend to decompose into aldehyde end-groups in aqueous media. The hydrolysis of the alkene chain ends to form aldehyde chain ends during dialysis of the deprotected PVP with water and with 0.1 M HCl was problematic as it resulted in the formation of imine bonds between the amine chain ends and the aldehyde chain ends in organic solvents. This could prevent the derivatized amine end-groups from acting as initiators for the ROP of L-lysine NCAs. Furthermore, the method of choice for deprotection of the N^{ε}-(benzyloxycarbonyl)-L-lysine residues was acidolysis with HBr in a dioxane/dichloromethane solvent mixture (see Sections 8.2.2 and 8.3.1). Under these conditions, it is likely that any alkene groups would undergo electrophilic addition of HBr. The alkyl bromide could hydrolyze to also form a hydroxyl-terminated PVP, as illustrated in Scheme 6.1.

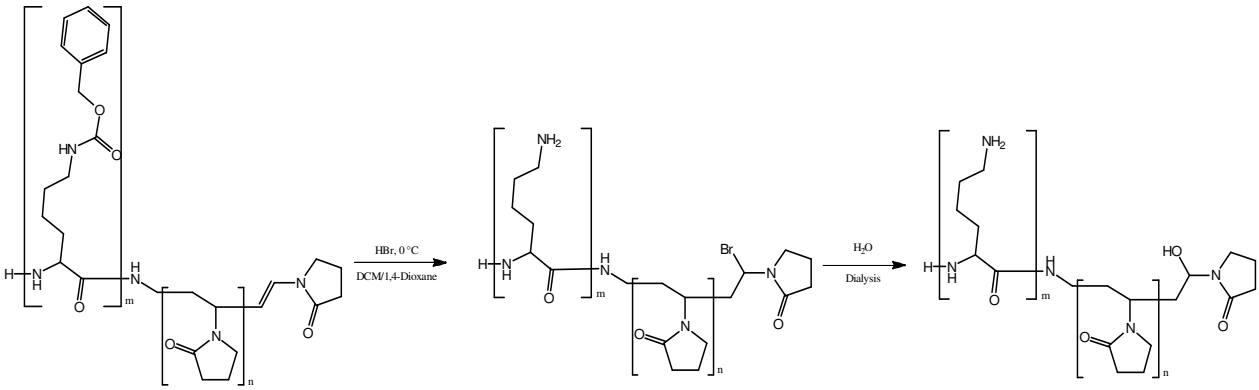

Scheme 6.1: Addition of HBr to Alkene End-Groups of PVP and Subsequent Hydrolysis of the Bromide.

On the other hand, the free amines on the lysine residues could attack the alkyl halide, resulting in the coupling of polymer chains. The hydroxyl-terminated PVP is known to convert to an aldehyde via elimination of pyrrolidone,[1,2] as illustrated in Scheme 6.2.

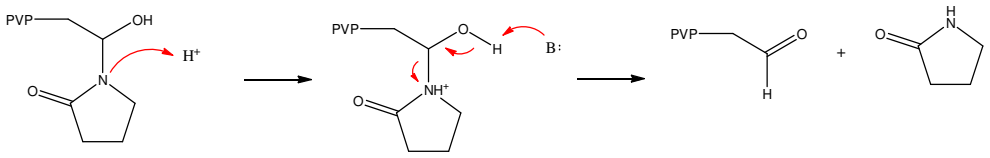

Scheme 6.2: Formation of Aldehyde End-Groups via Elimination of Pyrrolidone.

The presence of an aldehyde functional group on the PVP block of the block copolymer would be problematic as it could react with the primary amines of the lysine residues as well as that on the daunosamine residue of Doxorubicin. This could affect the micelle self-assembly, architecture or drug release profile. Thus it would be best to either protect or remove the aldehyde chain end after the acidolysis step or to remove the xanthate end-group via another method. If the xanthate can be quantitatively converted to an aldehyde chain end without affecting the phthalimide chain end, it could be removed before the amine is deprotected. Reduction or oxidation of the aldehyde are two possible methods for its selective removal. Phthalimides are generally insensitive to most oxidizing agents that are powerful enough to convert an aldehyde to a carboxylic acid.[3] Phthalimides are also not deprotected by sodium borohydride but are instead converted to 2-(hydroxymethyl)benzamides.[3,4] These functional groups readily hydrolyze in acidic solutions at elevated temperatures, releasing the primary amine.[3,5] Thus the primary amine end-group can be deprotected via a two-step process, with the aldehyde end-groups being transformed into the more stable primary hydroxyl end-groups during the first step. This deprotection procedure is illustrated in Scheme 6.3.

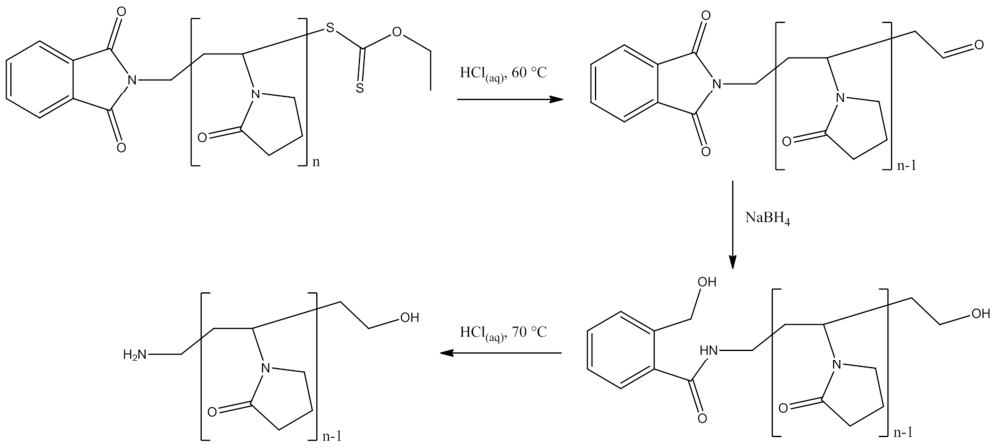

Scheme 6.3: Two-Step Removal of Phthalimide Protecting Group with Simultaneous Reduction of Aldehyde End-Groups.

The mechanism by which the xanthate chain end is converted to a hydroxyl chain end was unclear. Three possible mechanisms were considered. The first mechanism involves nucleophilic attack on

the thiocarbonyl carbon followed by decomposition of the tetrahedral intermediate by elimination of the weakest base, as depicted in Scheme 6.4.

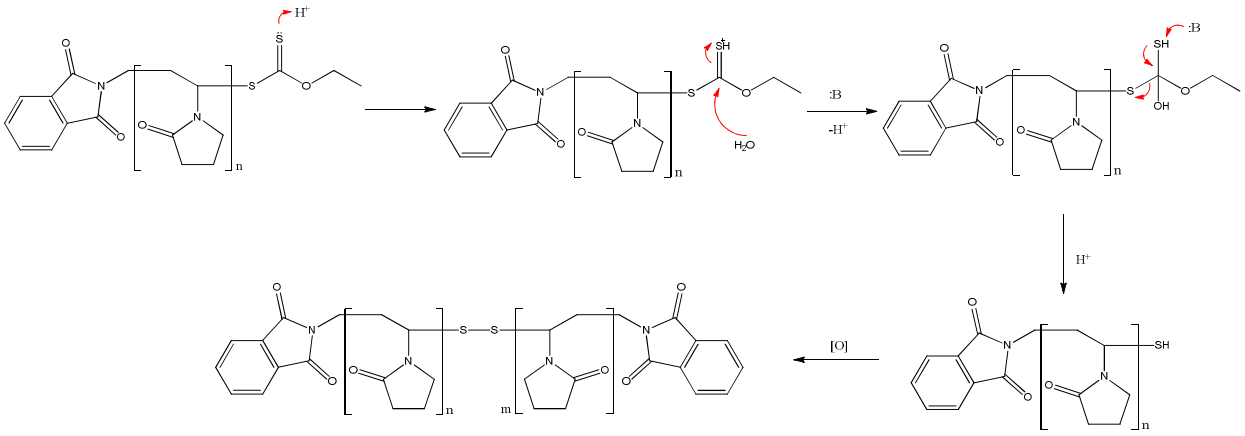

Scheme 6.4: Mechanism of Xanthate Hydrolysis by Nucleophilic Attack.

This mechanism indicates that a thiol chain end will be formed instead of a xanthate. The second mechanism involves elimination of xanthic acid, either via a bimolecular or unimolecular process, as depicted in Scheme 6.5.

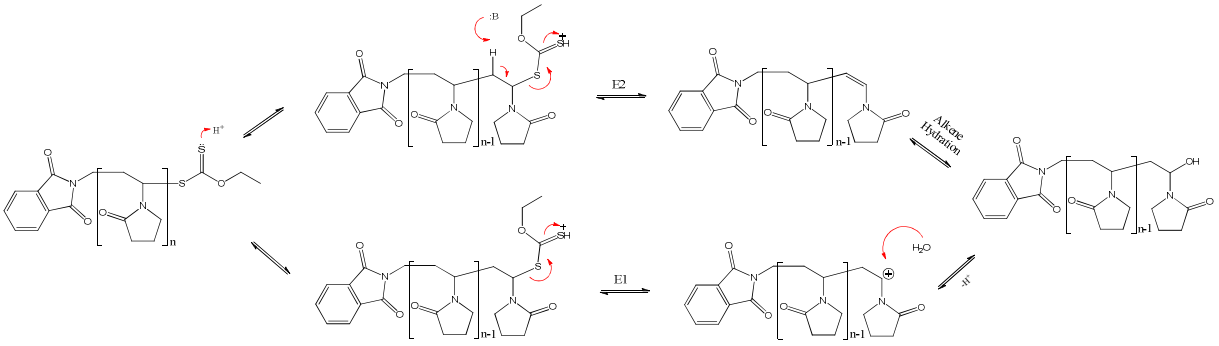

Scheme 6.5: Mechanism of Xanthate Hydrolysis by Elimination of Xanthic Acid.

However, the bimolecular process involves hydration of the alkene-terminated PVP. Alkene hydration usually does not occur readily at low temperatures without the addition of a strong acid catalyst. Hence, a unimolecular elimination mechanism is the most likely process by which the xanthate end-group is converted to an alcohol end-group in water. Water is a weak base and would be more likely to donate a pair of electrons to the carbocation than to extract a proton.

The final mechanism considered possible was nucleophilic substitution of xanthic acid with water, as depicted in Scheme 6.6.

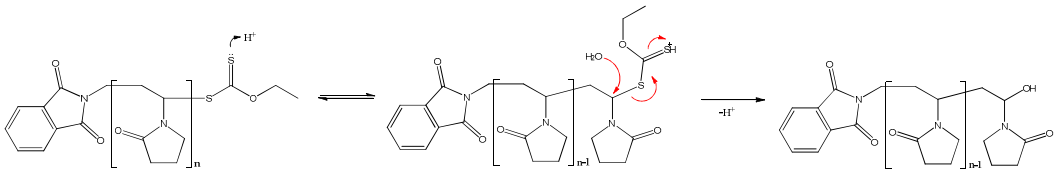

Scheme 6.6: Mechanism of Xanthate Hydrolysis by Substitution of Xanthic Acid with Water.

Formation of a hydroxyl end-group could be more likely to occur in acidic media than formation of a thiol end-group since xanthic acid decomposes into carbon disulfide and water under such conditions. This would drive the reaction towards the quantitative formation of the hydroxyl end-group. Four *in-situ* ^{1}H-NMR kinetic experiments were performed in order to get a better understanding of the rates of xanthate conversion to an alcohol, an aldehyde or a thiol under various conditions. This would help to optimize the reaction conditions for the conversion of the xanthate end-group to an aldehyde in the presence of a phthalimide protecting group. The simultaneous reduction of the aldehyde end-group and deprotection of the phthalimide end-group was also attempted.

6.2) Materials and Experimental Methods

Anhydrous calcium chloride, sodium hydrogen carbonate (ACS reagent grade), anhydrous sodium carbonate (Na_2CO_3), concentrated hydrochloric acid (32%), anhydrous calcium sulfate, concentrated sulfuric acid (95 – 97%) and D_2O were purchased from Merck and used as received. A seven inch long Wilmad® quick pressure valve medium wall NMR tube with a 5 mm diameter, benzophenone, 35% DCl in D_2O, sodium borohydride (98.5%) and chloroform-d 99.8 atom % were purchased from Sigma Aldrich and used as received. Methanol, dichloromethane and diethyl ether were purchased from KIMIX. Methanol was fractionally distilled before use. Dichloromethane was washed with concentrated sulfuric acid followed by 5% sodium bicarbonate solution and finally water before being dried over calcium chloride and fractionally distilled from calcium sulfate. Diethyl ether was distilled from sodium and benzophenone. Dimethylacetamide (Chromosolv® Plus, for HPLC ≥ 99.9%) was purchased from Sigma Aldrich and used as received. Butylated hydroxytoluene (BHT) 99% (GC) was purchased from Sigma Aldrich and used as received. Lithium chloride ≥ 98% was purchased from Riedel-de Haën and used as is. 0.45 µm Glass fiber prefilters were purchased from PALL Life Sciences. SnakeSkin® Dialysis tubing (3500 g/mol nominal molecular weight cutoff) was purchased from Thermo Scientific and used as is.

6.2.1) *In-Situ* ^{1}H-NMR Kinetic analysis of Xanthate End-Group Hydrolysis

Two *in-situ* ^{1}H-NMR experiments were performed in order to study the mechanisms and rates of xanthate end-group hydrolysis reactions in D_2O and 1 M DCl.

Xanthate-functionalized PVP (0.01 g, 2.48×10^{-6} mol), prepared in Section 4.5.2, ($M_{n,NMR}$ = 4,000 g/mol) was added to two separate vials.

0.75 mL D_2O was added to the first vial and the solution was placed in a Wilmad® quick pressure valve medium wall NMR tube. A vacuum was carefully applied for one minute in order to remove the residual organic solvents and the NMR tube was back-filled with nitrogen. The time taken from addition of the D_2O until the NMR analysis began was measured. A Varian VNMRS 300 MHz spectrometer was used for the analysis. A scan of the initial conditions at 25 °C was taken, the sample was withdrawn and the temperature in the probe was raised to 40 °C. The sample was re-inserted, the deuterium feed-back loop was locked and the magnetic field was shimmed before the analysis was continued. The time taken to do this was recorded. A spectrum was recorded every 388 seconds, using 64 scans with an acquisition time and relaxation delay of 4 seconds each, for a total acquisition time of 512 seconds and a total analysis time of 13 hours. The PVP was isolated from the reaction mixture by evaporation of the D_2O under vacuum, dissolving the residue in DCM and precipitation from diethyl ether. SEC analysis was performed on the isolated sample.

For the second vial, the sample was prepared as described for the first vial except that 0.068 mL 35% (w/w) DCl in D_2O (0.085 g, 7.94×10^{-4} mol) was added to the NMR tube quickly before analysis. The time taken from this addition until the initial conditions could be recorded was measured. The analysis was performed on a Varian Inova 400 MHz NMR spectrometer with nitrogen gas being used for the VT control. After the initial conditions at 25 °C were recorded, the sample was removed and the temperature of the probe was raised to 60 °C before re-inserting the sample, locking the deuterium feed-back loop, shimming the magnetic field and continuing with the analysis. The time taken to do this was recorded. A spectrum was recorded every 1608 seconds, using 16 scans with an acquisition time of 4 seconds and a relaxation delay of 8 seconds, for a total acquisition time of 192 seconds per spectrum and a total analysis time of 64 hours. The PVP was isolated from the reaction mixture by adding sodium carbonate (0.065 g, 6.13×10^{-4} mol) and measuring the pH (pH = 11), evaporation of the D_2O, dissolving the residue in DCM and precipitation from diethyl ether. SEC analysis was performed on the isolated sample.

6.2.2) *In-Situ* ^{1}H-NMR Kinetic analysis of Alkene End-Group Hydrolysis

Two *in-situ* ^{1}H-NMR experiments were performed in order to study the mechanisms and rates of alkene end-group hydrolysis reactions in D_2O and 1 M DCl.

Thermolyzed PVP (0.01 g, 2.48×10^{-6} mol), prepared as described in Section 5.2.1 from PVP synthesized by the SDSB in Section 4.5.3 ($M_{n,NMR}$ = 7,000 g/mol), was added to two separate vials.

0.75 mL D_2O was added to the first vial and the sample was prepared as described for vial 1 in Section 6.2.1. The kinetic analysis was measured for 64 hours at 65 °C. A spectrum was recorded every 3216 seconds, using 32 scans with an acquisition time of 4 seconds and a relaxation delay of 8 seconds, for a total acquisition time of 384 seconds. The PVP was isolated from the reaction mixture by evaporation of the D_2O, dissolving the residue in DCM and precipitation from diethyl ether. SEC analysis was performed on the isolated sample.

For the second vial, the sample was prepared as described for vial 2 in Section 6.2.1. The kinetic analysis was measured for 15 hours at 65 °C. A spectrum was recorded every 1416 seconds, using 32 scans with an acquisition time of 4 seconds and a relaxation delay of 8 seconds, for a total acquisition time of 384 seconds. The PVP was isolated from the reaction mixture by addition of sodium bicarbonate (0.06 g, 7.14×10^{-4} mol), evaporation of the D_2O, dissolving the residue in DCM and precipitation from diethyl ether. SEC analysis was performed on the isolated sample.

6.2.3) Reduction of the Aldehyde End-Group with Simultaneous Phthalimide Deprotection

1 g of the crude PVP reaction mixture, prepared by the CDSB as described in Section 4.5.2, ($M_{n,NMR}$ = 10,100 g/mol) was dissolved in 5 mL of 1 M HCl and dialyzed with 1 M HCl at 60 °C for 16 hours. The solution was then dialyzed with deionized water until it was neutral. 1 mL of the solution was isolated by evaporation of the water under vacuum, dissolving the residue in DCM and precipitation from diethyl ether. The isolated polymer was analyzed by ^{1}H-NMR. Another 2 mL of the solution was placed in a separate vial and sodium borohydride (0.02 g, 2.64×10^{-4} mol) was added. The sample was stirred at ambient temperature for 16 hours before being dialyzed with three portions of 100 mL deionized water. 1 mL of the solution was removed and the PVP was isolated for NMR as well as SEC analysis as described above. 0.15 mL 35% HCl was added to the remaining solution and the reaction mixture was heated at 60 °C for 8 hours. The solution was dialyzed to neutral pH with deionized water and the PVP was isolated for NMR and SEC analysis by evaporating the water under vacuum, dissolving the residue in DCM and precipitation in diethyl ether. The product was

derivatized with PFBA, as described in Section 5.2.5, before NMR analysis in order to determine the fraction of free primary amine end-groups. SEC analysis was also performed on the final product.

6.3) Results and Discussion

6.3.1) Hydrolysis of the Xanthate End-Group

NMR Analysis

The ^{1}H-NMR spectrum of the initial conditions for the *in-situ* NMR experiment performed on vial 1 in Section 6.2.1 is illustrated in Figure 6.1. The spectrum was normalized by setting the integral for the phthalimide protons at δ = 7.74 – 7.99 ppm to 4. This was cross-referenced with the polymer backbone peaks at δ = 2.98 – 4.02 ppm. The fraction of xanthate end-groups remaining during the *in-situ* hydrolysis in D_2O was measured from the integral intensity for the α-protons to the xanthate at δ = 5.65 – 5.9 ppm.

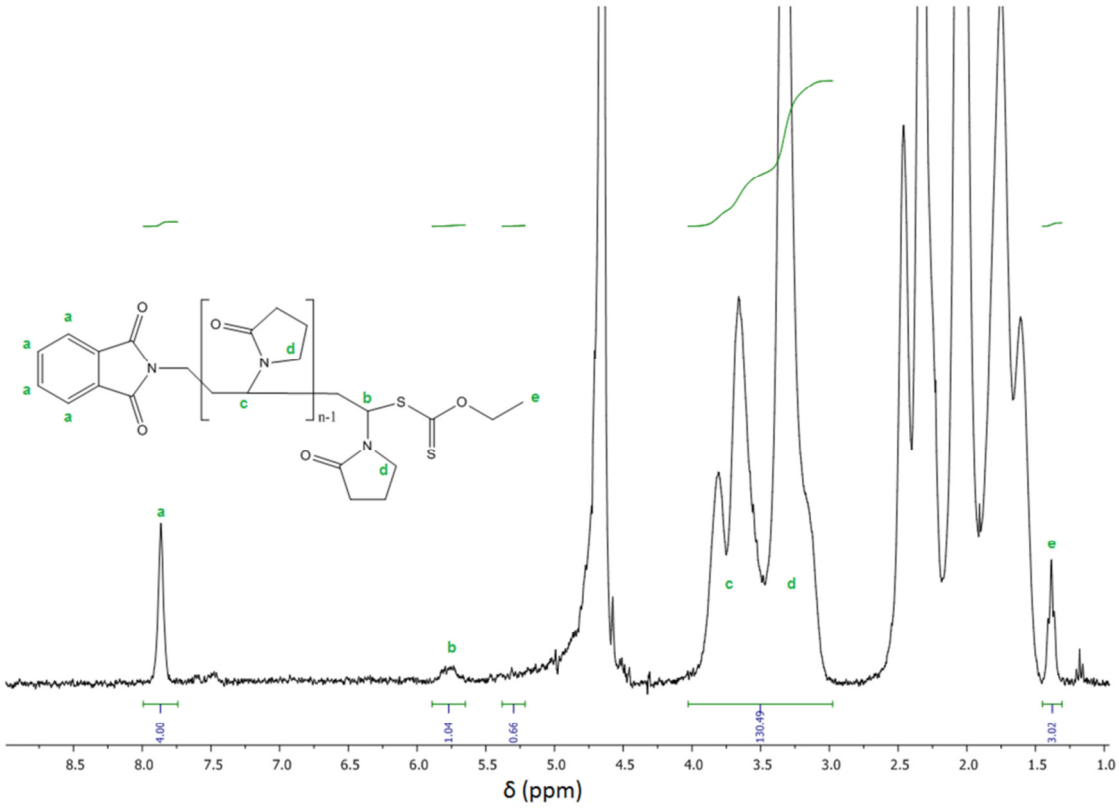

Figure 6.1: Initial Conditions for the *in-situ* NMR Experiment Performed on Vial 1 in Section 6.2.1.

The concentration profiles for the xanthate end-group during hydrolysis in D_2O as well as in 1 M DCl were plotted in Figure 6.2.

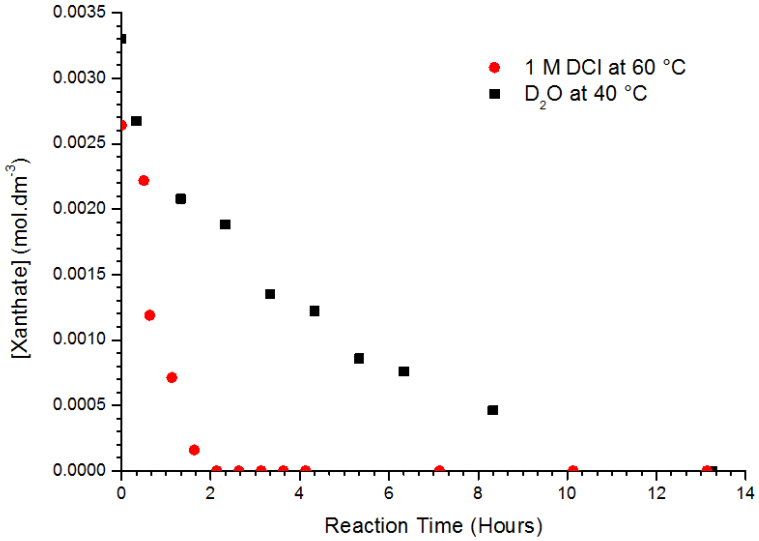

Figure 6.2: Concentration Profile for the Xanthate End-Group during Hydrolysis in D_2O at 40 °C and in 1M DCl at 60 °C.

The hydrolysis of the xanthate chain ends appeared to occur quite readily in D_2O at 40 °C, having a half-life of about 3 hours. No aldehyde chain ends were detectable. The major product was the hydroxyl end-group, as illustrated in Figure 6.3 (δ = 5.25 – 5.40 ppm). It could not be accurately quantified due to the interfering water peak. The peak at δ = 7.41 – 7.66 ppm could not be accounted for but was present from the initial measurement and its intensity did not change throughout the kinetic analysis. Some alkene end-groups were detected at the end of the analysis (δ = 6.78 – 7.02 ppm) as illustrated in Figure 6.3. The integral for the alkene protons was 0.24, suggesting that 24% of the xanthate end-groups were converted to alkene end-groups.

Increasing the temperature and adding DCl increased the rate of decomposition greatly. The half-life for xanthate hydrolysis in this case was approximately 9 minutes. Accurate measurement of the initial conditions was difficult as time was required for the sample temperature to equilibrate as well as to lock and shim the instrument. The phthalimide group was quite stable under acidic conditions. Only about 7% had ring-opened after 64 hours at 60 °C and the 2-carbamoylbenzoic acid formed was still acting as a protecting group for the amine. The rate of phthalimide ring-opening in H_2O may be greater, however, due to the kinetic isotope effect.[6-8] The aldehyde end-group could not be detected under acidic conditions. It was only slightly detectable in D_2O due to the partial hydration of the aldehyde. This caused some of the carbonyl protons to resonate in the region of the spectrum that is dominated by the water resonance.

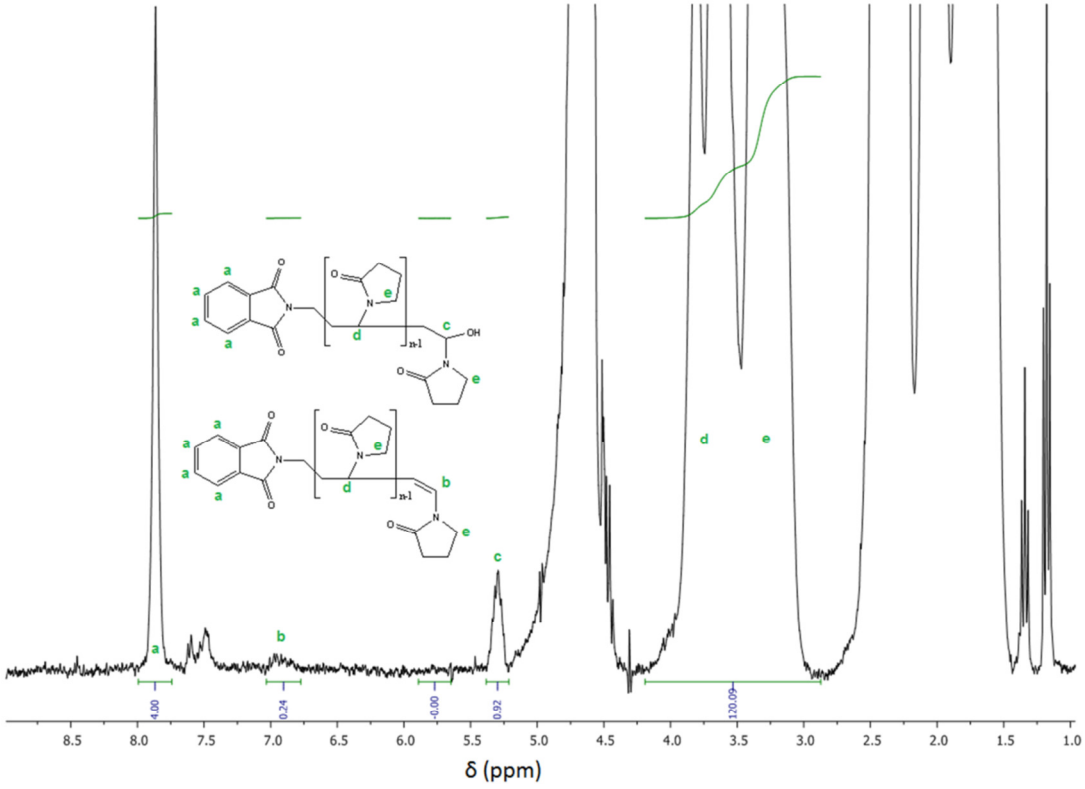

Figure 6.3: Conditions at the end of the *in-situ* NMR Experiment Performed on Vial 1 in Section 6.2.1.

To determine the amount of aldehyde present, the hydrolyzed PVP was isolated as described in Section 6.2.1. It was intended to only raise the pH to 7 by adding 0.75 equivalents of Na_2CO_3 to DCl but the resulting pH was 11. Either some of the DCl had evaporated during the kinetic analysis or there was an error in the weighing of Na_2CO_3 or DCl. The ^{1}H-NMR spectrum of the isolated sample in $CDCl_3$ is illustrated in Figure 6.4.

The phthalimide protons peak could no longer be used as an internal reference as over 50% of the phthalimide end-groups had ring-opened. This is characteristic of phthalimides in alkaline solution. Hence, the NMR spectrum was normalized by adjusting the PVP backbone peak to 130.49 – the value for the starting material, taking into account the interference from the diethyl ether, as described in Section A10. No alkene end-groups could be detected and integration of the aldehyde protons peak indicated over 80% of the xanthate end-group was converted to an aldehyde end-group. The peak at δ = 5.94 – 6.05 ppm indicated that aldol condensation took place. The presence of three distinct aldehyde peaks also implies the presence of aldol condensation products as well as aldol addition products. Since the concentration of DCl in the reaction mixture could not be accurately neutralized with Na_2CO_3, a milder base should be employed for the neutralization. Titration of less than 1 mL of solution would prove difficult and would dilute the concentration of

polymer in the product solution. That would make end-group analysis by NMR more difficult and less accurate.

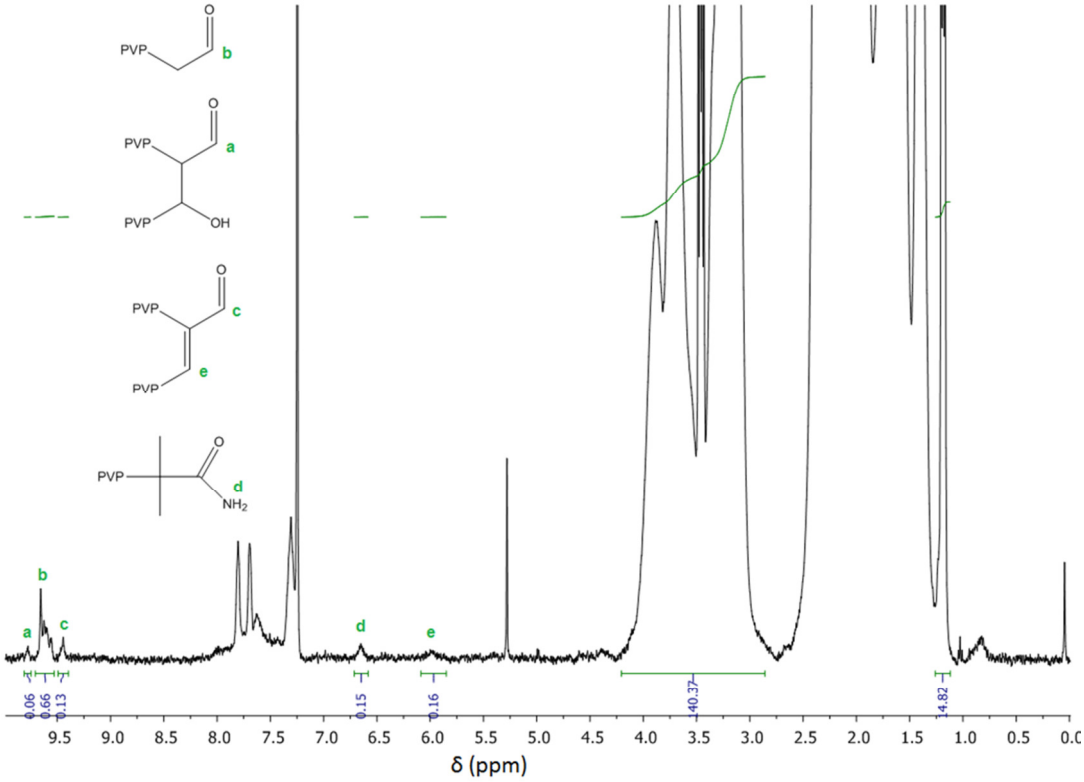

Figure 6.4: ^{1}H-NMR spectrum of the PVP Isolated after Hydrolysis of the Xanthate End-Group in 1 M DCl at 60 °C.

The aldol addition and condensation products are each formed by the conjugation of two aldehyde-functionalized PVP chains. Hence, the initial fraction of aldehyde end-groups relative to xanthate-functionalized PVP, before any aldol addition or condensation reactions had occurred, was calculated to be 1.04 using Equation 6.1.

$$\chi_{CHO} = 2 \times \int_{\delta=9.39}^{\delta=9.49} f(\delta)d\delta + \int_{\delta=9.53}^{\delta=9.70} f(\delta)d\delta + 2 \times \int_{\delta=9.75}^{\delta=9.81} f(\delta)d\delta \quad (6.1)$$

Thus the conversion of the xanthate end-group to an aldehyde end-group is quantitative under acidic conditions and moderate temperatures. The xanthate hydrolysis is also selective in the presence of the phthalimide end-group.

The peak at δ = 6.59 – 6.69 ppm is indicative that the nitrile end-group of the initiator-derived PVP chains had hydrolyzed to form a primary amide.[9-11] If the hydrolysis was quantitative and no further degradation to carboxylic acid had taken place, the integral of the amide protons divided by 2 indicated that the concentration of initiator-derived PVP chains was 7.5% of the xanthate end-group

concentration. Thus χ_{α_R} would be 0.93 and χ_{ω_X} would be 0.96. This is in close agreement with the calculations in Section 4.2

SEC Analysis

The SEC traces for the xanthate-functionalized PVP and its products of hydrolysis in D_2O at 40 °C as well as in 1 M DCl at 60 °C were normalized, as described in Appendix A1. The normalized distributions were plotted in Figure 6.5.

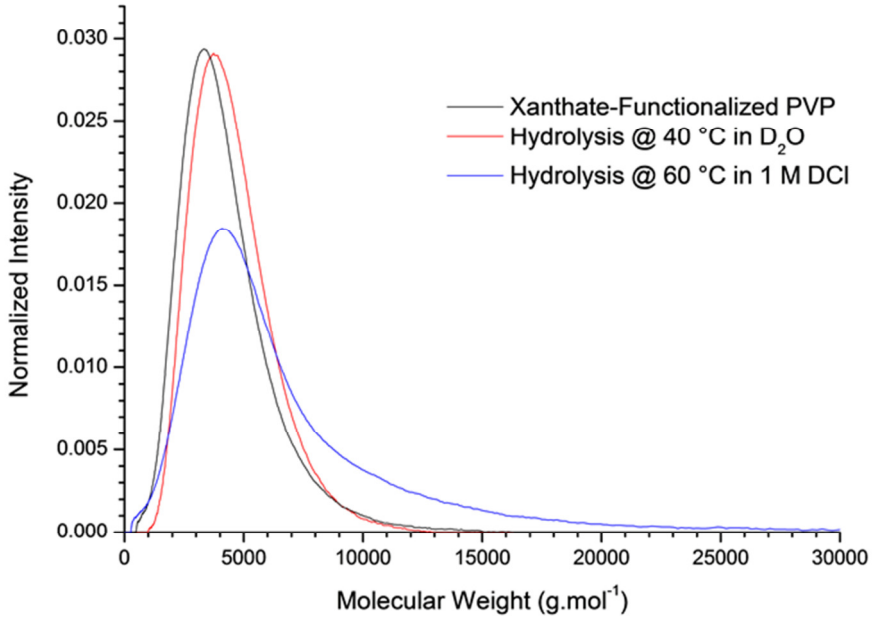

Figure 6.5: Normalized Molecular Weight Distributions for the Hydrolysis of the Xanthate End-Group in D_2O and 1 M DCl.

$M_{n,SEC}$ for the product of hydrolysis in D_2O increased by 300 g/mol and $Đ$ decreased by 0.07. These values are quite low and within experimental error. The end-group effects discussed in Section 5.3.2 may be plausible in this case as $M_{n,SEC}$ for this polymer is relatively low so the end-group effects would be more pronounced. The baseline of the SEC trace was not that stable either. The SEC trace for the product of hydrolysis in D_2O at 40 °C is illustrated in Figure 6.6.

$M_{n,SEC}$ for the product of hydrolysis in 1 M DCl increased by 2,622 g/mol and $Đ$ increased by 0.34, indicating that a significant amount of chain coupling had occurred. This result provides further evidence towards the theory that aldol addition and condensation reactions had occurred during the isolation of the PVP from the reaction mixture. Hence, alkaline conditions should be avoided when isolating aldehyde end-functional PVP.

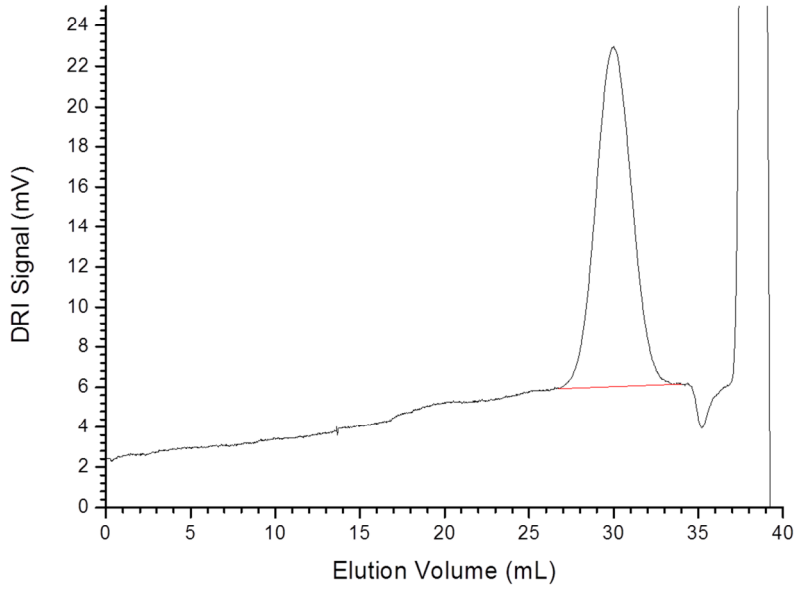

Figure 6.6: SEC Trace for the Xanthate-Functionalized PVP Hydrolyzed at 40 °C in D_2O.

6.3.2) Hydrolysis of the Alkene End-Group

NMR Analysis

The ^{1}H-NMR spectra of the alkene-functionalized PVP that was used for the hydrolysis experiments in Section 6.2.2 were taken in both D_2O and $CDCl_3$. These are illustrated in Figure 6.7. The concentration profiles for the alkene end-group during hydrolysis in D_2O as well as in 1 M DCl were plotted in Figure 6.8.

Hydrolysis of the alkene end-group did not occur to any measurable extent in D_2O, even at 65 °C. In contrast, 81% had decomposed after 22 minutes in 1 M DCl at 25 °C (the time taken for sample preparation and setting up the initial scan.) Thus, in acidic solutions, the alkene end-group was more susceptible towards hydrolysis than the xanthate end-group. However, alkene end-group formation is not the most likely intermediate during the hydrolysis of the xanthate end-group in D_2O as the latter hydrolyzed readily in neutral aqueous solutions. Hence, hydroxyl end-group formation most likely follows an S_N1 mechanism, as indicated in Scheme 6.5, by E1 elimination followed by hydration of the carbocation.

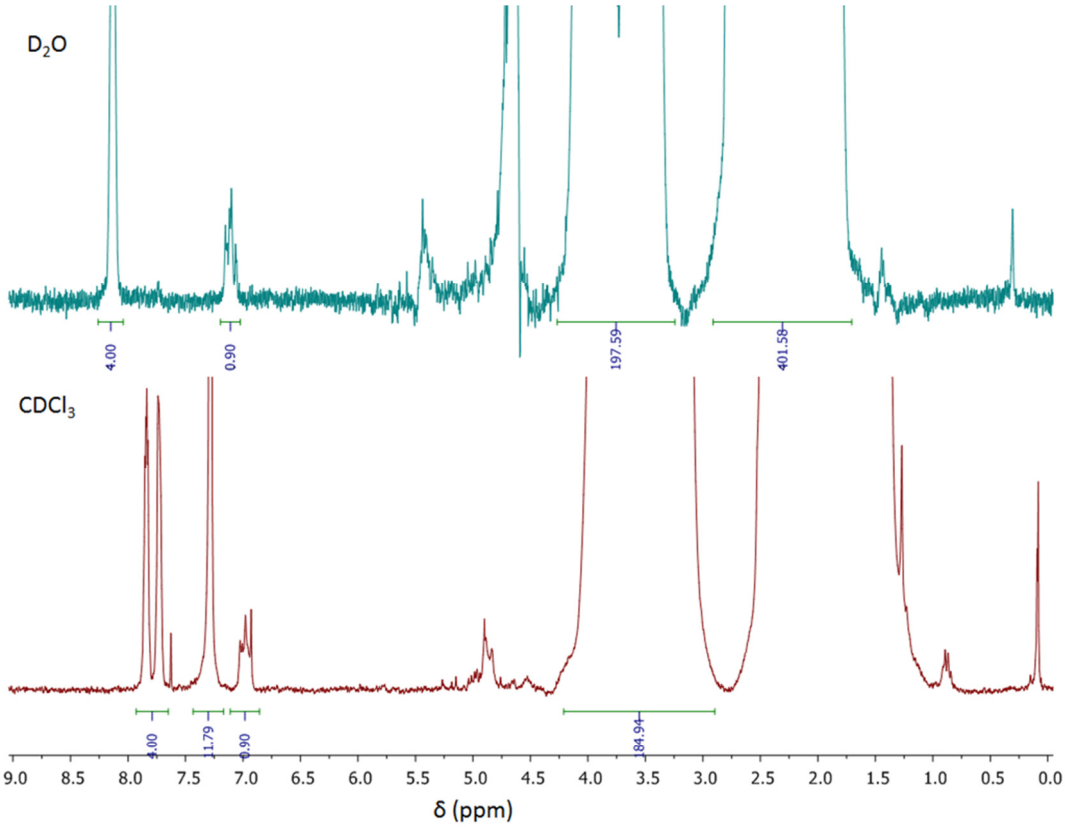

Figure 6.7: ^{1}H-NMR of Alkene-Functionalized PVP used for the Hydrolysis Experiments Described in Section 6.2.2.

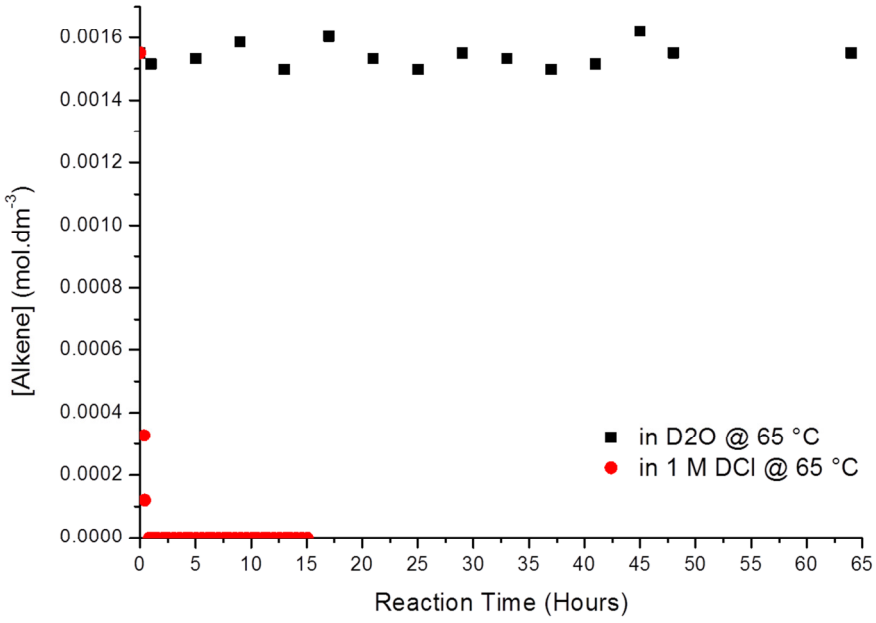

Figure 6.8: Concentration Profiles for the Alkene End-Group during Hydrolysis in D_2O as well as in 1 M DCl.

Some hydroxyl-functionalized PVP was detected briefly while the probe temperature was still 25 °C though it rapidly decomposed once the temperature was increased to 65 °C. The ^{1}H-NMR spectrum of the alkene-functionalized PVP after hydrolysis in 1 M DCl at 65 °C is plotted in Figure 6.9.

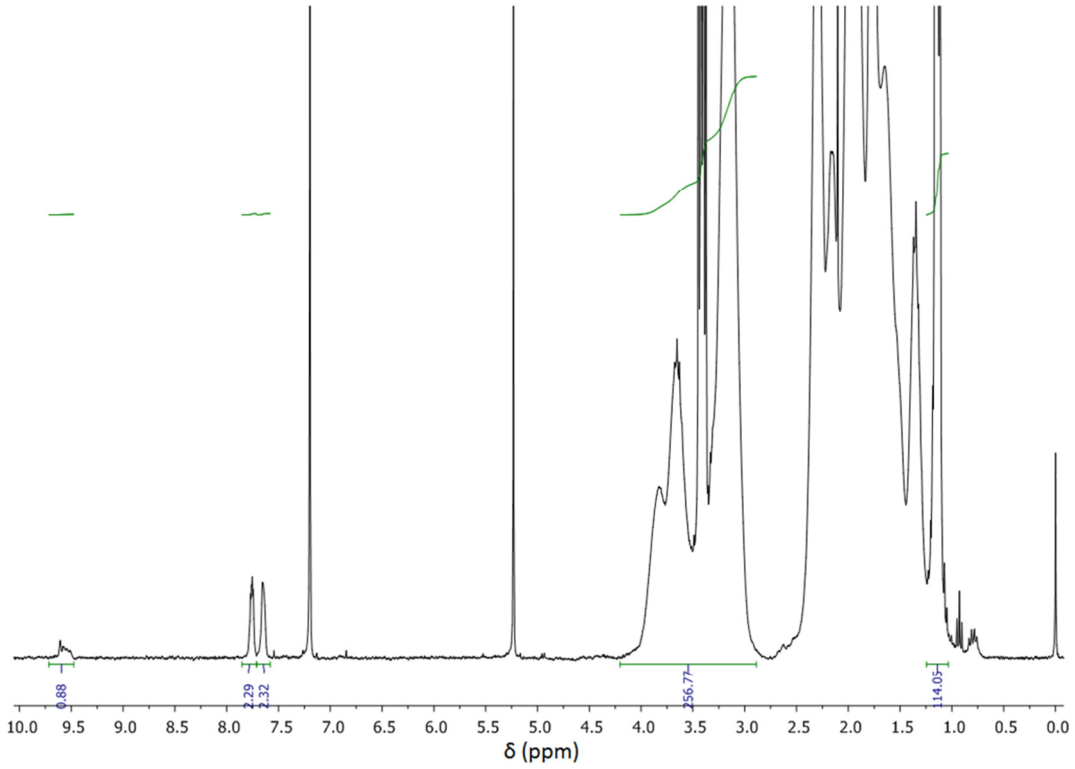

Figure 6.9: ^{1}H-NMR Spectrum of Alkene-Functionalized PVP after Hydrolysis in 1 M DCl at 65 °C.

The spectrum was normalized by adjusting the PVP backbone peaks to 180.74, the value for the same peaks in the NMR spectrum the starting material in $CDCl_3$. The interference from the absorbed diethyl ether was accounted for using the procedure described in Appendix A10. According to this normalization, the conversion of the alkene end-group on PVP to an aldehyde was quantitative - the integral intensity for the Alkene end-groups of the starting material was 0.84 in $CDCl_3$. No alkene, xanthate or hydroxyl end-groups could be detected in the product.

The integrals for the phthalimide protons were significantly larger than expected and this could not be accounted for. However, it seems more likely that there was a small interference in the region of the phthalimide protons resonance frequencies from an adventitious impurity in the isolated product than a large interference in the region of the PVP backbone peaks for the starting material.

While the conversion of alkene end-groups to aldehyde end-groups was quantitative, the concentrations of the alkene and aldehyde end-groups in the starting material and product, respectively, were still less than the concentration of the phthalimide end-groups. Extended

relaxation delays were used when acquiring the spectra so that protons with long T1 relaxation times would not lose relative signal intensity with an increase in the number of scans. Thus the loss of the xanthate end-group during the synthesis of this polymer sample may have occurred by a different mechanism than just thermolysis.

SEC Analysis

The SEC traces for the xanthate-functionalized PVP starting material, the thermolyzed PVP and the product of hydrolysis in 1 M DCl at 65 °C were normalized, as described in Appendix A1. The normalized distributions were plotted in Figure 6.10.

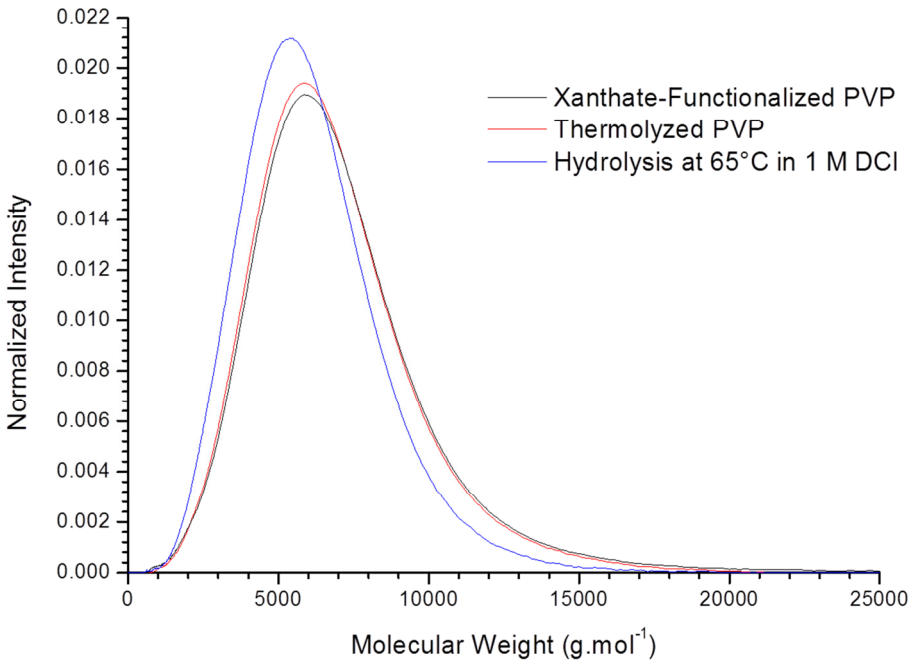

Figure 6.10: Normalized Molecular Weight Distributions for the Thermolysis of the Xanthate End-Group and its Hydrolysis in 1 M DCl at 65 °C.

$M_{n,SEC}$ for the product of hydrolysis in 1 M DCl decreased by 700 g/mol and $Đ$ decreased by 0.01, indicating that no chain coupling had occurred. The decrease in $M_{n,SEC}$ and $Đ$ could be from the end-group effects discussed in Section 5.3.2 but it may also be due to experimental error.

6.3.3) Reduction of the Aldehyde End-Group with Simultaneous Phthalimide Deprotection

NMR Analysis

The ^{1}H-NMR spectrum for the PVP isolated after hydrolysis and dialysis of the crude reaction mixture is illustrated in Figure 6.11.

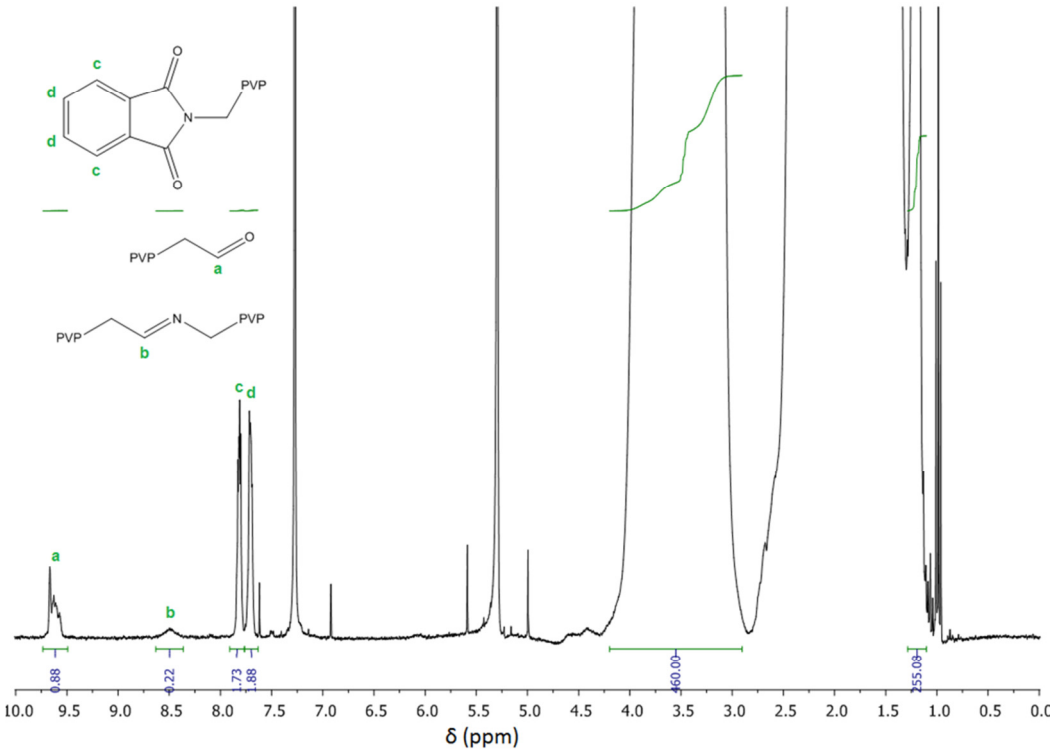

Figure 6.11: ^{1}H-NMR Spectrum of PVP Isolated for Crude Reaction Mixture by Dialysis and Hydrolysis.

The spectrum was normalized by adjusting the integral of the PVP backbone protons peak at δ = 2.9 – 4.2 ppm to 290, the value for the same region of the PVP isolated by precipitation. The difference in the amount of diethyl ether in the sample compared to the precipitated PVP was accounted for by the procedure described in Appendix A10. After normalization, the amount of phthalimide end-groups was about 6% less than that for the starting product. Some imine protons were also detected (δ = 8.5 ppm). Their relative amount was 22% of the amount of phthalimide end-groups present on the xanthate-functionalized starting material. These results suggested that some of the phthalimide end-groups may have decomposed during the hydrolysis, releasing the primary amine that could have formed a Schiff base with the aldehyde end-groups. However, this seems unlikely as the phthalimide end-group appeared to be stable under the hydrolysis conditions described in Section 6.2.1 and the amount of imine protons detected is also greater than the decrease in the amount of phthalimide end-groups. The rate of phthalimide hydrolysis may have been slower in DCl due to the kinetic isotope effect.[6-8] It was considered that some of the NVP oligomerized during the hydrolysis,

increasing the amount of PVP backbone protons as well as the amount of aldehyde end-groups. This is feasible since the crude reaction mixture still contained residual AIBN. Also, the hydrolysis of some of the monomer present may have occurred, producing acetaldehyde. This is indicated by the sharp peak overlapping with the broad aldehyde protons peak at δ = 9.49 – 9.74 ppm in Figure 6.11. This meant that the normalization of the spectrum would no longer be equal to that for the precipitated PVP. This is possible if the dialysis was not performed for sufficiently long to allow equilibration to occur before changing the dialysis solvent.

The NMR spectrum for the PVP isolated after reduction with sodium borohydride is illustrated in Figure 6.12. The same normalization procedure was used as described above. No aldehyde end-groups could be detected and all the detectable phthalimide end-groups were converted to 2-(hydroxymethyl)benzamides.

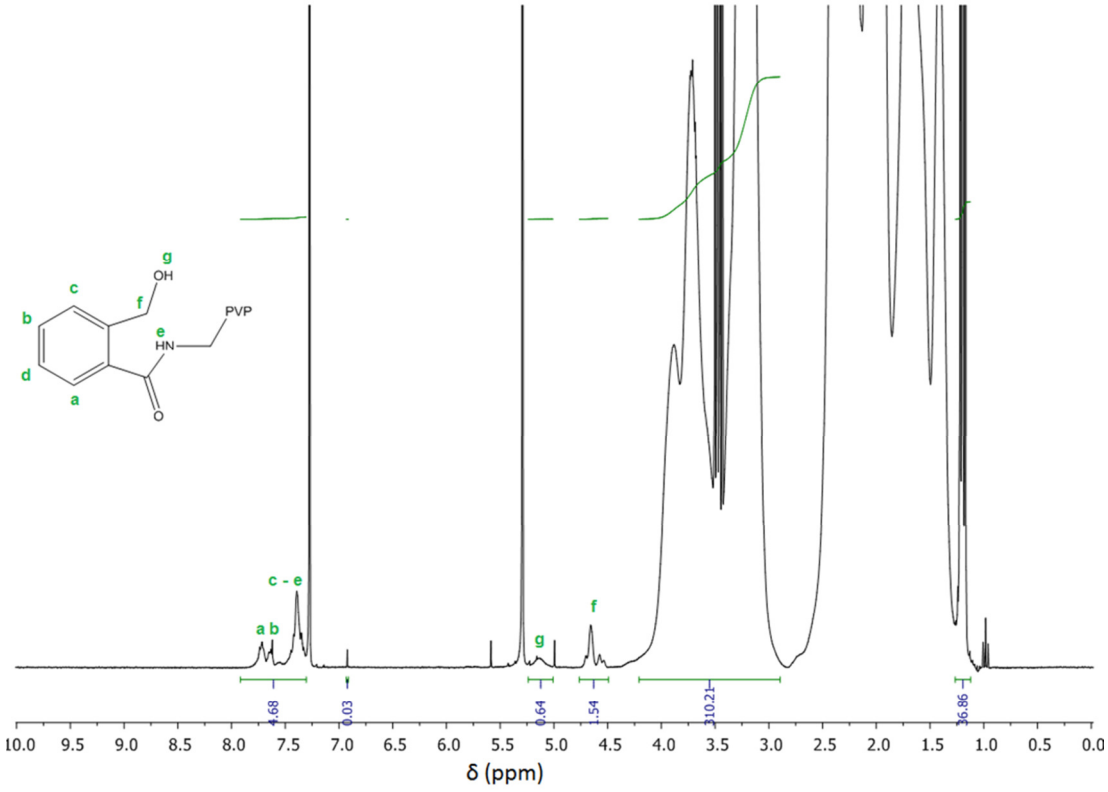

Figure 6.12: ^{1}H-NMR Spectrum of PVP after Reduction with $NaBH_4$.

The ^{1}H-NMR spectrum of the reduced PVP after hydrolysis and PFBA-derivatization is illustrated in Figure 6.13. The spectrum was normalized as described above. The integral of the imine protons peak indicated that over 96% of the phthalimide end-groups had been successfully deprotected by the procedure.

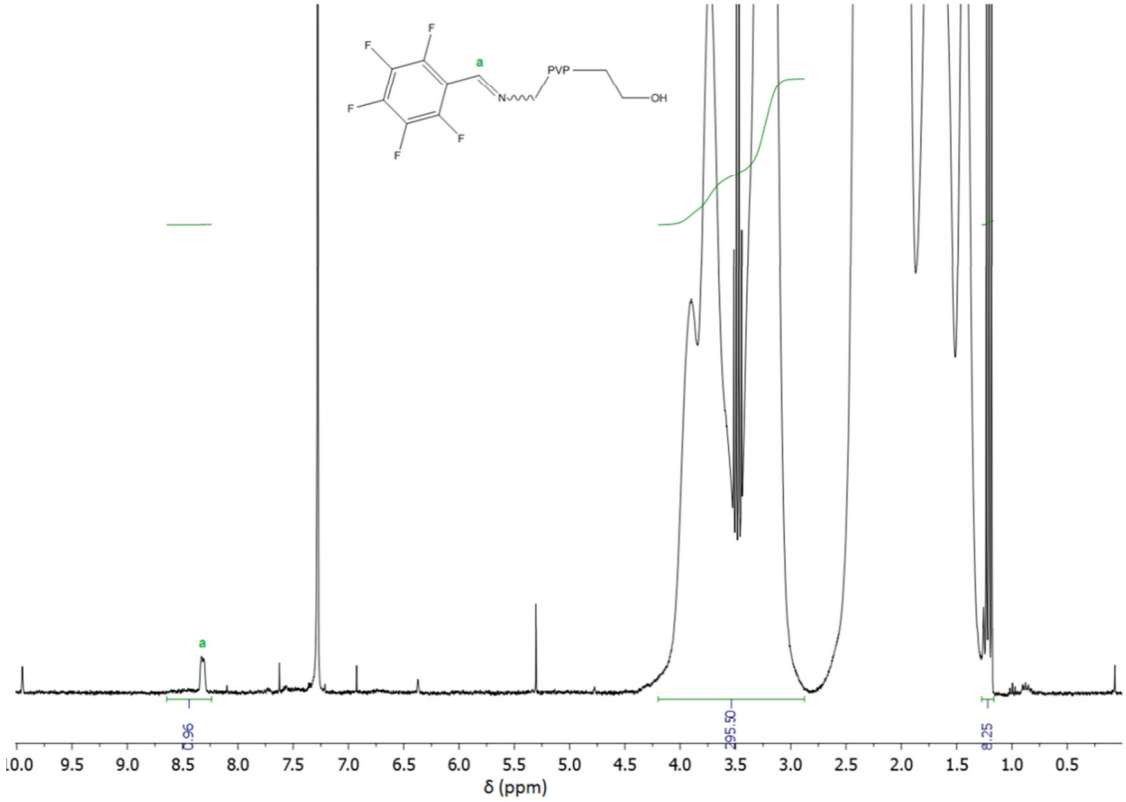

Figure 6.13: ^{1}H-NMR Spectrum of the Reduced PVP after hydrolysis and PFBA-Derivatization.

SEC Analysis

The SEC traces for the xanthate-functionalized PVP starting material and the product of deprotection by hydrolysis and reduction were normalized by the procedure described in Appendix A1 and the normalized distributions were plotted as functions of molecular weight in Figure 6.14.

$M_{n,SEC}$ of the deprotected product had increased by 1500 g/mol though $Đ$ stayed constant. The constant $Đ$ indicated that the increase in $M_{n,SEC}$ was either due to propagation during the initial hydrolysis of the crude reaction mixture that contained both AIBN and NVP or the different end-groups causing a change in the hydrodynamic volume of the polymer chains rather than coupling reactions. Hence, even in the presence of some amine-functionalized PVP, the aldehyde end-group can be quantitatively reduced in H_2O by $NaBH_4$ without any significant amount of imine bonds being formed or reduced.

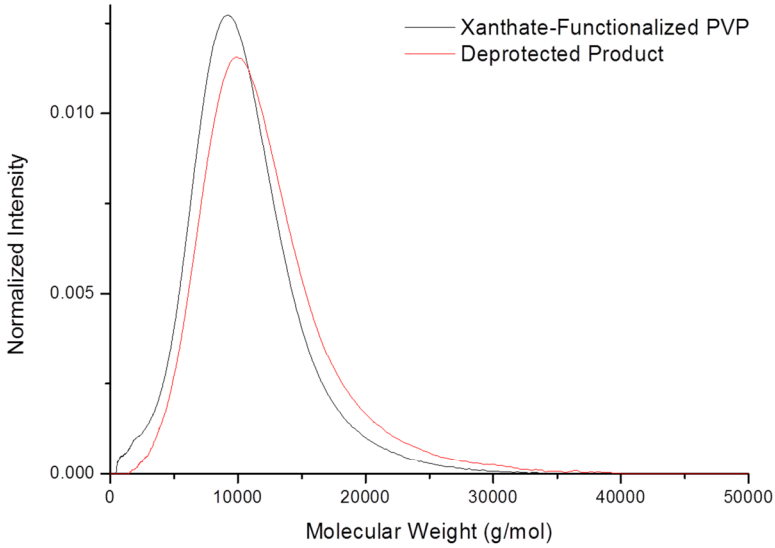

Figure 6.14: Normalized Molecular Weight Distributions Obtained by SEC for the Xanthate-Functionalized PVP and the Product of Deprotection by Hydrolysis and Reduction.

6.4) Conclusions

The hydrolysis of the xanthate end-group in D_2O leads to the formation of hydroxyl-functionalized PVP. The reaction rate is increased dramatically in the presence of a strong acid and further decomposition of the hydroxyl end-group to an aldehyde end-group occurs more readily. The alkene end-group is more stable towards hydrolysis than the xanthate end-group in D_2O but is more readily hydrolyzed in the presence of a strong acid. Both the xanthate and the alkene end-groups of PVP decompose quantitatively to aldehyde end-groups when hydrolyzed at around 60 °C in 1 M DCl. The nitrile end-group of the initiator-derived PVP chains also appeared to hydrolyze when the hydrolysis was performed for an extended time at 60 °C in 1 M DCl. The phthalimide end-groups were stable in acidic solutions but readily ring-opened under alkaline conditions.

Some of the primary amine end-groups appeared to be deprotected during the hydrolysis of xanthate-functionalized PVP in 1 M HCl at 60 °C.

More work needs to be performed to fully understand the rates of hydrolysis for the different end-groups but, from the preliminary results, it appears that the selective hydrolysis of the xanthate and alkene end-groups in the presence of the phthalimide protecting group is possible. Studies using HCl need to be performed to avoid any kinetic isotope effects.

6.5) References

1. Pound, G.; McKenzie, J. M.; Lange, R. F. M.; Klumperman, B. Polymer-protein conjugates from small omega]-aldehyde end-functional poly(N-vinylpyrrolidone) synthesised via xanthate-mediated living radical polymerisation. *Chem. Commun.* **2008**, 3193-3195.

2. Jacobs, J.; Pound-Lana, G.; Klumperman, B. Poly(N-vinylpyrrolidone-b-(gamma]-benzyl-l-glutamate)) - synthesis and self-assembly into pH-sensitive micelles. *Polym. Chem.* **2012**, *3*, 2551-2560.

3. Wuts, P. G. M.; W. Greene, T. W. *Greene's Protective Groups in Organic Synthesis;* John Wiley and Sons, Inc.: Hoboken, New Jersey, 2012.

4. Horii, Z.; Iwata, C.; Tamura, Y. Reduction of Phthalimides with Sodium Borohydride. *J. Org. Chem.* **1961**, *26*, 2273-2276.

5. Osby, J. O.; Martin, M. G.; Ganem, B. An exceptionally mild deprotection of phthalimides. *Tetrahedron Lett.* **1984**, *25*, 2093-2096.

6. Anslyn, E. V.; Dougherty, D. A. *Modern Physical Organic Chemistry;* University Science: USA, 2006.

7. Kresge, A. J. Solvent Isotope Effect in H_2O-D_2O Mixtures. *Pure Appl. Chem.* **1964**, *8*, 243-258.

8. Leskovac, V. In *Kinetic Isotope Effects;* Comprehensive Enzyme Kinetics; Springer: USA, 2003; pp 353-390.

9. Snyder, H. R.; Elston, C. T. Polyphosphoric Acid as a Reagent in Organic Chemistry. VI.1 The Hydrolysis of Nitriles to Amides. *J. Am. Chem. Soc.* **1954**, *76*, 3039-3040.

10. Moorthy, J. N.; Singhal, N. Facile and Highly Selective Conversion of Nitriles to Amides via Indirect Acid-Catalyzed Hydration Using TFA or AcOH-H_2SO_4. *J. Org. Chem.* **2005**, *70*, 1926-1929.

11. Ritter, J. J.; Minieri, P. P. A New Reaction of Nitriles. I. Amides from Alkenes and Mononitriles1. *J. Am. Chem. Soc.* **1948**, *70*, 4045-4048.

CHAPTER 7

Preparation of Poly(*N*-vinylpyrrolidone-*Block*-L-lysine) Copolymers by *N*-Carboxyanhydride Ring-Opening Polymerization

7.1) Introduction

The preparation of block copolymers can be achieved by two approaches. One approach is to functionalize the first block with a functional group that can act as a macroinitiator for the monomer of the second block. This is essentially what is known as a grafting-from approach in the preparation of graft copolymers as well as modified surfaces.[1] The other approach is to link the two blocks together by a coupling reaction after functionalizing the respective blocks with complementary functional groups. This is analogous to the grafting-to approach.[1] Both approaches have benefits as well as pitfalls and these are usually complementary. For our purposes of preparing poly(*N*-vinylpyrrolidone-b*lock*-L-lysine) copolymers, a grafting-from approach seems more feasible since most coupling reactions between two macromolecules are not very efficient even if the coupling reaction is very efficient for small molecules. The main reasons for this are the generally poor diffusion coefficients for the end-groups compared to those for small molecules as well as greater steric hindrance caused by the polymer backbone. A grafting-to approach would also require three preparation and isolation procedures while the grafting to approach would only require two. NCA ring-opening polymerization is one of the best ways to prepare a homopolypeptide such as poly(L-lysine) and it has recently been demonstrated that polymer-peptide block copolymers as well as block copolypeptides can be readily prepared by using a macroinitiator for the NCA polymerization.[2-5] Hence it would be a well suited reaction process for the preparation of our desired copolymer. The polymerization of N^{ε}-(benzyloxycarbonyl)(L-lysine) NCA by a primary amine-functionalized macroinitiator to prepare block copolymers of various molecular weights and architectures has been achieved by performing the polymerization at low temperature[2] (0 °C), low pressure[6] (1×10^{-5} bar) or both.[3] Since the best results were obtained by applying both low temperatures and pressures during the NCA polymerization, this was the route followed in our research.

Lysine has two primary amine functional groups, the alpha amino group (N^{α}) adjacent to the carboxyl group and an epsilon amino group (N^{ε}) on the side chain. Thus in order to prepare a stable *N*-carboxyanhydride of lysine (Lys-NCA), the ε-amine must be appropriately protected. This was most often achieved with the benzyloxycarbonyl (CBZ) protecting group.[2,3,7-11] The α-amine can be

protected during the reaction that introduces the CBZ protection by forming a Cu(II) complex with the α-amine and carboxyl group, as depicted in Scheme 7.1. The copper can be removed from the protected amino acid by washing with a solution of EDTA.

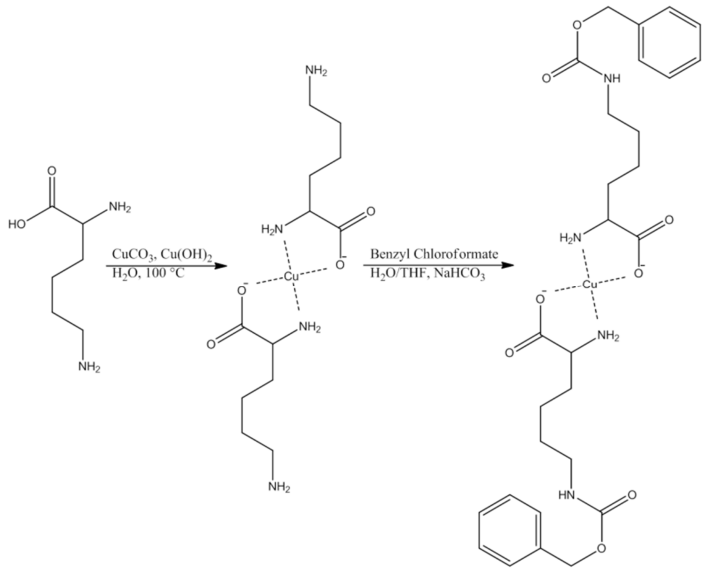

Scheme 7.1: Preparation of N^{ε}-(Benzyloxycarbonyl)-L-Lysine.

N^{ε}-(benzyloxycarbonyl)-L-Lysine *N*-carboxyanhydride (N^{ε}-(CBZ)-Lys-NCA) has been prepared by the optimized Fuchs-Farthing method[2,3,6,9,12] (Scheme 7.2), isolated and polymerized successfully.

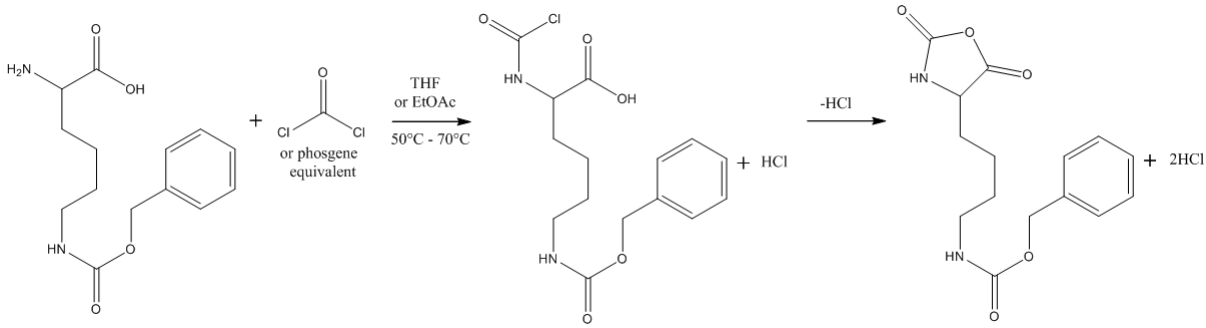

Scheme 7.2: Synthesis of N^{ε}-(CBZ)-Lys-NCA by the Fuchs-Farthing Method.

A modified Leuch's method (Scheme 7.3) for the preparation of N^{ε}-(CBZ)-Lys-NCA has also been reported. It was a one pot protection and cyclization procedure using benzyl chloroformate followed by phosphorus pentachloride (PCl_5).[13] Purification of the NCAs prepared this way to the level required for living polymerization may prove difficult due to the formation of phosphorus oxide chloride which has been known to co-crystallize with NCAs.[14]

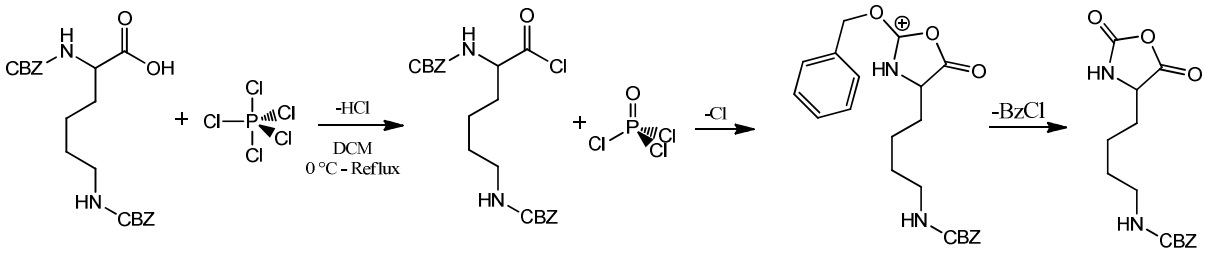

Scheme 7.3: Synthesis of N^{ε}-(CBZ)-Lys-NCA by the Modified Leuch's Method.

An article by Kramer *et al.*[8] involving the purification of NCAs by flash chromatography was found. However, the NCAs from their group were prepared using either phosgenation or α,α-dichloromethylmethyl ether as the halogenating agent. Thus it was unclear if this procedure would work for NCAs prepared with PCl_5 or other halogenating agents such as thionyl chloride, phosphorus trichloride or phosphorus tribromide. Some papers have also eluded the decomposition of NCAs during aqueous extraction techniques by cooling the water and organic phase to 0 °C during the separation and drying stages.[7,15]

Removal of the CBZ protecting group from the lysine residues in peptides has been achieved either through acidolysis[7,9,10,16,17] or catalytic hydrogenation.[7,16,18,19]

7.2) Materials and Experimental Methods

L-lysine hydrochloride was purchased from Wuhan Pharma Chemical Co., Ltd. and used as received. Bis(trichloromethyl)carbonate (99%), benzyl chloroformate, dimethyl sulfoxide-d6 (DMSO-d6), benzophenone, *α*-pinene, anhydrous *N*,*N*-dimethylformamide (DMF), *N,N*-dimethylacetamide (Chromosolv® Plus, for HPLC ≥ 99.9%), butylated hydroxytoluene (BHT) 99% (GC), calcium hydride and basic copper(II) carbonate were purchased from Sigma Aldrich and used as received. 2000 g/mol nominal molecular weight cut-off (MWCO) benzoylated dialysis tubing was purchased from Sigma Aldrich and soaked in 3 portions of deionized water before use to remove the sodium azide preservative. 4Å molecular sieves (8 – 12 mesh) were also purchased from Sigma Aldrich, dried in a vacuum oven at 165 °C for 5 hours and allowed to cool to room temperature under vacuum before use. Sodium, sodium bicarbonate, sodium carbonate, disodium ethylenediaminetetraacetic acid dihydrate (EDTA), anhydrous magnesium sulfate and glacial acetic acid were purchased from Merck and used as received. Diethyl ether, *n*-hexane and tetrahydrofuran (THF) were purchased from Kimix and distilled from sodium and benzophenone before use. DCM was purchased from Kimix and washed with concentrated sulfuric acid followed by 5% sodium bicarbonate solution and finally

water before being dried over calcium chloride and fractionally distilled from 4Å molecular sieves. Methanol was purchased from Kimix and fractionally distilled before use. Ethanol was purchased from Kimix and dried by refluxing with calcium oxide. Dry ethanol was distilled off after 6 hours and stored over 4Å molecular sieves. Ethyl acetate was purchased from Kimix and washed with sodium bicarbonate solution followed by water before drying with magnesium sulfate and 4Å molecular sieves. Dry ethyl acetate was fractionally distilled and stored over 4Å molecular sieves. 1-Octylamine was purchased from Sigma Aldrich and was dried as well as distilled from calcium hydride under reduced pressure. SnakeSkin® Dialysis tubing (10,000 g/mol and 3,500 g/mol nominal molecular weight cutoff) was purchased from Thermo Scientific and used as is. Lithium chloride ≥ 98% was purchased from Riedel-de Haën and used as is. 0.45 µm Glass fiber prefilters were purchased from PALL Life Sciences.

7.2.1) Synthesis of N^{ε}-(Benzyloxycarbonyl) L-Lysine

L-lysine monohydrochloride (32 g, 0.1752 mol) was dissolved in 300 mL deionized water. Basic copper(II) carbonate ($CuCO_3 \cdot Cu(OH)_2$, 37 g, 0.1673 mol) was added and the solution was refluxed for 30 minutes before being cooled down to room temperature and being filtered. Sodium bicarbonate (17 g, 0.2023 mol) was added and the solution was cooled to 0 °C in a three-neck round bottom flask fitted with a dropping funnel and a mineral oil bubbler. Benzyl chloroformate (20 g, 0.1172 mol) was dissolved in 150 mL THF and the solution was charged into the dropping funnel. The benzyl chloroformate solution was then added dropwise to the lysine copper complex solution while maintaining the temperature at 0 °C for two hours. The reaction mixture was then heated at 40 °C overnight. The THF was removed by evaporating under vacuum and the precipitate was filtered and washed with three 100 mL portions of deionized water.

EDTA (22 g, 0.0591 mol) and sodium carbonate (8 g, 0.0755 mol) were dissolved in 300 mL deionized water and added to the precipitate. The mixture was heated at 60 °C with gentle mixing for 1 hour before being cooled to 0 °C and filtered. This procedure was repeated 2 more times to ensure all the copper was removed from the product. The precipitate was washed with three 50 mL portions of deionized water and dried in a vacuum oven at 60 °C overnight. Product Yield: 22.65 g (69%) IR (ATR):[20] 3334 cm^{-1} (m, N-H secondary urethane), 2599 cm^{-1} (w, br, N-H amine), 2131 cm^{-1} (w, br, N-H amine), 1692 cm^{-1} (s, C=O carbamate), 1522 cm^{-1} (s, C=O acid).

7.2.2) Synthesis of N^{ε}-(CBZ) Lys-NCA

N^{ε}-(Benzyloxycarbonyl)-L-Lysine (4 g, 14.27 mmol) was placed in a 250 mL three-neck round bottom flask and 120 mL dry THF was added along with α-pinene (4 g, 29.36 mmol). The round bottom was fitted with a dropping funnel, reflux condenser and mineral oil bubbler. The reaction mixture was sparged with argon for 10 minutes before heating to 65 °C. Triphosgene (1.64 g, 5.527 mmol) was dissolved in 40 mL dry THF and the solution was charged in the dropping funnel. The triphosgene solution was added to the reaction mixture dropwise over thirty minutes with vigorous stirring and occasional sparging with argon. Initially, a dense slurry formed. However, it would dissolve as the reaction progressed provided it was sufficiently broken up by the stirring process. After 90 minutes, the reaction mixture was cooled to 0 °C and run through a celite column (5.0 cm × 2.2 cm) that had been dried in a vacuum oven at 140 °C. Argon was used to flush the solution rapidly through the column. The filtrate was concentrated to ca. 40 mL under vacuum and the product was precipitated by adding dropwise to 200 mL of hexane with rapid stirring. The suspension was sealed and left in a freezer overnight to ensure complete precipitation of the product before filtering. The product was recrystallized from THF and hexane two more times, cooling the THF solution to 0 °C and running it rapidly through a dry silica column (2.0 cm × 2.2 cm) each time. Product Yield: 3.42 g (78%) ^{1}H-NMR ($CDCl_3$): δ = 7.27 ppm (br, 5H, phenyl hydrogens), 6.84 ppm (br, 1H, N-H carbamate), 5.03 ppm (br, 2H, benzyl hydrogens), 4.86 ppm (br, 1H, N-H NCA ring), 4.19 ppm (br, 1H, α-hydrogen), 3.13 ppm (br, 2H, ε-hydrogens), 2.05 – 1.05 ppm (br, 6H, β, γ and δ-hydrogens.)

7.2.3) Polymerization of N^{ε}-(CBZ) Lys-NCA Using 1-Octylamine

In order to assure that the NCAs synthesized were sufficiently pure to allow for a controlled ring-opening polymerization as well as to have a reference of the peaks corresponding to the protons of the lysine residues in the ^{1}H-NMR spectrum of the PVP-poly(L-lysine) block copolymer, a polymerization was performed using a small molecule primary amine initiator. 1-Octylamine was used as an initiator as this amine was not very volatile and hence would remain in a DMF solution at 0 °C when the pressure is below 1 mbar. The methyl protons on the initiator would also serve as an internal reference for the ^{1}H-NMR spectrum of the polypeptide which would allow for the direct measurement of the average number of residues in the product.

A 10% (w/w) stock solution of 1-octylamine was prepared by adding 0.9 g DMF to 0.1 g 1-octylamine. An aliquot of the stock solution (0.168 g, 1.30×10^{-4} mol) was added to 7 mL anhydrous DMF. The solution was cooled to 0 °C in an ice bath at 0.6 mbar for 15 minutes. N^{ε}-(CBZ) Lys-NCA

(1.42 g, 4.64×10^{-3} mol) was quickly added to the reaction and the pressure was reduced to 0.6 mbar again. The initiator-to-NCA ratio was 35. The pressure and temperature were maintained for 5 hours, after which it was noted that the reaction mixture had become a gel. In order to avoid excessive loss of solvent, the Schlenk tube was sealed for the remainder of the reaction. The reaction was allowed to continue at 0 °C for 24 hours. The product was precipitated from diethyl ether, using THF as a solvent. The precipitate was suspended in 10 mL methanol and 1 mL glacial acetic acid was added. The dispersion was dialyzed, using 2000 g/mol MWCO dialysis tubing, with 3 portions of methanol followed by 6 portions of deionized water. The polypeptide was isolated by lyophilization and analyzed by ^{1}H-NMR in DMSO-d6.

7.2.4) Polymerization of N^{ε}-(CBZ) Lys-NCA Using Amine-functionalized PVP

Polymerization was carried out at several different initiator-to-NCA ratios and, due to a limited amount of prepared PVP macroinitiator, several different amine-functionalized PVP samples were used. $M_{n,SEC}$ for the various PVP initiator samples was kept within 12 kDa to 17 kDa as PVP with molecular weight greater than 25 kDa is known to bioaccumulate within the body.[21-23] PVP prepared by the semi-batch RAFT polymerizations described in Chapter 4 has a much lower weight fraction of polymer chains with a molecular weight greater than 25,000 g/mol than conventional PVP with a K-value of 17 that is used for parenteral formulations. The added molecular weight of the polypeptide block should not pose a problem as polypeptides prepared from NCAs of L-amino acids are biodegradable.

In a typical polymerization, amine-functionalized PVP (prepared as described in Section 4.5.2 and deprotected as described in Chapter 5) was dissolved in dry DCM and anhydrous sodium carbonate was added (10% w/w compared to polymer) along with 4Å molecular sieves. The mixture was sealed and allowed to dry for 16 hours at 4 °C before filtering through glass wool and placing in a Schlenk tube. The DCM was carefully removed by evaporation under vacuum and replaced with DMF (10 mL per gram of polymer.) The Schlenk tube was placed in an ice bath and the pressure was reduced to 0.6 mbar for 2 hours. N^{ε}-(CBZ) Lys-NCA (150% of the amount intended to be used) was dissolved in a minimum amount of ethyl acetate and eluted through a column of silica (120 × 8 mm for 1.5 g), that had been washed with 10 mL ethyl acetate. Ethyl acetate was used as the mobile phase and nitrogen gas was used to perform flash chromatography. A beaker containing hexane was used to determine when the NCA began to emerge from the column by capturing a drop every few seconds until a precipitate was seen to form. This was also used to determine when the NCA had finished eluting.

The NCA was precipitated from hexane, filtered and dried under vacuum. The required amount was added to the reaction mixture rapidly at 0 °C. The pressure in the Schlenk tube was reduced to 0.6 mbar and left at 0 °C for 5 hours, after which the tube was sealed and kept at 0 °C for 24 hours. The product was isolated from the reaction mixture by precipitating from diethyl ether, using THF as a solvent. The isolate was further purified by dissolving in methanol and dialyzing, using 10,000 MWCO dialysis tubing, with three portions of methanol followed by six portions of deionized water. The polymer was isolated from the dialysis solution by lyophilization. The isolated sample was analyzed by ^{1}H-NMR in DMSO-d6, DMAC SEC, transmission electron microscopy in vitreous ice (cryo-TEM) and dynamic light scattering (DLS) in H_2O as well as DMF.

7.2.5) Preparation of Colloidal Dispersion of PVP-*block*-poly(N^{ε}-(CBZ)-L-lys) in H_2O

The PVP-*block*-poly(N^{ε}-(CBZ)-L-lys) was amphiphilic and formed a colloidal dispersion when dialysed from methanol into water. Thus a sample of PVP-*block*-poly(N^{ε}-(CBZ)-L-lys) dispersed in H_2O was imaged using cryo-TEM to obtain an impression of the size of the micelles formed. 2 mg of the isolated block copolymer sample was dispersed in 1 mL deionized water. 1 mL methanol was added to the dispersion and the mixture was shaken vigorously until it became homogeneous. The methanol was removed by heating gently under vacuum until only about 0.9 mL of solution remained. A solution of PVP-*block*-poly(N^{ε}-(CBZ)-L-lys) in DMF was also prepared at a concentration of 2 mg/mL. Both samples were filtered with 0.45 µm glass fiber SEC filters before analysis.

DLS analysis of the dispersion of PVP-*block*-poly(N^{ε}-(CBZ)-L-lys) in H_2O, as well as the solution in DMF, was performed on a Malvern PN3704 Zetasizer S173. The complex refractive index of the dispersion was set to 1.59 + 0.01i. This was an approximation as no refractive index measurement equipment was available. This is the complex refractive index of a poly(styrene) latex[24] and since the dispersion of PVP-*block*-poly(N^{ε}-(CBZ)-L-lys) in H_2O resembled this type of latex and contained many phenyl functional groups, it was assumed that the complex refractive index of the latex would be a close approximation to that for PVP-*block*-poly(N^{ε}-(CBZ)-L-lys) in H_2O. The dispersant refractive index was set to 1.330 and its viscosity was set to 0.8872 cP.[25] The complex refractive index of the DMF solution was set to 1.45 + 0.001i. This is an approximation, assuming the average refractive index increment for a protein in DMF solution is about 0.2 mL/g.[26] This approximation was considered to be closer to the refractive index of PVP-*block*-poly(N^{ε}-(CBZ)-L-lys) in DMF than that of a polystyrene latex. Unfortunately, these approximations are quite speculative and their degree of error cannot be determined. However, since no previous work on determining these values could be found, it was

the only option. Also, the main variable being observed for the DLS experiments was the change in the average hydrodynamic diameter due to aggregation or dissociation so accurate values for the mean hydrodynamic diameter were not crucial. The solvent refractive index was set to 1.431 and its viscosity was set to 0.9200 cP. Three measuremens were taken at 25 °C for both samples. Each measurement consisted of 14 scans with an acquisition time of 60 seconds. The average of the three measurements was used to construct a particle size distribution of the colloidal suspension and the solution. The data was converted from an intensity distribution to a number distribution for both samples.

cryo-TEM of the dispersion was performed using a Tecnai F20 transmission electron microscope operating at 200kV for the field emission gun and fitted with a US 4000 Gatan CCD camera.

7.3) Results and Discussion

7.3.1) Synthesis of poly(N^{ε}-(CBZ)-L-lysine)

NMR Analysis

The ^{1}H-NMR spectrum of poly(N^{ε}-(CBZ)-L-lysine) initiated by 1-octylamine is illustrated in Figure 7.1. Using the methyl protons peak at δ = 0.84 ppm as an internal reference and normalizing its integration intensity to 3, the average number of lysine residues per peptide chain was calculated by measuring the integration intensity of the benzyl protons on the CBZ group at δ = 4.96 ppm and dividing the value by 2. This calculation indicated that the degree of polymerization was approximately 32. This is well within the desired block size for the DDS and the correspondence between the degree of polymerization at that monomer conversion indicated that the polymerization was well controlled. If the polymerization was not well controlled, many of the oligomers formed would be lost during the dialysis step and DP for the product would not correlate with the expected value of 35.

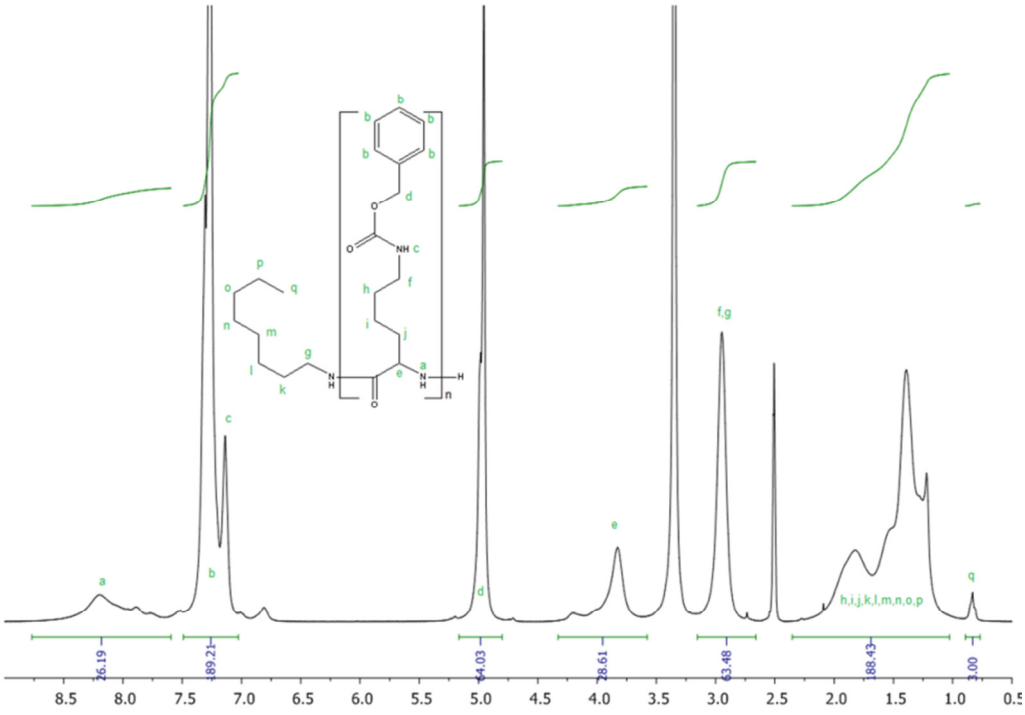

Figure 7.1: 1H-NMR of poly(N^{ε}-(CBZ)-L-lysine).

7.3.2) Synthesis of PVP-block-poly(N^{ε}-(CBZ)-L-lysine)

NMR Analysis

Of the several trials attempted for the NCA ROP using amine-functionalized PVP as the macroinitiator, only one was successful at preparing a significantly large peptide block. The introduction of water or other impurities, such as residual phosgene or HCl, could have resulted in the loss of control of the ROP. That is why all the materials used for the ROP should be as pure as possible. An inadequate temperature or pressure regulation could also have led to poorer control. This trial used a 15.8 kDa PVP macroinitiator and had a initiator-to-NCA ratio of 50. The ^{1}H-NMR spectrum of the isolated block copolymer in DMSO-d6 is illustrated in Figure 7.2. Due to the large amount of water in the sample, the water peak was presaturated in order to obtain a better dynamic range for the spectrum. Since the water peak overlapped with the PVP backbone peaks at δ = 2.8 – 4.1 ppm, the PVP backbone peaks at δ = 1.14 – 2.43 ppm were used as an internal reference. The interfering peaks for the lysine residues (e) were accounted for using an iterative protocol as described in Appendix A12.

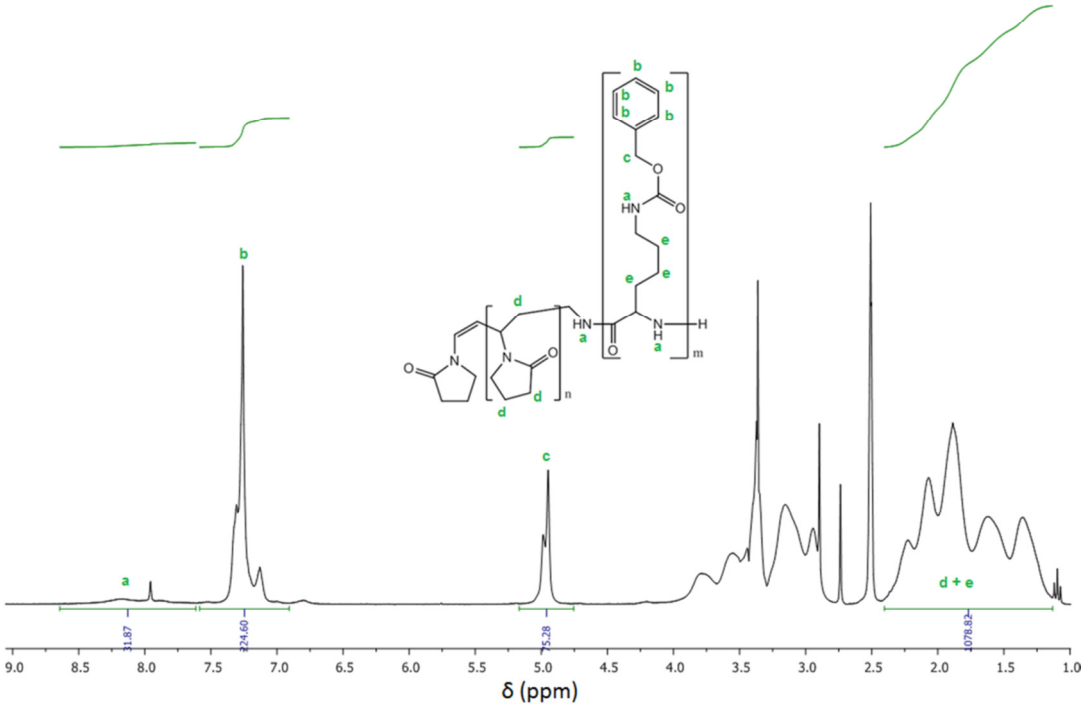

Figure 7.2: ^{1}H-NMR Spectrum of PVP-*block*-poly(N^{ε}-(CBZ)-L-lys) with Presaturation of the Water Peak.

After normalization, dividing the integral for the phenyl protons peak (b – Figure 7.2) by 5 indicated that the average number of lysine residues per PVP chain was approximately 45. This is close to the expected value for the initiator-to-NCA ratio used. Dividing the integral for the benzyl protons peak (c – Figure 7.2) by 2 indicated that the average number of lysine residues per PVP chain was approximately 38. These are in close agreement and the difference may be due to the precision of the integration or differences in T1 as the acquisition time plus the relaxation delay was only 5 seconds. The integral for amide protons peak would not be useful as chemical exchange with water would result in a reduction in signal intensity during the presaturation stage of the NMR spectral acquisition. However, its broadness is indicative that the average molecular weight of the molecules containing lysine residues must be quite large.

SEC Analysis

SEC analysis for the PVP-*block*-poly(N^{ε}-(CBZ)-L-lys) was performed as described in Appendix A1 for block copolymers. The normalized molecular weight distributions for the PVP macroinitiator as well as the block copolymer product are illustrated in Figure 7.3.

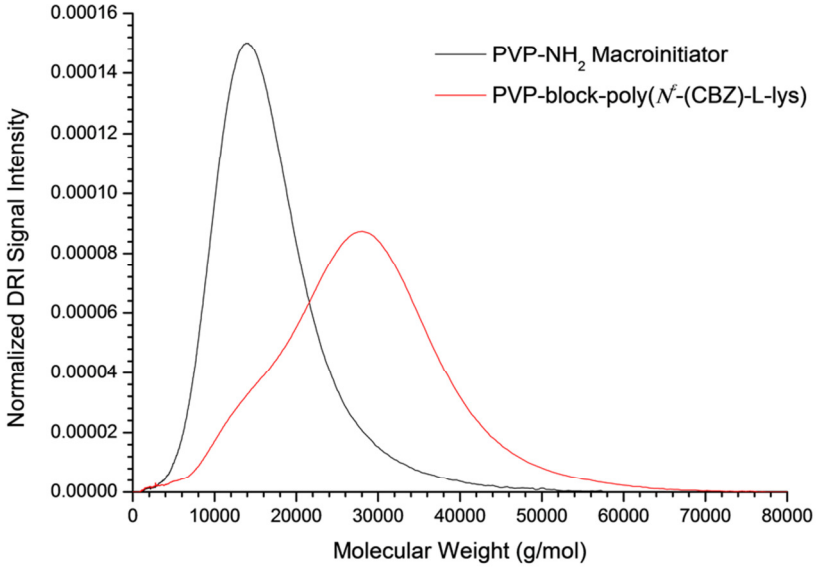

Figure 7.3: Normalized Molecular Weight Distributions for the PVP-Amine Macroinitiator and the PVP-*block*-poly(N^{ε}-(CBZ)-L-lys) Product.

M_n and $Đ$ for the PVP-*block*-poly(N^{ε}-(CBZ)-L-lys) were 28300 g/mol and 1.13, respectively. M_n and $Đ$ for the PVP macroinitiator were 16800 g/mol and 1.17, respectively. Thus the average molecular weight of the polymer had increased by 11500 g/mol. This corresponds to an average increase in DP by approximately 44 N^{ε}-(CBZ)-L-lys repeat units. The low dispersity of the product indicates that the polymerization was well controlled. The bimodal distribution indicates that not all of the PVP chains had initiated ring-opening polymerization of the NCA. This is to be expected since some of the PVP chains were initiator-derived. Deconvolution of the molecular weight distribution could aid in determining the fraction of initiator-derived PVP chains in the product but, in order to be able to perform such a calculation, the distributions of the mono-functional and bi-functional R-group functionionalized PVP chains is required. These are the only polymer chains that would be able to initiate ROP of the N^{ε}-(CBZ)-L-lys NCA. The degree of deprotection and fraction of amine end-groups that successfully initiate ROP of N^{ε}-(CBZ)-L-lys NCA also needs to be accurately known, provided the assumption that these fractions are not chain-length dependent is correct. Models of the RAFT-mediated polymerization and ROP polymerization would then be prepared to fit the respective parameters. The distribution models would require the rate constants for the elementary steps of the polymerization reaction mechanisms to be determined. Very few of these constants were actually found in the literature, as described in Chapter 4, and obtaining some of them would require instrumentation that was not available to us. Also, peak-position relative calibration with PMMA would introduce substantial errors due to differences in the hydrodynamic volume of the block copolymer and PMMA. Hence, either universal calibration or direct molecular weight

determination, using a static light scattering detector, is necessary for all the SEC analyses. A more in depth study is required to accurately determine the fraction of initiator-derived PVP chains.

Cryo-Transmission Electron Microscopy analysis

The colloidal dispersion prepared in Section 7.2.5 was analyzed by cryo-TEM. A representative cryo-TEM image is illustrated in Figure 7.4.A.

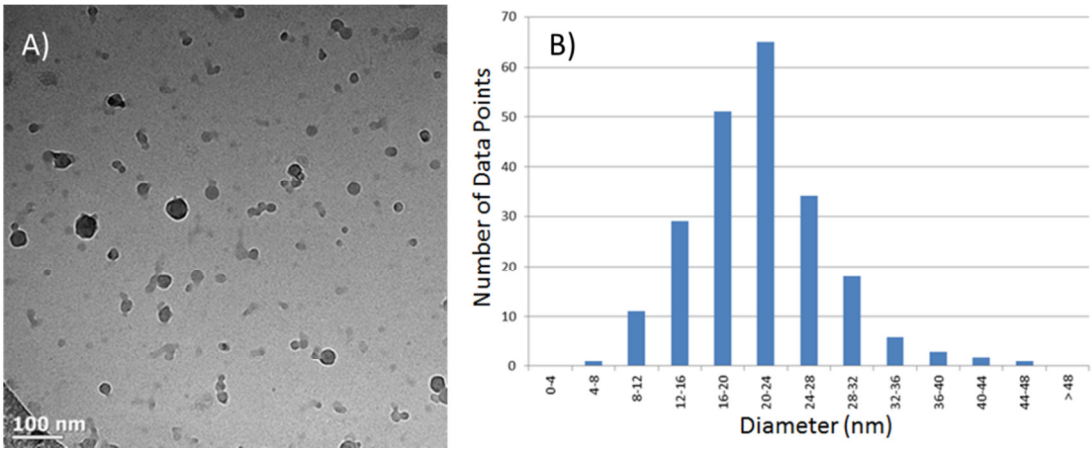

Figure 7.4: A) Representative Cryo-TEM Image of PVP-*block*-poly(N^{ε}-(CBZ)-L-lys) Collodial Dispersion. B) Histogram of Measured Micelle Diameters.

The particle sizes were measured in all the images taken using the AxioVision LE 4.4 software package and a histogram of the collected data was plotted in Figure 7.4.B. The mean measured micelle diameter was 21.5 nm with a standard deviation of 6.5 nm. This indicated that the average size of the micelles was within the desired range. Some cylindrical micelles were also present in the sample though they appeared to have a different density to the spherical ones. It was unclear why two types of micelles were present but it was considered that perhaps block copolymers with low-molecular weight PVP chains and relatively high molecular weight peptide chains would have a larger critical packing parameter and form the cylindrical micelles with a different packing density. Due to the variation in perspective with the depth of each particle within the sample, these measurements are only an approximation of the actual values.

DLS Analysis

The size distributions obtained from the DLS analysis of the PVP-*block*-poly(N^{ϵ}-(CBZ)-L-lys) colloidal suspension in H_2O as well as the solution of PVP-*block*-poly(N^{ϵ}-(CBZ)-L-lys) in DMF are illustrated in Figure 7.5. Comparison of the two distributions indicated that PVP aggregates in H_2O to form micelles with an average diameter of 57 nm and a standard deviation of 21 nm while the average size of each polymer chain in solution is 3.8 nm with a standard deviation of 1.2 nm. Since the exact values of the complex refractive index for the solution or the colloidal suspension were not known, these values are only an approximation and the results of cryo-TEM may be closer to the actual values.

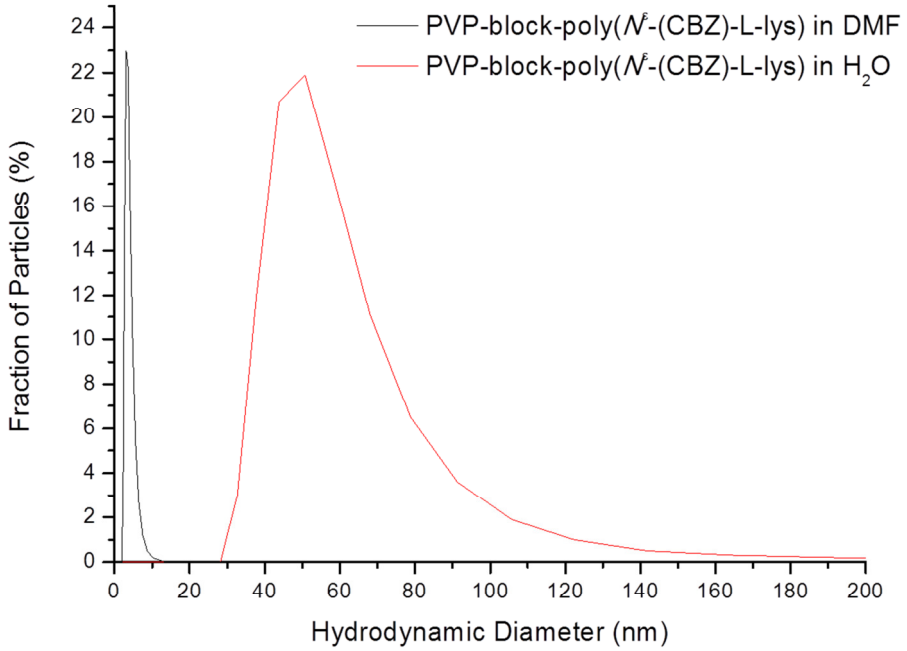

Figure 7.5: DLS Analysis of PVP-*block*-poly(N^{ϵ}-(CBZ)-L-lys) in DMF and in H_2O.

7.4) Conclusions

The ring-opening polymerization of (N^{ϵ}-(CBZ)-L-lys) NCA using a primary amine-functionalized PVP was successfully used to prepare the block copolymer PVP-*block*-poly(N^{ϵ}-(CBZ)-L-lys) with a relatively high molecular weight. NMR as well as SEC analysis confirmed the polymerization was well controlled. DLS and cryo-TEM analysis indicated that the block copolymer was amphiphilic and self-assembled in H_2O to form micelles within the desired size range.

7.5) References

1. Minko, S. In *Grafting on Solid Surfaces: "Grafting to" and "Grafting from" Methods;* Springer Berlin Heidelberg: 2008; pp 215-234.

2. Habraken, G. J. M.; Peeters, M.; Dietz, C. H. J. T.; Koning, C. E.; Heise, A. How controlled and versatile is N-carboxy anhydride (NCA) polymerization at 0°C? Effect of temperature on homo-, block- and graft (co)polymerization. *Polym. Chem.* **2010***, 1*, 514-524.

3. Habraken, G. J. M.; Wilsens, K. H. R. M.; Koning, C. E.; Heise, A. Optimization of N-carboxyanhydride (NCA) polymerization by variation of reaction temperature and pressure. *Polym. Chem.* **2011***, 2*, 1322-1330.

4. Deming, T. J. Facile synthesis of block copolypeptides of defined architecture. *Nature* **1997***, 390*, 386-389.

5. Cheng, J.; Deming, T. J. In *Synthesis of Polypeptides by Ring-Opening Polymerization of α-Amino Acid N-Carboxyanhydrides;* Deming, T., Ed.; Peptide-Based Materials; Springer Berlin Heidelberg: 2012; Vol. 310, pp 1-26.

6. Aliferis, T.; Iatrou, H.; Hadjichristidis, N. Living Polypeptides. *Biomacromolecules* **2004***, 5*, 1653-1656.

7. Hernández, J. R.; Klok, H. Synthesis and ring-opening (co)polymerization of L-lysine N-carboxyanhydrides containing labile side-chain protective groups. *J. Polym. Sci. A Polym. Chem.* **2003***, 41*, 1167-1187.

8. Kramer, J. R.; Deming, T. J. General Method for Purification of α-Amino acid-N-carboxyanhydrides Using Flash Chromatography. *Biomacromolecules* **2010***, 11*, 3668-3672.

9. Sun, J.; Chen, X.; Deng, C.; Yu, H.; Xie, Z.; Jing, X. Direct Formation of Giant Vesicles from Synthetic Polypeptides. *Langmuir* **2007***, 23*, 8308-8315.

10. Deng, C.; Chen, X.; Yu, H.; Sun, J.; Lu, T.; Jing, X. A biodegradable triblock copolymer poly(ethylene glycol)-b-poly(l-lactide)-b-poly(l-lysine): Synthesis, self-assembly, and RGD peptide modification. *Polymer* **2007***, 48*, 139-149.

11. Toncheva, V.; Wolfert, M. A.; Dash, P. R.; Oupicky, D.; Ulbrich, K.; Seymour, L. W.; Schacht, E. H. Novel vectors for gene delivery formed by self-assembly of DNA with poly(L-lysine) grafted with hydrophilic polymers. *Biochim. Biophys. Acta* **1998***, 1380*, 354-368.

12. Harada, A.; Kataoka, K. Formation of Polyion Complex Micelles in an Aqueous Milieu from a Pair of Oppositely-Charged Block Copolymers with Poly(ethylene glycol) Segments. *Macromolecules* **1995***, 28*, 5294-5299.

13. Cotarca, L.; Eckert, H. *Phosgenations: A Handbook;* Wiley: Weinheim, Germany, 2006.

14. Penczek, S. *Models of Biopolymers By Ring-Opening Poylmerization;* Taylor & Francis: Florida, 1989.

15. Poché, D. S.; Moore, M. J.; Bowles, J. L. An Unconventional Method for Purifying the N-carboxyanhydride Derivatives of γ-alkyl-L-glutamates. *Synth. Commun.* **1999**, *29*, 843-854.

16. Wuts, P. G. M.; W. Greene, T. W. *Greene's Protective Groups in Organic Synthesis;* John Wiley and Sons, Inc.: Hoboken, New Jersey, 2012.

17. Shiraishi, K.; Kawano, K.; Minowa, T.; Maitani, Y.; Yokoyama, M. Preparation and in vivo imaging of PEG-poly(L-lysine)-based polymeric micelle MRI contrast agents. *J. Control. Release* **2009**, *136*, 14-20.

18. ElAmin, B.; Anantharamaiah, G. M.; Royer, G. P.; Means, G. E. Removal of benzyl-type protecting groups from peptides by catalytic transfer hydrogenation with formic acid. *J. Org. Chem.* **1979**, *44*, 3442-3444.

19. Qiongjiao, Y.; Juan, L.; Shipu, L.; Yixia, Y.; Ping, Z. Synthesis and RGD peptide modification of poly(lactic acid)-co-(glycolic acid)-alt-(L-lysine). *e-Polymers* **2013**, *8*, 295.

20. Socrates, G. *Infrared Characteristic Group Frequencies;* John Wiley & Sons Ltd.: Chichester, England, 1994.

21. Gärtner, K.; Vogel, G.; Ulbrich, M. Untersuchungen zur Penetration von Makromolekülen (Polyvinylpyrrolidon) durch glomeruläre und postglomeruläre Capillaren in den Harn und die Nierenlymphe und zur Größe der extravasalen Umwälzung von 131J-Albumin im Interstitium der Niere. *Pflüger's Archiv* **1968**, *298*, 305-321.

22. Wessel, W.; Schoog, M.; Winkler, E. Polyvinylpyrrolidone (PVP), its diagnostic, therapeutic and technical application and consequences thereof. *Arzneimittel-Forschung* **1971**, *21*, 1468-1482.

23. Pramanick, S.; Singodia, D.; Vikas, C. Excipient Selection in Parenteral Formulation Development. *Pharma Times* **2013**, *45*, 65-77.

24. Xiaoyan Ma, X.; Lu, J. Q.; Brock, R. S.; Jacobs, K. M.; Yang, P.; Hu, X. H. Determination of complex refractive index of polystyrene microspheres from 370 to 1610 nm. *Phys. Med. Biol.* **2003**, *48*, 4165.

25. Píchal, M.; Šifner O. *Properties Of Water And Steam: Proceedings Of The 11th International conference;* Taylor & Francis: USA, 1990.

26. Zhao, H.; Brown, P. H.; Schuck, P. On the Distribution of Protein Refractive Index Increments. *Biophys. J.* **2011**, *100*, 2309-2317.

CHAPTER 8

Deprotecting the N^{ε}-Amine of the Lysine Residues on PVP-*block*-poly(N^{ε}-(CBZ)-L-lys)

8.1) Introduction

As mentioned in Chapter 7, there are two main methods of deprotecting the N^{ε}-amine of lysine from the benzyloxycarbonyl protecting group. These are acidolysis with hydrobromic acid in trifluoroacetic acid[1-5] (TFAA) or catalytic hydrogenation (CH) with a palladium catalyst.[5-7] Since no previous papers dealt with the deprotection of PVP-*block*-poly(N^{ε}-(CBZ)-L-lys), both methods were investigated. Deprotection via CH also offered the advantage of reducing the alkene end-group of PVP, preventing aldehyde or alkyl halide end-group formation.

8.2) Materials and Experimental Methods

Anhydrous calcium chloride, anhydrous calcium sulfate, concentrated sulfuric acid (95 – 97%), DMSO-d6, glacial acetic acid sodium hydrogen carbonate (ACS reagent grade), anhydrous sodium carbonate, concentrated hydrochloric acid (32%), hydrogen bromide (25% in acetic acid), Celite® 545, sodium chloride and sodium metal were purchased from Merck and used as received. Benzophenone, pentafluorobenzaldehyde (PFBA), trifluoroacetic acid, 10% Pd/C and chloroform-d 99.8 atom % were purchased from Sigma Aldrich and used as received. 4Å molecular sieves (8 – 12 mesh) were also purchased from Sigma Aldrich, dried in a vacuum oven at 165 °C for 5 hours and allowed to cool to room temperature under vacuum before use. Dichloromethane, 1,4-dioxane and absolute ethanol were purchased from KIMIX. Dichloromethane was washed with concentrated sulfuric acid followed by 5% sodium bicarbonate solution and finally water before being dried over calcium chloride and fractionally distilled from calcium sulfate. 1,4-Dioxane was distilled from sodium and benzophenone. Ethanol was dried by refluxing with calcium oxide. Dry ethanol was distilled off after 6 hours and stored over 4Å molecular sieves. SnakeSkin® Dialysis tubing (10,000 g/mol nominal molecular weight cutoff (MWCO)) was purchased from Thermo Scientific and used as is.

8.2.1) Deprotection of the CBZ Group by Acidolysis with HBr in TFAA

PVP-*block*-poly(N^{ε}-(CBZ)-L-lys) (0.4 g, 3.2×10^{-5} mol) with $M_{n,NMR}$ of the PVP block equal to 11,000 g/mol and $M_{n,NMR}$ of the peptide block equal to 5,300 g/mol was dissolved in 3 mL TFAA. The solution was cooled to 0 °C and 1 mL of HBr (25% in acetic acid) was added. The reaction mixture was stirred for four hours at 0 °C and then 10 mL of H_2O with 3.2 g Na_2CO_3 was added slowly. The reaction mixture was dialyzed, using 10,000 MWCO dialysis tubing, with four 250 mL portions of H_2O and the polymer was isolated by lyophilization. The product and starting material were analyzed by ^{1}H-NMR. The starting material was dissolved in $CDCl_3$ and the product was dissolved in DMSO-d6.

8.2.2.) Deprotection of the CBZ Group by Acidolysis with HBr in a 1,4-Dioxane and DCM Mixture

1 mL DCM and 1 mL 1,4-dioxane was added to PVP-*block*-poly(N^{ε}-(CBZ)-L-lysine) (0.05 g, 1.77×10^{-6} mol). The solution was cooled to 0 °C in an ice bath and 1 mL HBr (25% in acetic acid) was added. The reaction mixture was kept at 0 °C for 3 hours. Na_2CO_3 (1.0 g, 9.4×10^{-3} mol) was dissolved in 10 mL H_2O and this solution was slowly added to the reaction mixture. The DCM and 1,4-dioxane were removed by evaporation under vacuum and the solution was dialyzed with four 250 mL portions of H_2O, using 10,000 MWCO dialysis tubing. The polymer was isolated by lyophilization.

8.2.3) Deprotection of the CBZ Group by Catalytic Hydrogenation

PVP-*block*-poly(N^{ε}-(CBZ)-L-lysine) (0.1 g, 4.50×10^{-6} mol) was dissolved in 4 mL ethanol with gentle heating. 1 mL glacial acetic acid and 0.05 g 10% Pd/C was added. The reaction mixture was heated to 45 °C and sparged with H_2 gas for four hours. 1 g NaCl dissolved in 5 mL 0.4 M HCl and this solution was added to the reaction mixture. The catalyst was removed by centrifugation at 5000 rpm for 20 minutes followed by filtering through celite. Sodium bicarbonate (0.2 g, 2.4 mmol) was slowly added and the solution was dialyzed with four 250 mL portions of H_2O, using 10,000 MWCO dialysis tubing. The polymer was isolated by lyophilization.

8.3) Results and Discussion

8.3.1) Deprotection of PVP-*block*-poly(N^{ε}-(CBZ)-L-lys) by Acidolysis with HBr

NMR Analysis

The ^{1}H-NMR spectrum of the PVP-*block*-poly(N^{ε}-(CBZ)-L-lys) starting material that was deprotected by acidolysis with HBr in TFAA (HBr Method 1) was normalized by the procedure described in Appendix A12. The average number of lysine residues on the starting material was determined to be 20.39. The ^{1}H-NMR spectrum of the product was normalized by adjusting the integral for the polymer backbone peaks at δ = 0.98 – 2.42 ppm to equal that for the starting material. The degree of deprotection achieved by HBr Method 1 was determined by measuring the change in the integral for the benzyl protons peak at δ = 4.77 – 5.15 ppm of the normalized ^{1}H-NMR spectra for the starting material and the product. This turned out to be 70%. A possible reason for the incomplete deprotection could be due to the poor solubility of PVP in TFAA that resulted in the precipitation of the block copolymer at 0 °C. The ^{1}H-NMR spectrum of the PVP-*block*-poly(L-lysine) deprotected by HBr Method 1 is illustrated in Figure 8.1.

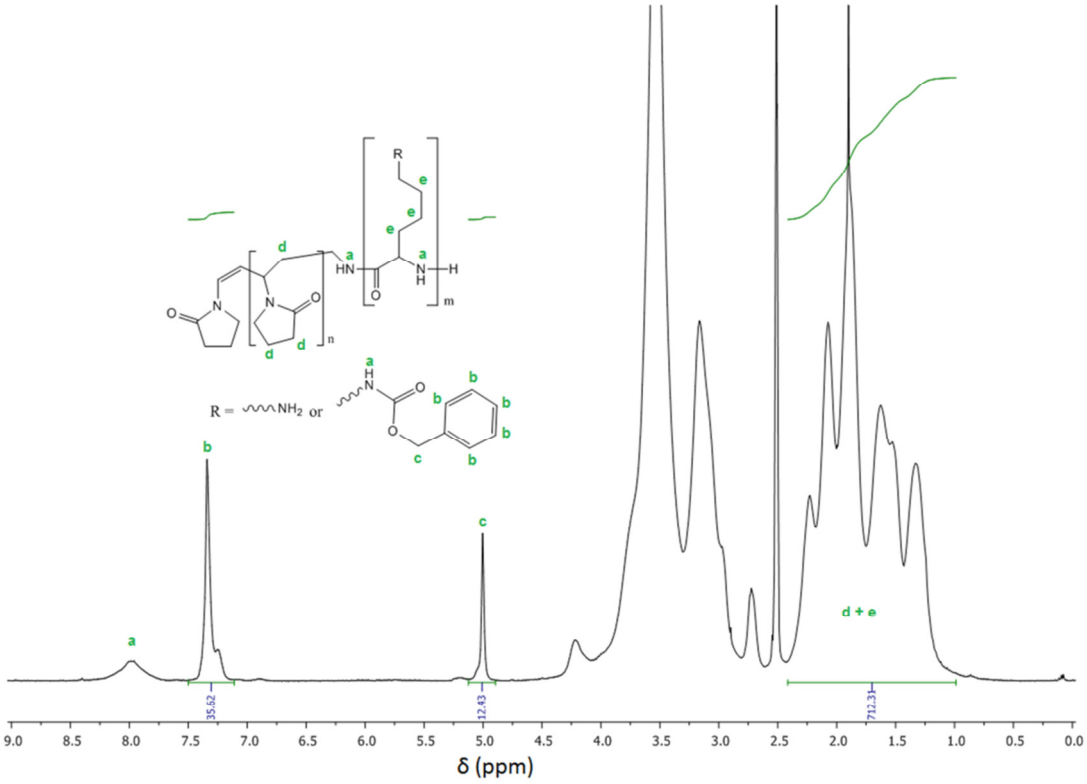

Figure 8.1: ^{1}H-NMR Spectrum of PVP-*block*-poly(L-lysine) Deprotected with HBr in TFAA.

Using the same analytical procedure, the degree of deprotection achieved by acidolysis with HBr in the DCM and 1,4-dioxane solvent mixture (HBr Method 2) was determined to be about 100% as no benzyl protons peak could be detected. The product was derivatized with PFBA and its ^{1}H-NMR spectrum is illustrated in Figure 8.2. After adjusting the integral of the backbone protons peaks at δ = 0.98 – 2.42 ppm to equal that for the starting material, the integral of the imine protons peak at δ = 7.95 – 8.68 ppm was equal to 28.72. This was less than the expected value of ca. 40. A possible reason for this could be that the acidolysis step resulted in partial hydrolysis of the lysine residues. However, a more likely reason is that the presence of water (δ = 3.3) and acetic acid (peaks – g and h) were causing an equilibrium to be established, resulting in only a partial imine derivatization.

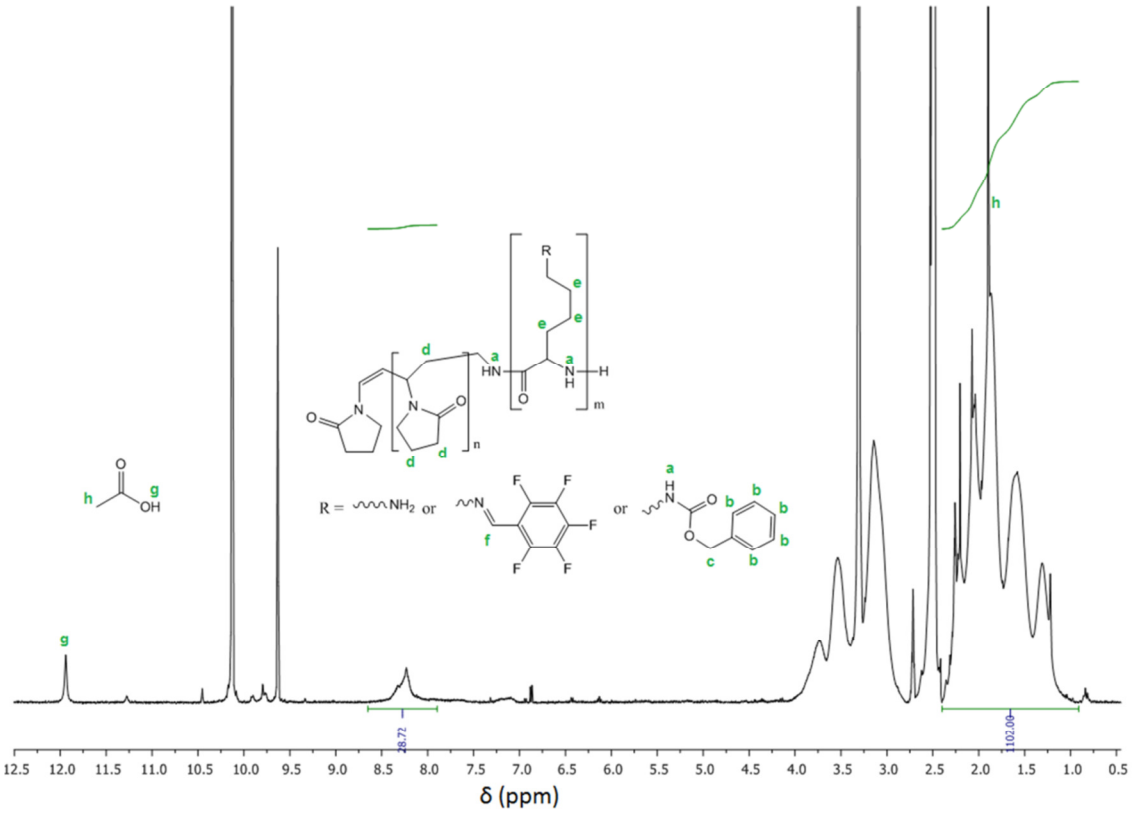

Figure 8.2: ^{1}H-NMR Spectrum of PVP-*block*-poly(L-lysine) Deprotected with HBr in a Mixture of 1,4-Dioxane and DCM.

DLS Analysis

The product of the HBr Method 2 as well as the PVP macroinitiator used to prepare it were analyzed by DLS in H_2O. The hydrodynamic diameter distributions were plotted in Figure 8.3. The results indicated that PVP-*block*-poly(L-lysine) has a larger hydrodynamic diameter in H_2O than the PVP

macroinitiator but a much smaller one than PVP-*block*-poly(N^{ε}-(CBZ)-L-lys). Thus PVP-*block*-poly(L-lysine) most likely does not self-assemble into micelles in H_2O.

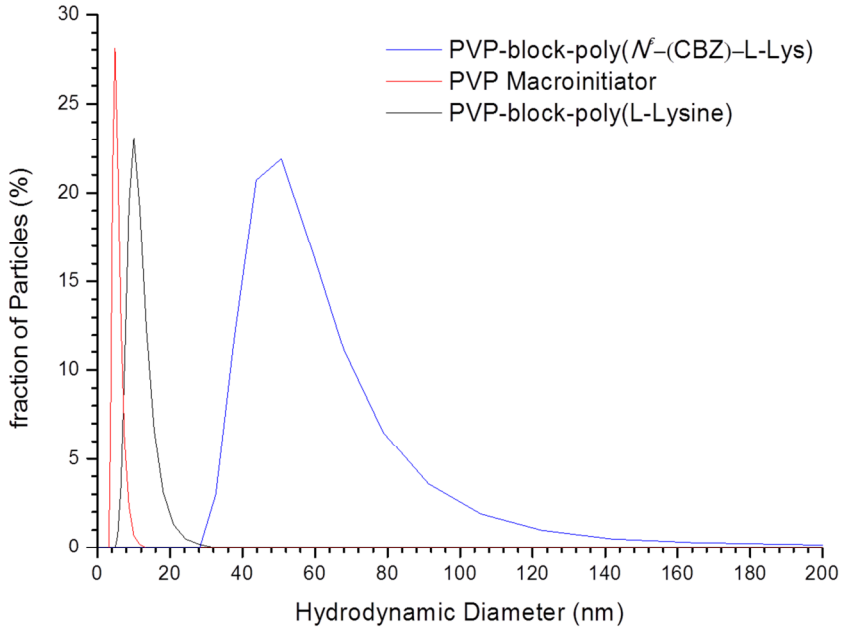

Figure 8.3: DLS Results for PVP-*block*-poly(L-lysine), Deprotected by Acidolysis in the 1,4-Dioxane and DCM Solvent Mixture, as well as that of the PVP Macroinitiator Used to Prepare it.

8.3.2) Deprotection of PVP-*block*-poly(N^{ε}-(CBZ)-L-lys) by Catalytic Hydrogenation

NMR Analysis

The ^{1}H-NMR spectrum of the PVP-*block*-poly(N^{ε}-(CBZ)-L-lys) starting material that was deprotected by CH was normalized by the procedure described in Appendix A12. The average number of lysine residues on the starting material was determined to be 23.55. The degree of deprotection by CH was determined by the same method as described in Section 8.3.1. For CH, the degree of deprotection turned out to be 85%. The ^{1}H-NMR spectrum of the PVP-*block*-poly(N^{ε}-(CBZ)-L-lys) starting material and that for the product of deprotection by CH are superimposed on each other in Figure 8.4. Though this procedure was generally milder than the acidolysis procedures and more effective than the HBr Method 1, it was still not quantitative and it was not possible to remove all of the heterogenous Pd catalyst from the product even with our extensive isolation procedure. PVP is known to adsorb strongly to the surface of colloidal noble metal particles as it stabilizes their surface energy and stabilizes their dispersion through steric hindrance.[8,9] It was not possible to remove all of

the catalyst from the reaction mixture by centrifugation, even when acid and a large amount of electrolyte was added. This confirmed that the Pd nanoparticles must be sterically stabilized.[10,11] Filtering over celite also failed to remove all of the catalyst. However, due to time restraints, this was only confirmed qualitatively by noting that the solution remained light brown. Thus acidolysis by the HBr Method 2 proved to be the simplest and most effective method for deprotecting the lysine residues of PVP-*block*-poly(N^{ε}-(CBZ)-L-lys).

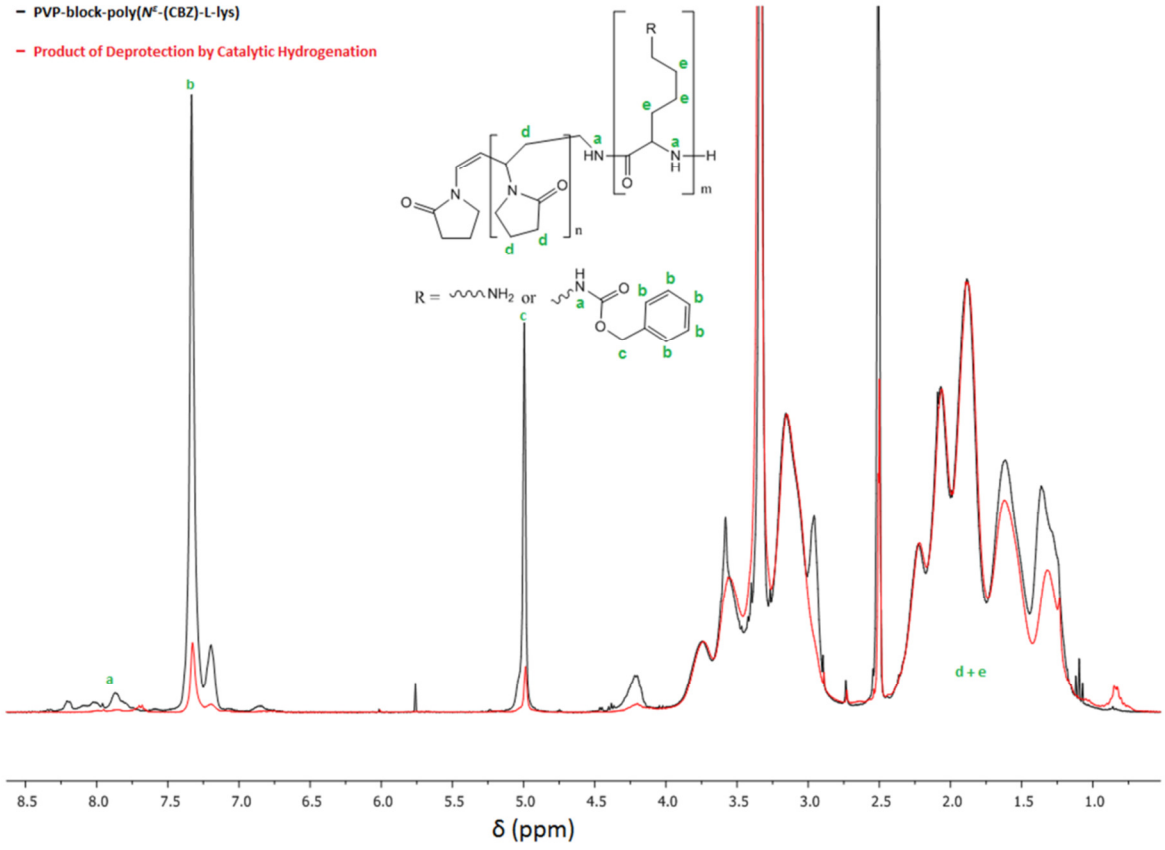

Figure 8.4: ^{1}H-NMR Spectrum for PVP-*block*-poly(L-lysine) Deprotected by Catalytic Hydrogenation and that of its Starting Material.

8.4) Conclusions

The deprotection of PVP-*block*-poly(N^{ε}-(CBZ)-L-lysine) was most effective when performed by acidolysis with HBr in a 1,4-dioxane and DCM solvent mixture at 0 °C. Though deprotection by catalytic hydrogenation was almost quantitative and could be optimized to provide quantitative deprotection, complete removal of the noble metal catalyst proved to be extremely difficult due to the strong stabilizing interaction of the colloidal metal particles with PVP.

8.5) References

1. Deng, C.; Chen, X.; Yu, H.; Sun, J.; Lu, T.; Jing, X. A biodegradable triblock copolymer poly(ethylene glycol)-b-poly(l-lactide)-b-poly(l-lysine): Synthesis, self-assembly, and RGD peptide modification. *Polymer* **2007***, 48*, 139-149.

2. Shiraishi, K.; Kawano, K.; Minowa, T.; Maitani, Y.; Yokoyama, M. Preparation and in vivo imaging of PEG-poly(L-lysine)-based polymeric micelle MRI contrast agents. *J. Control. Release* **2009***, 136*, 14-20.

3. Toncheva, V.; Wolfert, M. A.; Dash, P. R.; Oupicky, D.; Ulbrich, K.; Seymour, L. W.; Schacht, E. H. Novel vectors for gene delivery formed by self-assembly of DNA with poly(L-lysine) grafted with hydrophilic polymers. *Biochim. Biophys. Acta* **1998***, 1380*, 354-368.

4. Hernández, J. R.; Klok, H. Synthesis and ring-opening (co)polymerization of L-lysine N-carboxyanhydrides containing labile side-chain protective groups. *J. Polym. Sci. A Polym. Chem.* **2003***, 41*, 1167-1187.

5. Wuts, P. G. M.; W. Greene, T. W. *Greene's Protective Groups in Organic Synthesis;* John Wiley and Sons, Inc.: Hoboken, New Jersey, 2012.

6. ElAmin, B.; Anantharamaiah, G. M.; Royer, G. P.; Means, G. E. Removal of benzyl-type protecting groups from peptides by catalytic transfer hydrogenation with formic acid. *J. Org. Chem.* **1979***, 44*, 3442-3444.

7. Qiongjiao, Y.; Juan, L.; Shipu, L.; Yixia, Y.; Ping, Z. Synthesis and RGD peptide modification of poly(lactic acid)-co-(glycolic acid)-alt-(L-lysine). *e-Polymers* **2013***, 8*, 295.

8. Nguyen, V. L.; Nguyen, D. C.; Hirohito, H. H.; Ohtaki, M.; Hayakawa, T.; Nogami, M. Chemical synthesis and characterization of palladium nanoparticles. *Adv. Nat. Sci: Nanosci. Nanotechnol.* **2010***, 1*, 35012.

9. Zhao, Y.; Baeza, J. A.; Koteswara Rao, N.; Calvo, L.; Gilarranz, M. A.; Li, Y. D.; Lefferts, L. Unsupported PVA- and PVP-stabilized Pd nanoparticles as catalyst for nitrite hydrogenation in aqueous phase. *J. Catal.* **2014***, 318*, 162-169.

10. Somasundaran, P. *Encyclopedia of Surface and Colloid Science;* Taylor & Francis: 2006.

11. Pashley, R.; Karaman, M. *Applied Colloid and Surface Chemistry;* John Wiley & Sons: England, 2005.

CHAPTER 9

Conjugation of Doxorubicin to PVP-*block*-poly(L-lysine)

9.1) Introduction

This chapter focusses on the preliminary study of the synthesis as well as self-assembly and stability of PVP-*block*-poly(L-lysine) conjugates with Doxorubicin as well as other compounds via imine linkages. Imines form when a primary amine reacts with an aldehyde or ketone, forming a carbon-nitrogen double bond and eliminating water. They belong to a class of functional groups known as Schiff bases. The general mechanism of Schiff base formation is illustrated in Scheme 9.1.

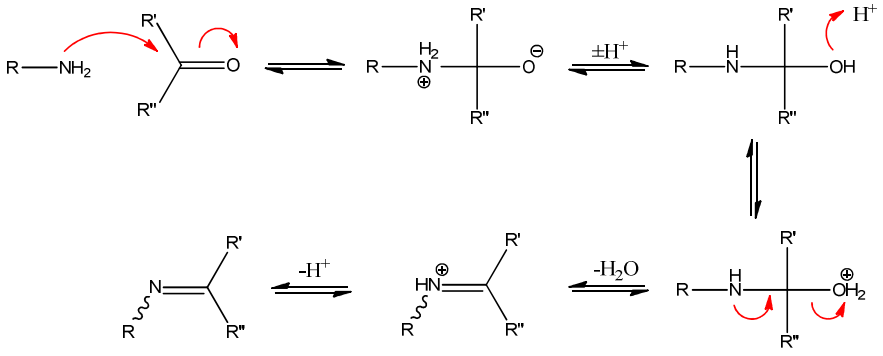

Scheme 9.1: General Mechanism of Schiff Base Formation.

Schiff bases are usually unstable in aqueous solutions and decompose readily into their starting materials.[1] However, their stability can be improved if electron-withdrawing groups are attached to the nitrogen or carbonyl carbon. Ketones also generally decompose more slowly than aldehydes. Due to their tunable hydrolysis rates, Schiff bases are often investigated as acid-labile linkers. Acyl hydrazones are among the most well-known of the acid-labile linkers and Etrych *et al.* have studied the conjugation of Doxorubicin via hydrazone bonds to its α-hydroxy ketone extensively.[2-5] Some research has also been published where the conjugation of Doxorubicin to macromolecules is achieved via an imine bond of an aldehyde to its daunosamine residue.[6-8] These techniques are based on incorporating the hydrolytically-labile imine bond within the hydrophobic domain of a hydrogel or micelle.

9.2) Materials and Experimental Methods

Benzaldehyde was purchased from Sigma Aldrich and used as received. Sodium bicarbonate was purchased from Merck and used as received. Doxorubicin hydrochloride was purchased from Taizhau Crene Biotechnology and used as received. Methanol was purchased from Kimix and fractionally distilled before use. 0.45 µm Glass fiber prefilters were purchased from PALL Life Sciences.

9.2.1) Synthesis of PVP-*block*-poly(L-lysine)-Doxorubicin Dispersion in H_2O

PVP-*block*-poly(L-lysine) (4 mg, 1.94×10^{-7} mol, *ca.* 7.29×10^{-6} mol of lysine residues) with $M_{n,NMR}$ of the PVP block equal to 15,800 g/mol and $M_{n,NMR}$ of the poly(L-lysine) block equal to 4,800 g/mol (DP = 38) was dissolved in 2 mL methanol. Doxorubicin.HCl (0.010 g, 1.72×10^{-5} mol) was added along with $NaHCO_3$ (0.005 g, 5.95×10^{-5} mol). The solution was left to react at 4 °C in the absence of light for 48 hours. 2 mL of H_2O was added and the methanol was removed by evaporating under vacuum. The sample was filtered through a 0.45 µm glass SEC prefilter, stored in a glass vial and frozen in liquid nitrogen for transportation to cryo-TEM analysis. DLS was performed immediately after preparation as well as after 24 hours at 25 °C in the absence of light.

9.2.2) Synthesis of PVP-*block*-poly(L-lysine)-Benzaldehyde Dispersion in H_2O

Benzaldehyde (0.040 g, 3.77×10^{-4} mol) was dissolved in 20 mL methanol. PVP-*block*-poly(L-lysine) (4 mg, 1.94×10^{-7} mol, *ca.* 7.29×10^{-6} mol of lysine residues) with $M_{n,NMR}$ of the PVP block equal to 15,800 g/mol and $M_{n,NMR}$ of the poly(L-lysine) block equal to 4,800 g/mol (DP = 38) was dissolved in 2 mL of the benzaldehyde solution along with $NaHCO_3$ (0.005 g, 5.95×10^{-5} mol). The solution was left to react at 4 °C in the absence of light for 48 hours. 2 mL of H_2O was added and the methanol was removed by evaporating under vacuum. The sample was filtered through a 0.45 µm glass SEC prefilter, stored in a glass vial and frozen in liquid nitrogen for transportation to cryo-TEM analysis. DLS was performed immediately after preparation as well as after 24 hours at 25 °C in the absence of light.

9.2.3) Synthesis of Doxorubicin Dispersion in H_2O

Doxorubicin.HCl (0.010 g, 1.72×10^{-5} mol) was added to 2 mL methanol along with $NaHCO_3$ (0.005 g, 5.95×10^{-5} mol). The solution was left to react at 4 °C in the absence of light for 48 hours. 2 mL of H_2O was added and the methanol was removed by evaporating under vacuum. The sample was filtered through a 0.45 µm glass SEC prefilter and DLS was performed immediately after preparation.

9.3) Results and Discussion

9.3.1) Synthesis of PVP-*block*-poly(L-lysine)-Doxorubicin as well as free Doxorubicin Dispersions

DLS Analysis

The complex refractive index of the PVP-*block*-poly(L-lysine)-Doxorubicin dispersion was set to 1.59 + 0.01i. This was the same approximation used in Section 7.2.5 as no refractive index measurement instrumentation was available. The dispersant refractive index was set to 1.330 and its viscosity was set to 0.8872 cP. The hydrodynamic diameter distributions of the PVP-*block*-poly(L-lysine)-Doxorubicin dispersion, measured by DLS, immediately after sample preparation as well as after 24 hours at 25 °C are illustrated in Figure 9.1. The initial mean hydrodynamic diameter was 194 nm, substantially larger than the 57 nm measured for the PVP-*block*-poly(N^{ε}-(CBZ)-L-lys) dispersion. The standard deviation of the distribution was significantly low (83 nm) indicating that the dispersion was most likely the result of self-assembly into micelles rather than aggregation into a colloidal precipitate.

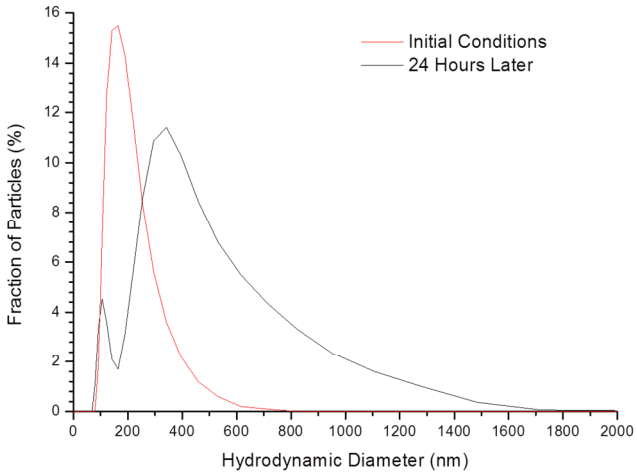

Figure 9.1: Hydrodynamic Diameter Distributions for the PVP-*block*-poly(L-lysine)-Doxorubicin Dispersion.

The increase in particle size could be due to the larger size of the Doxorubicin molecule compared to the CBZ protecting group as well as the oligomerization of Doxorubicin on some of the lysine residues, as illustrated in Scheme 9.2.

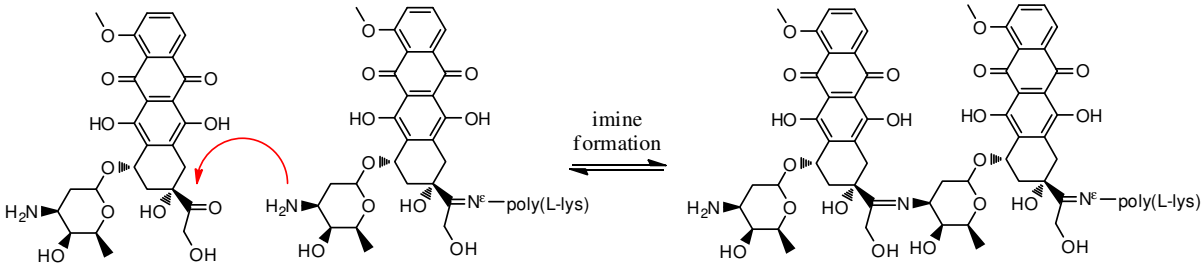

Scheme 9.2: Oligomerization of Doxorubicin on Lysine Residues of PVP-*block*-poly(L-lysine).

Both the mean hydrodynamic diameter and the standard deviation of the PVP-*block*-poly(L-lysine)-Doxorubicin dispersion increased to 461 nm and 293 nm, respectively, after 24 hours. This was indicative of aggregation occurring, resulting in the formation of a colloidal precipitate. The formation of a precipitate was visible and sedimented at the bottom of the sample vial after it was left standing for a sufficient amount of time. The hydrodynamic diameter distribution of the Doxorubicin dispersion measured by DLS is illustrated in Figure 9.2.

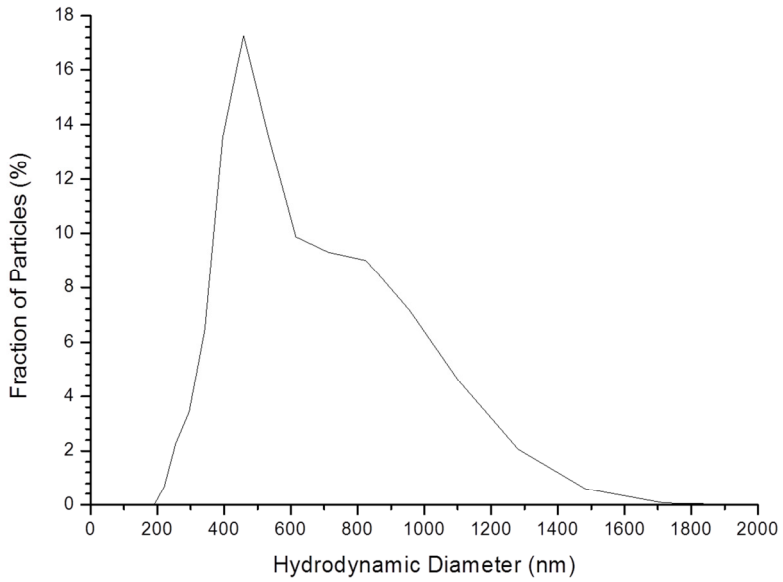

Figure 9.2: Hydrodynamic Diameter Distribution for the Free Doxorubicin Dispersion.

The mean hydrodynamic diameter and the standard deviation of this dispersion were calculated to be 602 nm and 251 nm, respectively. This distribution closely resembles that of the PVP-*block*-poly(L-lysine)-Doxorubicin dispersion after 24 hours, complementing the theory that the imine

bonds conjugating Doxorubicin to the PVP-*block*-poly(L-lysine) were hydrolyzed and the free Doxorubicin had aggregated to form a precipitate.

Cryo-TEM Analysis

Cryo-TEM analysis of the PVP-*block*-poly(L-lysine)-Doxorubicin dispersion was performed to obtain a more accurate measurement of the average particle diameter as well as to visualize the morphology of the micelles. A representative image of those acquired is illustrated in Figure 9.3.A. 119 particle diameters were measured from 18 images and a histogram of the measured values was plotted in Figure 9.3.B.

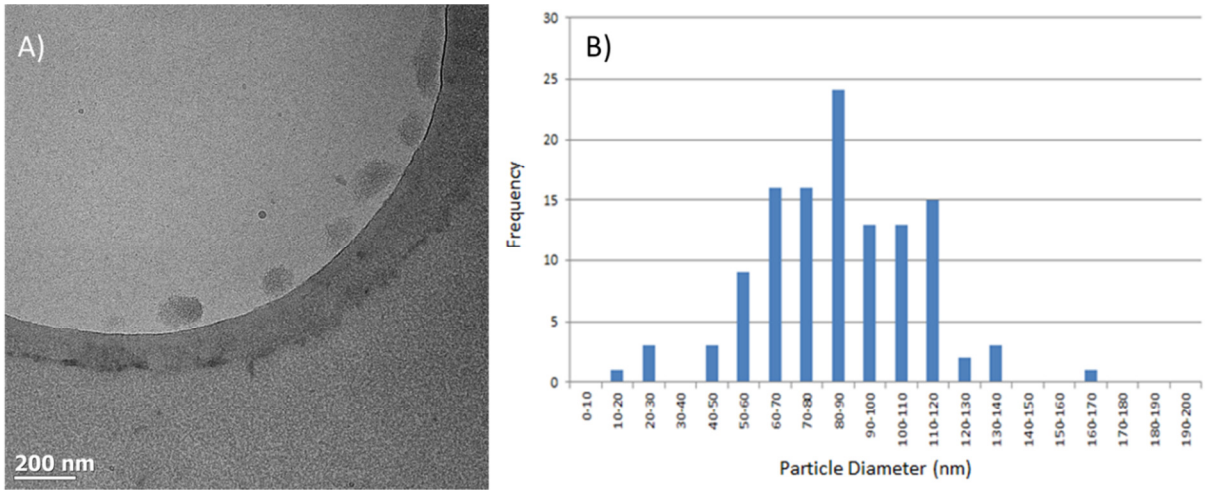

Figure 9.3: A) Cryo-TEM Image of PVP-*block*-poly(L-lysine)-Doxorubicin Dispersion. B) Histogram of Measured Particle Diameters.

The average particle diameter measured from the cryo-TEM images was 86 nm with a standard deviation of 25 nm. There were many cylindrical micelles observed, indicating that the hydrophobic block of the block copolymer had indeed increased in size, compared to that of the PVP-*block*-poly(N^{ε}-(CBZ)-L-lys) dispersion, causing an increase in the critical packing parameter.[9]

9.3.2) Synthesis of PVP-*block*-poly(L-lysine)-Benzaldehyde Dispersion

DLS Analysis

The complex refractive index of the PVP-*block*-poly(L-lysine)-benzaldehyde dispersion was set to 1.59 + 0.01i. This was an approximation as no refractive index measurement equipment was available. The dispersant refractive index was set to 1.330 and its viscosity was set to 0.8872 cP. The

hydrodynamic diameter distributions, measured by DLS, immediately after sample preparation as well as after 24 hours at 25 °C are illustrated in Figure 9.4. The initial mean hydrodynamic diameter was 50 nm with a standard deviation of 16 nm. This indicated that the PVP-*block*-poly(L-lysine)-benzaldehyde conjugates would self-assemble in aqueous solution to form micelles as the mean hydrodynamic diameter of PVP-*block*-poly(L-lysine) was 11 nm.

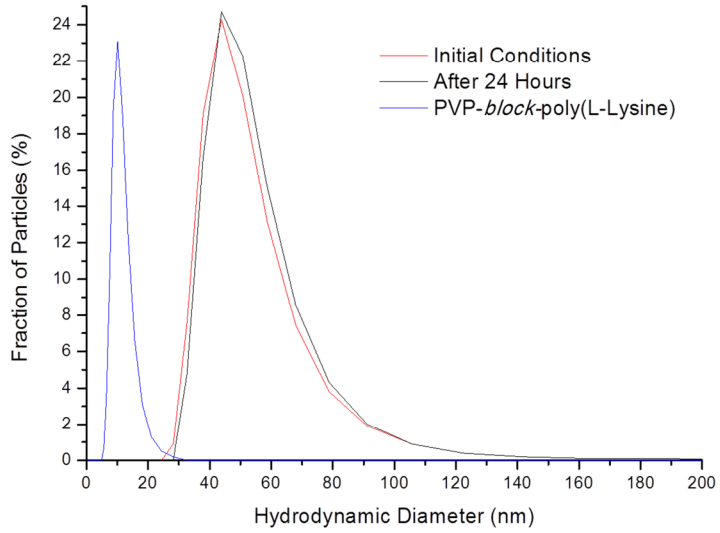

Figure 9.4: Hydrodynamic Diameter Distributions for the PVP-*block*-poly(L-lysine)-benzaldehyde Dispersion as well as that for PVP-*block*-poly(L-lysine).

The mean hydrodynamic diameter as well as the standard deviation of the PVP-*block*-poly(L-lysine)-benzaldehyde dispersion did not change much after 24 hours at 25 °C (52 nm and 16 nm, respectively.) Thus it appeared as though the PVP-*block*-poly(L-lysine)-benzaldehyde dispersion was stable under ambient conditions and at pH ≈ 7.5. This cannot be confirmed by DLS alone and quantification of the release of benzaldehyde from the dispersion with time needs to be determined. This could be achieved by high performance liquid chromatography (HPLC),[10] field-flow fractionation (FFF)[11] or dynamic dialysis.[12,13] However, due to time constraints, this was left for future work.

Cryo-TEM Analysis

12 cryo-TEM images of the PVP-*block*-poly(L-lysine)-benzaldehyde dispersion were taken to study the morphology of the micelles as well as to gain a closer approximation of their mean particle diameter. A representative cryo-TEM image of the PVP-*block*-poly(L-lysine)-benzaldehyde dispersion

is illustrated in Figure 9.5.A. 234 particle diameters were measured and a histogram of the data is illustrated in Figure 9.5.B. The average measured particle diameter was 12 nm with a standard deviation of 1.1 nm.

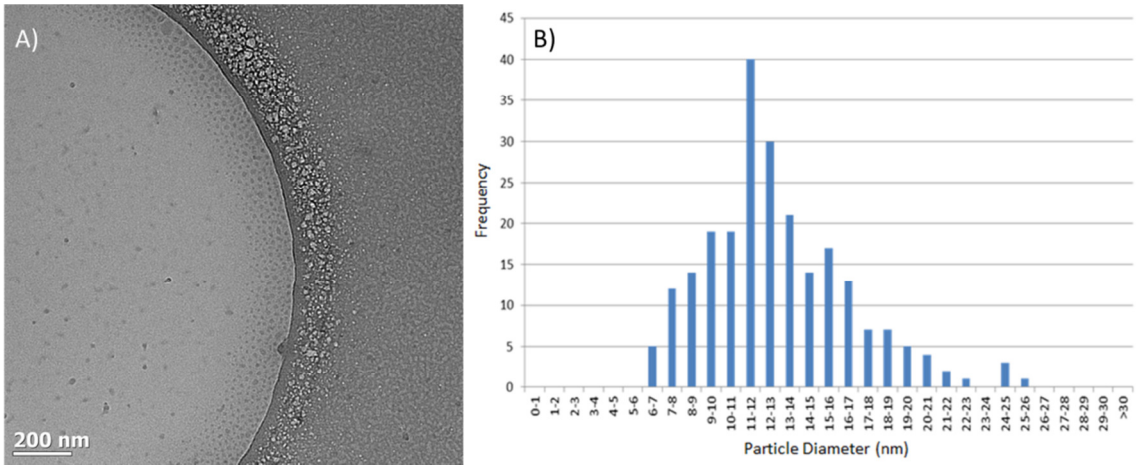

Figure 9.5: A) Cryo-TEM Image of PVP-*block*-poly(L-lysine)-benzaldehyde Dispersion. B) Histogram of Measured Particle Diameters.

The particle morphology was far more uniform – only spherical micelles were observed in all the images. This indicated that the hydrophobic block of the PVP-*block*-poly(L-lysine)-benzaldehyde conjugate was smaller in size than that of the PVP-*block*-poly(N^{ε}-(CBZ)-L-lys), causing a decrease in the critical packing parameter.

The apparent stability and uniform morphology of the PVP-*block*-poly(L-lysine)-benzaldehyde conjugate may be the key to improving the retention of Doxorubicin in the core. Instead of conjugating Doxorubicin alone to the PVP-*block*-poly(L-lysine), a formulation with benzaldehyde could be used. Benzaldehyde would also act as a capping agent, preventing the oligomerization of Doxorubicin and increasing the hydrophobicity of the peptide block. It could also be used to modulate the size of the micelles. The addition of a cross-linking agent, such as terephthalaldehyde, may increase the stability of the dispersion further.[14-16]

9.4) Conclusions

The conjugation of Doxorubicin and benzaldehyde to PVP-*block*-poly(L-lysine) via imine bonds occurred readily in methanol. These conjugates self-assembled into micelles in aqueous solution. PVP-*block*-poly(L-lysine)-Doxorubicin was not stable in H_2O and dissociated into free Doxorubicin, that aggregated into a precipitate, and polymer. PVP-*block*-poly(L-lysine)-benzaldehyde was stable in

H_2O. The stability of the PVP-*block*-poly(L-lysine)-Doxorubicin conjugates in H_2O may be improved by preparing a formulation with benzaldehyde, that would act by diluting the concentration of Doxorubicin conjugated to the peptide block (allowing control of the micelle size and morphology) as well as improving the hydrophobicity of Doxorubicin by capping the free amine of its daunosamine residue. This would also prevent the oligomerization of Doxorubicin. A cross-linking agent, such as terephthalaldehyde may also be added to the formulation to improve the stability of the conjugates further.

9.5) References

1. Clayden, J.; Greeves, N.; Warren, S. *Organic Chemistry;* Oxford University Press: New York, 2012.

2. Etrych, T.; Jelínková, M.; Říhová, B.; Ulbrich, K. New HPMA copolymers containing doxorubicin bound via pH-sensitive linkage: synthesis and preliminary in vitro and in vivo biological properties. *J. Control. Release* **2001***, 73*, 89-102.

3. Chytil, P.; Etrych, T.; Koňák, Č; Šírová, M.; Mrkvan, T.; Říhová, B.; Ulbrich, K. Properties of HPMA copolymer–doxorubicin conjugates with pH-controlled activation: Effect of polymer chain modification. *J. Control. Release* **2006***, 115*, 26-36.

4. Vetvicka, D.; Hruby, M.; Hovorka, O.; Etrych, T.; Vetrik, M.; Kovar, L.; Kovar, M.; Ulbrich, K.; Rihova, B. Biological Evaluation of Polymeric Micelles with Covalently Bound Doxorubicin. *Bioconjugate Chem.* **2009***, 20*, 2090-2097.

5. Sirova, M.; Mrkvan, T.; Etrych, T.; Chytil, P.; Rossmann, P.; Ibrahimova, M.; Kovar, L.; Ulbrich, K.; Rihova, B. Preclinical Evaluation of Linear HPMA-Doxorubicin Conjugates with pH-Sensitive Drug Release: Efficacy, Safety, and Immunomodulating Activity in Murine Model. *Pharm. Res.* **2010***, 27*, 200-208.

6. Xiao, N.; Liang, H.; Lu, J. Degradable and biocompatible aldehyde-functionalized glycopolymer conjugated with doxorubicinvia acid-labile Schiff base linkage for pH-triggered drug release. *Soft Matter* **2011***, 7*, 10834-10840.

7. Saito, H.; Hoffman, A. S.; Ogawa, H. I. Delivery of Doxorubicin from Biodegradable PEG Hydrogels Having Schiff Base Linkages. *J. Bioact. Compat. Polym.* **2007***, 22*, 589-601.

8. Yu, J.; Ha, W.; Chen, J.; Shi, Y. pH-Responsive supramolecular hydrogels for codelivery of hydrophobic and hydrophilic anticancer drugs. *RSC Adv.* **2014***, 4*, 58982-58989.

9. Pashley, R.; Karaman, M. *Applied Colloid and Surface Chemistry;* John Wiley & Sons: England, 2005.

10. Tucker, R.; Parcher, B.; Jones, E.; Desai, T. Single-Injection HPLC Method for Rapid Analysis of a Combination Drug Delivery System. *AAPS PharmSciTech* **2012***, 13*, 605-610.

11. Zattoni, A.; Roda, B.; Borghi, F.; Marassi, V.; Reschiglian, P. Flow field-flow fractionation for the analysis of nanoparticles used in drug delivery. *J. Pharm. Biomed. Anal.* **2014***, 87*, 53-61.

12. Zambito, Y.; Pedreschi, E.; Di Colo, G. Is dialysis a reliable method for studying drug release from nanoparticulate systems?—A case study. *Int. J. Pharm.* **2012***, 434*, 28-34.

13. Modi, S.; Anderson, B. D. Determination of Drug Release Kinetics from Nanoparticles: Overcoming Pitfalls of the Dynamic Dialysis Method. *Mol. Pharmaceutics* **2013***, 10*, 3076-3089.

14. Shuai, X.; Merdan, T.; Schaper, A. K.; Xi, F.; Kissel, T. Core-cross-linked polymeric micelles as paclitaxel carriers. *Bioconjug. Chem.* **2004***, 15*, 441-448.

15. Xu, P.; Tang, H.; Li, S.; Ren, J.; Van Kirk, E.; Murdoch, W. J.; Radosz, M.; Shen, Y. Enhanced stability of core-surface cross-linked micelles fabricated from amphiphilic brush copolymers. *Biomacromolecules* **2004***, 5*, 1736-1744.

16. Wu, Y.; Chen, W.; Meng, F.; Wang, Z.; Cheng, R.; Deng, C.; Liu, H.; Zhong, Z. Core-crosslinked pH-sensitive degradable micelles: A promising approach to resolve the extracellular stability versus intracellular drug release dilemma. *J. Control. Release* **2012***, 164*, 338-345.

CHAPTER 10

Epilogue

10.1) Thesis Synopsis

The RAFT-mediated controlled radical polymerization of NVP, using *O*-ethyl-*S*-(phthalimidylmethyl)xanthate (XA2) as the chain transfer agent, was demonstrated to suffer from slow pre-equilibrium phase kinetics as the phthalimidylmethyl radical was less stable than the propagating radical. The probability of radical transfer from a propagating radical to the phthalimidylmethyl leaving group at a given time during the polymerization was demonstrated to increase with a decrease in the ratio of monomer to RAFT agent. The optimization of this transfer probability was achieved by designing a semi-batch process for the RAFT polymerization of NVP with XA2. This semi-batch process ensured the ratio of monomer to RAFT agent was as low as possible while the pre-equilibrium phase was still active, taking into account the increase in reaction time as well as initiator-derived and terminated polymer chains. By this process, the effects of the poor pre-equilibrium phase kinetics were mitigated and an improvement in the main equilibrium phase kinetics was also noted.

A primary amine end-group functional PVP was prepared by reacting the phthalimide end-group with hydrazine in methanol. The xanthate end-group had to be removed beforehand to avoid its aminolysis. It was converted to an alkene end-group by thermolysis under vacuum. It was found that both the xanthate as well as the alkene end-groups were susceptible to hydrolysis in dilute acid solutions at ambient temperatures. Both formed an *N*-(1-hydroxyalkyl)amide end-group that would eliminate pyrrolidone at elevated temperatures and form an aldehyde end-group. The simultaneous removal of the xanthate and phthalimide end-groups was achieved by a three stage one-pot process. It involved the hydrolysis of the xanthate end-group to an aldehyde, reduction of the aldehyde end-group to a primary alcohol with the simultaneous reduction of the phthalimide end-group to a 2-(hydroxymethyl)benzamide and the acid hydrolysis of the benzamide to a primary amine.

The amine-functionalized PVP was used as a macroinitiator for the ROP of N^{ε}-(CBZ)-L-lys NCA to form a PVP-*block*-poly(N^{ε}-(CBZ)-L-lys) block copolymer. The CBZ protecting group was removed by acidolysis with HBr in a 1,4-dioxane and DCM solvent mixture at 0 °C. Hydrogenation over a palladium catalyst proved promising as a milder alternative deprotection protocol but removal of

the catalyst after the reaction proved to be extremely difficult due to the stabilizing adsorption of PVP to the palladium nanoparticle surface.

The conjugation of Doxorubicin as well as benzaldehyde to the lysine residues via imine linkages was achieved in methanol and these conjugates were shown to self-assemble into micelles when dispersed in H_2O. The Doxorubicin conjugates were quite unstable in aqueous solution at ambient temperatures while the benzaldehyde conjugates appeared to be relatively stable.

10.2) Implications of the Research

The improvement in the probability of radical transfer, when RAFT-mediated polymerization is performed in semi-batch mode, may also be observed for other RAFT agent-monomer systems that suffer from slow pre-equilibrium kinetics. The improvement in the probability of radical transfer between the propagating and dormant polymer chains of different length during the main equilibrium of a RAFT-mediated polymerization may also be observed. However, the degree that this effects the measurable parameters may vary, due to the increase in both initiator-derived and terminated polymer chains, and has yet to be accurately measured for the NVP-XA2 system.

The deprotection of a phthalimide end-group was quantitative when hydrazine in methanol was used. However, hydrazine is extremely toxic and also can act as an initiator for the ROP of NCAs hence needs to be quantitatively removed from the product. This was achieved by extensive dialysis. The deprotection of the phthalimide end-group by reduction and subsequent hydrolysis proved to be quantitative and avoided the introduction of toxic or potentially interfering compounds, making product isolation less stringent.

While the PVP-block-poly(L-lysine)-Doxorubicin conjugates were not sufficiently stable on their own, the observed stability of the PVP-block-poly(L-lysine)-benzaldehyde conjugates may be induced in the former by preparing a formulation of Doxorubicin and benzaldehyde with PVP-*block*-poly(L-lysine). The benzaldehyde would also modulate the size of the hydrophobic block and prevent the oligomerization of Doxorubicin. Cross-linking agents, such as terephthalaldehyde, may also be incorporated into the formulation to further improve micelle stability.

If a formulation of Doxorubicin with benzaldehyde and PVP-*block*-poly(L-lysine) proves to be sufficiently stable under the physiological conditions of blood plasma, the formulation can be transformed or enhanced through the substitution or addition of other chemotherapy drugs, such as

Paclitaxel or Rapamycin, to the conjugate. The only limitation for such changes is that the new drugs must contain an aldehyde or ketone functional group.

10.3) Future Research and Developments

In order to ensure that the proposed drug-delivery system is considered for clinical trials, regardless of its efficacy, it needs to be composed entirely of biodegradable or excretable components. While the peptide block is biodegradable and should not pose a problem, the PVP block is not and thus needs to be below the renal excretion threshold. The PVP block cannot be too short either as this would affect the critical packing parameter for micelle morphology. Thus the lengths of the PVP and poly(L-lysine) blocks need to be optimized. The PVP block must be removable from the body via renal excretion while still providing a sufficiently low critical packing parameter for the block copolymer. The poly(L-lysine) block needs to be sufficiently long to induce the desired cell-penetrating property.

The work done so far focused on determining the stability of the imine conjugates in H_2O. The future formulations should have their stability tested under the physiological conditions of blood plasma. Once a sufficiently stable formulation is devised, its dissociation sensitivity at endosomal pH (pH ≈ 4 – 6) needs to be measured and the formulation should then be further optimized to ensure that the dissociation is sufficiently rapid.

Another modification that could be performed to improve the stability of the micelles is to incorporate a ternary block to the block copolymer that is composed of a well-established pH-sensitive polymer. Poly(L-histidine) is one such polypeptide. Since poly(L-histidine) and poly(L-lysine) both have relatively stiff backbones, incorporating a short poly(L-histidine) block between the PVP and poly(L-lysine) blocks should improve the stability of the imine bonds in the core of the micelle as the poly(L-histidine) block would form a shell around the core, preventing direct contact with the aqueous phase. Such a synthesis should be relatively simple since the transition between the histidine block and the lysine block does not need to be discrete. For instance, a gradient copolypeptide could be prepared by initiating the ROP of L-histidine NCAs with an amine end-functional PVP and after a significant NCA conversion is reached, L-lysine NCAs are added. Ideally, the length of the histidine block should be as short as possible to avoid an excessive reduction in the cell-penetrating potential of the poly(L-lysine) block. However, studies accessing the effect of the poly(L-histidine) block length on the cell penetrating potential of the poly(L-lysine) block should be performed to determine the exact effect.

Since the main reason for developing the imine conjugates as drug delivery systems was to incorporate poly(L-lysine) for its cell-penetrating potential, this property needs to be demonstrated for the block copolymer PVP-*block*-poly(L-lysine). If the PVP block prevents the poly(L-lysine) from performing non-classical membrane transport, a labile linker needs to be incorporated between the two blocks. Since the cell penetrating peptide should only be active within a tumor, an acid-labile linker should be used. One such linker is the acyl hydrazone bond that was discussed in Chapter 9. A theoretical method for forming an acyl hydrazone bond between the PVP and poly(L-lysine) blocks was devised and is illustrated in Scheme 10.1.

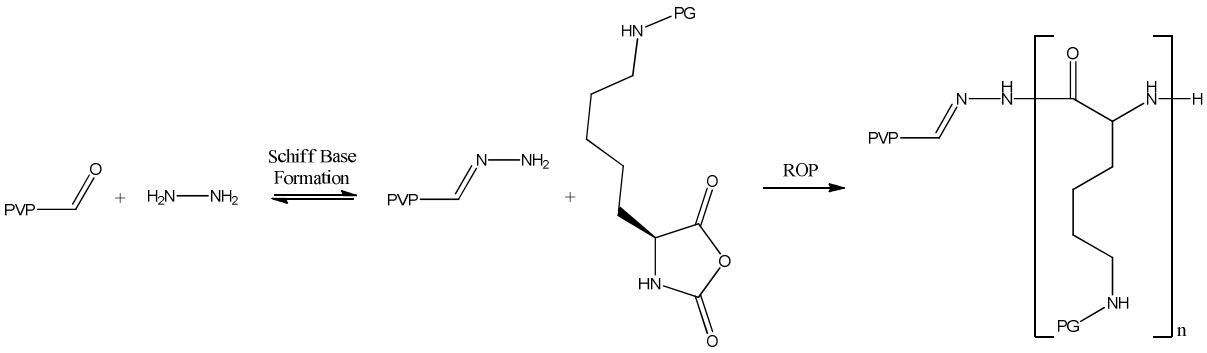

Scheme 10.1: Preparation of PVP-*block*-poly(L-lysine) with an Acyl Hydrazone Bond Between the two Blocks.

This method involves the formation of a Schiff base between hydrazine and an aldehyde end-functional PVP, under conditions that ensure minimal cross-linking occurs. This hydrazone end-functional PVP would then be used as a macroinitiator for the ROP of L-lysine NCAs. Since the hydrazone bond is acid-labile, an orthogonal protecting group, such as the 9-fluorenylmethyloxycarbonyl protecting group. No literature on such an initiator for NCAs has been found hence model studies should be performed to ensure such a reaction is possible.

The ability of poly(L-lysine) to improve the uptake of chemotherapy drugs within various cancer cells, including multi-drug resistant ones, via the reversible imine bonds should also be investigated. Even though the imine bonds should be unstable in acidic media, their formation and dissociation is reversible and is most rapid at pH = 5 – 6. Hence there should be a certain fraction of drugs that are conjugated to the poly(L-lysine) block as it passes through a cell membrane. This type of transport needs to be demonstrated. Any inherent chemotherapeutic effects of poly(L-lysine) also needs to be measured.

Appendices

A1) Conversion of SEC Traces to Molecular Weight Distributions

A linear calibration curve was used for the SEC analysis with the following general form:

$$\log(MW)_{PMMA} = a_c + b_c V_e \quad \text{(A1.1)}$$

Where

MW = Molecular weight as a function of elution volume

PMMA = Poly(methyl methacrylate)

V_e = Elution volume in mL

a_c and b_c are the calibration constants.

After linear baseline correction, the DRI signal was normalized according to Equation A1.2.

$$Norm_i = \frac{n_i}{\sum W_i n_i} \quad \text{(A1.2)}$$

Where

n_i = Baseline-corrected DRI signal at ith data point

W_i = Weight of the ith data point = $\frac{MW_i - MW_{i+1}}{111.14 g/mol}$

MW_i = Molecular weight corresponding with ith elution volume

111.14 g/mol = molar mass of the repeating unit for PVP

Weighting $Norm_i$ was performed to take into account the discrete distribution of possible molecular weights as well as to account for the biased sampling of the data points, as depicted in Equation A1.3.

$$N_i = Norm_i \times W_i \quad \text{(A1.3)}$$

M_n, M_w and $Đ$ were then calculated using Equations A1.4, A1.5 and A1.6 respectively.

$$M_n = \frac{\sum MW_i N_i}{\sum N_i} \quad \text{(A1.4)}$$

$$M_w = \frac{\sum (MW_i)^2 N_i}{\sum MW_i N_i} \quad \text{(A1.5)}$$

$$Đ = \frac{M_w}{M_n} \quad \text{(A1.6)}$$

For the analysis of copolymers, W_i could not be determined without knowledge of the number of polymer chains between each data point. Hence, the data was treated as a continuous distribution.

n_i was normalized by computing the integral between each adjacent data pair numerically, using the Trapezoidal rule, and adding them up:

$$\int_{i+1}^{i} ndMW \approx \frac{(MW_i - MW_{i+1})(n_i + n_{i+1})}{2} \quad \text{(A1.7)}$$

$$\int_{i=n}^{0} ndMW \approx \sum \int_{i+1}^{i} ndMW \quad \text{(A1.8)}$$

$$N_i = \frac{n_i}{\int_{i=n}^{0} ndMW} \quad \text{(A1.9)}$$

M_n, M_w and $Đ$ were then calculated using Equations A1.10, A1.11 and A1.12 respectively.

$$M_n = \sum \int_{i+1}^{i} MW_i N_i \, dMW \quad \text{(A1.10)}$$

$$M_W = \frac{\sum \int_{i+1}^{i} (MW_i)^2 N_i dMW}{\sum \int_{i+1}^{i} MW_i N_i dMW} \quad \text{(A1.11)}$$

$$Đ = \frac{M_w}{M_n} \quad \text{(A1.12)}$$

A2) Least Squares Approximation of Kinetic Data

A2.1) Kinetic Data from Section 3.2.4

$$[NVP] = 2.6518e^{\left(-\frac{t}{7819.3595}\right)} + 0.3861 \quad \text{(A2.1)}$$

$$[XA2] = 0.3627e^{\left(-\frac{t}{3449.6420}\right)} + 0.1362e^{\left(-\frac{t}{13175.5702}\right)} + 0.1377 \quad \text{(A2.2)}$$

The first derivatives for [NVP] and [XA2] were calculated from Equations A2.1 and A2.2:

$$\frac{d[NVP]}{dt} = (-3.3914 \times 10^{-4})e^{-1.2789\times10^{-4}t} \quad \text{(A2.3)}$$

$$\frac{d[XA2]}{dt} = (-1.0515 \times 10^{-4})e^{-2.8989\times10^{-4}t} - (1.0340 \times 10^{-5})e^{-7.5898\times10^{-5}t} \quad \text{(A2.4)}$$

A2.2) Kinetic Data from Sections 3.2.2 and 3.2.3

$$[NVP]_{R=117} = 9.0182e^{\left(-\frac{t}{11982.3890}\right)} - 0.0379 \quad \text{(A2.5)}$$

$$[XA2]_{R=117} = 0.0456e^{\left(-\frac{t}{6207.9710}\right)} + 4.4536 \times 10^{-4} \quad \text{(A2.6)}$$

$$[NVP]_{R=196} = 7.7998e^{\left(-\frac{t}{17935.3834}\right)} + 1.2546 \quad \text{(A2.7)}$$

$$[XA2]_{R=196} = 0.0456e^{\left(-\frac{t}{6207.9710}\right)} - 1.1693 \times 10^{-3} \quad \text{(A2.8)}$$

A2.3) Comparison of P(T) for XA2 with that for *O*-ethyl-*S*-(cyanoisopropyl)xanthate

The following least squares approximations were made, using the data provided by Pound *et al.*,[1] for the RAFT-mediated polymerization of NVP with *O*-ethyl-*S*-(cyanoisopropyl)xanthate (X1).

$$[NVP]_{X1,R=6} = 0.8420e^{\left(-\frac{t}{28241.6450}\right)} + 1.3057 \quad \text{(A2.9)}$$

$$[X1]_{X1,R=6} = 1.3355e^{\left(-\frac{t}{47706.5515}\right)} - 0.9378 \quad \text{(A2.10)}$$

A3) Calculating [M] for a Continuous Semi-Batch Process (CSB)

The rate of initiator decomposition is described by the rate law:

$$-\frac{d[I]}{dt} = k_d[I] \quad \text{(A3.1)}$$

Where

$[I]$ = concentration of initiator (mol.dm^{-3})

k_d = rate constant for initiator decomposition (s^{-1})

t = reaction time (s)

The analytical solution is found by the separation of variables technique:

$$\frac{d[I]}{[I]} = -k_d dt \quad \text{(A3.2)}$$

$$[I]_t = [I]_0 e^{(-k_d t)} \quad \text{(A3.3)}$$

Since this is a unimolecular decomposition:

$$I_t = I_0 e^{(-k_d t)} \quad \text{(A3.4)}$$

Where

I = No. of mols of initiator

The rate of initiator-derived radical formation is given by the rate law:

$$-\frac{d[I^\bullet]}{dt} = 2fk_d[I] \quad \text{(A3.5)}$$

Where

$[I^\bullet]$ = concentration of initiator-derived radicals (mol.dm^{-3})

f = efficiency factor for the initiator in the specific reaction mixture

The rate of initiation in the absence of alternative radical reaction pathways and in the presence of a large excess of monomer can be considered as:

$$R_i = -\frac{d[I^\bullet]}{dt} = 2fk_d[I] \quad \text{(A3.6)}$$

Where

R_i = rate of initiation (mol.dm^{-3}.s^{-1})

The rate of termination is described by the rate law:

$$R_t = \sum_i \sum_j 2k_t^{i,j} [P_i^\bullet][P_j^\bullet] \quad \text{(A3.7)}$$

Where

R_t = rate of termination of propagating radicals (mol.dm^{-3}.s^{-1})

$k_t^{i,j}$ = rate constant for the termination of propagating chains of length i with chains of length j (dm^3.mol^{-1}.s^{-1})

The rate law can be simplified as follows:

$$R_t = 2k_t^*[P^\bullet]^2 \quad \text{(A3.8)}$$

Where

k_t^* = IUPAC average termination rate constant (dm^3.mol^{-1}.s^{-1})

$[P^\bullet]$ = concentration of propagating radicals (mol.dm^{-3})

Under the steady state approximation, the rate of initiation is equal to the rate of termination:

$$R_i = R_t$$

$$2fk_d[I] = 2k_t^*[P^\bullet]^2 \quad \text{(A3.9)}$$

Since the volume of the reaction mixture does not influence the number of initiator molecules which undergo homolytic scission, equation A3.9 can be rewritten as:

$$[P^{\bullet}]_t = \sqrt{\frac{fk_d[I]_t}{k_t^*}} = \sqrt{\frac{fk_d I_0 e^{(-k_d t)}}{k_t^* V}} \quad \text{(A3.10)}$$

Where

V = Volume of reaction mixture (dm^3)

The rate of propagation is described by the rate law:

$$-\frac{d[M]}{dt} = \sum_i k_p^i [P_i^{\bullet}][M] \quad \text{(A3.11)}$$

Where

k_p^i = rate constant for propagation of chains with length i ($dm^3.mol^{-1}.s^{-1}$)

Under a similar analogy to that for the termination rate constant, the rate law can be simplified to Equation A3.12.

$$-\frac{d[M]}{dt} = k_p[P^{\bullet}][M] \quad \text{(A3.12)}$$

$$= k_p[M]\sqrt{\frac{fk_d I_0 e^{(-k_d t)}}{k_t^* V}} \quad \text{(A3.13)}$$

Where

k_p = average propagation rate constant ($dm^3.mol^{-1}.s^{-1}$)

In a semi-batch reactor, the change in concentration of monomer with respect to time can be described as follows:

$$\frac{d[M]}{dt} = \frac{d}{dt}\left(\frac{M_0+M_r}{V}\right) + \frac{1}{V}\frac{dM_f}{dt} = \frac{d}{dt}\left(\frac{M_0}{V}\right) + \frac{d}{dt}\left(\frac{M_r}{V}\right) + \frac{1}{V}\frac{dM_f}{dt} \quad \text{(A3.14)}$$

Where

M_0 = initial amount of monomer in the reactor (mol)

M_f = total amount of monomer fed into reactor from t_0 until t (mol)

M_r = monomer which has been converted to polymer (mol)

The first term describes the dilution of initial monomer molecules as the volume of the reaction mixture is increased.

$$\frac{d}{dt}\left(\frac{M_0}{V}\right) = -\frac{M_0}{V^2}\frac{dV}{dt} \tag{A3.15}$$

The second term describes the change in concentration of the monomer due to propagation (the change in monomer concentration due to initiation being considered negligible).

$$\frac{d}{dt}\left(\frac{M_r}{V}\right) = -k_p[M]\sqrt{\frac{fk_dI_0e^{(-k_dt)}}{k_t^*V}} \tag{A3.16}$$

The third term describes the change in concentration of monomer in the reaction mixture due to the monomer feed. The amount of monomer fed into the reactor from t_0 until t is given by Equation A3.17.

$$M_f = C_m v \tag{A3.17}$$

Where

C_m = Concentration of monomer in the feed (mol.dm^{-3})

v = total volume of monomer feed added to the reactor from t_0 until t (dm^3)

the rate at which monomer is fed into the reactor is given by Equation A3.18.

$$\frac{dM_f}{dt} = C_m\frac{dv}{dt} \tag{A3.18}$$

Substituting Equations A3.15, A3.16 and A3.18 into Equation A3.14 provides a complete explicit differential equation for the monomer concentration.

$$\frac{d[M]}{dt} = -\frac{M_0}{(V)^2}\frac{dV}{dt} + \frac{C_m}{V}\frac{dv}{dt} - k_p[M]\sqrt{\frac{fk_dI_0e^{(-k_dt)}}{k_t^*V}} \quad \text{(A3.19)}$$

Since $V = V_0 + v$

$$\frac{dV}{dt} = \frac{dv}{dt} \quad \text{(A3.20)}$$

Hence

$$\frac{d[M]}{dt} = -\frac{M_0}{(V_0+v)^2}\frac{dv}{dt} + \frac{C_m}{(V_0+v)}\frac{dv}{dt} - k_p[M]\sqrt{\frac{fk_dI_0e^{(-k_dt)}}{k_t^*(V_0+v)}} \quad \text{(A3.21)}$$

This is a non-linear first-order ordinary differential equation of three functions ($[\mathrm{M}](\mathrm{t})$, $C_m(t)$ and $v(t)$) of one variable (t). Hence two more equations are required to be able to simultaneously solve the system of differential equations. For instance, if the monomer concentrations in the reactor and the monomer feed are kept constant from t_0 to t, then the rate of monomer addition to the semi-batch reactor can be computed from Equation A3.22.

$$-\frac{M_0}{(V_0+v)^2}\frac{dv}{dt} + \frac{C_m}{(V_0+v)}\frac{dv}{dt} - k_pC\sqrt{\frac{fk_dI_0e^{(-k_dt)}}{k_t^*(V_0+v)}} = 0 \quad \text{(A3.22)}$$

Where

C = the constant concentration of monomer in the reaction mixture (mol.dm^{-3})

Equation A3.23 expresses Equation A3.22 explicitly with respect to $\frac{dv}{dt}$.

$$\frac{dv}{dt} = \frac{k_pC}{\left(C_m - \frac{M_0}{(V_0+v)}\right)}\sqrt{\frac{fk_dI_0e^{(-k_dt)}(V_0+v)}{k_t^*}};\ v(0) = 0 \quad \text{(A3.23)}$$

Equation A3.23 provides the rate at which the monomer feed needs to be added to the reactor during the reaction.

Approximate solutions to the initial value problem can be obtained via numerical methods such as Euler's Method, Predictor-Corrector or Runge-Kutta Methods. This will be useful in order to determine the concentration of the RAFT agent with time. Knowing that would allow us to calculate $M_{n,theory}$.

A4) Calculation of [M] for a Discrete Semi-Batch Process (DSB)

The rate of propagation for the time interval $t_i \leq t < t_{i+1}$ between monomer additions can be described by the kinetic mechanism for a batch process.

$$-\frac{d[M]}{dt} = k_p[M]\sqrt{\frac{fk_dI_ie^{(-k_d(t-t_i))}}{k_t^*V_i}} \quad \text{(A4.1)}$$

Where

I_i = number of moles of initiator in the reaction mixture at time t_i

V_i = Volume of reaction mixture at time t_i (dm^3)

This differential equation can be solved analytically by the separation of variables technique.

$$\frac{d[M]}{[M]} = -k_p\sqrt{\frac{fk_dI_ie^{(-k_d(t-t_i))}}{k_t^*V}}\,dt \quad \text{(A4.2)}$$

$$ln[M] = \frac{2k_p}{k_d}\sqrt{\frac{fk_dI_i}{k_t^*V}}e^{\left(-\frac{k_d(t-t_i)}{2}\right)} + C_{int} \quad \text{(A4.3)}$$

Where

C_{int} = integration constant

At the beginning of each time interval:

$$[M](t) = [M]_i \quad \text{(A4.4)}$$

$$ln[M]_i - \frac{2k_p}{k_d}\sqrt{\frac{fk_dI_i}{k_t^*V}} = C_{int} \quad \text{(A4.5)}$$

Hence the concentration of monomer at any given time during the interval can be determined by the piecewise function in Equation A4.6.

$$ln[M] = \frac{2k_p}{k_d}\sqrt{\frac{fk_dI_i}{k_t^*V}}\left(e^{\left(-\frac{k_d(t-t_i)}{2}\right)} - 1\right) + ln[M]_i \quad for\ t_i \leq t < t_{i+1} \tag{A4.6}$$

A5) Calculating Observed Rate Constants

The parameters calculated for the determination of φ for the polymerization of NVP with XA2 at various monomer to RAFT agent ratios are given in Table A5.1. φ for the trial with R = 5 was computed by computing the slope of each adjacent data pair because although the linear correlation coefficient was 0.976, visual examination of the data (plotted in Figure A5.1.A) indicated that there was a non-linear correlation of the data at high monomer conversions.

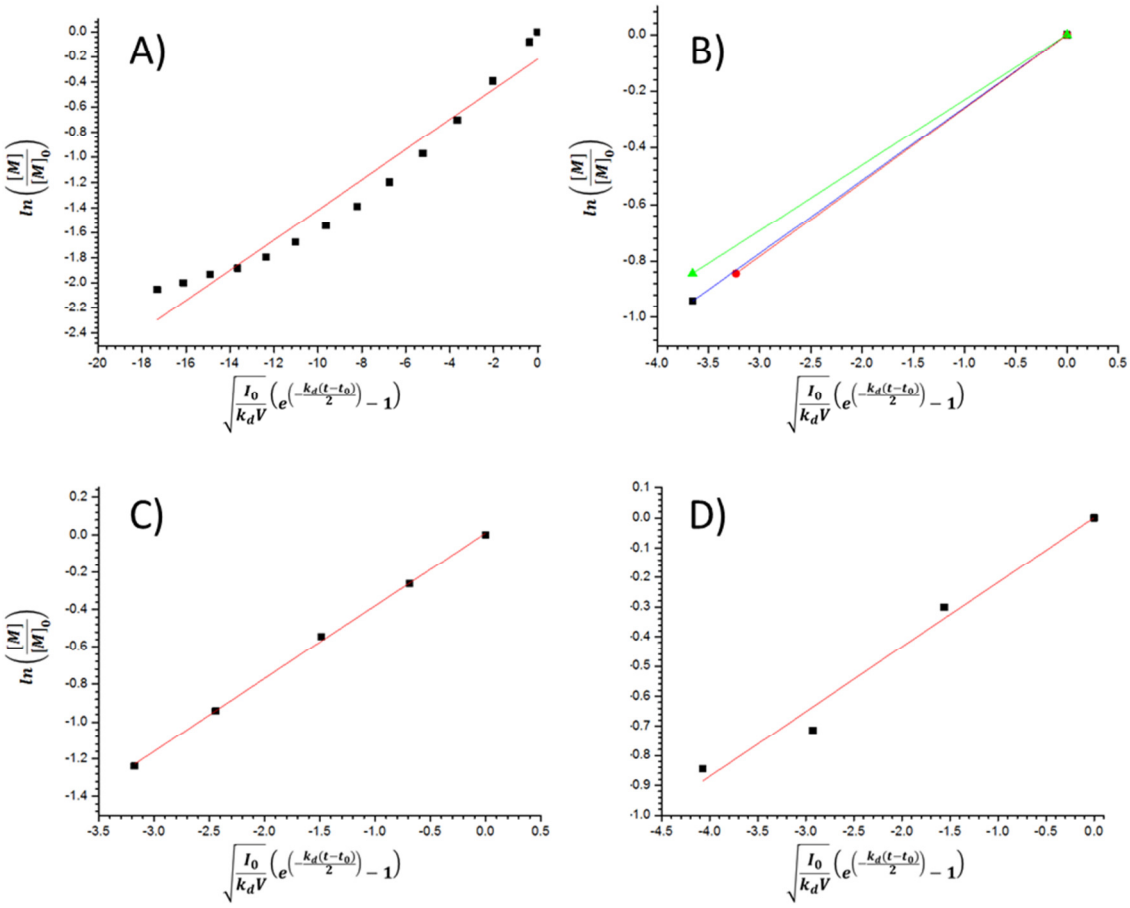

Figure A5.1: Plots of $ln\left(\frac{[M]}{[M]_0}\right)$ versus $\sqrt{\frac{I_0}{k_dV}}\left(e^{\left(-\frac{k_d(t-t_0)}{2}\right)} - 1\right)$ for the Polymerizations Performed in Sections A) 3.2.4, B) 4.5.1, C) 3.2.3 and D) 3.2.2.

Table A5.1: Parameters for the Calculation of φ for the Polymerization of NVP with XA2 at Various Monomer to RAFT Agent Ratios.

$\frac{[M]_0}{[X]_0}$	Time (s)	[M]	I_0 (mol)	V (dm^3)	$ln\left(\frac{[M]}{[M]_0}\right)$	$\sqrt{\frac{I_0}{k_d V}}\left(e^{\left(-\frac{k_d(t-t_0)}{2}\right)}-1\right)$	φ
5	0	3.033	5.48079E-05	0.00089	0	0	N/A
5	664.992	2.80246	5.48079E-05	0.00089	-0.079054626	-0.376796789	0.209807058
5	3664.98	2.04601	5.48079E-05	0.00089	-0.393660674	-2.044316744	0.188667036
5	6665.004	1.49849	5.48079E-05	0.00089	-0.705094294	-3.660147789	0.192738976
5	9664.992	1.14548	5.48079E-05	0.00089	-0.973728466	-5.225854571	0.171573742
5	12664.98	0.91494	5.48079E-05	0.00089	-1.198449018	-6.743010473	0.148119618
5	15665.004	0.75645	5.48079E-05	0.00089	-1.38867107	-8.213138373	0.129391499
5	18664.992	0.64838	5.48079E-05	0.00089	-1.542830563	-9.637661827	0.10821829
5	21665.016	0.56914	5.48079E-05	0.00089	-1.673181058	-11.01802865	0.094431779
5	24665.004	0.5043	5.48079E-05	0.00089	-1.794136179	-12.35557548	0.090430569
5	27664.992	0.46107	5.48079E-05	0.00089	-1.883757632	-13.65164643	0.069148571
5	30665.016	0.43946	5.48079E-05	0.00089	-1.931760807	-14.90754245	0.038222253
5	33665.004	0.41064	5.48079E-05	0.00089	-1.999590589	-16.12447965	0.055738112
5	36664.992	0.38903	5.48079E-05	0.00089	-2.053651046	-17.30368095	0.045844978
20	0	8.033625543	5.48079E-05	0.00112	0	0	N/A
20	7500	3.133113962	5.48079E-05	0.00112	-0.94160854	-3.655655212	0.257575861
20	0	8.033625543	5.48079E-05	0.00112	0	0	N/A
20	6600	3.454458984	5.48079E-05	0.00112	-0.84397007	-3.23202437	0.261127
20	0	8.033625543	5.48079E-05	0.00112	0	0	N/A
20	7500	3.454458984	5.48079E-05	0.00112	-0.84397007	-3.655655212	0.230867
117	0	8.998	2.07052E-05	0.002	0	0	N/A
117	3000	6.92846	2.07052E-05	0.002	-0.261364764	-0.688499111	0.379615253
117	6600	5.21884	2.07052E-05	0.002	-0.544727175	-1.486575066	0.355056946
117	11100	3.50922	2.07052E-05	0.002	-0.94160854	-2.442668663	0.41510723
117	14700	2.60942	2.07052E-05	0.002	-1.237874356	-3.17567458	0.404179297
196	0	8.998	1.82693E-05	0.002	0	0	N/A
196	7400	6.659	1.82693E-05	0.002	-0.301033007	-1.559172272	0.193072
196	14400	4.409	1.82693E-05	0.002	-0.713354424	-2.92663743	0.301522
196	20700	3.869	1.82693E-05	0.002	-0.844006255	-4.074303639	0.113841

A6) Calculating the Feed Times for the CDSB

For the first interval, the time it would take for the reaction to reach 60% monomer conversion can be computed by Equation A5.1.

$$t_1 - t_0 = -\frac{2}{k_d}\ln\left(1 + \ln(0.4)\frac{k_d}{2k_p}\sqrt{\frac{k_t^*}{f k_d [I]_0}}\right) \quad \text{(A5.1)}$$

The following parameters were set:

$$M_0 = [M]_0 V_0 = M_{1i} \quad \text{(No. of moles of monomer at } t = 0\text{)} \tag{A5.2}$$

$$M_1 = [M]_1 V_0 = M_{1f} = 0.4 M_0 \quad \text{(No. of moles of monomer at } t = t_1\text{)} \tag{A5.3}$$

$$M_{add} = [M]_{add} \frac{1}{b} V_0 \text{ (No. of moles of monomer added at the end of each interval)} \tag{A5.4}$$

$$I_0 = I_i \text{ (No. of moles of initiator at the beginning of each interval.)} \tag{A5.5}$$

If the concentration of the monomer solution being added is that of the undiluted monomer and the reaction is done in the absence of solvent:

$$[M]_{add} \approx [M]_0 \tag{A5.6}$$

For the second interval, the concentration of monomer in the reaction mixture after addition of the monomer feed is:

$$[M]_{2i} = \frac{0.4[M]_0 V_0 + \frac{[M]_0 V_0}{b}}{\left(1+\frac{1}{b}\right)V_0} = \frac{\left(0.4+\frac{1}{b}\right)}{\left(1+\frac{1}{b}\right)}[M]_0 \tag{A5.7}$$

Where $\frac{1}{b}$ is the volume fraction of monomer added relative to V_0. The constant b can be considered as the dilution factor for monomer additions during the discrete semi-batch processes.

The concentration of monomer after the second reaction interval is complete will be:

$$[M]_{2f} = 0.4[M]_0 \tag{A5.8}$$

Hence the reaction time for the second interval can be computed by:

$$t_2 - t_1 = -\frac{2}{k_d}\ln\left(1 + \frac{k_d}{2k_p}\sqrt{\frac{k_t^*\left(1+\frac{1}{b}\right)V_0}{f k_d I_0}}\, ln\left(0.4 \div \frac{\left(0.4+\frac{1}{b}\right)}{\left(1+\frac{1}{b}\right)}\right)\right) \tag{A5.9}$$

$$= -\frac{2}{k_d}\ln\left(1 + \frac{k_d}{2k_p}\sqrt{\frac{k_t^*\left(1+\frac{1}{b}\right)V_0}{f k_d I_0}}\, ln\left(\frac{\left(0.4+\frac{2}{5b}\right)}{\left(0.4+\frac{1}{b}\right)}\right)\right) \tag{A5.10}$$

$$= -\frac{2}{k_d}\ln\left(1 + \frac{k_d}{2k_p}\sqrt{\frac{k_t^*\left(1+\frac{1}{b}\right)V_0}{f k_d I_0}}\, ln\left(\frac{\left(1+\frac{1}{b}\right)}{\left(1+\frac{5}{2b}\right)}\right)\right) \tag{A5.11}$$

For the third interval:

$$[M]_{3i} = \frac{0.4[M]_0\left(1+\frac{1}{b}\right)V_0+\frac{[M]_0V_0}{b}}{\left(1+\frac{2}{b}\right)V_0} = \frac{\left(0.4\left(1+\frac{1}{b}\right)+\frac{1}{b}\right)}{\left(1+\frac{2}{b}\right)}[M]_0 = \frac{\left(0.4\left(1+\frac{7}{2b}\right)\right)}{\left(1+\frac{2}{b}\right)}[M]_0 \quad \text{(A5.12)}$$

$$[M]_{3f} = 0.4[M]_0 \quad \text{(A5.13)}$$

$$t_2 - t_1 = -\frac{2}{k_d}\ln\left(1 + \frac{k_d}{2k_p}\sqrt{\frac{k_t^*\left(1+\frac{2}{b}\right)V_0}{fk_dI_0}}\,ln\left(0.4 \div \frac{\left(0.4\left(1+\frac{7}{2b}\right)\right)}{\left(1+\frac{2}{b}\right)}\right)\right) \quad \text{(A5.14)}$$

$$= -\frac{2}{k_d}\ln\left(1 + \frac{k_d}{2k_p}\sqrt{\frac{k_t^*\left(1+\frac{2}{b}\right)V_0}{fk_dI_0}}\,ln\left(\frac{\left(1+\frac{2}{b}\right)}{\left(1+\frac{7}{2b}\right)}\right)\right) \quad \text{(A5.15)}$$

Suppose that for a certain reaction interval $t_{k+1} - t_k$:

$$t_{k+1} - t_k = -\frac{2}{k_d}\ln\left(1 + \frac{k_d}{2k_p}\sqrt{\frac{k_t^*\left(1+\frac{k}{b}\right)V_0}{fk_dI_0}}\,ln\left(\frac{\left(1+\frac{k}{b}\right)}{\left(1+\frac{3+2k}{2b}\right)}\right)\right) \quad \text{(A5.16)}$$

Then for the interval $t_{k+2} - t_{k+1}$:

$$[M]_{(k+1)i} = \frac{0.4[M]_0\left(1+\frac{k}{b}\right)V_0+\frac{[M]_0V_0}{b}}{\left(1+\frac{k}{b}\right)V_0+\frac{1}{b}V_0} = \frac{\left(0.4\left(1+\frac{k}{b}\right)+\frac{1}{b}\right)}{\left(1+\frac{k+1}{b}\right)}[M]_0 = \frac{\left(0.4\left(1+\frac{2k+5}{2b}\right)\right)}{\left(1+\frac{k+1}{b}\right)}[M]_0 = \frac{\left(0.4\left(1+\frac{2(k+1)+3}{2b}\right)\right)}{\left(1+\frac{k+1}{b}\right)}[M]_0 \quad \text{(A5.17)}$$

$$[M]_{(k+1)f} = 0.4[M]_0 \quad \text{(A5.18)}$$

$$t_{k+2} - t_{k+1} = -\frac{2}{k_d}\ln\left(1 + \frac{k_d}{2k_p}\sqrt{\frac{k_t^*\left(1+\frac{k}{b}\right)V_0}{fk_dI_0}}\,ln\left(0.4 \div \frac{\left(0.4\left(1+\frac{2(k+1)+3}{2b}\right)\right)}{\left(1+\frac{k+1}{b}\right)}\right)\right) \quad \text{(A5.19)}$$

$$= -\frac{2}{k_d}\ln\left(1 + \frac{k_d}{2k_p}\sqrt{\frac{k_t^*\left(1+\frac{k+1}{b}\right)V_0}{fk_dI_0}}\,ln\left(\frac{\left(1+\frac{k+1}{b}\right)}{1+\frac{3+2(k+1)}{2b}}\right)\right) \quad \text{(A5.20)}$$

Thus, by mathematical induction:

$$t_{i+1} - t_i = -\frac{2}{k_d}\ln\left(1 + \frac{k_d}{2k_p}\sqrt{\frac{k_t^*\left(1+\frac{i}{b}\right)V_0}{fk_dI_0}}\,ln\left(\frac{\left(1+\frac{i}{b}\right)}{\left(1+\frac{3+2i}{2b}\right)}\right)\right) \quad \text{(A5.21)}$$

A7) Calculating the Reaction Time as well as χ for R-group and Xanthate-Functionalized Chains for the CDSB

Considering Equation A3.4, the number of initiator-derived propagating radicals that are formed from t_i to t_{i+1} (N_{Ii}) can be calculated by equation A6.1.

$$N_{Ii} = 2fI_i(1 - e^{(-k_d(t_{i+1}-t_i)})) \quad \text{(A7.1)}$$

The fraction of ω-xanthate functionalized chain ends can be computed as follows:

Termination by combination is described by the rate law in Equation A3.8. By the steady-state approximation, $[P^\bullet]_t$ can be calculated using Equation A3.10.

Since every pair of radicals which undergo termination by combination form one terminated polymer chain, the formation of terminated polymer chains can be described as follows:

$$\frac{d[PT]}{dt} = -0.5\frac{d[P^\bullet]_{ter}}{dt} = 0.5 \times 2k_t^*[P^\bullet]^2 \quad \text{(A7.2)}$$

$$[PT] = k_t^* \int_{t_0}^{t} \frac{fk_dI_0e^{(-k_dt)}}{k_t^*V} dt \quad \text{(A7.3)}$$

$$= \frac{fk_dI_0}{V} \int_{t_0}^{t} e^{(-k_dt)} dt \quad \text{(A7.4)}$$

$$= -\frac{fI_0}{V}(e^{(-k_dt)} - e^{(-k_dt_0)}) \quad \text{(A7.5)}$$

$$PT = -fI_0(e^{(-k_dt)} - e^{(-k_dt_0)}) \quad \text{(A7.6)}$$

Thus the number of terminated chains that form during the interval $t_{i+1} - t_i$ is:

$$PT_i = fI_0(1 - e^{(-k_d(t_{i+1}-t_i))}) \quad \text{(A7.7)}$$

The fraction of dormant chains after n intervals can be computed by:

$$\chi_{\omega_X} = \frac{X_0}{(\sum_{i=0}^{n} PT_i)+X_0} \quad \text{(A7.8)}$$

Where

PT_i = the number of terminated chains formed during interval i

A8) Calculating the Reaction Time as well as χ for R-group and Xanthate-Functionalized Chains for the SDSB

The first interval was kept identical to the CDSB. The initial rate of dilution will also be the same. Hence, the change in [M] is:

$$[M]_{2i} = \frac{0.4[M]_0V_0+[M]_0V_0}{V_0+V_0} = \frac{1.4}{2}[M]_0 = 0.7[M]_0 \quad \text{(A8.1)}$$

This translates to a decrease in the monomer conversion from 60% to 30%. Thus $\frac{[M]_{2f}}{[M]_{2i}}$ for the second interval will be:

$$\frac{[M]_{2f}}{[M]_{2i}} = \frac{0.4[M]_0}{0.7[M]_0} = 0.5714 \quad \text{(A8.2)}$$

For the third interval, $\frac{[M]_{3f}}{[M]_{3i}}$ will be the same as for the second interval. Hence, the amount of monomer needed to make $[M]_{3i} = 0.7[M]_0$ can be calculated as follows:

$$0.7[M]_0 = \frac{0.4[M]_0\times 2V_0+x[M]_0}{2V_0+x} \quad \text{(A8.3)}$$

$$0.7[M]_0(2V_0 + x) - 0.4[M]_0 \times 2V_0 = x[M]_0 \quad \text{(A8.4)}$$

$$0.6[M]_0V_0 = 0.3x[M]_0 \quad \text{(A8.5)}$$

$$x = 2V_0 \quad \text{(A8.6)}$$

It would seem that the volume added at the end of each interval is twice that which was added at the end of the previous interval. To prove this, suppose the following relation is true:

$$x_i = 2x_{i-1} \quad \text{(A8.7)}$$

Then for interval i:

$$0.7[M]_0 = \frac{0.4[M]_0\times V_{i-1}+x_i[M]_0}{V_{i-1}+x_i} \quad \text{(A8.8)}$$

$$0.7[M]_0(V_{i-1} + x_i) - 0.4[M]_0 \times V_{i-1} = x_i[M]_0 \quad \text{(A8.9)}$$

$$0.3[M]_0V_{i-1} = 0.3x_i[M]_0 \quad \text{(A8.10)}$$

$$0.3[M]_0V_{i-1} = 0.3x_i[M]_0 \quad \text{(A8.11)}$$

$$x_i = V_{i-1} \quad \text{(A8.12)}$$

For interval $i+1$

$$0.7[M]_0 = \frac{0.4[M]_0\times(2V_{i-1})+x_{i+1}[M]_0}{2V_{i-1}+x_{i+1}} \quad \text{(A8.13)}$$

$$0.7[M]_0(2V_{i-1} + x_{i+1}) - 0.4[M]_0 \times (2V_{i-1}) = x_{i+1}[M]_0 \quad \text{(A8.14)}$$

$$0.6[M]_0V_{i-1} = 0.3x_{i+1}[M]_0 \quad \text{(A8.15)}$$

$$x_{i+1} = 2V_{i-1} = 2x_i \quad \text{(A8.16)}$$

Thus, by mathematical induction:

$$x_{i+1} = 2x_i \quad \forall\, i > 1, i \in \mathbb{N} \quad (x_0 = 0, x_1 = V_0) \quad \text{(A8.17)}$$

The length of each reaction interval after the first can be determined by:

$$t_{i+1} - t_i = -\frac{2}{k_d} ln\left(1 + \frac{1}{\varphi}\sqrt{\frac{k_dV_i}{I_0}} ln(0.5714)\right) \quad \text{(A8.18)}$$

Where

$$V_i = V_0 + \sum_{n=0}^{i} x_n \quad \text{(A8.19)}$$

A9) Calculating the Reaction Time as well as χ for R-group and Xanthate-Functionalized Chains for the s-CSB

The rate of formation of initiator-derived chain ends NI can be computed by solving the equation:

$$-\frac{dNI}{dt} = 2fk_dI_0 \quad \text{(A9.1)}$$

$$NI(t) = 2fk_dI_0(t + t_0) \quad \text{(A9.2)}$$

χ_{α_R} can be calculated by:

$$\chi_{\alpha_R} = \frac{X_0}{X_0+2fk_dI_0(t_0+t)} \quad \text{(A9.3)}$$

The number of radicals at any time during the reaction can be computed by:

$$[P^{\bullet}]_t = \sqrt{\frac{fk_dI_0}{k_t^*(V_0+v)}} \quad \text{(A9.4)}$$

Thus

$$\frac{dPT}{dt} = (V_0 + v) \times k_t^* \left(\sqrt{\frac{fk_dI_0}{k_t^*(V_0+v)}}\right)^2 = fk_dI_0 \quad \text{(A9.5)}$$

Thus

$$PT = fk_dI_0(t + t_0) \quad \text{(A9.6)}$$

χ_{ω_X} can be calculated by Equation A9.7.

$$\chi_{\omega_X} = \frac{X_0}{X_0+fk_dI_0(t_0+t)} \quad \text{(A9.7)}$$

A10) Determining the Amount of Diethyl Ether in a Polymer Sample with a Known $M_{n,NMR}$

The difference in the amount of residual diethyl ether absorbed in two PVP samples that were derived from the same polymer but were isolated independantly can be accounted for by using the relation shown in Equation A10.1. This is especially useful if there is no longer a detectable end-group to use as an internal reference for one of the samples and the backbone resonance at δ = 2.9 – 4.2 ppm needs to be used.

$$\int_{\delta=2.9}^{\delta=4.2} f_1(\delta)d\delta - \frac{2}{3}\int_{\delta=1.15}^{\delta=1.25} f_1(\delta)d\delta = \int_{\delta=2.9}^{\delta=4.2} f_2(\delta)d\delta - \frac{2}{3}\int_{\delta=1.15}^{\delta=1.25} f_2(\delta)d\delta \quad \text{(A10.1)}$$

Where

$f_1(\delta)$ = the ^{1}H-NMR spectrum of the PVP sample that has a detectable end-group.

$f_2(\delta)$ = the ^{1}H-NMR spectrum of the PVP sample without a detectable end-group.

To normalize the ^{1}H-NMR spectrum obtained for the sample prepared in Section 5.2.4 with respect to number of PVP chains for the sample prepared in Section 5.2.1, the left-hand side (LHS) of Equation A10.1 was computed and found to be equal to 377.46. Hence, Equation A10.1 can be reduced to Equation A10.2.

$$\int_{\delta=2.9}^{\delta=4.2} f_2(\delta)d\delta = \frac{2}{3}\int_{\delta=1.15}^{\delta=1.25} f_2(\delta)d\delta + 377.46 \quad \text{(A10.2)}$$

A numerical iterative procedure was performed to approximate this integral. The first data set in the iteration is given below.

$$\left(\int_{\delta=2.9}^{\delta=4.2} f_2(\delta)d\delta\right)_1 = \int_{\delta=2.9}^{\delta=4.2} f_1(\delta)d\delta = 398.16$$

$$\left(\int_{\delta=1.15}^{\delta=1.25} f_2(\delta)d\delta\right)_0 = \int_{\delta=1.15}^{\delta=1.25} f_1(\delta)d\delta = 31.04$$

This approximation assumes that the amount of diethyl ether in both cases was the same. The integral for the methyl protons of diethyl ether at the first normalization iteration was measured and the difference between the initial assumption and the first iteration was computed.

$$\left(\int_{\delta=1.15}^{\delta=1.25} f_2(\delta)d\delta\right)_1 = 24.6$$

$$\left(\int_{\delta=1.15}^{\delta=1.25} f_2(\delta)d\delta\right)_1 - \left(\int_{\delta=1.15}^{\delta=1.25} f_2(\delta)d\delta\right)_0 = -6.44 = \varepsilon_1$$

$\varepsilon < 0$ Indicates that there was less residual diethyl ether in the PVP sample that was being normalized than in the PVP sample with a detectable end-group.

The iteration was repeated until it converged to a value for ε that was lower than the precision of the NMR data. The procedure is given below.

$$\left(\int_{\delta=2.9}^{\delta=4.2} f_2(\delta)d\delta\right)_{n+1} = \left(\int_{\delta=2.9}^{\delta=4.2} f_2(\delta)d\delta\right)_n + \frac{2}{3} \times \varepsilon_n$$

$$\left(\int_{\delta=1.15}^{\delta=1.25} f_2(\delta)d\delta\right)_{n+1} \; is\; measured$$

$$\varepsilon_{n+1} = \left(\int_{\delta=1.15}^{\delta=1.25} f_2(\delta)d\delta\right)_{n+1} - \left(\int_{\delta=1.15}^{\delta=1.25} f_2(\delta)d\delta\right)_n$$

The results of the iterations are tabulated in Table A10.1.

Table A10.1: Results of Iterative Procedure for Normalizing the ^{1}H-NMR Spectrum obtained for the sample prepared in Section 5.2.4 with respect to number of PVP chains for the sample prepared in Section 5.2.1.

n	$\left(\int_{\delta=2.9}^{\delta=4.2} f_2(\delta)d\delta\right)_n$	$\left(\int_{\delta=1.15}^{\delta=1.25} f_2(\delta)d\delta\right)_n$	ε_n
0	N/A	31.04	N/A
1	398.16	24.6	-6.44
2	393.87	24.33	-0.27
3	393.69	24.32	-0.01
4	393.68	24.32	0.00

A11) Normalizing the NMR Spectrum of the PFBA-Derivatized PVP using the Peak for the Vinyl Protons

The fraction of xanthate-functionalized chains before thermolysis of the PVP sample was determined in Section 4.6.3 to be 0.85 compared to phthalimide chain ends. Since thermolysis quantitatively converts the xanthate end-group to an alkene, the fraction of alkene end-groups compared to phthalimide chain ends should also be 0.85. Hence the ^{1}H-NMR spectrum for the PFBA-derivatized PVP can be normalized using the alkene protons peak at δ = 6.75 – 7.01 ppm. The interference from the carbon satellite of the chloroform peak has to be taken into account. This interference can be computed using Equation A11.1.

$$\int_{\delta=6.75}^{\delta=7.01} f_1(\delta)d\delta - \frac{0.011}{2}\int_{\delta=7.14}^{\delta=7.33} f_1(\delta)d\delta = 0.85 \qquad \text{(A11.1)}$$

Where

$f_1(\delta)$ = the ^{1}H-NMR spectrum of the PFBA-derivatized PVP sample.

A first approximation assumed that there was no interference from the carbon satellite.

$$\left(\int_{\delta=7.14}^{\delta=7.33} f_1(\delta)d\delta\right)_0 = 0.00$$

$$\left(\int_{\delta=6.75}^{\delta=7.01} f_1(\delta)d\delta\right)_0 = 0.85$$

$\left(\int_{\delta=7.14}^{\delta=7.33} f_1(\delta)d\delta\right)_1$ was then measured and found to be equal to 3.05

The error in the first approximation for $\int_{\delta=7.14}^{\delta=7.33} f_1(\delta)d\delta$ was computed

$$\varepsilon_1 = \left(\int_{\delta=7.14}^{\delta=7.33} f_1(\delta)d\delta\right)_0 - \left(\int_{\delta=7.14}^{\delta=7.33} f_1(\delta)d\delta\right)_1$$

$\left(\int_{\delta=6.75}^{\delta=7.01} f_1(\delta)d\delta\right)_1$ could then be calculated using the general iterative procedure:

$\left(\int_{\delta=7.14}^{\delta=7.33} f_1(\delta)d\delta\right)_n$ is measured and ε_n is computed using

$$\varepsilon_n = \left(\int_{\delta=7.14}^{\delta=7.33} f_1(\delta)d\delta\right)_{n-1} - \left(\int_{\delta=7.14}^{\delta=7.33} f_1(\delta)d\delta\right)_n$$

$$\left(\int_{\delta=6.75}^{\delta=7.01} f_1(\delta)d\delta\right)_{n+1} = \left(\int_{\delta=6.75}^{\delta=7.01} f_1(\delta)d\delta\right)_n - \frac{0.011}{2}\varepsilon_n$$

The results of the iteration are shown in Table A11.1.

Table A11.1: Results for the Iterative Procedure, Described in Appendix A11.

$\boldsymbol{n}$	$\left(\int_{\delta=7.14}^{\delta=7.33} \boldsymbol{f_1(\delta)d\delta}\right)_n$	$\left(\int_{\delta=6.75}^{\delta=7.01} \boldsymbol{f_1(\delta)d\delta}\right)_n$
0	0	0.85
1	3.05	0.87
2	3.12	0.87

A12) Normalizing the ^{1}H-NMR Spectrum of PVP-block-poly(N^{ε}-(CBZ)-L-lysine)

The PVP backbone peaks of the ^{1}H-NMR spectrum for PVP-block-poly(N^{ε}-(CBZ)-L-lysine) at δ = 1.14 – 2.43 ppm were used as an internal reference. There are 6 hydrogen atoms on the lysine residues that also resonate in the region of interest. Since the benzyl hydrogens peak of the lysine residues are resolved from any interferences, their integration intensity can be used to determine the integration intensity of the interfering hydrogen peaks. This was achieved using Equation A12.1.

$$\int_{\delta=1.14}^{\delta=2.43} f_1(\delta)d\delta - 3\int_{\delta=4.77}^{\delta=5.15} f_1(\delta)d\delta = 2\int_{\delta=2.9}^{\delta=4.2} f_2(\delta)d\delta \qquad \text{(A12.1)}$$

Where

$f_1(\delta)$ = the ^{1}H-NMR spectrum for PVP-block-poly(N^{ε}-(CBZ)-L-lysine)

$f_2(\delta)$ = the ^{1}H-NMR spectrum of the thermolyzed PVP used to prepare the macroinitiator

The first data set in the iteration was:

$$\left(\int_{\delta=1.14}^{\delta=2.43} f_1(\delta)d\delta\right)_1 = 2\int_{\delta=2.9}^{\delta=4.2} f_2(\delta)d\delta = 2 \times 426.17 = 852.98$$

$$\left(\int_{\delta=4.77}^{\delta=5.15} f_1(\delta)d\delta\right)_1 = 59.52$$

The error in the first approximation for $\int_{\delta=1.14}^{\delta=2.43} f_1(\delta)d\delta$ was computed using Equation A12.2.

$$\left(\int_{\delta=1.14}^{\delta=2.43} f_1(\delta)d\delta\right)_1 - 3\left(\int_{\delta=4.77}^{\delta=5.15} f_1(\delta)d\delta\right)_1 = 2\int_{\delta=2.9}^{\delta=4.2} f_2(\delta)d\delta + \varepsilon_1 \qquad \text{(A12.2)}$$

$$\varepsilon_1 = -178.56$$

The subsequent data sets were computed using the following general iterative formulae.

$$\left(\int_{\delta=1.14}^{\delta=2.43} f_1(\delta)d\delta\right)_{n+1} = \left(\int_{\delta=1.14}^{\delta=2.43} f_1(\delta)d\delta\right)_n - \varepsilon_n$$

$\int_{\delta=1.14}^{\delta=2.43} f_1(\delta)d\delta$ normalized to $\left(\int_{\delta=1.14}^{\delta=2.43} f_1(\delta)d\delta\right)_{n+1}$

$\left(\int_{\delta=4.77}^{\delta=5.15} f_1(\delta)d\delta\right)_{n+1}$ measured from spectrum

$$\varepsilon_{n+1} = \left(\int_{\delta=1.14}^{\delta=2.43} f_1(\delta)d\delta\right)_{n+1} - 3\left(\int_{\delta=4.77}^{\delta=5.15} f_1(\delta)d\delta\right)_{n+1} - 2\int_{\delta=2.9}^{\delta=4.2} f_2(\delta)d\delta$$

The results of the iterative procedure are tabulated in Table A12.1.

Table A12.1: Results of Iterative Procedure for Normalizing the ^{1}H-NMR Spectrum for PVP-block-poly(N^{ε}-(CBZ)-L-lysine).

n	$\left(\int_{\delta=1.14}^{\delta=2.43} f_1(\delta)d\delta\right)_n$	$\left(\int_{\delta=4.77}^{\delta=5.15} f_1(\delta)d\delta\right)_n$	ε_n
1	852.98	59.52	-178.56
2	1031.54	71.98	-37.38
3	1068.92	74.59	-7.83
4	1076.75	75.14	-1.65
5	1078.40	75.25	-0.33
6	1078.73	75.28	-0.09
7	1078.82	75.28	0

A13) References

1. Pound, G.; McLeary, J. B.; McKenzie, J. M.; Lange, R. F. M.; Klumperman, B. In-Situ NMR Spectroscopy for Probing the Efficiency of RAFT/MADIX Agents. *Macromolecules* **2006**, *39*, 7796-7797.